UNIVERSITY OF OKLAHOMA

GRADUATE COLLEGE

A STUDY OF HYPOSELENOCYANITE AND THE KINETICS AND MECHANISM OF THE LACTOPEROXIDASE SYSTEM

A DISSERTATION

SUBMITTED TO THE GRADUATE FACULTY

In partial fulfillment of the requirements for the

Degree of

DOCTOR OF PHILOSOPHY

By

KELLYE CUPP-SUTTON
Norman, Oklahoma
2018

A STUDY OF HYPOSELENOCYANITE AND THE KINETICS AND MECHANISM OF THE LACTOPEROXIDASE SYSTEM

A DISSERTATION APPROVED FOR THE
DEPARTMENT OF CHEMISTRY AND BIOCHEMISTRY

BY

Dr. Michael T. Ashby, Chair

Dr. Robert White

Dr. Shaorong Liu

Dr. George Richter-Addo

Dr. Tohren Kibbey

ACKNOWLEDGEMENTS

First, I would like to extend my sincere thanks to my research advisor Dr. Ashby. His guidance, patience, and encouragement during my studies have been invaluable. I would also like to acknowledge my current and former committee members Drs. White, Liu, Richter-Addo, Kibbey, and Thomson for their help and encouragement. A special thanks to Dr. Richter-Addo for accepting me as an honorary member of his lab during Dr. Ashby's sabbatical in South Africa.

I would also like to extend my gratitude to Drs. Susan Nimmo and Steven Foster for their support both in areas of research and teaching assistantship and to the Department of Chemistry and Biochemistry for continued financial support during my research. Thank you also to Rachel Roccanova, a fellow Analytical Chemistry graduate student, whose reassurance helped me through some of the more strenuous of times in the program.

Lastly, but most importantly, I want to thank my family. To my husband Blair whose endless support I could not appreciate more. To my parents, Brad and Dianne Cupp, and grandparents, Charles and Carol Cupp, for their support and encouragement that made me believe I could do anything. To my sister, Karye Allard, whose pride in me during this undertaking made me sure I could not fail. And to my mother-in-law, Elaine Sutton, and father-in-law, Dr. Wendell Sutton, who deserves special thanks for the countless hours he spent editing the dissertation you are about to read. Thank you for everything.

TABLE OF CONTENTS

LIST OF TABLES

LIST OF FIGURES

LIST OF ABBREVIATIONS

Cat	Catalase
Cpd I	Compound I
Cpd II	Compound II
DTNB	5,5'-dithiobis-(2-nitrobenzoic acid)
E/EE	Lactoperoxidase Native Enzyme
EE0	Initial lactoperoxidase
EOx	Lactoperoxidase bound to hydrogen peroxide
EPO	Eosinophil Peroxidase
E_T	Total lactoperoxidase concentration
EX	Lactoperoxidase bound to halide or pseudohalide
H_2O_2	Hydrogen Peroxide
HOBr	Hypobromous Acid
HOCl	Hypochlorous Acid
HOI	Hypoiodous acid
HOSCN	Hypothiocyanous Acid
HOSeCN	Hyposelenocyanous Acid
HOX	Hypo(pseudo)halous acid
K_D	Dissociation constant
LPO	Lactoperoxidase
MPO	Myeloperoxidase
N	Hill coefficient
Na_2HPO_4	Disodium phosphate
NaH_2PO_4	Monosodium phosphate
NaOH	Sodium Hydroxide
OBr^-	Hypobromite
OCl^-	Hypochlorite
OI^-	Hypoiodite
$OSCN^-$	Hypothiocyanite
$OSeCN^-$	Hyposelenocyanite
Ox	Hydrogen peroxide
Ox0	Initial hydrogen peroxide
P	Hypohalite product
PsX^-	Pseudohalide
S	Reducing substrate
SCN^-	Thiocyanate
$SeCN^-$	Selenocyanate
SF	Stopped-Flow
TNB	5-thio-2-nitrobenzoic acid
UV-Vis	Ultraviolet-visible spectroscopy
X^-	Halide

$\Delta A_{max-min}$	Change in absorbance at the maximum and minimum of the difference spectra
E	Molar absorptivity
Θ	Ratio of bound to unbound lactoperoxidase
λ_{max}	Wavelength of maximum absorbance
T	Age time

ABSTRACT

The lactoperoxidase system, defined as lactoperoxidase in the presence of hydrogen peroxide and thiocyanate, is a powerful method of host defense, particularly in mammalian secretory mucosae. The product of this system, hypothiocyanite, functions as an antimicrobial by oxidizing bacterial sulfhydryls, thereby inhibiting bacterial respiration. The lactoperoxidase system and its product, hypothiocyanite, have been the focus of study for over a century. We explore herein the function of selenocyanate as a substrate of the lactoperoxidase system and we reinterpret the mechanism of the lactoperoxidase system with is natural substrate, thiocyanate.

There is new evidence in the literature that selenocyanate, the selenium derivative of thiocyanate, is present in mammals and concentrated in the secretory mucosae using the same active membrane transport mechanism as thiocyanate. However, the ability of lactoperoxidase to utilize selenocyanate as a substrate for the lactoperoxidase system has never been studied. Furthermore, the selenium derivative of hypothiocyanite, hyposelenocyanite, has not been previously characterized.

We successfully synthesized hyposelenocyanite via the oxidation of selenocyanate by hypochlorous acid at alkaline pH and using the lactoperoxidase system. Hyposelenocyanite produced at alkaline pH was characterized spectrophotometrically by comparison with the known spectrum of hypothiocyanite. The rate of oxidation of selenocyanate by hypochlorous acid at alkaline pH is faster than the oxidation of thiocyanate by hypochlorous acid by two orders of magnitude which is expected given the higher reactivity of selenium analogs of sulfur compounds. Similarly, the decomposition

of hyposelenocyanite at alkaline pH is several orders of magnitude faster than the hydrolysis of hypothiocyanite under the same conditions.

The lactoperoxidase system was also used to synthesize hyposelenocyanite, which was observed spectrophotometrically via the reaction of hyposelenocyanite with 5-thio-2-nitrobenzoic acid. Remarkably, while observing the ability of the lactoperoxidase system to catalyze selenocyanate oxidation, we observed unexpected kinetics that could not be explained by the accepted mechanism of catalysis.

The reported literature mechanism of lactoperoxidase catalysis of halide and pseudohalide oxidation by hydrogen peroxide is known as the halogen cycle. The halogen cycle is reported in the literature as an ordered sequential mechanism where lactoperoxidase is oxidized in a two-electron oxidation reaction by hydrogen peroxide to produce compound I. Compound I then reacts with a halide or pseudo-halide to produce native lactoperoxidase and the hypo(pseudo)halous acid. When the reaction of compound I with hydrogen peroxide is rate-limiting, as has been reported for thiocyanate, the kinetics of the halogen cycle reaction are expected to be first-order in hydrogen peroxide and independent of reducing substrate concentration.

We performed a series of stopped-flow UV-Vis experiments with varying concentrations of reactants and enzyme and found that at high concentration of reducing substrate (relative to the concentration of hydrogen peroxide) the kinetics observed for the lactoperoxidase-catalyzed oxidation of thiocyanate and selenocyanate reflect what is expected according to the halogen cycle literature mechanism (although we reinterpret the kinetics in terms of a new mechanism). However, at low concentration of reducing

substrate (relative to hydrogen peroxide) the reaction becomes biphasic, a first-order reaction followed by a zeroth-order reaction.

We propose a new mechanism which accounts for the kinetics that are observed under all reaction conditions. The proposed mechanism is an ordered sequential mechanism where the initial reaction is the binding of lactoperoxidase with the reducing substrate. This bound lactoperoxidase species then reacts with hydrogen peroxide to produce native lactoperoxidase and the hypo(pseudo)halite. However, hydrogen peroxide, in addition to acting as the oxidizing substrate, also acts as a tight binding inhibitor of lactoperoxidase to produce a lactoperoxidase-hydrogen peroxide bound species which is inactive or less active in catalysis. Experimental data were fit to the proposed model for the lactoperoxidase-catalyzed oxidation of thiocyanate and selenocyanate to elucidate absolute rate constants for the mechanism.

The biological significance of the kinetics we observe when the concentration of hydrogen peroxide exceeds the concentration of the thiocyanate substrate, when hydrogen peroxide inhibition of lactoperoxidase is observed, depends on the reaction conditions *in vivo*. Concentration conditions that promote hydrogen peroxide inhibition of lactoperoxidase are not expected to be prevalent in healthy humans. However, it is conceivable that certain disease conditions promote the higher hydrogen peroxide concentrations and lower thiocyanate concentrations required for lactoperoxidase inhibition by hydrogen peroxide. Using the oral cavity as an example, inflammation of the gingival crevasse promotes phagocytosis that results in the extracellular production of hydrogen peroxide. Inflammation of gingival tissue also promotes the excretion of gingival crevicular fluid, which naturally lowers the concentration of thiocyanate. Since many oral

pathogenic bacteria are obligate anaerobes, it may be advantageous to deactivate the defensive peroxidases to raise the local concentration of hydrogen peroxide for the purpose of staving off infection. A better argument for such a defensive mechanism could be made if the other principal defensive peroxidase of the oral cavity, myeloperoxidase, is inhibited by hydrogen peroxide via a similar mechanism. Accordingly, additional mechanistic studies of the other defensive peroxidases are warranted.

Chapter 1 – INTRODUCTION

1.1 Lactoperoxidase

Lactoperoxidase is a mammalian heme peroxidase enzyme and a member of a family of defensive peroxidases which includes myeloperoxidase, eosinophil peroxidase, thyroid peroxidase, and the recently discovered vascular peroxidase.[1] While myeloperoxidase, lactoperoxidase, and eosinophil peroxidase have similar primary functions *in vivo*, thyroid peroxidase is distinct compared with the other mammalian heme peroxidases because it is membrane bound at the surface of thyrocytes and primarily serves to catalyze the iodination of tyrosine residues in thyroid hormones.[2] Lactoperoxidase has been the focus of study since the early 1900s when it was found that milk possessed intrinsic antibacterial activity.[3-5] Eventually, lactoperoxidase was determined to be the source of antimicrobial activity in milk when in the presence of hydrogen peroxide and thiocyanate.[6] In addition to its presence in milk, lactoperoxidase has been found to be widespread in secretory mucosa including saliva, tears, and breast milk as well as lung, intestinal, and cervical mucous. The widespread presence of lactoperoxidase in a variety of mucosal excretions has led to the relabeling of lactoperoxidase as milk peroxidase, salivary peroxidase (first discussed in 1951),[7-8] uterine peroxidase,[9] and airway peroxidase.[10] The numerous pseudonyms make researching the early history of lactoperoxidase challenging as it was not apparent to early researchers that they were observing the same enzyme.

Lactoperoxidase is one of the more heavily studied members of the mammalian peroxidase family due to the comparative ease with which it is isolated compared to

myeloperoxidase and eosinophil peroxidase.[11] As such, lactoperoxidase is the main focus of a book[12] as well as many book chapters[13-15] and review articles.[11, 16-18]

The lactoperoxidase system, which consists of lactoperoxidase, hydrogen peroxide, and a halide or pseudohalide substrate, usually thiocyanate, acts as a powerful method of host defense *in vivo*.[8] It is also commonly used commercially to inhibit microbial growth in milk and infant formula,[19] fruits, vegetables, meat,[10, 20] and cosmetics.[21] Lactoperoxidase is also used medically to treat oral health conditions such as xerostomia[22] and for the treatment of viral and bacterial infections.[23-24] This section presents a review of the working knowledge of the structure, function, and mechanisms of lactoperoxidase.

1.1.1 Lactoperoxidase Structure

Lactoperoxidase is a glycoprotein with a covalently linked iron containing heme, a protoporphyrin IX derivative, at its catalytic center. Two isoforms of lactoperoxidase are known, the enzymatically active heme containing species, and a non-heme or apo form of the enzyme which is enzymatically inactive.[25] The molecular weights of the isoforms are apparently the same according to SDS-PAGE analysis.[26] However, the non-heme species lacks a Soret band at 412 nm, which is characteristic of the presence of porphyrin π-π^* transitions, when examined using ultraviolet-visible absorption spectroscopy.[25-26] The biological significance of the non-heme protein is not known, but it has been proposed that it may be a precursor or degradation product since it is expressed ubiquitously in secretions where catalytically active lactoperoxidase is present.[26]

The amino acid sequence of bovine lactoperoxidase was determined in 1991[27] and the protein was first crystallized in 1995.[28] The crystal structure was finally determined in

2007 and is remarkably similar to myeloperoxidase with the primary difference being that myeloperoxidase exists as a dimer while lactoperoxidase is a monomer.[29]

The prosthetic group that acts as the active site in lactoperoxidase is the iron-containing heme which is a derivative of protoporphyrin IX and is common to the mammalian peroxidase family of enzymes including myeloperoxidase, thyroid peroxidase, and eosinophil peroxidase.[15] The lactoperoxidase protoporphyrin IX heme derivative differs from typical protoporphyrin IX, common to plant and fungal peroxidases such as horseradish peroxidase, by the presence of two hydroxy methyl functional groups at the 1 and 5 positions, Figure 1.1.[30]

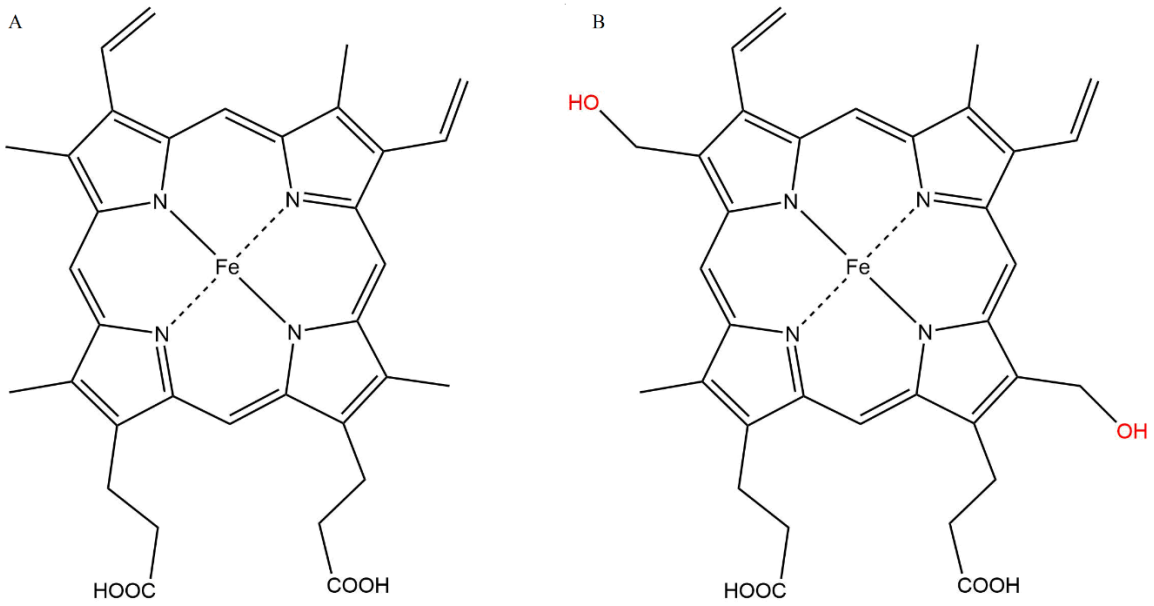

Figure 1.1 - The chemical structure of the protoporphyrin hemes, A, protoporphyrin IX and B, the protoporphyrin IX derivative found in mammalian heme peroxidases.

The hydroxyl modifications of the porphyrin structure allow covalent bonds of the heme to the protein backbone. These bonds are ester linkages which form between the hydroxyl groups and Asp225 and Glu375 in lactoperoxidase.[31] Analogous bonds are present in the other members of the family of mammalian peroxidases; however, myeloperoxidase also makes a third covalent bond to a vinyl β-carbon through a methionine residue.[32] The binding site for thiocyanate in lactoperoxidase differs from that of myeloperoxidase by the conformation of a loop which makes up one of the walls of the binding cavity.[33]

1.1.2 Lactoperoxidase Substrate Binding

There is some dissent in the literature when it comes to the binding site and orientation of the primary lactoperoxidase substrate, thiocyanate, based on the method of observation. The primary methods used to observe peroxidase structure and binding are NMR and X-ray crystallography; however, FTIR has also been used to study heme peroxidase enzymes, primarily horseradish peroxidase which utilizes a mechanism involving one-electron oxidations rather than the two-electron oxidations indicative of the primary mechanisms of lactoperoxidase, myeloperoxidase, and eosinophil peroxidase.[34-36]

It has been proposed that the binding site of thiocyanate is determined by an electrostatic interaction to a distal histidine residue. This has been indirectly observed via NMR studies which show pH dependent binding of thiocyanate which decreases rapidly as the pH nears 7.[37] This pH dependence correlates with the pKa of histidine at pH 6. A similar pH dependence is also present for iodide which indicates that thiocyanate and iodide bind to the same site.[38]

However, the electrostatic interaction of thiocyanate and iodide is not observed in X-ray crystallography studies. Singh et al. show that thiocyanate does not directly interact with any amino acid residues in the protein channel, but rather, is held in place by a conserved chain of hydrogen bonded water molecules in the catalytic pocket, through its nitrogen atom to an asparagine residue.[39] This chain of hydrogen bonded water molecules has also been proposed to function as a proton transfer chain.[33, 40] However, the aforementioned study crystallized lactoperoxidase in a cocktail of inorganic substrate anions and indicates that each substrate has a unique binding site.[39] The unique binding site of each substrate is used to determine if the position of the binding site has an effect on the preference of lactoperoxidase to catalyze oxidation and leads the authors to the conclusion that the order of substrate preference is Br^->Cl^->SCN^->I^-.[39] It is not clear whether the presence of multiple species of anion substrates influences the binding of the individual substrates to lactoperoxidase in solution. However, this claim on substrate preference is directly disputed by the results of a previous kinetic study of the rates of reaction of lactoperoxidase compound I with various inorganic substrates which indicates that the kinetic substrate preference is SCN^->I^->Br^- and that the oxidation of chloride is not catalyzed by lactoperoxidase.[41] Myeloperoxidase has a similar kinetic substrate preference to lactoperoxidase, but is also capable of catalyzing the oxidation of chloride, SCN^->I^->Br^->Cl^-.[42]

Another crystal structure, which shows the binding of thiocyanate only, indicates a much closer binding site for thiocyanate to the lactoperoxidase heme catalytic center.[33] While the crystal structure does not show a direct interaction of histidine to thiocyanate as predicted in the NMR studies,[37] it does show an interaction of thiocyanate to a water

molecule which is conserved and bound to the iron heme.[33] This water molecule, which is displaced when the heme is oxidized by hydrogen peroxide, is hydrogen bonded to a distal histidine.[33] It seems likely that this is the actual binding site of thiocyanate during catalysis.

The binding orientation of thiocyanate to lactoperoxidase is also not clear depending on whether NMR data or X-ray crystallography data is analyzed. NMR studies have shown that thiocyanate is oriented with the nitrogen toward the heme center.[43] However, the crystal structure shows that sulfur is oriented toward the heme center.[33] In myeloperoxidase, the orientation of thiocyanate in the distal position has been shown unambiguously to be with nitrogen toward the heme center.[44]

1.1.3 Biological Significance of Lactoperoxidase

In addition to similar structure, myeloperoxidase and lactoperoxidase have similar catalytic function. Myeloperoxidase and lactoperoxidase are both active in host defense via the production of hypo(halous)acids. Myeloperoxidase primarily produces hypochlorous acid and lactoperoxidase primarily produces hypothiocyanous acid through the oxidation of chloride and thiocyanate, respectively.[42] Curiously, myeloperoxidase does not oxidize chloride more efficiently than thiocyanate. In fact, myeloperoxidase compound I reacts with chloride and thiocyanate with apparent second-order rate constants of $2.5(3)\text{x}10^{4}$ $M^{-1}s^{-1}$ and $9.6(5)\text{x}10^{6}$ $M^{-1}s^{-1}$, respectively, indicating a kinetic preference for thiocyanate.[42] Lactoperoxidase compound I reacts with thiocyanate with the apparent second-order rate constant $2.0\text{x}10^{8}$ $M^{-1}s^{-1}$ and lactoperoxidase compound I is incapable of oxidizing chloride.[41]

The cause of the differing primary reducing substrate is a result of *in vivo* reducing substrate concentrations and the level of oxidative stress. In secretory fluids,

lactoperoxidase is the primary peroxidase present and thiocyanate is its primary reducing substrate. Concentrations of thiocyanate in these secretory fluids can range from 0.1-3000 μM depending on the source of the fluid and health of the subject.[45-46] However, under conditions of oxidative stress, myeloperoxidase can be introduced to the secretory fluids through the exocytosis of neutrophil granulocytes and its primary reducing substrate becomes thiocyanate.[47] In plasma, where the average concentration of chloride is approximately 100 mM, chloride is the primary reducing substrate of myeloperoxidase.[42, 48] However, hypochlorous acid produced by the myeloperoxidase-catalyzed oxidation of chloride reacts with thiocyanate with a rate constant of $2.34(9)x10^7$ $M^{-1}s^{-1}$, so it is likely that hypothiocyanite is still the active antibacterial species *in vivo*.[49]

1.2 Previous Understanding of Lactoperoxidase Mechanisms

Lactoperoxidase participates in three separate types of catalytic mechanisms. When hydrogen peroxide is present, but sufficient concentration of reducing substrate is absent, the enzyme acts as a catalase. Lactoperoxidase can also serve to catalyze the oxidation of various one-electron and two-electron reducing substrates through the peroxidase cycle and the halogen cycle. This section will review the literature on the accepted mechanism for each catalytic cycle relevant to lactoperoxidase as well as compare similar catalytic cycles for other heme enzymes.

1.2.1 Formation of Lactoperoxidase Compound I

The mechanisms of lactoperoxidase catalysis can be complicated, particularly due to the multiple active enzyme intermediates and multiple pathways by which these intermediates can be reached. Lactoperoxidase intermediate species vary in oxidation state of iron, oxidation equivalents, radicalization, and location of radicals, and all intermediates

have unique absorption spectra.[50] The absorption spectra of the lactoperoxidase intermediates differ in the Soret region, typically ranging between 400 and 500 nm, and also have notable differences in the Q bands, between 500 and 600 nm.[50] For example, Figure 1.2 shows the absorption spectra of native lactoperoxidase and two intermediate enzyme species, compound I and compound II.

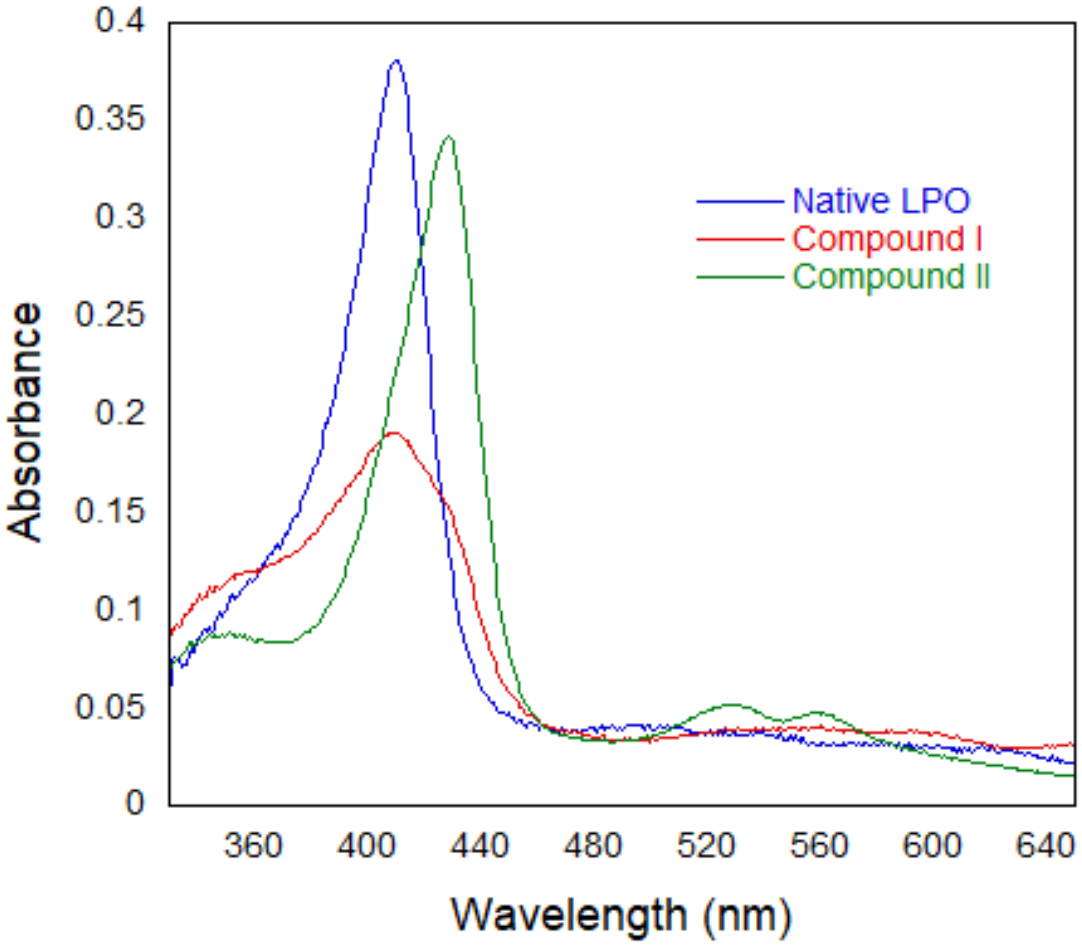

Figure 1.2 – Absorption spectra of lactoperoxidase enzyme species.

Regardless of the mechanism of catalysis, lactoperoxidase is always initially activated, by the two-electron oxidation of the native ferric enzyme, which contains an iron heme center with a 3+ oxidation state, by hydrogen peroxide. This forms an intermediate commonly known as compound I, which contains two oxidizing equivalents, Figure 1.3. The iron heme center of compound I has an oxidation state of 4+ accounting for one oxidizing equivalent and an unpaired electron localized to the porphyrin ring accounting for the second oxidizing equivalent. The unpaired electron of compound I is relatively unstable and quickly delocalizes to a nearby amino acid and forms a compound I isomer sometimes designated compound I*, Equation 1.1.[51]

$$aa\ Por^{+\cdot}Fe(III) + H_2O_2 \rightarrow aa^{+\cdot}PorFe(IV) + H_2O \qquad \text{Equation 1.1}$$

Compound I* has an absorption spectrum similar to that of compound II, an intermediate species resulting from the one-electron reduction of compound I, and still maintains two oxidizing equivalents. However, unlike compound I which can participate in a two-electron oxidation of a halide or pseudohalide, compound I* is relegated to participating in one-electron oxidations.[52] Because of the oxidizing limitations, formation of compound I* in the absence of a one-electron donor can effectively inactivate lactoperoxidase.

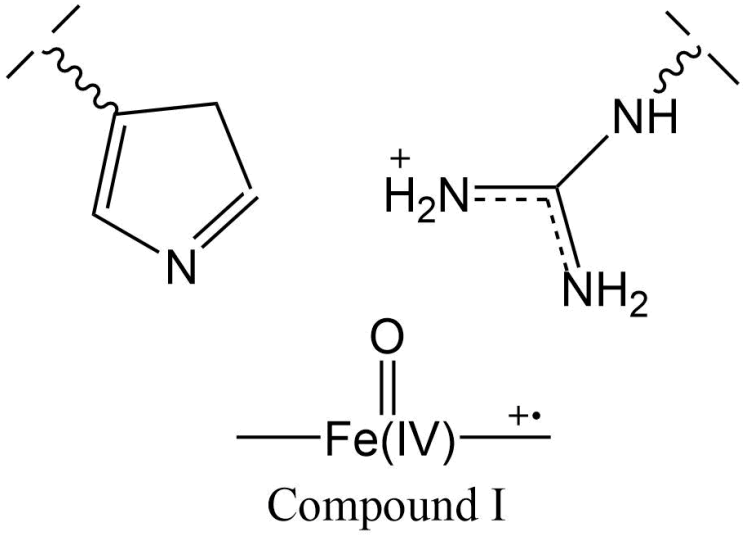

Figure 1.3 - Structure of lactoperoxidase compound I

1.2.2 The Peroxidase Cycle

The typical substrates of the lactoperoxidase peroxidase cycle are organic aromatic molecules which act as one-electron reductants. The kinetics and mechanism of the peroxidase cycle of lactoperoxidase and horseradish peroxidase were first studied by Chance in 1949[53] after the discovery of spectral evidence for multiple lactoperoxidase oxidized species was observed by Theorell and Akesson in 1943.[54] The peroxidase cycle of lactoperoxidase, which exists as a secondary mechanism in the absence of appropriate halide or pseudohalide substrate, is analogous to the primary catalytic reaction of horseradish peroxidase.[55]

The peroxidase cycle consists of three stages, Figure 1.4. The first stage is the oxidation of the native enzyme by hydrogen peroxide to produce compound I. In the absence of sufficient concentration of one-electron donating substrate a compound I isomer maintaining two oxidizing equivalents, compound I*, may be produced as discussed in

section 1.2.1. Compound I or compound I* is reduced in a one-electron oxidation reaction to compound II which contains one oxidizing equivalent in the iron(IV) catalytic center. Another one-electron reduction of compound II produces native LPO. These reductions produce two equivalents of radicalized substrate, A•, which subsequently react.[56]

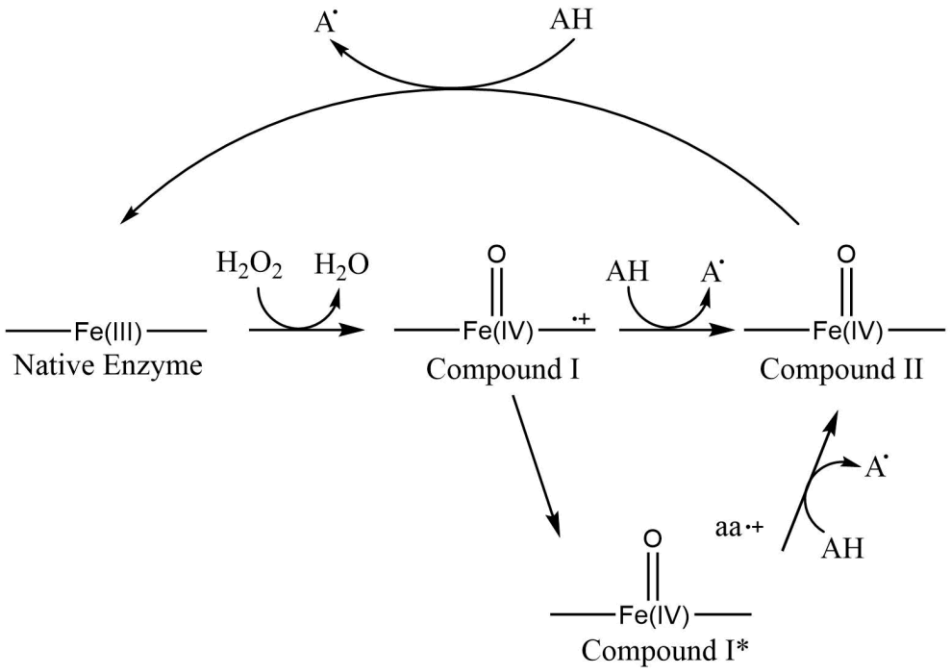

Figure 1.4 - Peroxidase cycle for the lactoperoxidase-catalyzed oxidation of one-electron reducing substrates.

1.2.3 The Halogen Cycle

The halogen cycle is the primary biologically relevant catalytic reaction of lactoperoxidase and is analogous to the halogen cycle catalytic mechanisms of myeloperoxidase and eosinophil peroxidase. It consists of a two-electron oxidation of a small inorganic anion, generally a halide or pseudo-halide, which produces a hypo(pseudo)halous acid which is active in host defense, discussed more in section 1.3 of this work.

The halogen cycle, like the peroxidase cycle, is initiated by the oxidation of the iron catalytic center by hydrogen peroxide to form compound I, Equation 1.2.1, as discussed in section 1.2.1. Compound I is reduced back to native enzyme in a two-electron redox reaction, generally by a halide or pseudohalide reducing substrate, Equation 1.2.2.[41]

$$LPO + H_2O_2 \overset{k_1}{\rightarrow} Cpd\ I + H_2O \qquad \text{Equation 1.2.1}$$

$$Cpd\ I + X^- \overset{k_2}{\rightarrow} LPO + OX^- \qquad \text{Equation 1.2.2}$$

The ability of compound I to oxidize a halide or pseudohalide depends on the relative redox potentials of the compound I/native enzyme and halide/hypohalous acid redox couples, Table 1. The compound I/native LPO redox couple has a reduction potential of 1.09 V at pH 7.[57] Lactoperoxidase compound I has a sufficient reduction potential to oxidize bromide, iodide, and thiocyanate which have reduction potentials of 0.93 V, 0.57 V, and 0.56, respectively.[58-59] However, chloride is unable to be oxidized by lactoperoxidase compound I as its reduction potential is, effectively, too high at 1.08 V.[58]

Table 1 - Two-electron oxidation potentials for LPO Cpd I, I^-, SCN^-, Br^- and Cl^- at pH 7

Redox Couple (pH 7)	E° (V)	Reference
$I^- + H_2O \rightarrow HOI + H^+ + 2e^-$	-0.56	56
$SCN^- + H_2O \rightarrow HOSCN + H^+ + 2e^-$	-0.57	57
$Br^- + H_2O \rightarrow HOBr + H^+ + 2e^-$	-0.93	56
$Cl^- + H_2O \rightarrow HOCl + H^+ + 2e^-$	-1.08	58
LPO Cpd I $\rightarrow$ LPO + $2e^-$	-1.09	57
MPO Cpd I $\rightarrow$ MPO + $2e^-$	-1.16	60
$2H_2O \rightarrow O_2 + 4H^+ + 4e^-$	-1.23	61

1.2.4 Catalase Activity

Catalase is a heme enzyme with a discovery predating that of lactoperoxidase by at least a decade, with the first discussion of the named enzyme occurring in 1900.[62] The main function of catalase is to catalyze the reduction of potentially cytotoxic hydrogen peroxide to water and molecular oxygen.

The mechanism of catalase action has been studied enzymatically, kinetically, and via computer model.[63-65] The long accepted mechanism is known as the Bonnichsen, Chance, and Theorell (BCT) mechanism which is similar to the mechanism of the halogen cycle of the mammalian peroxidases in that it involves a two-electron oxidation.[63] The first step of the mechanism is the oxidation of catalase by hydrogen peroxide to produce catalase compound I, Equation 1.2.3. Then catalase compound I oxidizes a second equivalent of hydrogen peroxide in a two-electron oxidation to produce molecular oxygen, Equation 1.2.4. This puts hydrogen peroxide in the position of being both the oxidizing and reducing substrate of the overall reaction which converts two equivalents of hydrogen peroxide to two water molecules and one molecular oxygen. The variation in the rate of hydrogen

peroxide consumption by catalase as compared to other heme enzymes that exhibit catalase-like activity has also been studied, Table 2.

$$Cat + H_2O_2 \xrightarrow{k_1} Cpd\ I + H_2O \qquad \text{Equation 1.2.3}$$

$$Cpd\ I + H_2O_2 \xrightarrow{k_2} Cat + H_2O + O_2 \qquad \text{Equation 1.2.4}$$

Table 2 - Maximum velocities of catalase activity for various catalase species and catalase-like activity for non-catalase heme enzymes.

Enzyme	**V ($M^{-1}s^{-1}$)**	**pH**	**References**
Erythrocyte Catalase	$3x10^7$	7	66
Bacterial Catalase	$6x10^7$	7	66
Micrococcus lysodeikticus catalase	$1x10^7$	7	67
Horse Blood Catalase	$4x10^7$	7	68
Myeloperoxidase	$2x10^6$	7.4	69
Chloroperoxidase	$2x10^5$	4.5	70
Horseradish Peroxidase	$5x10^2$	8	71
Bovine Cytochrome Oxidase	$2x10^2$	7	72

The second reaction, Reaction 1.2.4, is the rate-limiting reaction for catalysis and has been assumed to be a two-electron oxidation as discussed above, but there is still some debate over the intimate mechanism of this step. The second step is generally assumed to occur as a two-electron oxidation. However, there is evidence that two one-electron oxidations steps occur for the reduction of H_2O_2 by catalase. An isotopic labeling study indicates that the O-O hydrogen peroxide bond is not broken, but that a histidine residue nearby the catalytic center is involved in the oxidation[67] and a molecular modeling study

indicates that a histidine mediated acid-base reaction mechanism, Figure 1.5, or a radical mechanism, Figure 1.6, may more accurately describe the mechanism.[65]

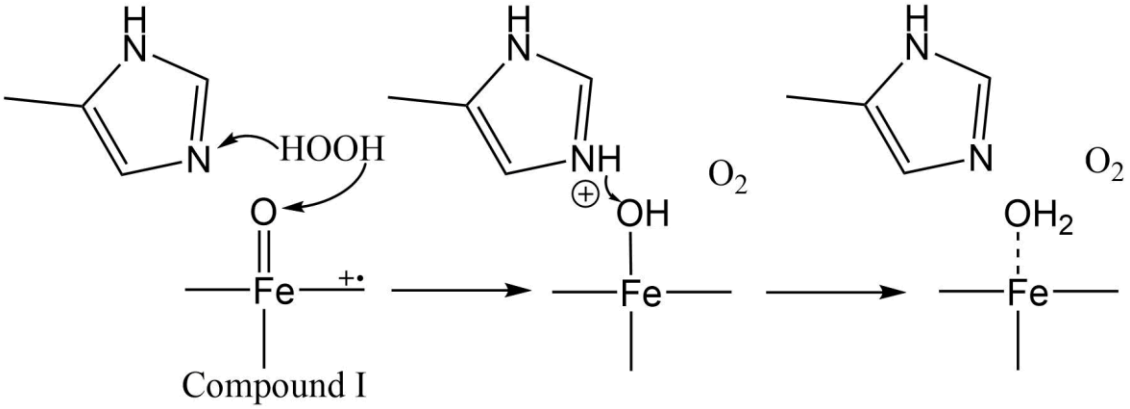

Figure 1.5 - Acid-base mediated reduction of hydrogen peroxide by catalase.

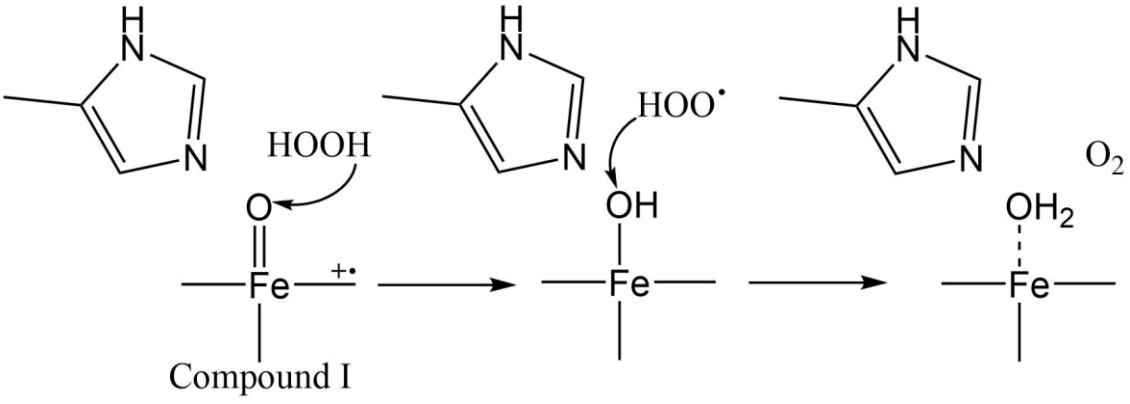

Figure 1.6 - Radical mechanism of the reduction of hydrogen peroxide by catalase.

The literature concerning the mechanism of the catalase-like action of heme peroxidases has been thoroughly reviewed by Obinger et al.[73] Most heme peroxidases are not capable of true catalase activity as described in Equations 1.2.3 and 1.2.4 with the exception of myeloperoxidase which has been shown to exhibit true catalase activity in addition to catalase-like activity unique to the other peroxidases.[69] This explains why myeloperoxidase has the highest rate of catalase activity as compared to other heme peroxidases, Table 2, although it is not as efficient as catalase enzymes.

Lactoperoxidase has been shown to exhibit pseudo-catalase activity via two different pathways, Figure 1.7.[50, 74] Lactoperoxidase pseudo-catalase activity can occur in the absence of typical reducing substrate and excess hydrogen peroxide with respect to enzyme concentration. Hydrogen peroxide acts, first, as a two-electron oxidant to oxidize native lactoperoxidase to produce compound I. Compound I is then reduced to compound II by a one-electron reduction by hydrogen peroxide producing superoxide. Compound II is then reduced back to native lactoperoxidase by superoxide completing the catalytic cycle.[74]

It should be noted at this point that there has been some contention in the literature about the species involved in the one-electron reduction of compound I to compound II during pseudo-catalase activity. Hydrogen peroxide may act as a one-electron reductant as discussed above; however, compound I is also capable of spontaneously undergoing one-electron reduction in the absence of excess hydrogen peroxide indicating that oxidizable groups such as nearby amino acid residues may also be active in compound I reduction.[50, 75]

When a large excess of hydrogen peroxide is introduced, compound I is produced by the reaction of native enzyme with hydrogen peroxide. Compound I is then reduced to

compound II either by hydrogen peroxide or by a nearby amino acid as discussed above. Compound II is oxidized to compound III by hydrogen peroxide in a two-electron oxidation. The fate of compound III depends on the reaction conditions. Compound III can release superoxide or molecular oxygen to form native enzyme or ferrous enzyme, respectively. If ferrous enzyme is formed, it can undergo two-electron oxidation by hydrogen peroxide to form compound II.[75] There is also evidence that compound III undergoes slow irreversible inactivation by the loss of heme iron in the presence of large excess of hydrogen peroxide.[76]

Lactoperoxidase catalase activity can also occur in the presence of iodide via the reaction of hydrogen peroxide with hypoiodite to produce two water molecules and molecular oxygen. In the first step, hypoiodite is produced through the lactoperoxidase halogen cycle which also produces water, section 1.2.3. Hypoiodite then oxidizes H_2O_2 to produce molecular oxygen and water.[77]

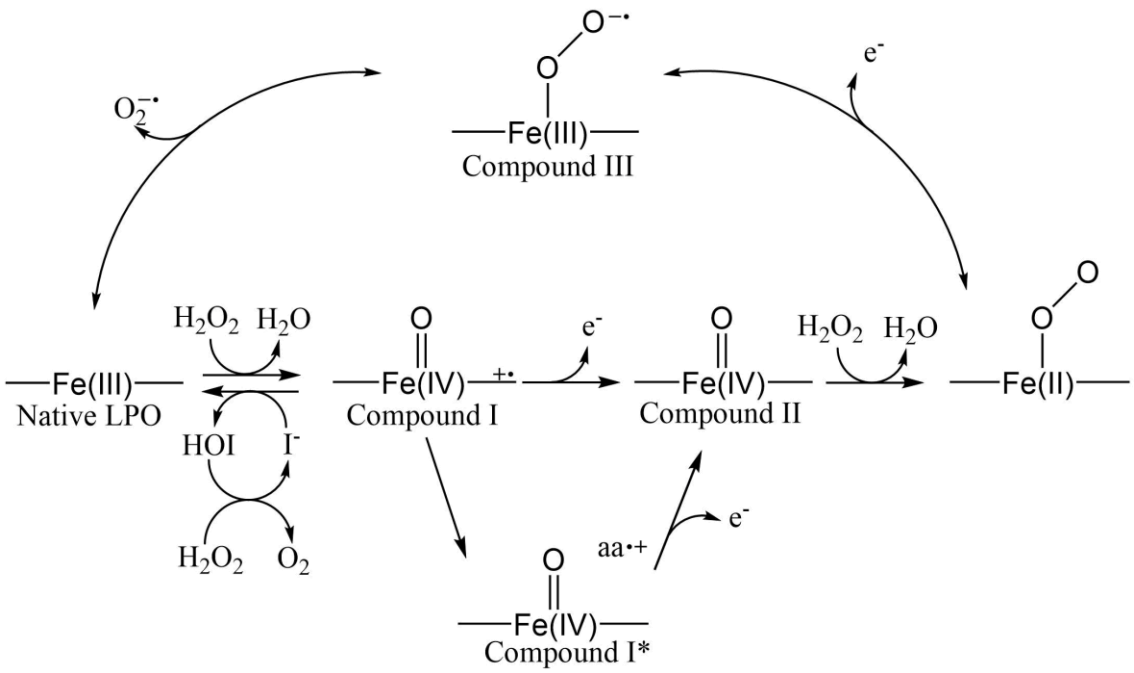

Figure 1.7 - Mechanism of pseudo-catalase action of lactoperoxidase.

1.2.5 Inhibition of Lactoperoxidase Activity

A variety of molecules have been studied as inhibitors of lactoperoxidase or its products. These methods of inhibition can be separated into two categories, which will be referred to here as enzyme inhibitors and product inhibitors. Enzyme inhibitors directly affect the ability of the enzyme to produce the desired product. Product inhibitors effect the ability of the product, usually hypothiocyanite, to act as desired.

One type of enzyme inhibitor which includes cyanide and fluoride react with the iron catalytic center. This blocks hydrogen peroxide from oxidizing the iron heme center preventing catalysis.[78-80] Hypothiocyanite is also known to indirectly cause enzyme inhibition by this mechanism through the production of cyanide and cyanate via the comproportionation of hypothiocyanite and thiocyanate at neutral pH.[81-82]

There are multiple methods by which lactoperoxidase can be irreversibly inactivated leading to enzyme inhibition. Hydrogen peroxide, which acts as the oxidizing

substrate for lactoperoxidase, can act as an enzyme inhibitor by diverting the enzyme to another catalytic cycle which does not produce HOX, see section 1.2.4, or inactivating the enzyme by overoxidation resulting in cleavage of the heme and release of iron.[74] Amitrole (3-amine-1,2,4-traizole) and 1-methylbenzymidazolidine-2-thione were also shown to cause suicide inhibition of lactoperoxidase by irreversible covalent binding of an intermediate to an important amino acid residue.[83-84]

There are also studies that indicate that some organic aromatic molecules can act as reversible enzyme inhibitors.[83-86] The mechanism of inhibition has not been thoroughly studied for all of the inhibitory molecules, but structural analysis of lactoperoxidase binding with organic aromatics which act as one-electron reducing substrates compared with organic aromatic molecules which act as inhibitors was reviewed by Sharma et al.[18] They noted that organic aromatic compounds which act as reducing substrates for lactoperoxidase bind to the binding pocket, but do not disturb the water molecule coordinated to the iron center which is displaced when hydrogen peroxide oxidizes the catalytic metal center discussed in section 1.1.2. However, the organic aromatic compounds which act as inhibitors displace the iron coordinated water and peroxide is unable to bind.[18]

Product inhibitors act by reacting with hypothiocyanite which inhibits its ability to interfere in microbial activity. There are few cases presented in the literature of product inhibition given the rapid rate of reaction of hypothiocyanous acid with bacterial thiols. Furthermore, kinetic experiments under conditions relevant to *in vivo* conditions are difficult to perform. However, cyanide, in addition to enzyme inhibition, may react competitively *in vivo* at neutral pH with hypothiocyanite leading to inhibition.[87]

Hypothiocyanite will also react rapidly with biological thiols such as reduced glutathione which may have an inhibitory effect on the antimicrobial action of hypothiocyanite.[88]

1.3 Hypothiocyanite

1.3.1 Biological Importance of Thiocyanate and Hypothiocyanite

Thiocyanate (SCN^-) is a pseudo-halide precursor compound for hypothiocyanite. Pseudo-halides are defined as polyatomic univalent anions which are chemically similar to halogens.[89] Thiocyanate was first found to be biologically active nearly a century before hypothiocyanite was proposed to be the possible product of the lactoperoxidase enzyme in milk and the source of the antibacterial properties of milk.[90] Common in physiological fluids, particularly in the secretory mucosae where lactoperoxidase is almost ubiquitously present, thiocyanate is supplemented into mammals by a plant based diet.[91-92] Thiocyanate is also produced as the product of the detoxification of cyanide.[93]

The function, properties, and reactions of hypothiocyanite were reviewed in 2012.[94] Hypothiocyanite/hypothiocyanous acid is a weak acid with a pKa of 5.3.[95] It has never been isolated, primarily as a consequence of its highly reactive nature, particularly near its pKa.[82] Hypothiocyanous acid is similar in structure and function to the hypohalous acids hypochlorous acid and hypobromous acid, the products of which are the mammalian heme peroxidases myeloperoxidase and eosinophil peroxidase, respectively. Like these hypohalous acids, hypothiocyanite displays potent antimicrobial, antifungal, and antiviral activity.[96-97]

Hypothiocyanite may be produced *in vivo* through two known methods. The method by which a majority of endogenous hypothiocyanite is produced is the lactoperoxidase-catalyzed oxidation of thiocyanate by hydrogen peroxide as discussed in

section 1.2.3. Hypothiocyanite may also be produced by the oxidation of thiocyanate by hypobromous acid and hypochlorous acid effectively neutralizing the more toxic hypohalous acids.[98]

The antimicrobial action of hypothiocyanite arises from the oxidation of bacterial sulfhydryls resulting in the production of sulfenyl thiocyanate and sulfenic acid derivatives. The oxidation causes bacterial crosslinking of sulfur residues inhibiting bacterial respiration.[99-100] Unlike hypochlorous acid and hypobromous acid, hypothiocyanite is unique in its ability to selectively oxidize bacterial sulfhydryls while leaving mammalian cells undamaged.[88, 101]

Hypothiocyanite also undergoes a decomposition at neutral pH via a cascade of comproportionation, disproportionation, and hydrolysis reactions which ultimately results in the decomposition products SO_3^{2-}, SO_4^{2-}, SCN^-, CN^-, and OCN^-, Equations 1.3.1-1.3.10.[82]

$$HOSCN \rightleftharpoons OSCN^- + H^+ \quad \text{Equation 1.3.1}$$

$$HOSCN + SCN^- \rightleftharpoons HO(SCN)_2^- \quad \text{Equation 1.3.2}$$

$$HO(SCN)_2^- \rightleftharpoons (SCN)_2 + OH^- \quad \text{Equation 1.3.3}$$

$$HO(SCN)_2^- + H^+ \rightleftharpoons (SCN)_2 + H_2O \quad \text{Equation 1.3.4}$$

$$(SCN)_2 + SCN^- \rightleftharpoons (SCN)_3^- \quad \text{Equation 1.3.5}$$

$$OSCN^- + (SCN)_2 \rightarrow NCS(=O)SCN + SCN^- \quad \text{Equation 1.3.6}$$

$$NCS(=O)SCN + H_2O \rightarrow O_2SCN^- + SCN^- + 2H^+ \quad \text{Equation 1.3.7}$$

$$O_2SCN^- + HOSCN \rightarrow O_3SCN^- + SCN^- + H^+ \quad \text{Equation 1.3.8}$$

$$O_3SCN^- + H_2O \rightarrow SO_4^{2-} + HCN + H^+ \quad \text{Equation 1.3.9}$$

$$O_3SCN^- + H_2O \rightarrow SO_3^{2-} + OCN^- + H^+ \quad \text{Equation 1.3.10}$$

1.4 Sulfur and Selenium

Sulfur and selenium belong to group 16 of the periodic table. They are, along with oxygen, tellurium, and polonium, members of the oxygen family also known as chalcogens. Sulfur and selenium are more similar in physical and chemical properties than any other two main-group elements. However, while they are both essential for life, only selenium is considered to be toxic.

This section discusses the similarities and differences between sulfur and selenium as well as the biological significance of selenium. This topic has been discussed thoroughly in *Biological Chemistry of Hydrogen Selenide*, a review article published in Antioxidants by myself and Dr. Michael T. Ashby.[102]

1.4.1 Physical and Chemical Properties of Sulfur and Selenium

Though sulfur is approximately 10,000 times more naturally abundant than selenium, and sulfur and selenium are more similar than any other main-group elements, selenium is an essential trace element selected for specific biological purposes. This must occur based on selenium's unique properties, the most significant being its high reactivity and low ionization energies as compared to sulfur, Table 3. The unique characteristics of selenium causes selenium congeners of sulfur molecules to react with faster rates[103] and maintain higher oxidation states than their sulfur counterparts.[104-105] These properties allow for the selection of selenium for specific biological purposes over the much more abundant sulfur discussed in section 1.4.2.

Table 3 - Chemical Properties of Sulfur and Selenium

Property		Sulfur	Selenium	Reference
Average atomic mass (amu)		32.06	78.96	–
Covalent radius (pm)		100	115	106
Bond Length		134 (S-H) 180 (S-C) 205 (S-S)	146 (Se-H) 196 (Se-C) 232 (Se-Se)	107
Bond Energy ($kJ•mol^{-1}$)	HX-H CH_3X-CH_3 CH_3X-XCH_3	381.6 (S-H) 307.9 (S-C) 273.6 (S-S)	334.9 (Se-H) 234 (Se-C) 197.6 (Se-Se)	108-111
Ionization Energies ($kJ•mol^{-1}$)	1^{st} 2^{nd} 3^{rd}	999.6 2251 3361	940.9 2045 2974	112
Electron affinity		200	195	113
Electronegativity		2.58	2.55	114
pK_{a1},(H_2X)		6.88	3.89	115-116
pK_{a2},(HX^-)		14.15	15.1	99,117

1.4.2 Physiological Significance of Selenium

The field of selenium chemistry began growing rapidly in 1957 when it was discovered to be a necessary trace element in mammalian physiology.[118] However, selenium is also a toxin, with a relatively narrow physiological concentration range earning it pseudonyms such as 'the essential poison' and 'the double edged sword.'[119-120] The physiological concentration of selenium in blood serum is normally between 70-150 ng/mL for humans over 1 year of age.[121] The U.S. Department of Health and Human Services sets a Recommended Daily Allowance of 55 ug/day and a Tolerable Upper Intake Level (UL) of 400 ug/day.[122-123] Exceeding the UL can lead to selenosis which can be acute or chronic and cause garlic odor of breath, vomiting, diarrhea, hair loss, brittleness of fingernails, and death.[124]

Selenium is considered a necessary trace element primarily due to its presence in the amino acid selenocysteine and is also presence in selenomethionine.[125-126] Selenocysteine is specifically selected for inclusion into the active sites of selenoproteins and selenomethionine is randomly incorporated into protein methionine sites.[127] As expected, given the status of selenium as a necessary trace element, a diet chronically lacking in selenium also leads to health issues. Selenium deficiency is associated with Kaschin-Beck Disease (Big Bone Disease)[128] and white muscle disease.[129]

Selenium is supplemented in mammals through diet in the form of the organic and inorganic selenium molecules: selenomethionine, selenocysteine, selenite, and selenate. Inorganic forms of selenium tend to be more toxic than organic forms although the reason is unknown.[130] However, increased toxicity of inorganic selenium species may be due to the interference of selenium compounds in sulfur redox equilibria.[131-132] Selenocyanate has also been discovered to be present in human fluids as a detoxification product of selenite[133] and has also been shown to concentrate in the secretory mucosae using the same transport mechanisms as thiocyanate.[134] The possible biological functions of selenocyanate, however, have not been studied until now.

1.5 Summary

Human peroxidases, by means of the formation of hypohalous acids, are extremely powerful in mammalian innate host defense. Hypothiocyanite is unique among the other hypohalous acid species in its ability to selectively inhibit bacteria without damaging host tissue.[88] The biological significance of hypothiocyanite in addition to the ease with which lactoperoxidase is isolated compared to myeloperoxidase and eosinophil peroxidase explains why it is one of the more well studied members of the peroxidase family.[11]

However, even given the similarities between sulfur and selenium, the role of selenocyanate in the lactoperoxidase system has not been studied. Furthermore, the selenium analog of hypothiocyanite, hyposelenocyanite, has never previously been observed.

The initial purpose of this research was to observe and characterize the novel species hyposelenocyanite by the study of its mechanisms of production using various synthetic methods and its stability as compared to analogous studies for the sulfur analog. The ability of lactoperoxidase to catalyze the oxidation of selenocyanate to produce hyposelenocyanite was of special interest as this would raise questions about the possible relevance of hyposelenocyanite *in vivo* or its possible therapeutic uses. However, our investigation of hyposelenocyanite as a substrate for lactoperoxidase resulted in data that challenged the literature mechanism for the lactoperoxidase halogen cycle. The research presented in this work compares hyposelenocyanite and its chemical properties to hypothiocyanite, but the main focus of this dissertation is our reexamination of the literature mechanism of the lactoperoxidase-catalyzed oxidation of halides and pseudo-halides.

Chapter 2 – PRODUCTION AND STUDY OF HYPOSELENOCYANITE

2.1 Introduction

The independent synthesis of the selenium derivative of hypothiocyanite ($OSCN^-$), hyposelenocyanite ($OSeCN^-$), using various synthetic methods, was used to determine if this molecule can be produced and to observe its physical and chemical properties. Chapter 2 will discuss the synthesis of $OSeCN^-$ using two methods: the oxidation of $SeCN^-$ by hypochlorous acid (HOCl) under alkaline conditions, and the LPO-catalyzed oxidation of $SeCN^-$ by H_2O_2. These synthesis methods were chosen due to their previous success being used to synthesize $OSCN^-$. Analysis of redox potentials was also performed to predict the ability of the methods to produce $OSeCN^-$. Using methods to synthesize $OSeCN^-$ by which $OSCN^-$ has been previously synthesized (and mechanisms and rate constants determined), allowed for the direct comparison of the production and decomposition rates of $OSeCN^-$ as compared to $OSCN^-$.

2.2 Production of Hyposelenocyanite by the Oxidation of Selenocyanate by Hypochlorous Acid Under Alkaline Conditions

$OSCN^-$ has been independently synthesized by the oxidation of SCN^- by hypohalous acids of higher oxidation potential at alkaline pH.[135-136] This independent synthesis has facilitated the study of $OSCN^-$ and its properties, reaction mechanisms and kinetics, and its likely action *in vivo* as discussed in section 1.3. Synthesis of $OSCN^-$ has also allowed for the independent characterization of hypothiocyanite via NMR,[137] UV-Vis,[137-138] and mass spectroscopy.[139]

The ability of SCN^- to be oxidized to $OSCN^-$ by a hypohalous acid or hydrogen peroxide is dependent upon the relative redox potentials of the species, Table 4. Hydrogen peroxide is known to oxidize SCN^- in an exceedingly slow pH-dependent reaction with a rate constant of $3.1(3)x10^{-2}$ $M^{-1}\cdot min^{-1}$ at pH 7 and $6.9x10^{-3}$ $M^{-1}\cdot min^{-1}$ at pH 13.[140] HOBr and HOCl oxidize SCN^- much faster with rate constants of $2.3x10^9$ $M^{-1}\cdot s^{-1}$ and $2.34(9)x10^7$ $M^{-1}\cdot s^{-1}$, respectively.[49, 98] The effective rate constants for the oxidation of SCN^- by HOBr and HOCl are pH dependent because the acids (HOX) have higher reactivities compared to the conjugate bases (OX^-) of the species.[49, 98]

The relative redox potentials of selenocyanate and hypochlorous acid indicate that the oxidation of $SeCN^-$ by HOI, HOBr, and HOCl should be possible, Table 4.[141] The oxidation of $SeCN^-$ by HOCl was observed via stopped-flow UV-Vis spectroscopic analysis to determine if $OSeCN^-$ is produced, the rate of its production and decomposition, and to observe its spectral features for characterization.

Table 4 – Standard two-electron oxidation potentials of halides, pseudohalides, and hydrogen peroxide.[94, 141]

Redox Couple	E° (V)
$2\ SeCN^- \rightarrow (SeCN)_2 + 2e^-$	-0.42
$2\ I^- \rightarrow I_2 + 2e^-$	-0.536
$2\ SCN^- \rightarrow (SCN)_2 + 2e^-$	-0.77
$2\ Br^- \rightarrow Br_2 + 2e^-$	-1.065
$2\ Cl^- \rightarrow Cl_2 + 2e^-$	-1.360

Redox Couple (pH 0)	E° (V)
$SeCN^- + H_2O \rightarrow HOSeCN + H^+ + 2e^-$	Unknown
$I^- + H_2O \rightarrow HOI + H^+ + 2e^-$	-0.987
$SCN^- + H_2O \rightarrow HOSCN + H^+ + 2e^-$	-0.82
$Br^- + H_2O \rightarrow HOBr + H^+ + 2e^-$	-1.331
$Cl^- + H_2O \rightarrow HOCl + H^+ + 2e^-$	-1.484
$2\ H_2O \rightarrow H_2O_2 + 2H^+ + 2e^-$	-1.77

Redox Couple (pH 14)	E° (V)
$SeCN^- + 2OH^- \rightarrow OSeCN^- + 2e^- + H_2O$	Unknown
$I^- + 2OH^- \rightarrow OI^- + 2e^- + H_2O$	-0.485
$SCN^- + 2OH^- \rightarrow OSCN^- + 2e^- + H_2O$	-0.44
$Br^- + 2OH^- \rightarrow OBr^- + 2e^- + H_2O$	-0.761
$Cl^- + 2OH^- \rightarrow OCl^- + 2e^- + H_2O$	-0.841
$3OH^- \rightarrow HO_2^- + H_2O + 2e^-$	-0.87

2.2.1 Kinetics of the Production of Hyposelenocyanite by the Oxidation of Selenocyanate by Hypochlorous Acid under Alkaline Conditions

$OSeCN^-$ was produced by the oxidation of $SeCN^-$ by HOCl at alkaline pH. $OSeCN^-$ was found to have a UV-Vis absorption peak with a λ_{max} at 378 nm, Figure 2.1. The λ_{max} observed for $OSeCN^-$ is only slightly shifted compared to the UV-Vis absorption peak for $OSCN^-$, λ_{max} = 376 nm.[94]

The reaction of HOCl with $SeCN^-$ at alkaline pH was observed spectrophotometrically at 292 nm to observe the change in absorbance of OCl^-, λ_{max} = 292 nm and ε_{292nm} = 350 $M^{-1}cm^{-1}$.[142] Pseudo-first-order concentration conditions with respect

to [$SeCN^-$] were used to observe the reaction of HOCl with $SeCN^-$. Pseudo-first-order conditions with respect to reductant were used to avoid overoxidation.[94] The traces collected for the change in [OCl^-] were fit to a first-order integrated rate equation to determine the effect of varying [$SeCN^-$] on the observed rate constants, Figure 2.2. The rate of the reaction of HOCl with $SeCN^-$ at pH 12.6 exhibited a pseudo-first-order dependency on [$SeCN^-$], Figure 2.3.

Since HOCl is the reactive species compared to the conjugate base OCl^-, varying the pH such that OCl^- becomes the dominant species in solution slows the reaction so that it can be observed more easily. The reaction of HOCl with SCN^- is dependent on the pH dependent equilibrium of HOCl and OCl^- according to equations 2.2.1 and 2.2.2. The steady-state approximation can be used to derive the rate law as shown by Ashby et al.[49] in equations 2.2.1-2.2.10:

$$OCl^- + H^+ \overleftrightarrow{k_1/k_{-1}} HOCl$$ Equation 2.2.1

$$HOCl + SCN^- \overrightarrow{k_2} Cl^- + OSCN^- + H^+$$ Equation 2.2.2

$$\frac{+d[HOCl]}{dt} = k_{-1}[H^+][OCl^-] - k_1[HOCl] - k_2[HOCl][SCN^-] = 0$$ Equation 2.2.3

$$\frac{+d[HOCl]}{dt} = k_{-1}[H^+][OCl^-] - (k_1 + k_2[SCN^-])[HOCl]$$ Equation 2.2.4

$$[HOCl]_{SS} = \frac{k_{-1}[H^+][OCl^-]}{k_1 + k_2[SCN^-]}$$ Equation 2.2.5

$$\frac{+d[OSCN^-]}{dt} = k_2[HOCl][SCN^-] = \frac{k_{-1}k_2[H^+][OCl^-][SCN^-]}{k_1 + k_2[SCN^-]}$$ Equation 2.2.6

When the reaction is under pseudo-first-order conditions ($k_1 >> k_2[SCN]$):

$$\frac{+d[OCl^-]}{dt} = k_{obs}[OCl^-] = \frac{k_{-1}k_2}{k_1}[H^+][OCl^-][SCN^-]$$ Equation 2.2.7

$$\frac{k_{-1}}{k_1} = \frac{1}{K_1} = 2.51 * 10^7 M^{-1}$$ Equation 2.2.8

$$k_{obs} = \frac{k_2[H^+][SCN^-]}{K_1}$$ Equation 2.2.9

$$k_2 = \frac{K_1 k_{obs}}{[H^+][SCN^-]}$$ Equation 2.2.10

The rate constant of the reaction of HOCl with SCN^- is reported to be $2.34(9)x10^7$ $M^{-1}s^{-1}$.[49] The observed second-order rate constant uncorrected for pH can be determined using equation 2.2.9 for the reaction of HOCl with SCN^- at pH 12.6 and was calculated to be $2.8(1)x10^2$ $M^{-1}s^{-1}$.[49] The observed rate constant of the reaction of HOCl with $SeCN^-$ at pH 12.6, $7.0(1)x10^3$ $M^{-1}s^{-1}$, is one order of magnitude higher than that of HOCl with SCN^- at pH 12.6, Figure 2.3. The rate constant k_2 for the reaction of HOCl with $SeCN^-$ can be calculated using equation 2.2.10 to be $1.2(2)x10^9$ $M^{-1}s^{-1}$, which is two orders of magnitude higher than that reported for the reaction of HOCl with SCN^-.

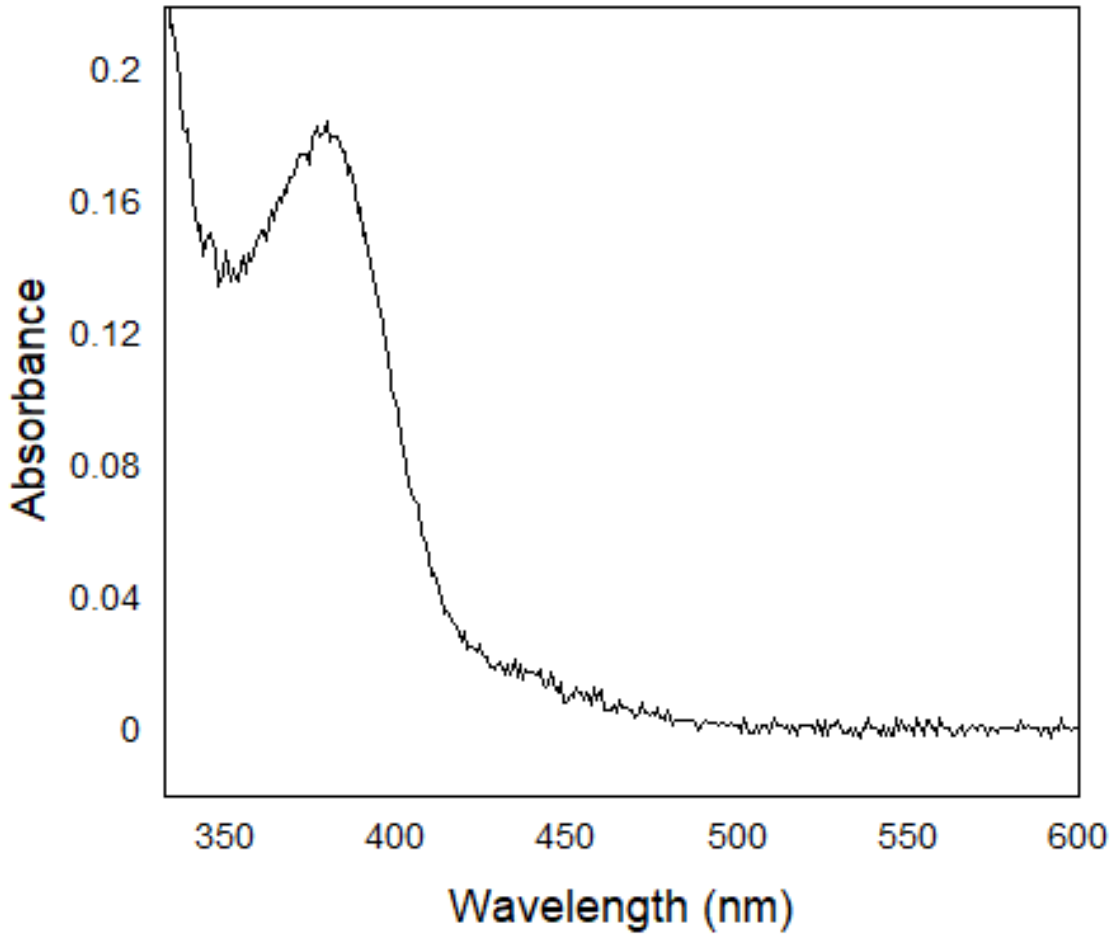

Figure 2.1 - Spectra of Hyposelenocyanite at pH 13 as produced by the oxidation of $SeCN^-$ by HOCl at pH 13. The post-mixing reactant concentrations were [HOCl] = 5 mM and [$SeCN^-$] = 5 mM in 0.1 M NaOH.

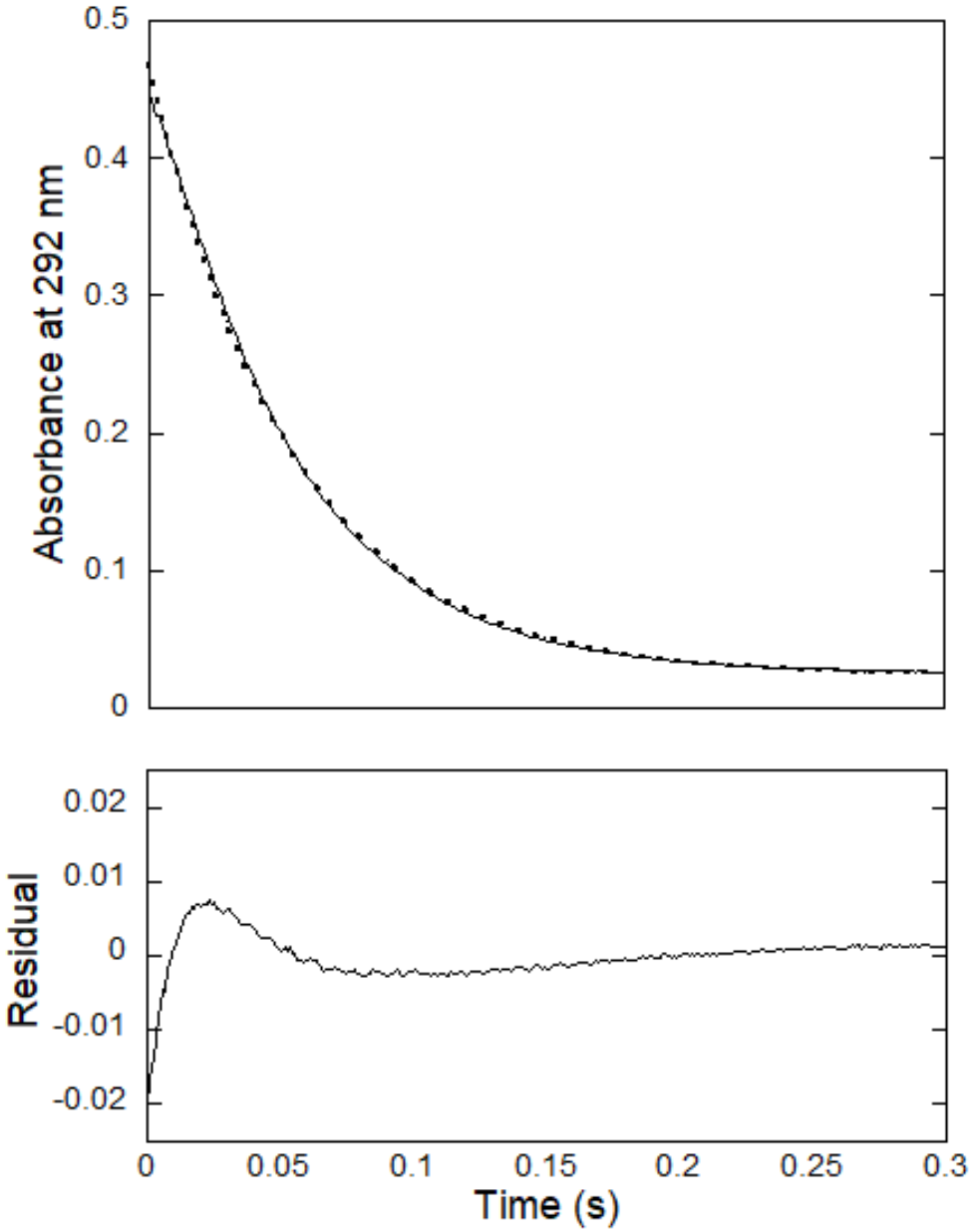

Figure 2.2 – Fitted trace of OCl^- at 292 nm upon mixing of [$SeCN^-$] = 5 mM with [OCl^-] = 5 mM at pH 13 in 0.1 M NaOH (after mixing concentrations). Traces from eight mixing cycles were averaged to obtain the final trace (solid line) and fit to the first-order integrated rate equation (dotted line).

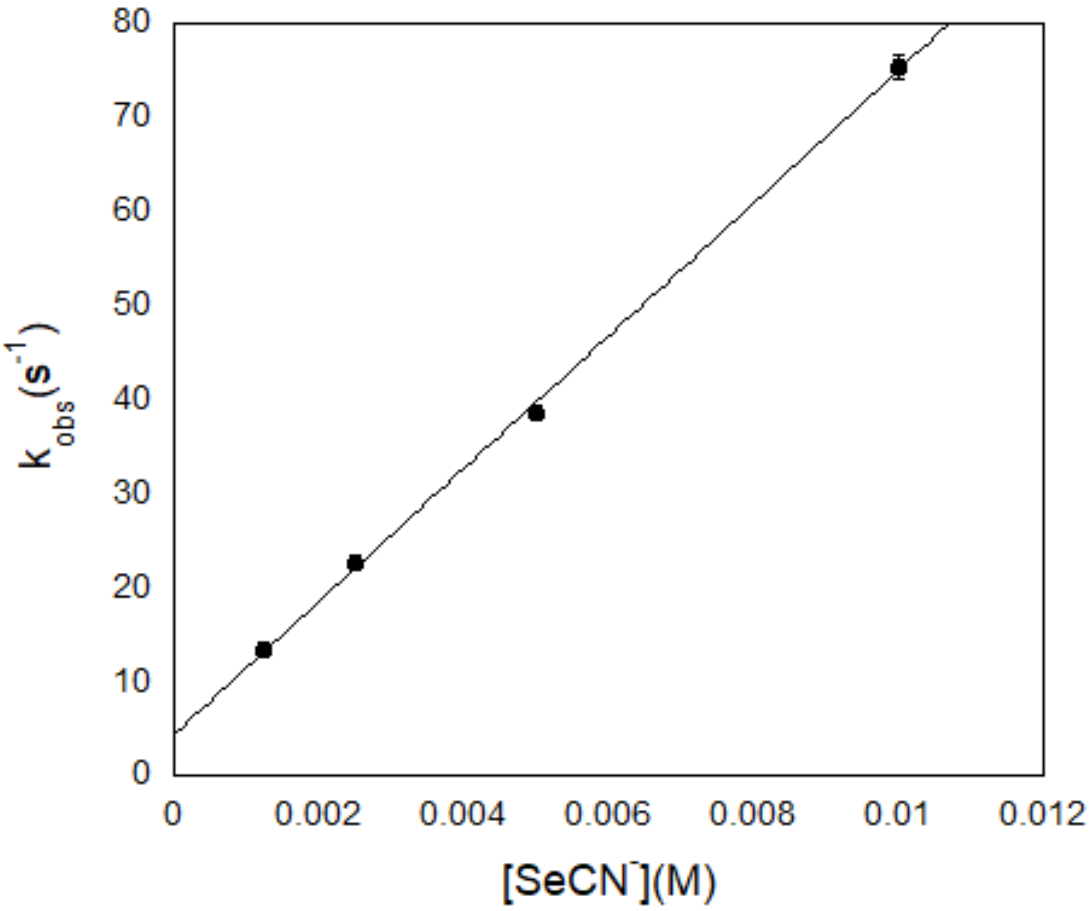

Figure 2.3 – [$SeCN^-$] dependency on the observed rate constant for the oxidation of $SeCN^-$ by HOCl at pH 12.6 in NaOH under pseudo-first-order conditions with respect to $SeCN^-$. Post-mixing concentration of [OCl^-] was held constant at 100 uM. The reaction was monitored at 292 nm to observe the decrease in [OCl^-]. The estimated error shown by the error bars for the individual rate constants is for a least-squares fit of an average of five kinetic traces. The slope of the line gives the second-order rate constant $7.0(1)x10^3$ $M^{-1}\cdot s^{-1}$ at pH 12.6.

2.2.2 Kinetics of the Decomposition of Hyposelenocyanite under Alkaline Conditions

Decomposition of $OSCN^-$ at alkaline pH occurs through the hydrolysis of $OSCN^-$ by OH^- to produce a thiocarbamate-S-oxide intermediate and finally NH_4^+, HCO_3^-, and elemental sulfur.[143] $OSCN^-$ hydrolysis at alkaline pH is a second-order reaction, first-order in both [OH^-] and [$OSCN^-$] and independent of [SCN^-] with a second-order rate constant of $4.24(5)x10^{-3}$ $M^{-1}s^{-1}$.[143]

The rate of decomposition of $OSeCN^-$ at alkaline pH was established to determine its lifetime and assess the type of analysis which can be done to characterize and test the properties of $OSeCN^-$. The decomposition rate of $OSeCN^-$ was measured at 378 nm to directly observe the decomposition of $OSeCN^-$ which has a λ_{max} at 378 nm and a molar absorption coefficient of approximately 28.5 $M^{-1}cm^{-1}$, Figure 2.4.

$OSeCN^-$ was synthesized by the oxidation of $SeCN^-$ by HOCl at pH 12.68 and the decomposition of $OSeCN^-$ was observed as a function of [OCl^-] and [$SeCN^-$] under pseudo-first-order conditions with respect to [$SeCN^-$]. The observed rate constant of decomposition of $OSeCN^-$ at pH 12.68 is 91.5(8) s^{-1} and is independent [$SeCN^-$] and [OCl^-] indicating the reaction is first-order in $OSeCN^-$ and independent of [$SeCN^-$], Tables 5 and 6. The observed rate constant of hydrolysis of $OSCN^-$ at pH 12.68 is $2.03(5)x10^{-4}$ s^{-1}, five orders of magnitude slower than $OSeCN^-$ decomposition at the same pH.[143] The independence of the rate of decomposition of $OSeCN^-$ on [$SeCN^-$] and first-order dependence on [OCl^-], are consistent with what is observed for the hydrolysis of $OSCN^-$ by [OH^-] at alkaline pH.[143] However, pH dependent studies as well as characterization of the products of the decomposition

should be done in the future to determine if the mechanism of decomposition is the same for $OSCN^-$ and $OSeCN^-$.

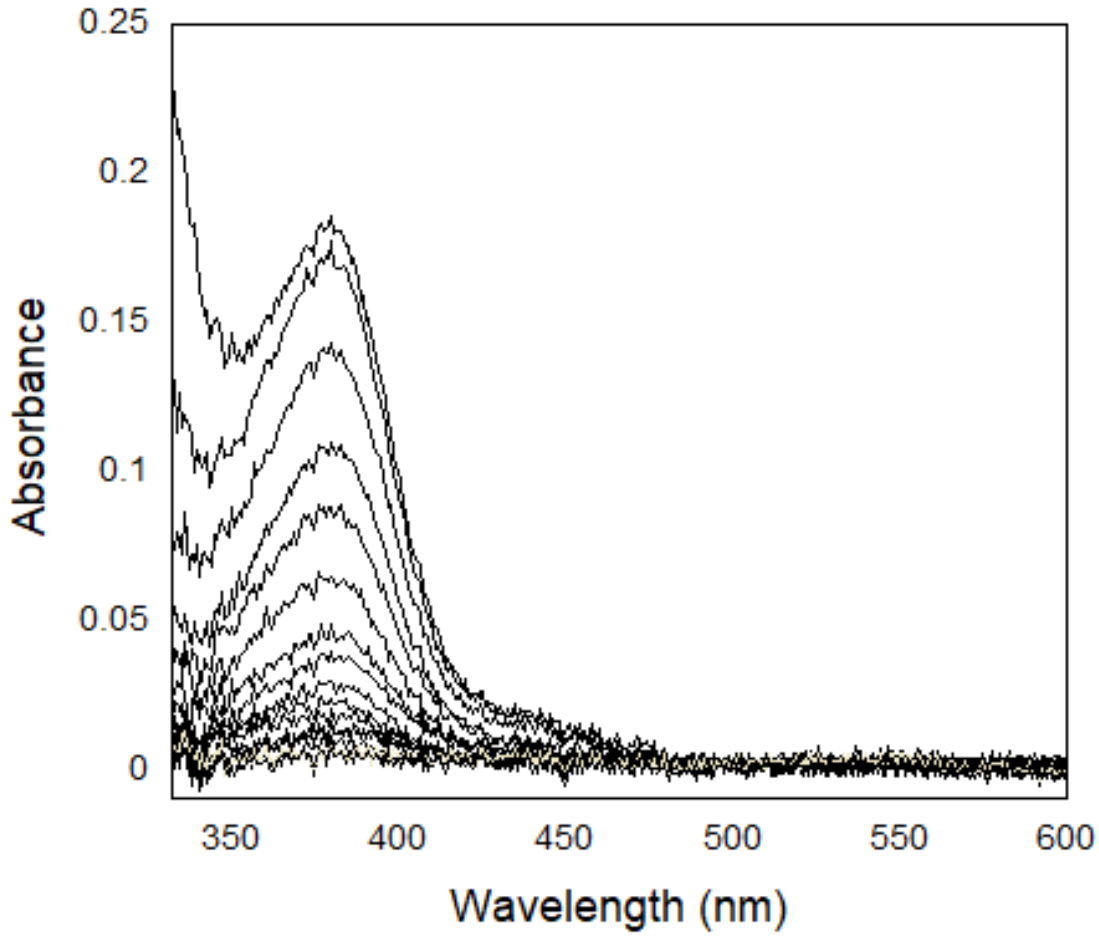

Figure 2.4 - Decomposition of $OSeCN^-$ produced by the oxidation of $SeCN^-$ by HOCl at alkaline pH.

Table 5 - Rate of decomposition of $OSeCN^-$ at pH 12.68 as $[OCl^-]$ is varied.

$[OCl^-]$(mM)	k (s^{-1})
3.4	93.9(2)
6.8	92.22(9)
13.6	90.07(9)
Average	92(2)

[σ]The post-mixing concentration of $[SeCN^-]$ was 200 mM (constant) and $[OCl^-]$ was varied from 3.4-13.6 mM in NaOH.

Table 6 - Rate of decomposition of $OSeCN^-$ at pH 12.68 as $[SeCN^-]$ is varied.

$[SeCN^-]$(mM)	k (s^{-1})
50	88.4(2)
100	90.6(1)
200	93.9(2)
Average	91(3)

[σ]The post- mixing concentration of $[OCl^-]$ was 3.4 mM (constant) and $[SeCN^-]$ was varied from 50-200 mM in NaOH.

2.3 Synthesis of Hyposelenocyanite by the Lactoperoxidase-Catalyzed Oxidation of Selenocyanate by Hydrogen Peroxide at Neutral pH

The lactoperoxidase-catalyzed oxidation of thiocyanate by hydrogen peroxide is a commonly used method to produce and study hypothiocyanite in a laboratory setting. The currently accepted mechanism of lactoperoxidase catalysis for thiocyanate oxidation is called the halogen cycle and is reviewed in section 1.2.3. However, the ability of lactoperoxidase to facilitate the oxidation of selenocyanate to produce hyposelenocyanite has never been determined. Time-resolved stopped-flow UV-Vis studies were conducted to determine the ability of lactoperoxidase to use selenocyanate as a reducing substrate to reduce hydrogen peroxide as well as to characterize the product of the reaction.

2.3.1 Characterization of Hyposelenocyanite Produced by the Lactoperoxidase-Catalyzed Oxidation of Selenocyanate by Hydrogen Peroxide at Neutral pH

LPO primarily catalyzes the oxidation of SCN^- by H_2O_2 via the halogen cycle using a two-electron redox reaction to produce $OSCN^-$ *in vivo*, section 1.2.3. However, LPO is also capable of utilizing halides such as I^- and Br^- as reducing substrates for the same two-electron oxidation. Here we explore the ability of LPO to utilize selenocyanate as a reducing substrate for the lactoperoxidase halogen cycle. As a dual functioning technique, a TNB (5-thio-2-nitrobenzoic acid) assay (which has been previously used to observe the kinetics of $OSCN^-$) has been used to simultaneously characterize $OSeCN^-$ and observe the kinetics of its production spectrophotometrically by the LPO system at neutral pH.[88, 144-145] Figure 2.5 shows the typical spectral change of the TNB spectra as the production of HOX is monitored by TNB assay.

TNB reacts rapidly with 2:1 stoichiometry with HOX to produce 5,5'-dithiobis-(2-nitrobenzoic acid), DTNB and X^-.[88] The reaction of $OSCN^-$ with TNB is very fast with an effective second-order rate constant of $4.37(3)x10^5\ M^{-1}s^{-1}$ at pH 7.4.[88] TNB and DTNB have strong visible absorption peaks at 412 nm and 324 nm, respectively. TNB has a large molar extinction coefficient of λ_{max} = 14,150 $M^{-1}cm^{-1}$.[146] As such, the HOX reaction kinetics are typically monitored at 412 nm to observe the decrease in [TNB] when the TNB assay is used, but may also be monitored at 324 nm to observe the production of DTNB.

The ability of TNB to react with the product of the LPO-catalyzed oxidation of $SeCN^-$ by H_2O_2 as well as the 2:1 stoichiometry of said reaction can be used to confirm that $OSeCN^-$ is the likely product of this reaction, Table 7. Furthermore, the first-order dependence of the observed rate constant of the LPO-catalyzed oxidation of $SeCN^-$ by H_2O_2 on [LPO] is a good indicator that the production of $OSeCN^-$ is observed by the TNB assay, Figure 2.6. The reaction of TNB with $OSeCN^-$ is not catalyzed by LPO so the reaction observed by the TNB assay must be the LPO-catalyzed oxidation of $SeCN^-$.

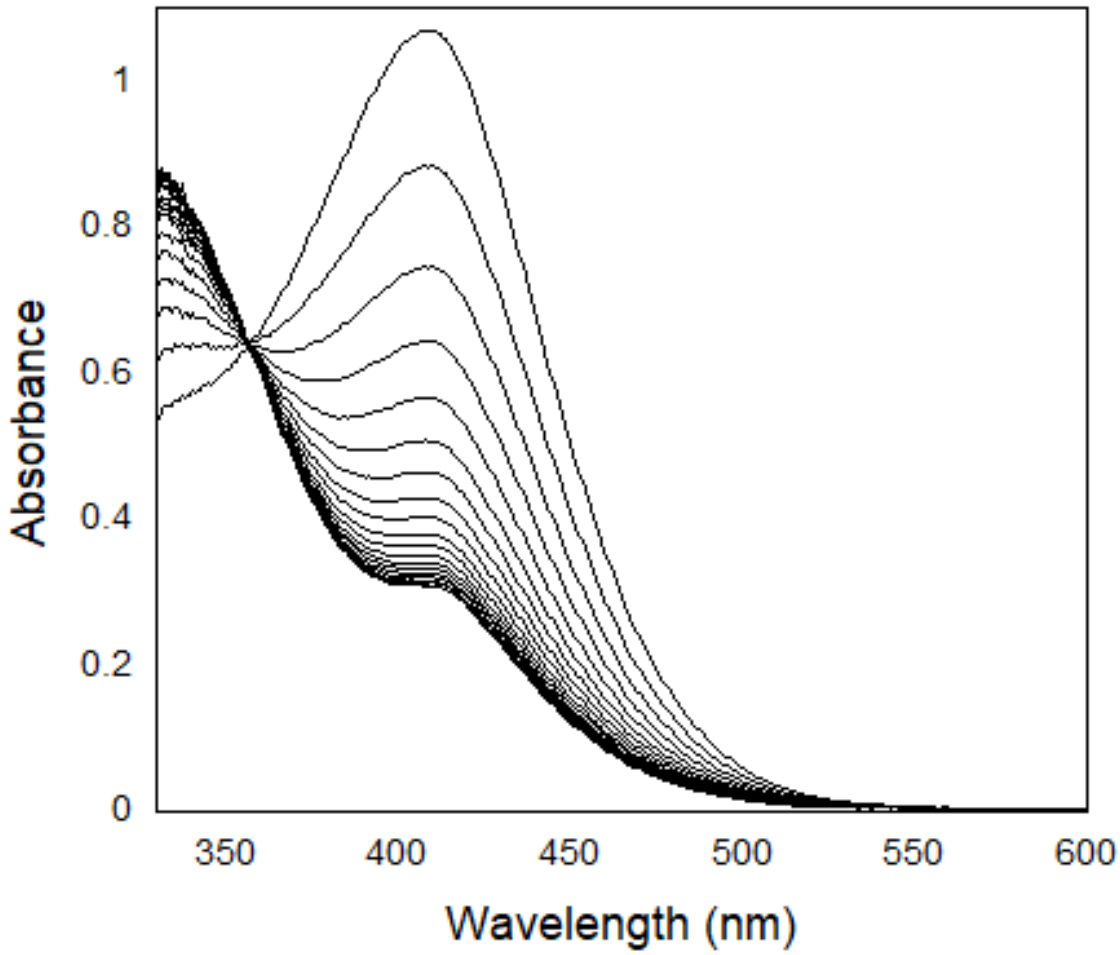

Figure 2.5 - Spectral change of TNB assay during the LPO-catalyzed oxidation of $SeCN^-$ by H_2O_2. The peak at 412 nm represents the decrease in [TNB] and the increase at 324 nm represents the increase in [DTNB].

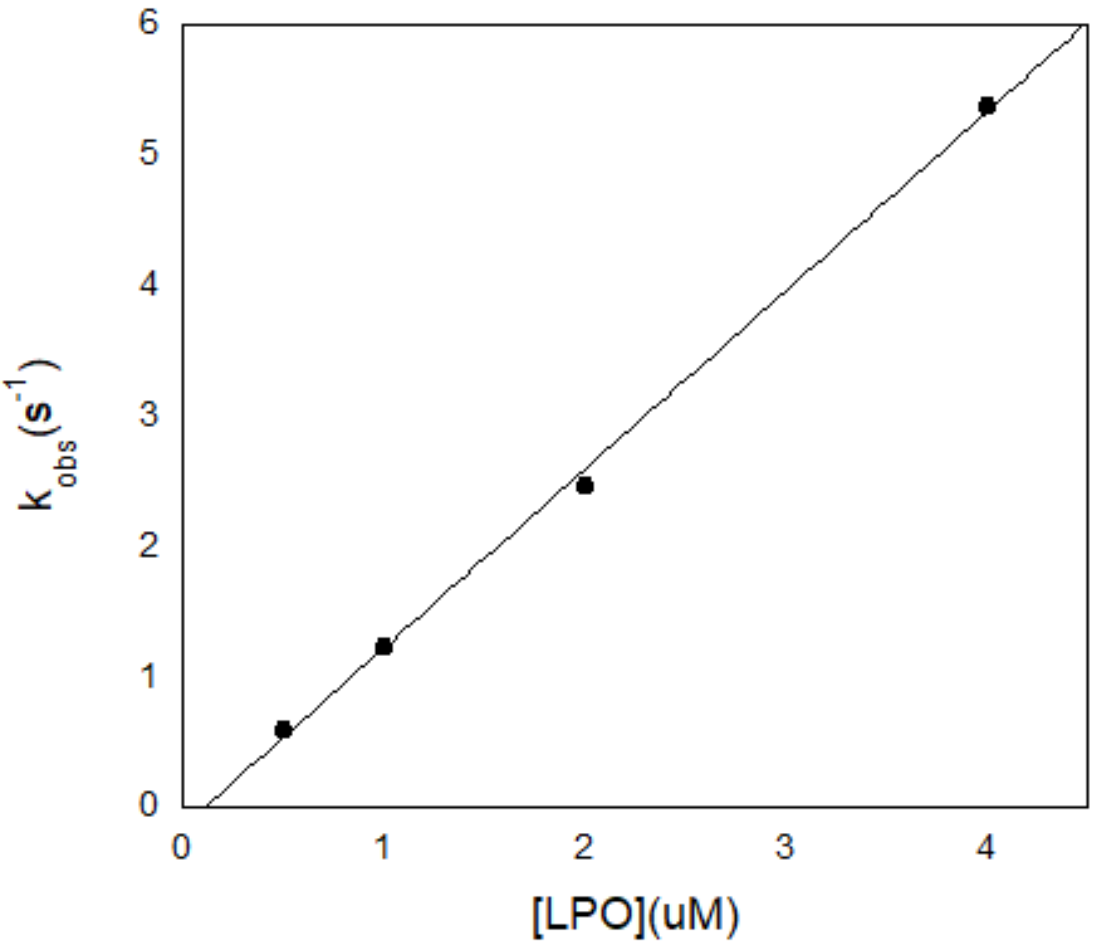

Figure 2.6 – Rate of the LPO-catalyzed oxidation of $SeCN^-$ by H_2O_2 as a function of [LPO]. Post-mixing concentrations were [$SeCN^-$] = 50 mM, [H_2O_2] = 40 uM, [TNB] = 274 uM, and [LPO] = 0.5-4 uM. The reaction was monitored at 324 nm to observe the rate of production of DTNB. The estimated error shown by the error bars for the individual rate constants is for a least-squares fit of an average of five kinetic traces and has been multiplied by a factor of 10 so that the error bars would be visible on the plot.

Table 7 - Ratio of $[H_2O_2]$ to change in [TNB] during the LPO-catalyzed oxidation of $SeCN^-$ by H_2O_2 as a function of $[H_2O_2]$

$[H_2O_2]$ (uM)	**Change Absorbance at 412 nm**	**Change in [TNB] (uM)**	**$[TNB]/[H_2O_2]$**
7.5	0.21	14.8	2.0
15	0.41	29	1.9
30	0.76	54	1.8

[a]The post-mixing concentrations were [LPO] = 1 uM, $[SeCN^-]$ = 1 mM, [TNB] = 70 uM, and $[H_2O_2]$ = 7.5-30 uM.

2.3.2 Stability of Hyposelenocyanite Near Neutral pH

Determination of the stability of hyposelenocyanite was necessary to assess what types of analysis could be performed to characterize the compound. Stopped-flow UV-Vis analysis and the TNB assay was used to determine the rate of decomposition of $OSeCN^-$ produced by the LPO-catalyzed oxidation of $SeCN^-$. A double-mixing experiment was used to react LPO, $SeCN^-$, and H_2O_2 to produce $OSeCN^-$ in the first mixing cycle. The age time following the first mixing cycle, τ, was varied to allow decomposition of $OSeCN^-$ before TNB was introduced in the second mixing cycle. The change in [TNB] was used to determine how much $OSeCN^-$ was present after each age time assuming that the biproducts would not react with TNB, though this may not be the case. Because the LPO system was used to produce $OSeCN^-$, the decomposition could not be measured until the production of $OSeCN^-$ was complete. Under the conditions used for these experiments, $[SeCN^-]$ = 1.3 mM, $[H_2O_2]$ = 40 uM, and [LPO] = 1 uM, the half-life of $OSeCN^-$ production was 57.98(2) ms. The minimum initial age time that could practically be used to determine

decomposition rate was approximately four times the half-life, 4 x $t_{1/2}$ = 0.23 s. At an age time of 0.2 seconds, it appears 24 uM of $OSeCN^-$ remains of what should be an initial 40 uM. However, as the age time is varied the rate of further decomposition is slower than expected given the initial concentration change, Figure 2.6. The large initial decomposition, at $\tau = 0.2$ seconds, and the slow decomposition that follows indicates that $OSeCN^-$ decomposes rapidly to a more stable decomposition product which also reacts quickly with TNB. The initial ratio of this decomposition product is approximately 1:2 with H_2O_2 indicating that the decomposition product might be the overoxidation product O_2SeCN^- which may also react with two equivalents of TNB to produce DTNB. $OSeCN^-$ can be determined to undergo rapid decomposition at pH 7, but the actual rate of decomposition cannot be determined due to the relatively slow method of production.

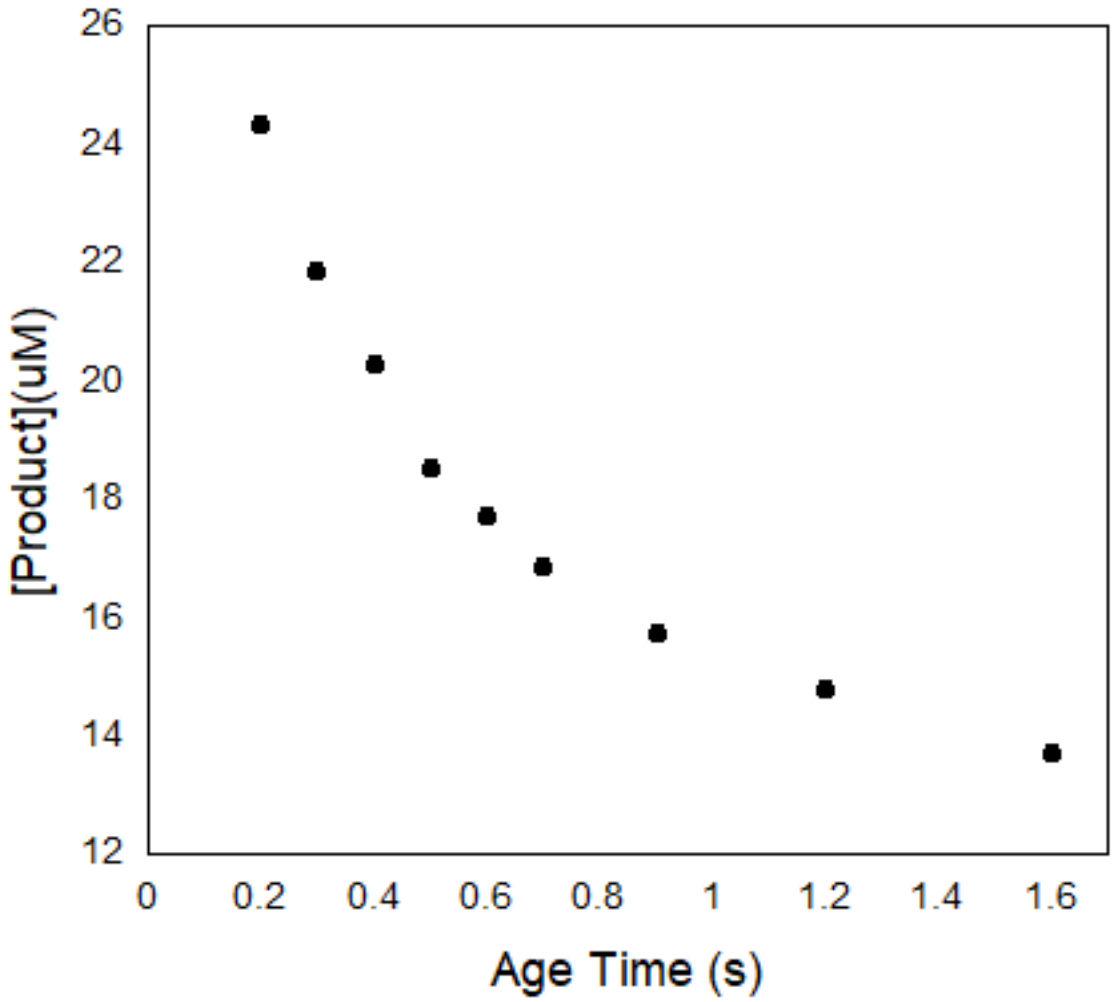

Figure 2.7 - Rate of decomposition of the hyposelenocyanite decomposition product at pH 7.4. Post-mixing concentration conditions of [$SeCN^-$] = 1.3 mM, [LPO] = 1 uM, [H_2O_2] = 40 uM, and [TNB] = 100 uM. A double mixing experiment was used where $OSeCN^-$ was produced in the first mixing cycle by the reaction of a mixture of $SeCN^-$ and LPO with H_2O_2. The product was then reacted with TNB in the second mixing cycle after varying age times and the absorbance at 412 nm was converted to product concentration using $\varepsilon_{TNB(412nm)}$ = 14,150 $M^{-1}cm^{-1}$ at a 2:1 stoichiometric ratio of TNB to product.

2.4 Conclusion

We have successfully synthesized $OSeCN^-$ using two different methods which have previously been used to produce $OSCN^-$. The oxidation of $SeCN^-$ by HOCl at alkaline pH produced $OSeCN^-$ at a significantly faster rate than $OSCN^-$ is produced using the analogous method. The rate of decomposition of $OSeCN^-$ at alkaline pH is also much faster than the hydrolysis of $OSCN^-$ under analogous pH conditions. The rapid decomposition of $OSeCN^-$ at alkaline pH, with a half-life of approximately 8 ms near pH 13, limits the types of characterization analysis which can be performed. The increased rate of production and decomposition of $OSeCN^-$ was not unexpected due to the reactive nature of selenium derivatives as compared to their sulfur analogs;[147-149] however, it is unfortunate because there are many characterization techniques which cannot be utilized for a species as short-lived as $OSeCN^-$ such as gas chromatography, mass spectrometry, ion chromatography, and NMR. However, the rapid decomposition of $OSeCN^-$ makes stopped-flow UV-Vis an ideal technique for analysis due to its ability to detect extremely short-lived species. This is especially true, given that not only is $OSeCN^-$ active in the UV-Vis range, but can also be analyzed via TNB assay.

2.5 Future Work

Since $OSeCN^-$ is a short-lived molecule the future studies which may be undertaken for its study are somewhat limited. However, a pH dependent stopped-flow study of the decomposition of $OSeCN^-$ can be used to determine the pH corrected rate constant of decomposition. Also, a double-mixing pH jump study which produces $OSeCN^-$ by the oxidation of $SeCN^-$ by HOCl at alkaline pH in the first mixing cycle and then decreases the pH in the second mixing cycle should be done to determine the rate of decomposition near

neutral pH. The rate of decomposition of $OSeCN^-$ at neutral pH should be determined to assess the likelihood of $OSeCN^-$ to have therapeutic significance. Determination of the final decomposition products of $OSeCN^-$ at alkaline and neutral pH may also shed light on its mechanism of decomposition, particularly at alkaline pH to determine if the selenium species analogous to thiocarbamate-S-oxide exists.[143] Studies at acidic pH would prove difficult due to the tendency of $SeCN^-$ to rapidly decompose into elemental selenium and hydrogen cyanide at low pH.[150]

Chapter 3 – LACTOPEROXIDASE MECHANISTIC STUDIES

3.1 Introduction

The rates of lactoperoxidase-catalyzed oxidation of various anionic reducing substrates by hydrogen peroxide have been studied alongside the other members of the oxidoreductase family of enzymes. This literature is reviewed in section 1.2. The biological reactions of the primary product of the lactoperoxidase system, hypothiocyanite, is reviewed in section 1.3.1. However, results reported here are inconsistent with mechanisms that have been reported in the literature, particularly under conditions of low concentration of reducing substrate where our results show the reaction becomes biphasic. These low concentration conditions may be physiologically relevant considering the concentration of thiocyanate in physiological fluids where lactoperoxidase is present can be as low as 0.1 uM.[46] The reason biphasic kinetics may not have been observed in previous studies of lactoperoxidase may be the consequence of the experimental methods employed. Enzyme kinetics are generally observed and analyzed differently than non-enzymic reaction kinetics. For instance, in many cases initial rates and Michaelis-Menten kinetics are used for analysis of enzymes. While these techniques offer valuable information about the maximum velocity of the catalysis, turnover numbers, and the concentration of substrate at which the enzyme becomes saturated under steady-state conditions, it is unsurprising that biphasic pre-steady-state kinetics may have gone unobserved in the majority of lactoperoxidase mechanistic studies. This is not to say that similar biphasic kinetics have not been observed previously in the literature, but they have not been fully explored or explained.[144] Biphasic kinetics are more often observed in myeloperoxidase research, but it is clear that the results discussed in this chapter are not analogous to the observations in

the myeloperoxidase studies which are often attributed to a change in the primary catalytic mechanism.[69, 145, 151]

In this chapter we will describe and mathematically model the expected kinetics of the accepted method for the lactoperoxidase-catalyzed halogen cycle, which describes the oxidation of halide and pseudohalide reducing substrates, X^-, by hydrogen peroxide, section 1.2.3. These models will be compared to experimental data under pseudo-first-order concentrations of X^- with respect to H_2O_2 as well as stoichiometric concentrations of H_2O_2 and X^-. The limitations of the accepted mechanism will be discussed and a new mechanism, which uses an ordered sequential mechanism where hydrogen peroxide acts as a tight binding inhibitor, will be proposed for the LPO-catalyzed oxidation of X^- by H_2O_2.

3.1.1 Literature Mechanism of Lactoperoxidase Halogen Cycle Catalysis – Ordered Sequential Mechanism

The accepted mechanism for the halogen cycle of lactoperoxidase catalysis, discussed in section 1.2.3, reflects a variation of an Ordered Sequential Mechanism, which is defined by the sequential binding of multiple enzyme substrates and has the general form shown in Equations 3.2.1-3.2.4.[152] Generally, in enzyme catalysis the rate- or turnover-limiting step is represented by equation 3.2.3 or 3.2.4. Sometimes these two steps are written as a single irreversible step representing the release of the final product.

$$E + A \rightleftharpoons EA \qquad \text{Equation 3.2.1}$$

$$EA + B \rightleftharpoons EAB \qquad \text{Equation 3.2.2}$$

$$EAB \rightleftharpoons EP \qquad \text{Equation 3.2.3}$$

$$EP \rightleftharpoons E + P \qquad \text{Equation 3.2.4}$$

In the accepted halogen cycle mechanism of lactoperoxidase, H_2O_2 oxidizes the iron(III) of the native LPO, which is the resting state of the enzyme, to iron(IV), Equation 3.2.5. This is a two-electron oxidation with the metal center and porphyrin ring both oxidized by a single electron so the oxidized form of the enzyme, compound I, carries two oxidizing equivalents. Compound I is easily observed spectrophotometrically and has unique spectral features, with the Soret band shifted to a λ_{max} at 431 nm as compared to native lactoperoxidase which has a λ_{max} at 412 nm.[41] Compound I is then reduced by a halide or pseudohalide of sufficient reduction potential, in a two-electron reduction, to produce LPO, Equation 3.2.6.

$$LPO + H_2O_2 \xrightarrow{k_1} Cpd\ I \qquad \text{Equation 3.2.5}$$

$$Cpd\ I + X^- \xrightarrow{k_2} LPO + OX^- \qquad \text{Equation 3.2.6}$$

The reaction is written as two consecutive irreversible reactions. The first reaction is generally considered to be irreversible due to inadequate redox potentials for compound I to oxidize water to hydrogen peroxide, Table 1. However, the production of compound I

can also be written as irreversible when it is rate-limiting so even if it were an equilibrium reaction, an equilibrium would not be relevant as compound I reacts as quickly as it is produced and a significant steady-state concentration of compound I cannot be reached. Reaction 3.2.5, the release of product, is often considered an irreversible step in enzyme mechanisms and is considered irreversible in this case.

Rate constants k_1 and k_2 in Equations 3.3.5 and 3.3.6 have been determined independently by Furtmüller et al. The rate constant for the production of compound I, k_1, is $1.1(1)x10^7$ $M^{-1}s^{-1}$. The rate constant for the reaction of X^- with compound I, k_2 in Equation 3.2.6, was determined for bromide, iodide, and thiocyanate to be $4.1(1)x10^4$, $1.20(4)x10^8$, and $2.0x10^8$ $M^{-1}s^{-1}$, respectively.[41] We have modeled these reactions for thiocyanate and bromide using Mathematica to see the expected behavior when Equations 3.2.5 and 3.2.6 were rate-limiting.

It is important to note that all models presented here consider $[X^-]$ to be constant, to reflect experimental pseudo-first-order reaction conditions. Experimentally, a TNB assay, as discussed in section 2.3.1, was used to observe the production of $OSeCN^-$ by the LPO-catalyzed oxidation of $SeCN^-$. The TNB assay produces X^- keeping the $[X^-]$ approximately constant during the LPO catalysis reaction, so the models were built to reflect the constant $[X^-]$ experimental conditions.

3.2 Literature Model of the Lactoperoxidase Halogen Cycle – Thiocyanate Reducing Substrate

The lactoperoxidase halogen cycle, shown in Equations 3.2.5 and 3.2.6, was modeled with the SCN^- k_2 rate constant using Mathematica. The active form of the enzyme

and the concentration dependencies of the reaction rates on LPO, H_2O_2, and SCN^- were modeled to predict the behavior which should be expected in laboratory experiments.

The rate constants used in the model, $k_1 = 1.1(1)x10^7\ M^{-1}s^{-1}$ and $k_2 = 2.0x10^8\ M^{-1}s^{-1}$, were calculated independently by Furtmüller et al.[41] As $k_2>k_1$, Equation 3.2.5, the production of compound I, is rate-limiting in this model. Under these conditions, the model presented in this section predicts a reaction with first-order kinetics overall and an observed rate constant with first-order dependence on [LPO]. The rate of the reaction observed was independent of X^- concentration and first-order with respect to H_2O_2. This model also predicts that the reaction should be independent of the second rate constant, k_2, as long as $k_2>k_1$. The effects of the second reaction, Equation 3.2.6, becoming rate-limiting, $k_1>k_2$, will be discussed in section 3.3.

3.2.1 Literature Model of the Lactoperoxidase Halogen Cycle– Thiocyanate Reducing Substrate – Enzyme Species

It is beneficial in catalytic mechanisms to observe the behavior of the enzyme during the reaction, particularly as equilibrium is reached and steady-state enzyme concentrations become relevant to the mechanism, to understand why the model reacts in any given way to varying reactant concentrations. In the case of thiocyanate as a reducing substrate for the lactoperoxidase system, the first reaction, Equation 3.2.5, is rate-limiting, so native LPO is the resting state of the enzyme during steady-state kinetics. A low steady-state concentration of compound I, is achieved quickly indicating that it is reacting almost as quickly as it is produced. Figure 3.1 shows the approach to equilibrium and the steady-state concentrations under the given conditions which were chosen to reflect conditions used in laboratory experiments.

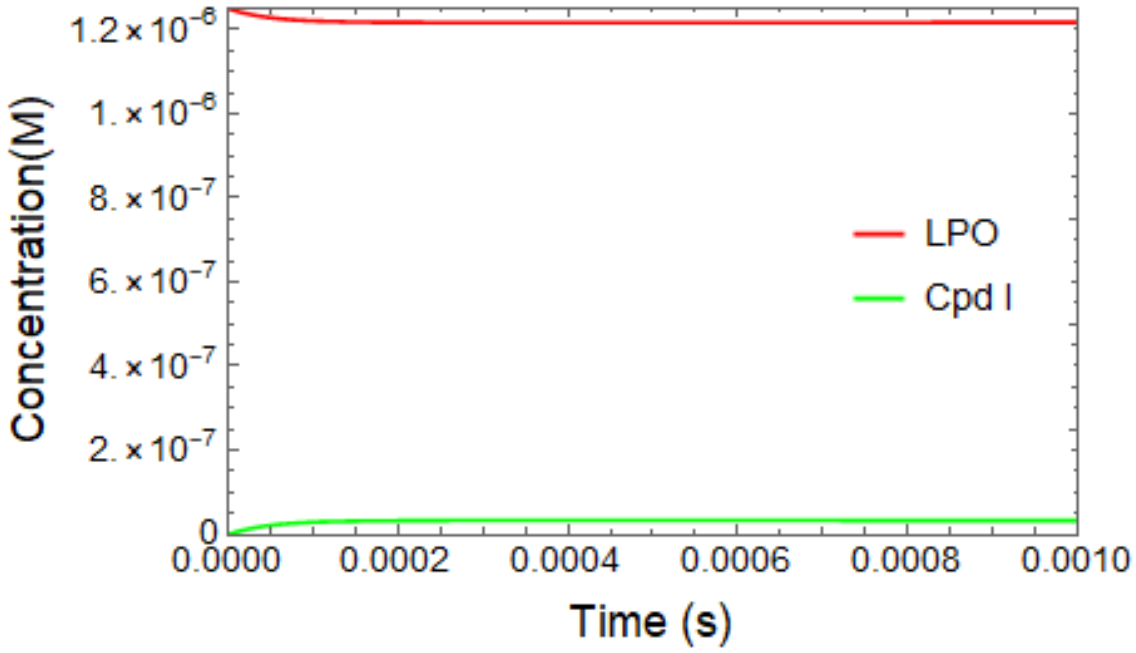

Figure 3.1 – Simulated concentrations of enzyme species during the lactoperoxidase-catalyzed oxidation of SCN^- by H_2O_2. Initial concentrations were [LPO] = 0.125 uM, [H_2O_2] = 50 uM, [SCN^-] = 100 uM (approximately constant).

3.2.2 Literature Model of the Lactoperoxidase Halogen Cycle – Thiocyanate Reducing Substrate – Effect of Lactoperoxidase Concentration

The effect of enzyme concentration on the observed rate constant of catalytic reactions is generally straight-forward with a first-order dependence on enzyme concentrations. Indeed, first-order dependence on [LPO] is observed in the LPO halogen cycle literature mechanism model for $0.125 \leq [LPO] \leq 2$ uM. These [LPO] conditions were chosen to reflect conditions used in laboratory experiments where the lactoperoxidase halogen cycle was observed. The overall reaction rate is first-order and the kinetic traces

can be seen in Figure 3.2. The linearity of the kinetic traces in the log plot make it clear that the reaction is first-order, Figure 3.3. Increasing slope of the log plot traces indicates an increasing observed rate constant as [LPO] is increased, Figure 3.3.

The kinetic traces were fit using the first-order integrated rate equation to calculate the simulated observed first-order rate constants, $k_{obs\text{-}sim}$. The linearity exhibited in Figure 3.4 of the relationship between $k_{obs\text{-}sim}$ and [LPO] indicates that the reaction is indeed first-order with respect to lactoperoxidase as expected.

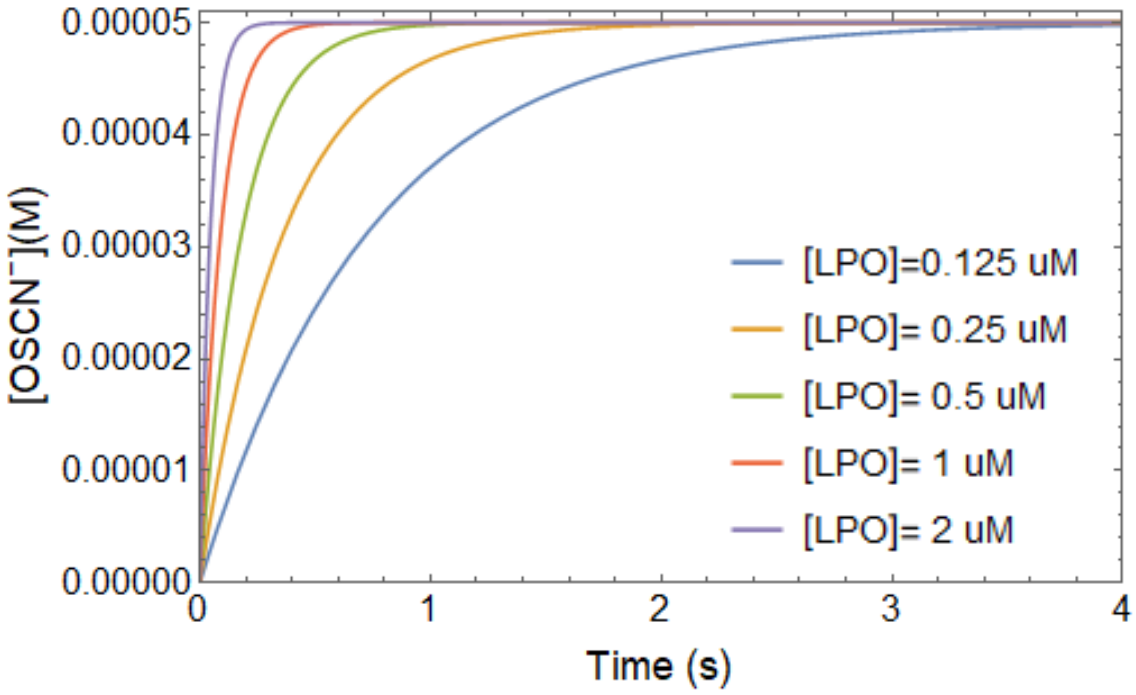

Figure 3.2 – Simulated kinetic traces of production of $OSCN^-$ by the LPO-catalyzed oxidation of SCN^- by H_2O_2 as LPO concentration is varied. Initial concentrations were [SCN^-] = 100 uM (approximately constant), [H_2O_2] = 50 uM, and [LPO] = 0.125-2 uM.

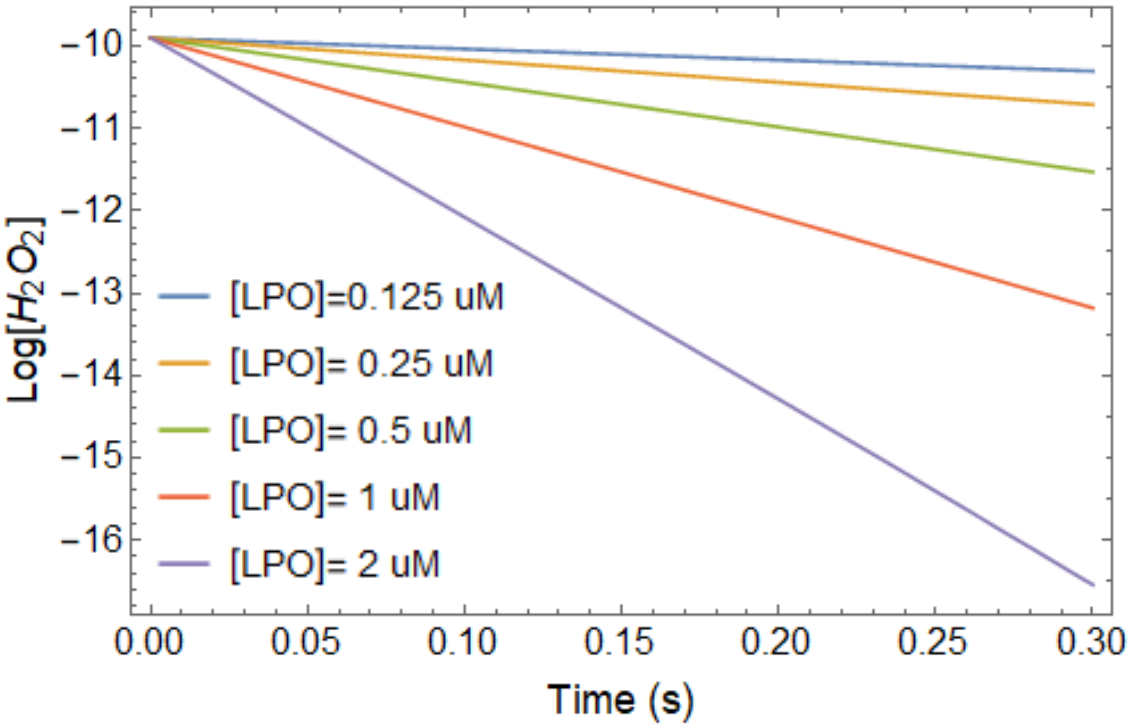

Figure 3.3 - Log plot of the simulated kinetic traces in Figure 3.2. Initial data is shown because the model became unstable when the individual reactions reached completion.

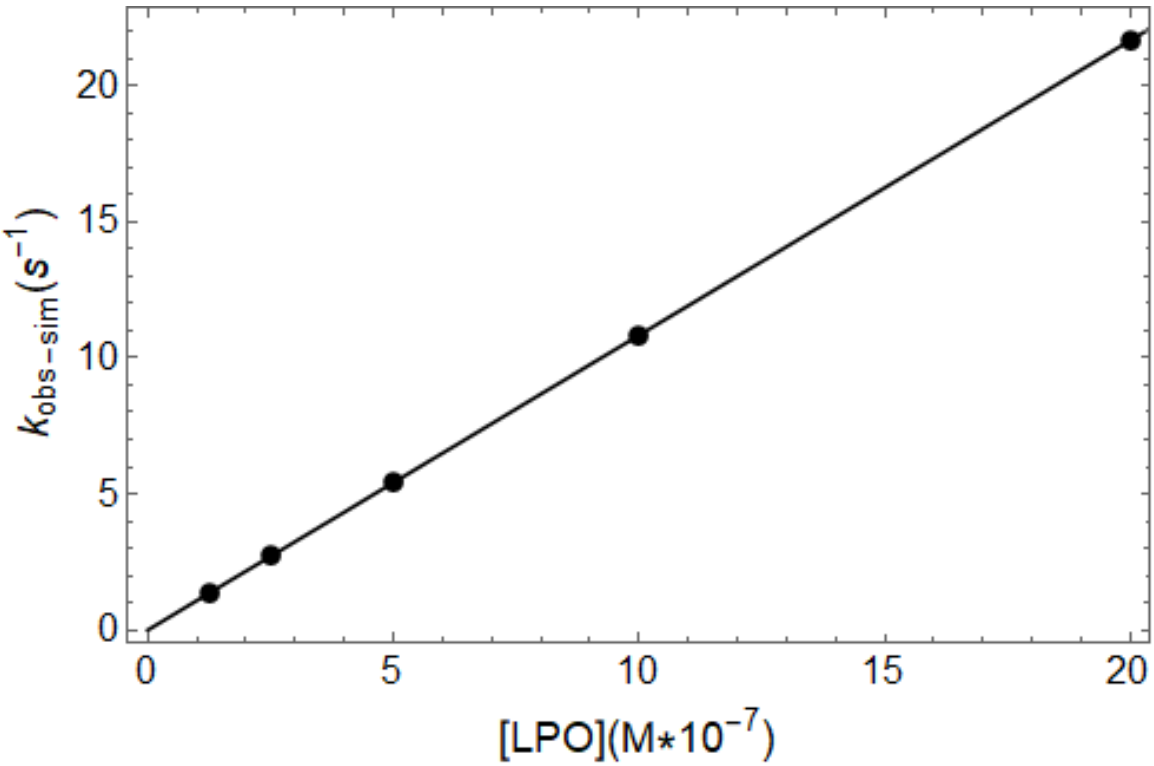

Figure 3.4 - Plot of the observed rate constants for the simulated LPO-catalyzed oxidation of SCN^- by H_2O_2 as a function of [LPO].

3.2.3 Literature Model of the Lactoperoxidase Halogen Cycle – Thiocyanate Reducing Substrate – Effect of Hydrogen Peroxide Concentration

During the LPO halogen cycle hydrogen peroxide acts as an oxidizing substrate for the iron catalytic center of lactoperoxidase to produce compound I, Equation 3.2.5. This reaction is rate-limiting when thiocyanate acts as a reducing substrate as the reaction of compound I with SCN^-, Equation 3.2.6, is faster than the production of compound I. In fact, as long as $[H_2O_2]$ does not greatly exceed $[SCN^-]$ the first reaction will be rate-limiting when SCN^- is the reducing substrate. As such, $[H_2O_2]$ was kept as the limiting reagent for

this model. As [H_2O_2] is the limiting reagent, the final concentration of $OSCN^-$ increases as the initial concentration of H_2O_2 is increased.

Given the pseudo-first-order conditions with respect to hydrogen peroxide when compared to lactoperoxidase it might be expected that the reaction should have a pseudo-first-order dependence on H_2O_2 if the stoichiometric reaction is considered outside of the context of a catalysis mechanism. However, the constant steady-state concentration of LPO, which exists due to its status as a catalyst, and the rate of LPO turnover controls the rate of this reaction. Individual traces can be observed in Figure 3.5 and the observed rate constant does not change but the total change in [$OSCN^-$] as a function of time increases with first-order dependence on [H_2O_2] indicating a first-order dependence with respect to H_2O_2. The constant slopes observed in the log plot of the individual kinetic traces in Figure 3.6 exhibit the independence of the observed rate constant on [H_2O_2]. This is further evidenced in Table 8 which shows the observed rate constants as calculated by fitting the first-order traces in Figure 3.5 to the first-order integrated rate equation.

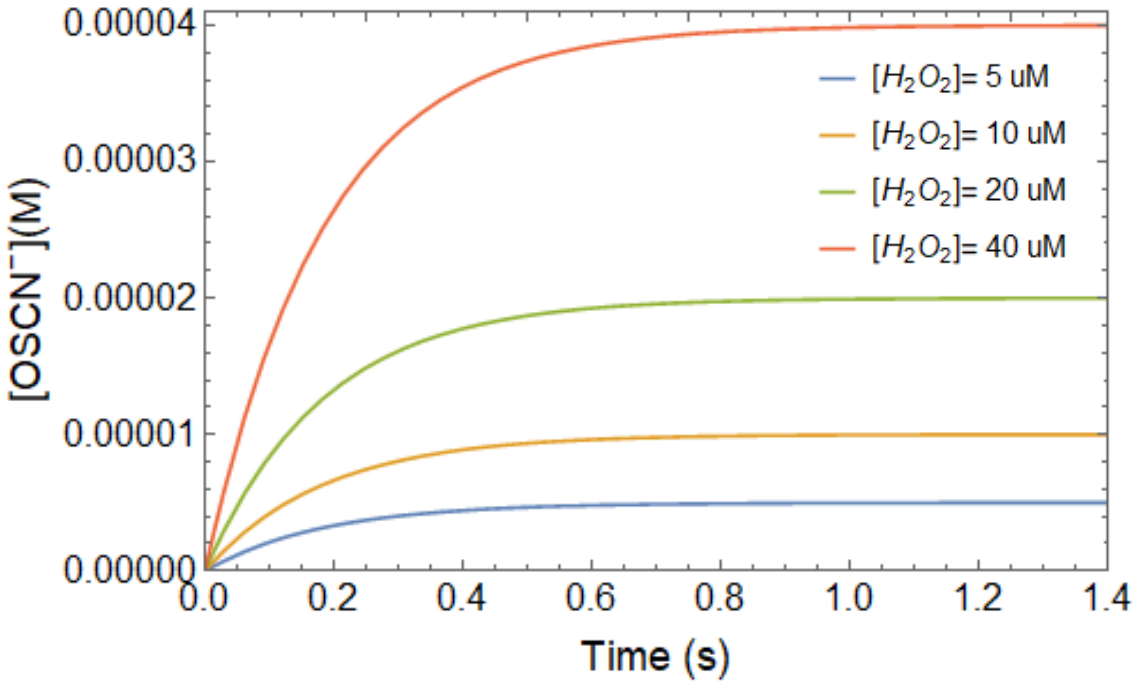

Figure 3.5 – Simulated kinetic traces for the production of $OSCN^-$ by the LPO-catalyzed oxidation of SCN^- by H_2O_2 as a function of $[H_2O_2]$ according to the model of the literature mechanism. Initial concentrations were [LPO] = 0.5 uM, $[SCN^-]$ = 100 uM (approximately constant), and $[H_2O_2]$ = 5-40 uM.

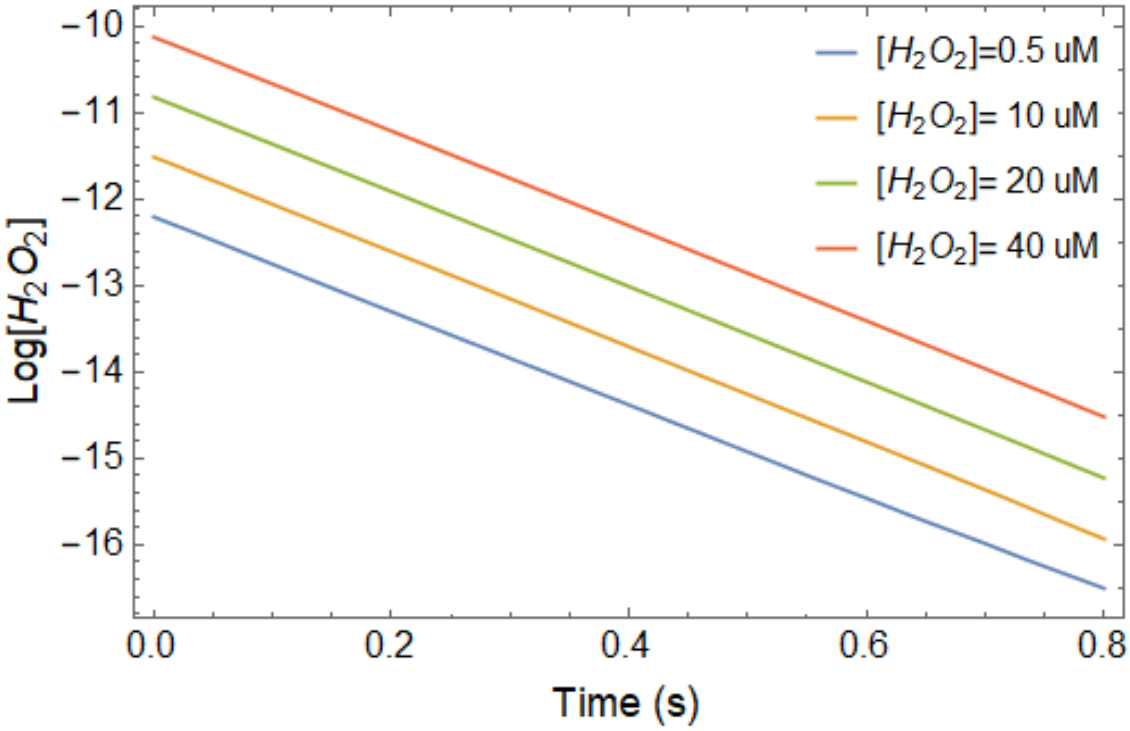

Figure 3.6 - Log plot of the simulated kinetic traces in Figure 3.5.

Table 8 - Observed rate constants for the literature model of the simulated LPO-catalyzed oxidation of SCN^- by H_2O_2 as a function of $[H_2O_2]$

$[H_2O_2]$(uM)	**k_{obs} (s^{-1})**
5	5.49
10	5.48
20	5.46
40	5.43

3.2.4 Literature Model of the Lactoperoxidase Halogen Cycle – Thiocyanate Reducing Substrate – Effect of Thiocyanate Concentration

Since the reaction of H_2O_2 with LPO to produce compound I, Equation 3.2.5, is rate-limiting when thiocyanate is the reducing substrate it would be expected that the rate of the reaction would be independent of thiocyanate concentration. This is true in the model of the halogen cycle mechanism for SCN^- acting as the reducing substrate, reported in Equations 3.2.5 and 3.2.6, as evidenced in Figure 3.7. In Figure 3.7 only a single trace is visible because the traces overlay completely. Table 9 shows that the calculated observed rate constants do not change as $[SCN^-]$ is varied.

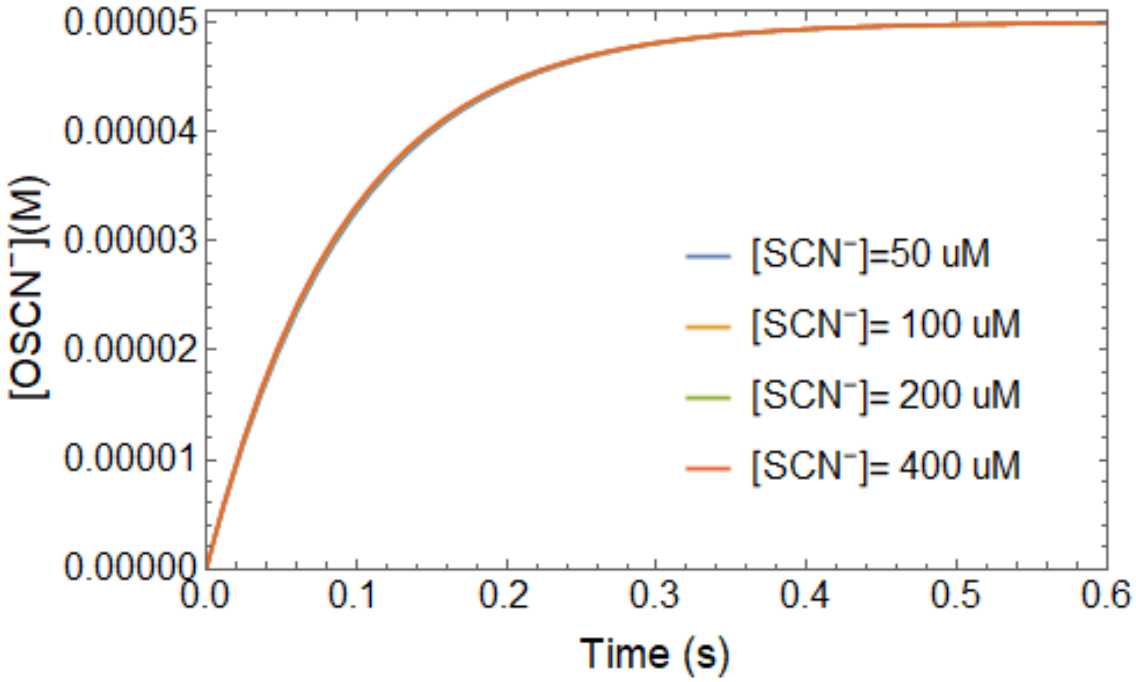

Figure 3.7 – Simulated kinetic traces of the LPO-catalyzed oxidation of SCN^- by H_2O_2 as a function of [SCN^-] according to the model of the literature mechanism. Only one trace is visible because the rate of the reaction is independent of [SCN^-]. Initial concentrations were [LPO] = 1 uM, [H_2O_2] = 50 uM, and [SCN^-] = 50-400 uM.

Table 9 - Observed rate constants for the Literature Model simulation of the LPO-catalyzed oxidation of SCN^- by H_2O_2 as a function of $[SCN^-]$

$[SCN^-](uM)$	$k_{obs}(s^{-1})$
50	10.67
100	10.83
200	10.92
400	10.96

3.3 Model of the Lactoperoxidase Halogen Cycle Literature Mechanism – Bromide Reducing Substrate

To highlight the significance of the rate-limiting step of the halogen cycle literature mechanism, we have developed a model of the lactoperoxidase-catalyzed oxidation of bromide. The reaction of Br^- with compound I has a reported rate constant, k_2, of $4.1(1)x10^4$ $M^{-1}s^{-1}$ which makes Equation 3.2.6 rate-limiting.[41] It should be noted that Br^- concentration conditions used in this model are low such that the second reaction, Equation 3.2.6, is rate-limiting. When $[Br^-]$ is sufficiently high with respect to $[H_2O_2]$, the first reaction, Equation 3.2.5, becomes rate-limiting and the kinetics reflect what is seen when thiocyanate is the reducing substrate in section 3.2.

3.3.1 Model of the Lactoperoxidase Halogen Cycle Literature Mechanism – Bromide Reducing Substrate – Enzyme Species

It is often useful to observe the primary enzyme species when steady-state catalysis reactions are observed. In the case of the LPO-catalyzed oxidation of Br^- by H_2O_2, since

the second reaction, Equation 3.2.6, is rate-limiting there is a buildup of compound I (referred to as Cpd I in the model) until it is the primary enzyme species, Figure 3.8. Compound I remains the primary enzyme species until H_2O_2 is depleted and the reaction is complete.

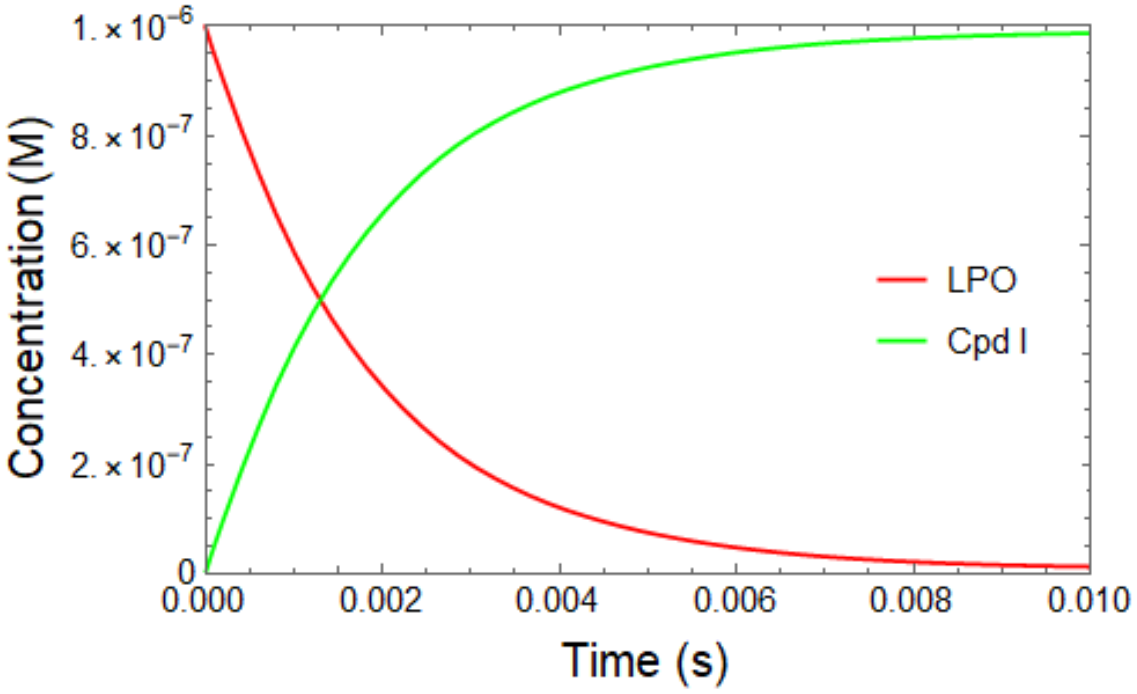

Figure 3.8 - Approach to steady-state concentrations of enzyme species during the simulated lactoperoxidase-catalyzed oxidation of Br^- by H_2O_2. Initial concentrations of reactants were [LPO] = 1 uM, [H_2O_2] = 50 uM, and [Br^-] = 100 uM (approximately constant).

3.3.2 Literature Model of the Lactoperoxidase Halogen Cycle – Bromide Reducing Substrate – Effect of Bromide Concentration

The rate of production of hypobromous acid is zeroth-order under the chosen conditions of relatively low [Br^-] as shown by the linear kinetic traces in Figure 3.9. The zeroth-order conditions are due to the unchanging concentration of Br^- which is experimentally relevant because of the TNB assay discussed in section 3.1.1. The zeroth-order reaction exhibits an observed rate constant with a first-order dependence on [Br^-], Figure 3.10, due to the presence of Br^- in the rate-limiting step, Equation 3.2.6.

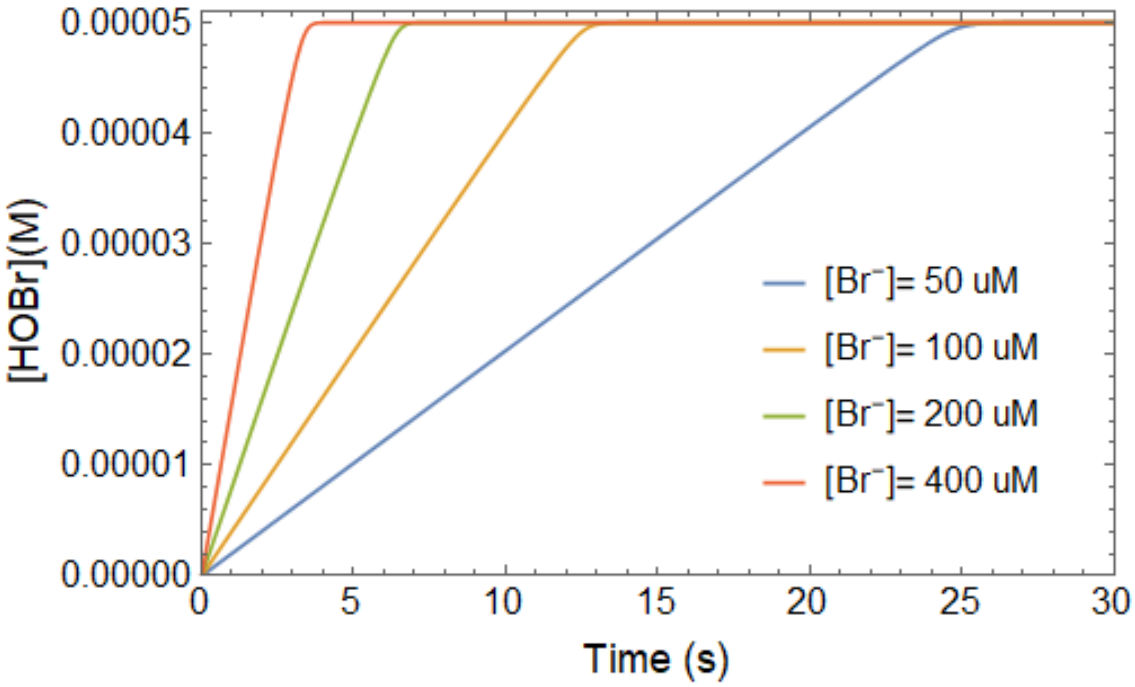

Figure 3.9 – Simulated kinetic traces of the lactoperoxidase-catalyzed oxidation of Br^- by H_2O_2 as [Br^-] is varied. The initial concentrations of reactant were [LPO] = 1 uM, [H_2O_2] = 50 uM, and [Br^-] = 50-400 uM.

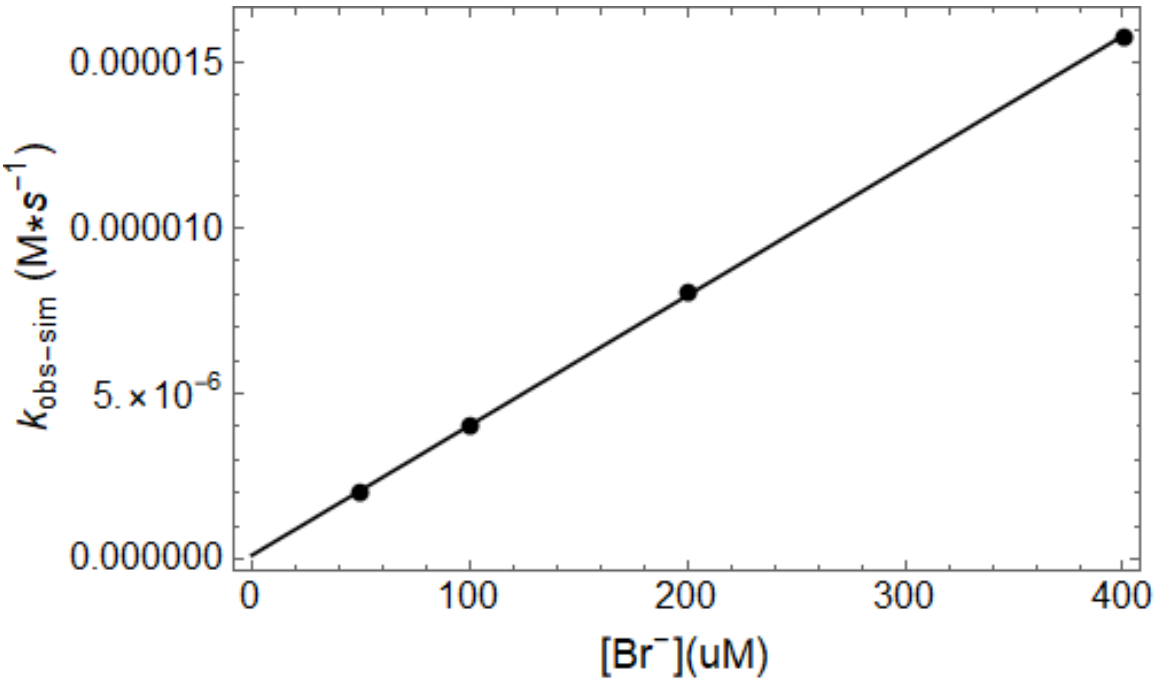

Figure 3.10 - Observed rate dependence on [Br^-] for the simulated lactoperoxidase-catalyzed oxidation of Br^- by H_2O_2 as [Br^-] is varied.

3.3.3 Literature Model of the Lactoperoxidase Halogen Cycle – Bromide Reducing Substrate – Effect of Lactoperoxidase Concentration

The effect of varying [LPO] on the rate of the LPO-catalyzed oxidation of Br^- by H_2O_2 was modeled according to Equations 3.2.5 and 3.2.6. The model responds to [LPO] variation as expected for an enzyme-catalyzed mechanism, with a first-order dependence of the observed rate constant on [LPO] exhibited in the linearity of Figure 3.12. The model maintains its zeroth-order kinetics as [LPO] is varied, Figure 3.11.

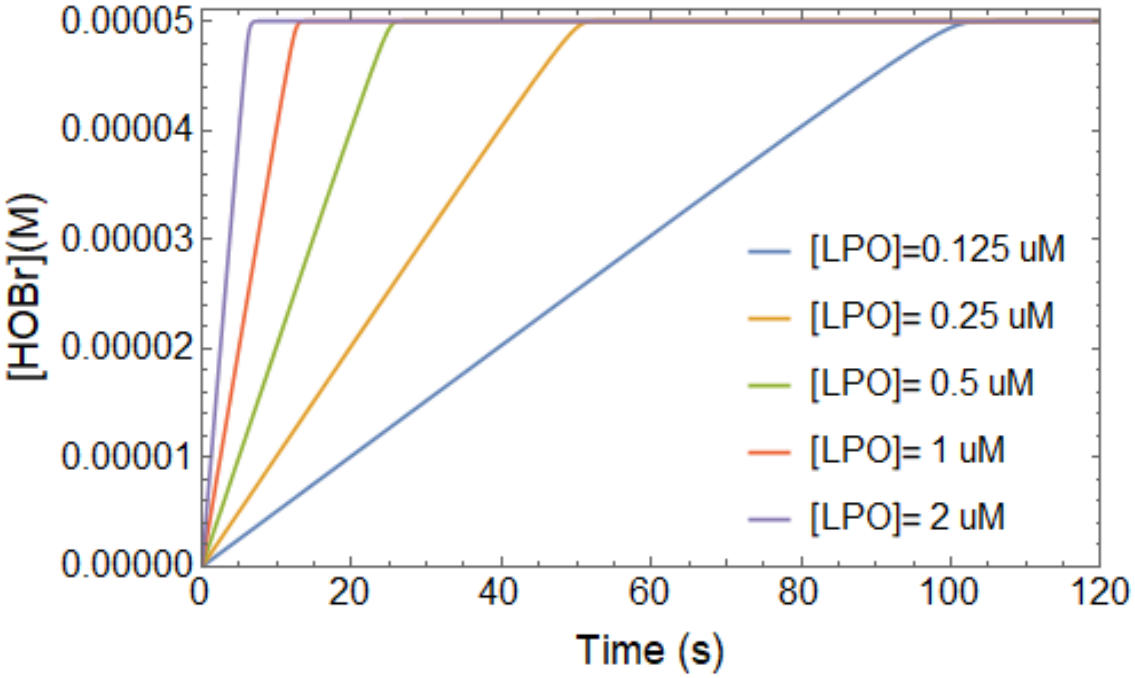

Figure 3.11 – Simulated kinetic traces of the lactoperoxidase-catalyzed oxidation of Br^- by H_2O_2 as LPO is varied. The initial concentrations of reactants were [Br^-] = 100 uM, [H_2O_2] = 50 uM, and [LPO] = 0.125-2 uM.

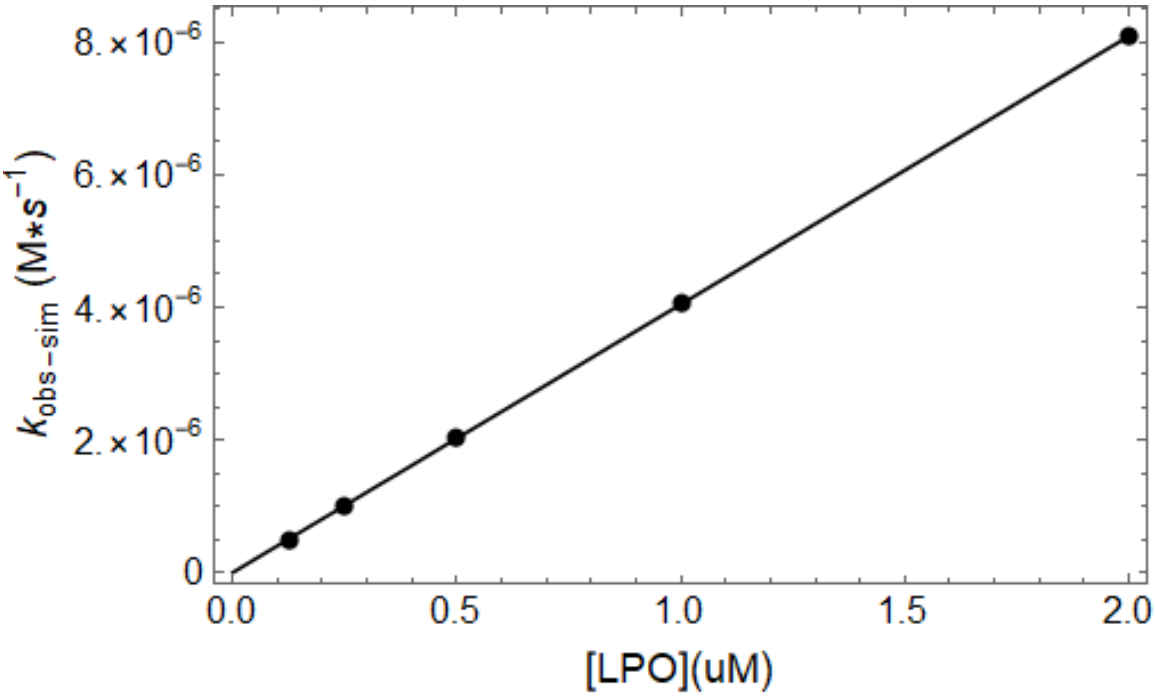

Figure 3.12 - Observed rate constant dependence on [LPO] for the simulated lactoperoxidase-catalyzed oxidation of Br^- by H_2O_2.

3.3.4 Literature Model of the Lactoperoxidase Halogen Cycle – Bromide Reducing Substrate – Effect of Hydrogen Peroxide Concentration

The effect of varying [H_2O_2] on the rate of the LPO-catalyzed oxidation of Br^- by H_2O_2 was modeled according to the halogen cycle literature mechanism, Equations 3.2.5 and 3.2.6. The modeled reaction is zeroth-order and the rate is independent of [H_2O_2], Figure 3.13 and Table 10. This is expected given the rate-limiting step does not involve H_2O_2 and that the production of compound I is considered irreversible.

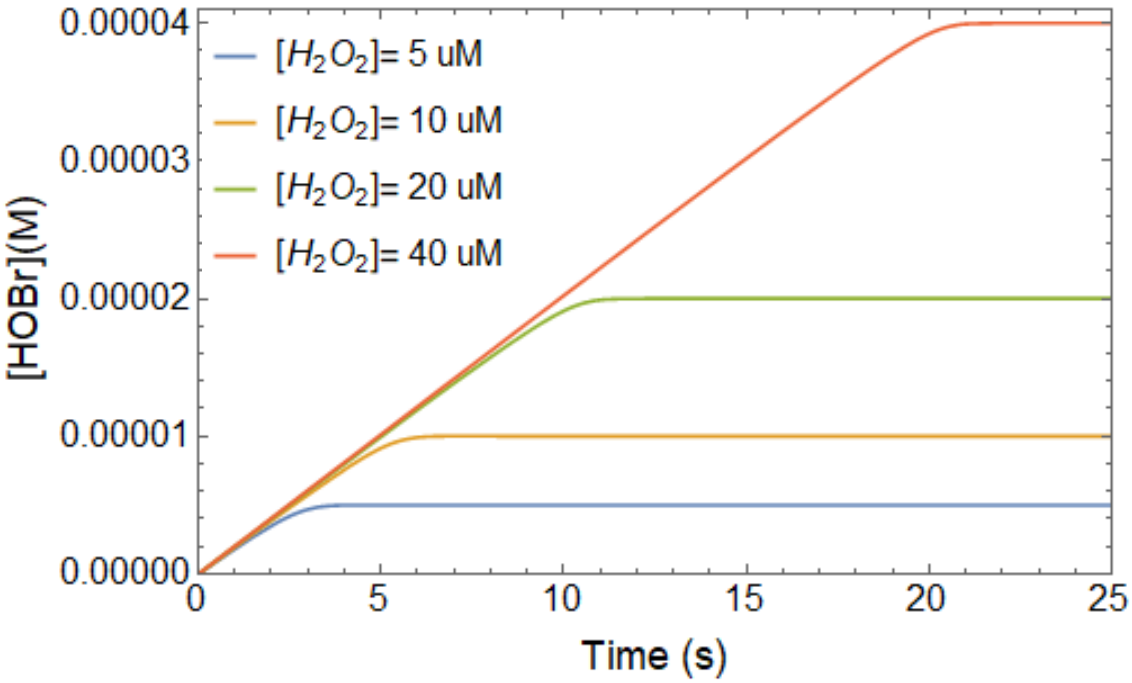

Figure 3.13 – Simulated kinetic traces of the lactoperoxidase-catalyzed oxidation of Br^- by H_2O_2 as [H_2O_2] is varied. The initial concentrations of the reactants were [LPO] = 0.5 uM, [Br^-] = 100 uM (approximately constant), and [H_2O_2] = 5-40 uM.

Table 10 - Observed zeroth-order rate constants for the simulated LPO-catalyzed oxidation of Br^- by H_2O_2 as a function of $[H_2O_2]$

$[H_2O_2]$(uM)	k_{obs}($M \cdot s^{-1}$)
5	1.82×10^{-6}
10	1.94×10^{-6}
20	1.99×10^{-6}
40	2.02×10^{-6}

[a]The variation in k_{obs} is due to the slight deviation from linearity as H_2O_2 is depleted.

3.4 Experimental Kinetics of the Lactoperoxidase-Catalyzed Oxidation of Thiocyanate and Selenocyanate Under Conditions of High Pseudohalide Concentration

Laboratory experiments to observe the lactoperoxidase-catalyzed oxidation of thiocyanate and selenocyanate by H_2O_2 were conducted to determine the effect of varying reactant concentrations on the mechanism. These studies have been grouped into two sets of reaction conditions simplified by the relative concentrations of pseudohalide reducing substrate, PsX^- (PsX^- = SCN^- and $SeCN^-$). The term "high concentration studies" refers, in general, to experiments we conducted where $[PsX^-] \geq 1$ mM, [LPO] ≥ 1 uM, and pseudo-first-order conditions of $[PsX^-]$ with respect to $[H_2O_2]$ were used. These conditions were optimized to observe the effects of varying reactant and enzyme concentrations where first-order reaction trace kinetics were observed.

Under conditions of high concentration of PsX^- the experimental data reflects the order dependencies predicted by the lactoperoxidase halogen cycle literature model in section 3.2 when Equation 3.2.5 is rate-limiting. First-order kinetics are observed with no rate dependence on [PsX^-], a first-order dependence [H_2O_2], and first-order dependence of the observed rate constant on [LPO] as shown for SCN^- in Tables 11 and 12 and Figure 3.14 and for $SeCN^-$ in Tables 13 and 14 and Figure 3.15. However, slight systematic dependence of the observed rate constant on [PsX^-] is observed for SCN^-, Table 11, which does not follow a strict order dependency.

Table 11 - Observed rate of the lactoperoxidase-catalyzed oxidation of SCN^- by H_2O_2 as a function of [H_2O_2]

[H_2O_2](uM)	**k_{obs} (s^{-1})**	**Model Predicted $k_{obs\text{-}sim}$ (s^{-1})**
7.5	6.56(4)	11.00
15	5.65(3)	11.00
30	7.02(8)	11.00
Average	6.4(7)	11.00

[a]A single mixing experiment with constant post-mixing concentrations of [LPO] = 1 uM, [SCN^-] = 4 mM, [TNB] = 70 uM, and [H_2O_2] = 7.5-30 uM.

[b]The estimated error, given by the parenthetical digits, for the individual rate constants is for a least-squares fit of an average of five kinetic traces.

[c]The average error was determined by the standard deviation of the individual fits.

Table 12 - Observed rate of the lactoperoxidase-catalyzed oxidation of SCN^- by H_2O_2 as a function of $[SCN^-]$

$[SCN^-]$(mM)	**k_{obs} (s^{-1})**	**Model Predicted $k_{obs\text{-}sim}$ (s^{-1})**
1.2	6.29(3)	11.00
2.1	7.96(2)	11.00
4.3	8.839(8)	11.00
8.6	8.93(1)	11.00
Average	–	11.00

[a]Single mixing experiment with constant post-mixing concentrations of [LPO] = 1 uM, $[H_2O_2]$ = 40 uM, and [TNB] = 100 uM.

[b]The estimated error, given by the parenthetical digits, for the individual rate constants is for a least-squares fit of an average of five kinetic traces.

[c]The average error of the model predicted rate constants was determined by the standard deviation of the individual fits.

[d] –, The average of the experimentally observed rate constants was not calculated due to systematic error.

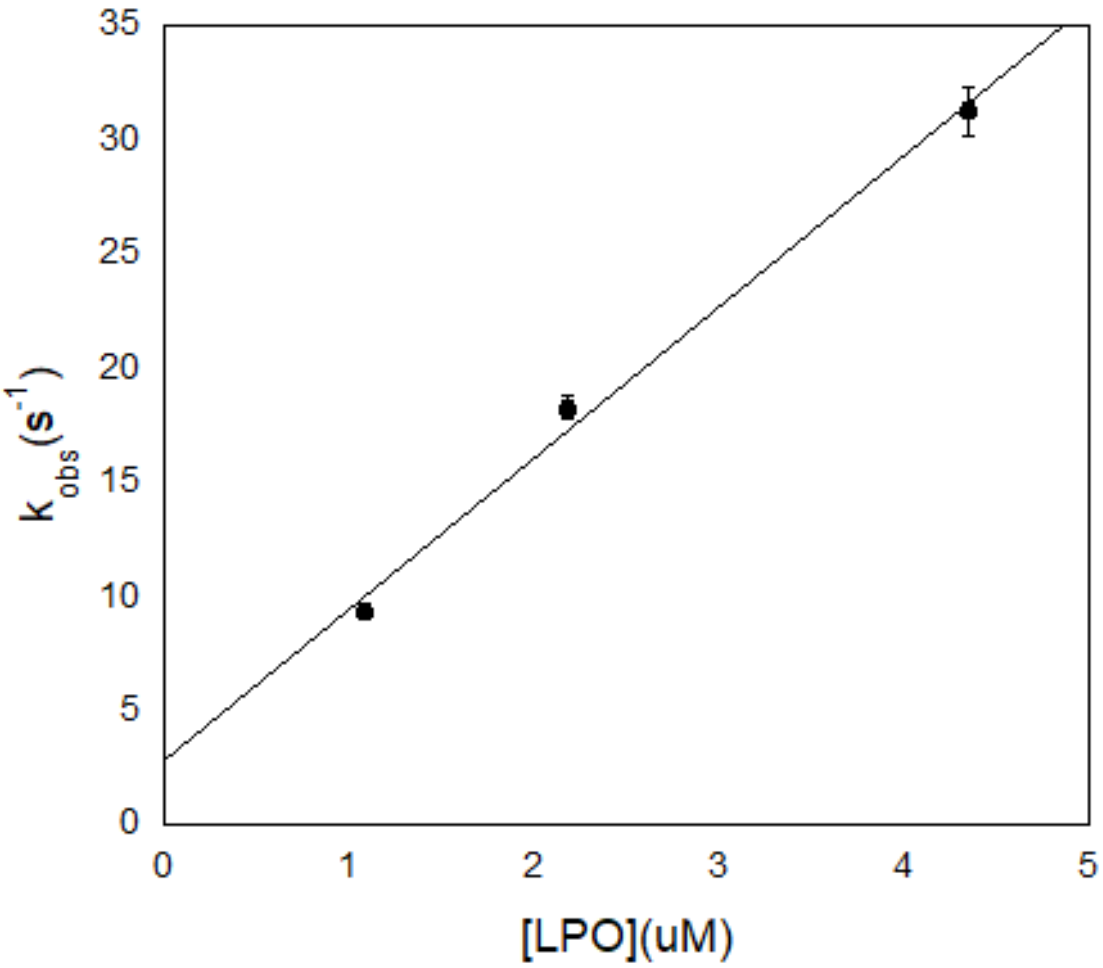

Figure 3.14 – [LPO] dependence on the rate of the LPO-catalyzed oxidation of SCN^- by H_2O_2. Post-mixing concentrations were [SCN^-] = 4 mM, [H_2O_2] = 40 uM, [TNB] = 100 uM, and [LPO] = 1.09-4.35 uM. The estimated error shown by the error bars for the individual rate constants is for a least-squares fit of an average of five kinetic traces and has been multiplied by a factor of 20 so that the error bars would be visible on the plot.

Table 13 - Observed rate of the LPO-catalyzed oxidation of $SeCN^-$ by H_2O_2 as a function of $[H_2O_2]$

$[H_2O_2]$(uM)	**k_{obs} (s^{-1})**
7.5	23.7(2)
15	24.23(8)
30	24.2(1)
Average	24.1(3)

[a]Single mixing experiment with post-mixing concentrations of [LPO] = 2.2 uM, $[SeCN^-]$ = 4 mM, [TNB] = 70 uM, and $[H_2O_2]$ = 7.5-30 uM.

[b]The estimated error, given by the parenthetical digits, for the individual rate constants is for a least-squares fit of an average of five kinetic traces.

[c]The average error of the model predicted rate constants was determined by the standard deviation of the individual fits.

Table 14 - Observed rate of the lactoperoxidase-catalyzed oxidation of $SeCN^-$ by H_2O_2 as a function of [$SeCN^-$]

[$SeCN^-$](mM)	**k_{obs} (s^{-1})**
1.0	8.73(1)
2.0	9.11(2)
4.0	8.45(1)
8.1	7.17(1)
Average	8.3(8)

[a] A single mixing experiment with post-mixing concentrations of [LPO] = 1 uM, [H_2O_2] = 40 uM, [TNB] = 100 uM, and [$SeCN^-$] = 1.0-8.1 mM.

[b]The estimated error, given by the parenthetical digits, for the individual rate constants is for a least-squares fit of an average of five kinetic traces.

[c]The average error of the model predicted rate constants was determined by the standard deviation of the individual fits.

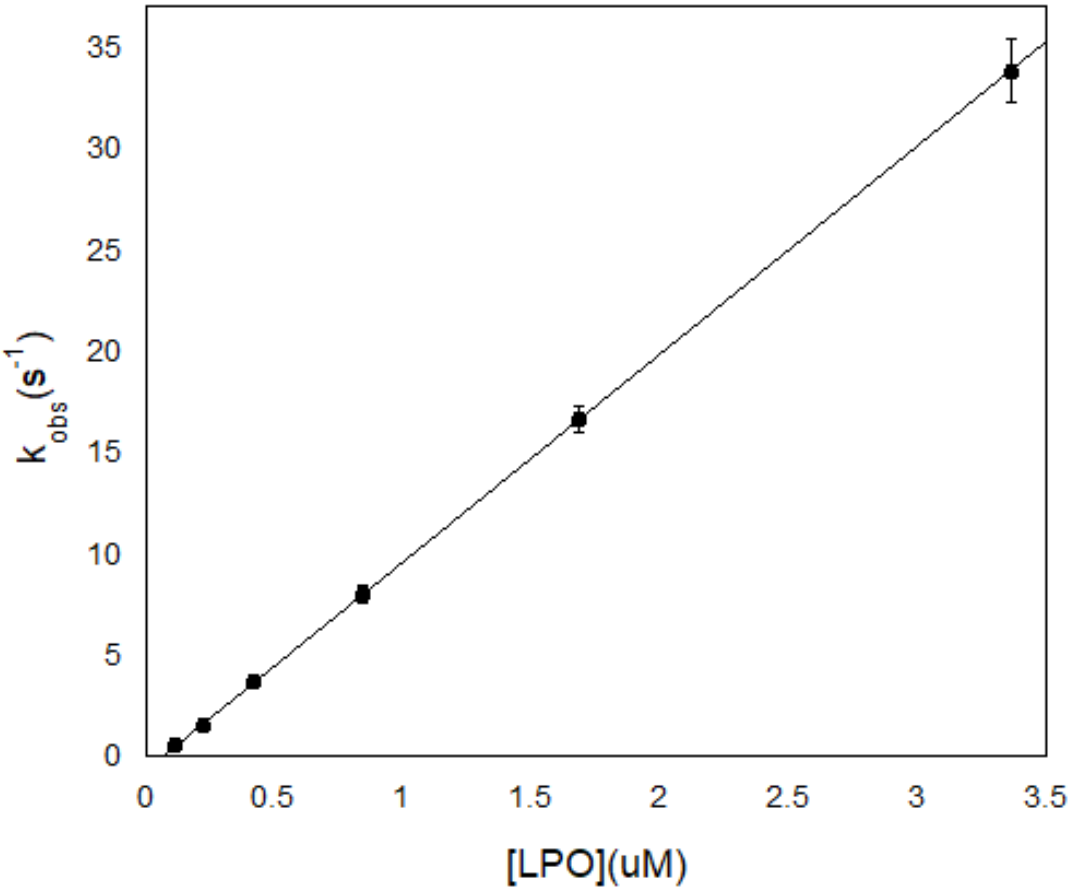

Figure 3.15 - Effect of varying [LPO] on the LPO-catalyzed oxidation of $SeCN^-$ by H_2O_2 under high [$SeCN^-$] conditions. Post-mixing concentrations of reactants were [$SeCN^-$] = 1 mM, [H_2O_2] = 15 uM, [TNB] = 70 uM, and [LPO] = 0.11-3.36 uM. The estimated error shown by the error bars for the individual rate constants is for a least-squares fit of an average of five kinetic traces and has been multiplied by a factor of 10 so that the error bars would be visible on the plot.

Again, in the case of both SCN^- and $SeCN^-$ acting as the reducing species, no dependence on the rate was observed when $[H_2O_2]$ was varied. However, a slight dependence on $[SCN^-]$ was observed, which is not explained by the model. When the halogen cycle literature mechanism was used to predict the results of the experiments in Tables 11 and 12 an observed rate constant of 11.0 s^{-1} was calculated whereas an average rate constant of 6.4(7) s^{-1} was observed experimentally as $[H_2O_2]$ was varied. A rate constant could not be calculated when $[SCN^-]$ was varied because of the systematic change in the data. The difference in the observed rate constant and predicted rate constant alone does not necessarily invalidate the model as differing sources or treatment of lactoperoxidase can cause changes in enzyme efficiency.

When $SeCN^-$ acts as the reducing substrate for the LPO system under identical conditions to SCN^- similar kinetics and dependencies are observed, that is a first-order reaction with a first-order dependency on $[H_2O_2]$ and independent $[SeCN^-]$ and a pseudo-first-order dependency on [LPO] was observed. The average observed rate of this reaction is 8.36(9) s^{-1}. This is slightly more than what is observed for SCN^-, but within the range of experimental error given the reactions slight dependence on $[PsX^-]$ observed under these conditions.

In the halogen cycle literature mechanism, the rate of compound I production by the oxidation of native LPO by H_2O_2 is rate-limiting, Equation 3.2.6. This causes the rate of the reaction to be independent of PsX^- concentration as it is not involved in the rate-limiting step. In turn, this would also cause the overall rate of catalysis to be independent of the rate constant of the reaction of PsX^- with compound I. That is, unless, as shown with

the lactoperoxidase-catalyzed oxidation of Br^- by H_2O_2 in section 3.3, the rate constant is small such that the reaction of X^- with compound I becomes rate-limiting.

An attempt was made to calculate the rate constant of the reaction of $SeCN^-$ with compound I, as was done for SCN^- by Furtmüller et al. but the reaction was too fast to be measured.[41] Under conditions of high [PsX^-] the overall reaction reflects what is observed in the literature model of the mechanism for the LPO-catalyzed oxidation of X^- by H_2O_2 presented in section 3.2.1, although there is a slight dependence on [PsX^-], especially observed for SCN^- which is not explained by the model.

3.5 Experimental Kinetics of the Lactoperoxidase-Catalyzed Oxidation of Pseudohalides by Hydrogen Peroxide Under Conditions of Low Pseudohalide Concentration

The lactoperoxidase halogen cycle literature mechanism given in Equations 3.2.5 and 3.2.6 does not predict any change in the kinetics under conditions of low [X^-] concentration, when $k_2>k_1$, unless [H_2O_2] greatly exceeds [PsX^-]. However, our studies show that under conditions of low concentrations of PsX^-, the LPO-catalyzed oxidation of PsX^- by H_2O_2 becomes biphasic with a first-order reaction followed by a zeroth-order reaction.

These traces appear, under initial inspection, to take on the aspects of burst phase enzyme kinetics which are also characterized by a first-order reaction followed by a zeroth-order reaction. Burst phase kinetics are observed as a result of a first-order pre-equilibrium reaction where the substrate reacts stoichiometrically with enzyme to produce the product at a faster rate than the rate of steady-state enzyme turnover.[152] The first-order burst phase reaction is followed by a zeroth-order steady-state reaction similar to what is observed in

our experiments. However, true burst phase kinetics only occur over a single catalytic turnover. In the experimental data presented here, multiple catalytic turnovers occur in the first step of the reaction indicating that simple burst phase kinetics cannot explain the observed kinetics. Moreover, the number of enzyme turnovers that occur during the first reaction increases with increasing [LPO] as well as increasing [PsX^-].

The results presented here probe the effect of varying reactant and enzyme concentrations on each step of the biphasic reaction observed under conditions of low [PsX^-]. The term "low concentration of [PsX^-]" is used here as a general term to refer to experiments conducted under conditions of [PsX^-] $\leq$ 1 mM, stoichiometric or near stoichiometric conditions of [PsX^-] with respect to [H_2O_2], and [LPO] $\leq$ 1 uM. These conditions were optimized to observe the effects of varying reactant and enzyme concentrations where biphasic and/or zeroth-order reaction trace kinetics were observed.

The observed rate constants were calculated to determine the effects of varying the concentrations of each reaction component on each step of the biphasic reaction observed at low [PsX^-]. This was done by fitting the kinetic traces to a simple first-order followed by zeroth-order biphasic kinetic model or fitting the rate constants of the reactions to first-order or zeroth-order models individually. Individual reaction fitting was achieved by truncation of the data to isolate a single reaction or selectively fixing the rate constants for the known reaction step according to expected values calculated from other data sets. Fixing known rate constants allowed the reaction in question to be fit when data truncation could not be used because the pre-steady-state and steady-state reactions were not well resolved.

Data was collected for both SCN^- and $SeCN^-$ with similar outcomes with respect to order dependencies and kinetic trace data. Therefore, representative data for SCN^- is presented here for discussion. The effect of differing PsX^- identity on rates and kinetic constants is discussed in section 3.6.

3.5.1 Effect of Varying Pseudohalide Concentration on the Lactoperoxidase-Catalyzed Oxidation of Pseudohalides by Hydrogen Peroxide at Low Concentrations of Pseudohalide

The lactoperoxidase-catalyzed oxidation of PsX^- by H_2O_2 was observed as a function of $[PsX^-]$ under conditions of low $[PsX^-]$ to determine the effects on the reaction rates. When the concentration of PsX^- was low, the overall reaction was biphasic with a first-order reaction followed by a zeroth-order reaction, Figure 3.16. However, as $[PsX^-]$ was increased, the number of enzyme turnovers that occurred in the first phase of the reaction increased, Figure 3.17. When the $[PsX^-]$ became sufficiently high, the reaction became strictly first-order and the reaction rate became largely independent of $[PsX^-]$ as seen in experiments conducted under conditions of high $[PsX^-]$ discussed in section 3.4.

When the pre-steady-state reaction was fit to a first-order model the observed rate constant decreased with increasing $[PsX^-]$, Figure 3.18. The $[PsX^-]$ versus k_{obs} relationship, however, is not linear and eventually, at sufficiently high $[PsX^-]$, the rate of the reaction becomes independent of $[PsX^-]$. It was first hypothesized that the PsX^- acts as an enzyme inhibitor; however, examination of initial reaction rates indicates that the reaction is independent of $[PsX^-]$. Instead, it appears that this initial reaction is a result of a pre-steady-state reaction, which is separate from the PsX^- oxidation catalysis and is inhibited by PsX^-.

In contrast to the pre-steady-state reaction, the number of enzyme turnovers which occur during the zeroth-order reaction decrease as [PsX^-] is increased. The reason for the decrease in the number of enzyme turnovers that occur during the steady-state reaction is two-fold. First, as H_2O_2 is the limiting reagent, the ratio of H_2O_2 reacted in the pre-steady-state versus the steady-state reaction increases until the steady-state reaction is no longer observed. Second, the rate of the steady-state reaction exhibits first-order dependency on [PsX^-], Figure 3.19. This causes the two reactions to become less resolved and more difficult to distinguish, particularly at higher [PsX^-] as seen in traces B and C in Figure 3.16.

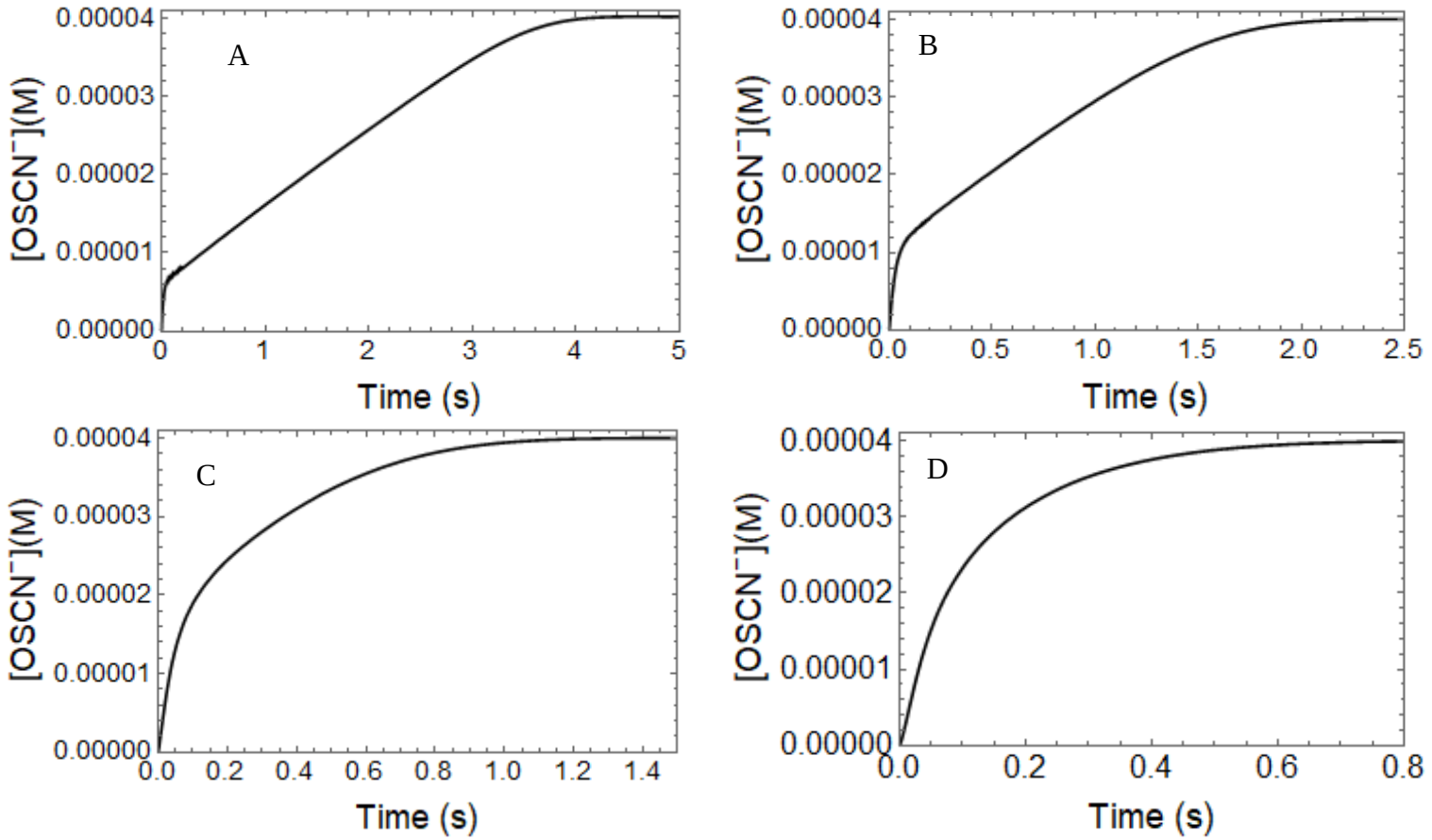

Figure 3.16 - Effect of varying [SCN^-] on the lactoperoxidase-catalyzed oxidation of SCN^- by H_2O_2 under conditions of low [PsX^-]. Post-mixing concentrations were [LPO] = 1.2 uM, [H_2O_2] = 40 uM, [TNB] = 100 uM, and [SCN] = 52, 106, 213, and 425 uM for A, B, C, and D, respectively.

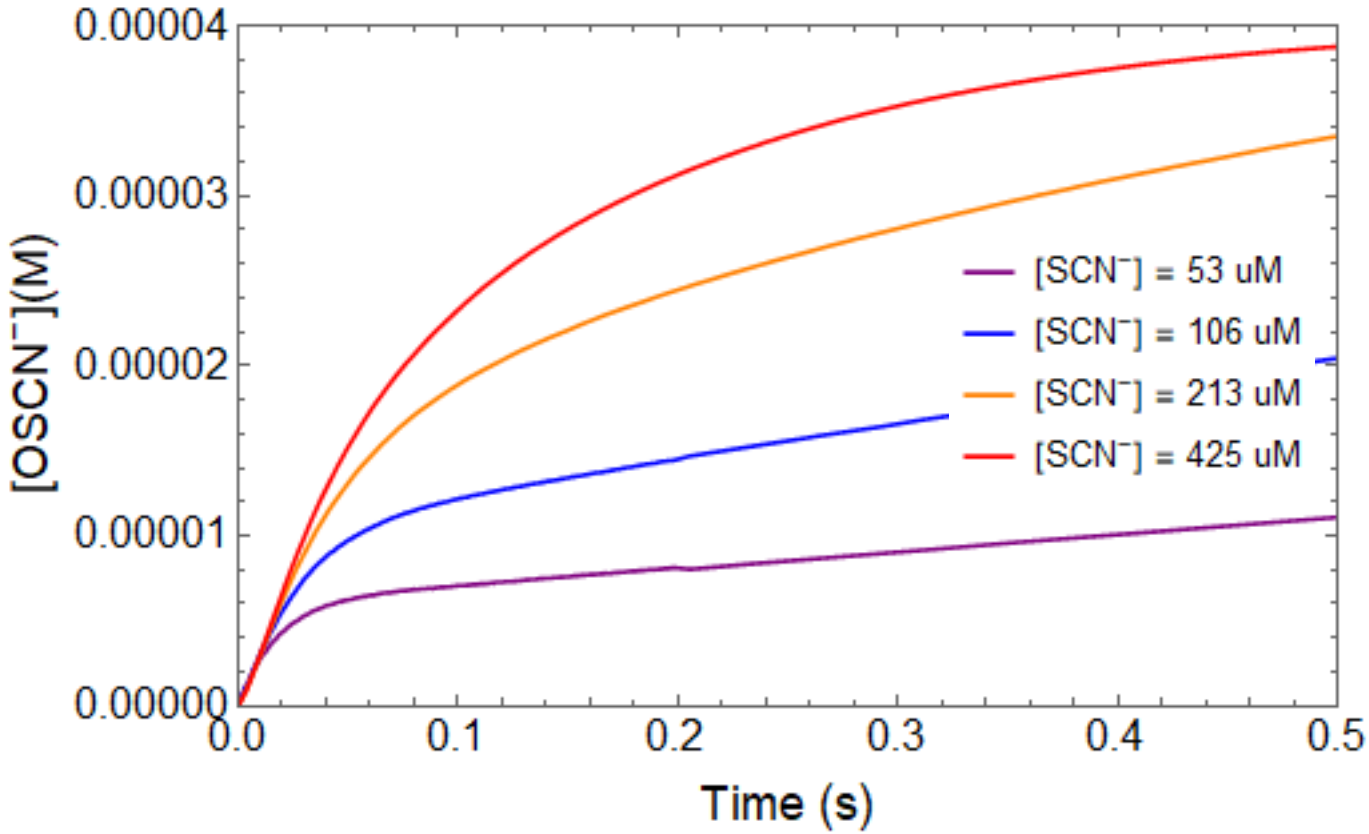

Figure 3.17 – Isolated view of the pre-steady-state reaction observed in Figure 3.16 for the lactoperoxidase-catalyzed oxidation of $[SCN^-]$ by H_2O_2 under low $[PsX^-]$ conditions. Post-mixing concentrations were [LPO] = 1.2 uM, $[H_2O_2]$ = 40 uM, [TNB] = 100 uM, and $[SCN^-]$ = 52, 106, 213, and 425 uM. Notably, the initial reaction rates do not vary and the number of enzyme turnovers that occur during the pre-steady-state reaction increase with increasing $[PsX^-]$.

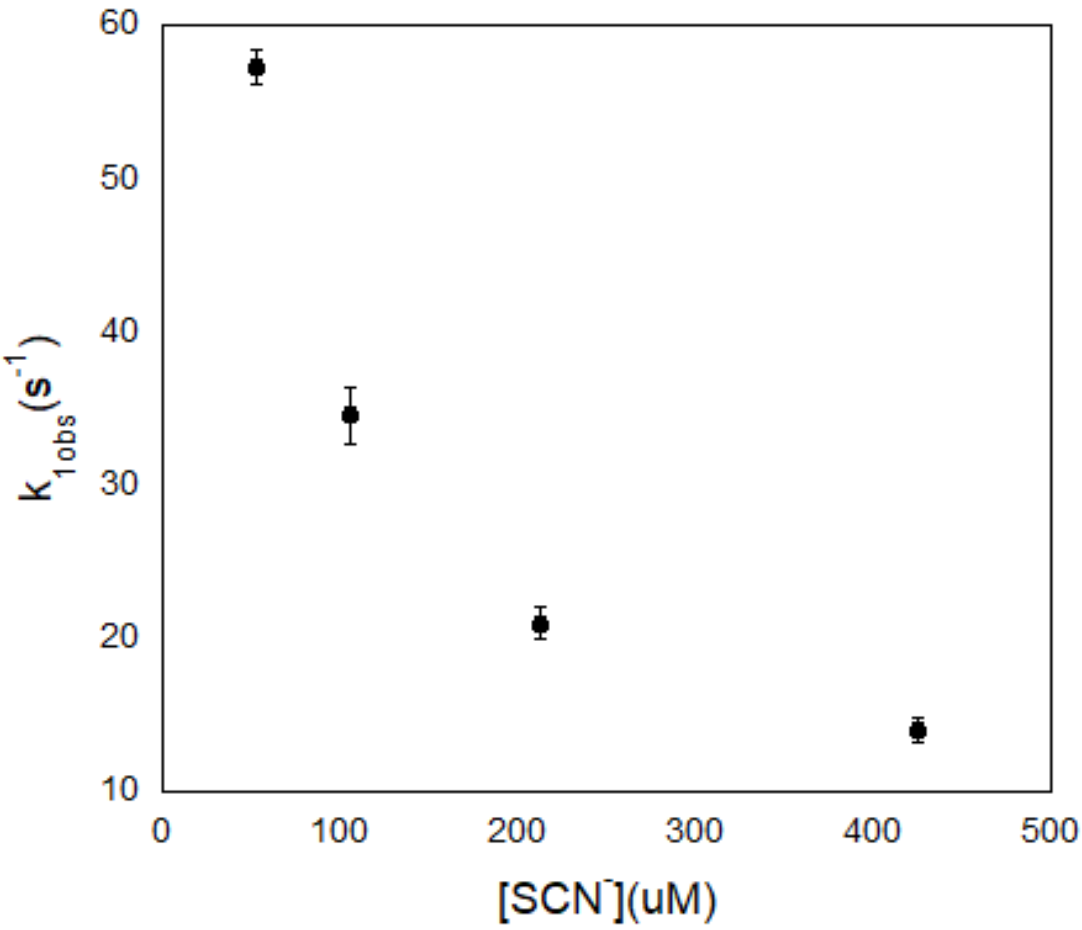

Figure 3.18 - Observed first-order rate constants for the pre-steady-state reaction in the lactoperoxidase-catalyzed oxidation of SCN^- by H_2O_2. Post-mixing concentrations were [LPO] = 1.2 uM, [H_2O_2] = 40 uM, [TNB] = 100 uM, and [SCN^-] = 52, 106, 213, and 425 uM. The estimated error shown by the error bars for the individual rate constants is for a least-squares fit of an average of five kinetic traces and has been multiplied by a factor of 10 so that the error bars would be visible on the plot.

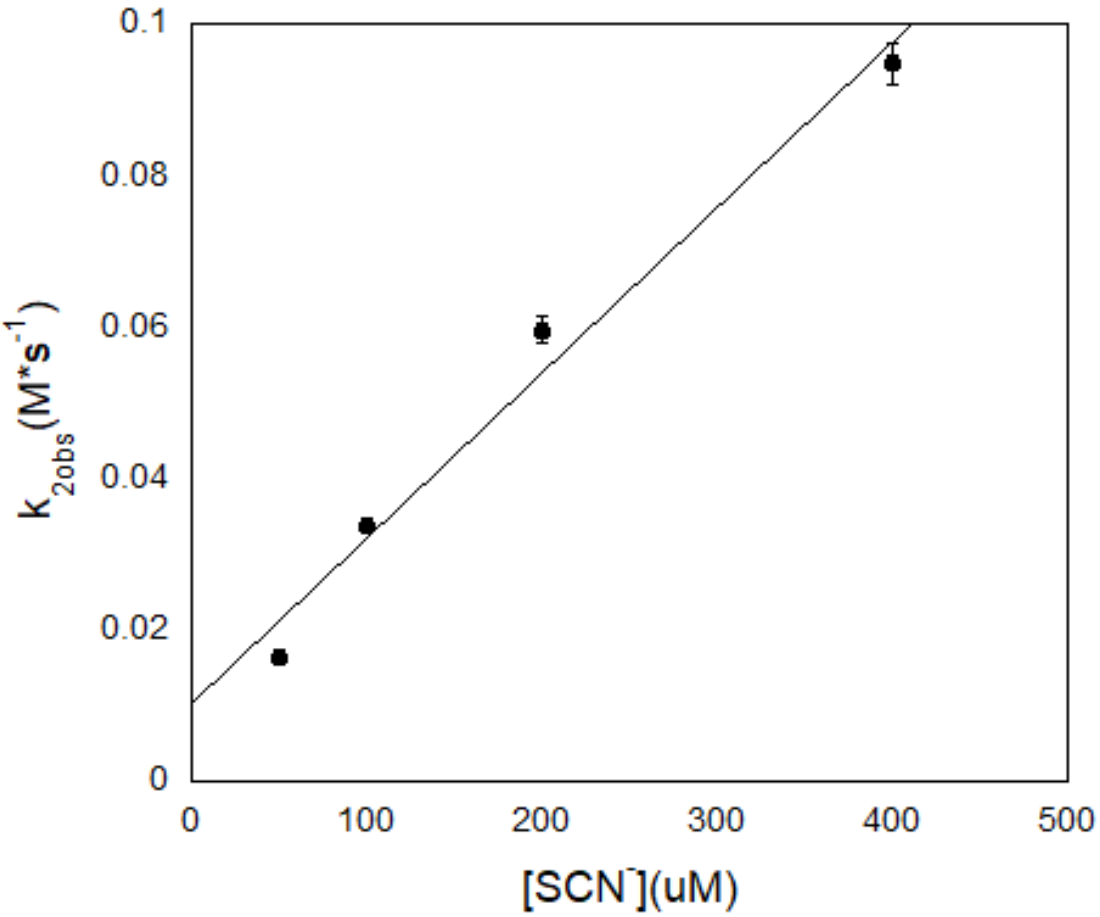

Figure 3.19 - Effect of varying [SCN^-] on the rate of the steady-state reaction during the lactoperoxidase-catalyzed oxidation of SCN^- by H_2O_2. Post-mixing concentrations were [LPO] = 0.1 uM, [H_2O_2] = 40 uM, [TNB] = 100 uM, and [SCN^-] = 50, 100, 200, and 400 uM. The estimated error shown by the error bars for the individual rate constants is for a least-squares fit of an average of five kinetic traces and has been multiplied by a factor of 10 so that the error bars would be visible on the plot.

3.5.2 Effect of Varying Hydrogen Peroxide Concentrations on the Lactoperoxidase-Catalyzed Oxidation of Pseudohalide by Hydrogen Peroxide Under Conditions of Low Pseudohalide Concentration

The lactoperoxidase-catalyzed oxidation of PsX^- by H_2O_2 under conditions of low $[PsX^-]$ was observed as a function of $[H_2O_2]$ to determine the effects on the reaction rates. Figure 3.20 shows the kinetic traces of the reactions at varying concentrations of $[H_2O_2]$. It should be noted that H_2O_2 is the limiting reagent in these experiments, so the production of $OSCN^-$ is proportional to $[H_2O_2]$.

The first step of the biphasic reaction, which represents the pre-steady-state reaction, exhibits a first-order dependency on $[H_2O_2]$ under the H_2O_2 concentration conditions which could be observed experimentally. Experimentally, the concentration of H_2O_2 was limited to approximately 5-50 uM due to the concentration changes that could be accurately observed spectrophotometrically using the TNB assay. The first-order dependency of the pre-steady-state reaction on $[H_2O_2]$ is shown by the linearity of the observed first-order rate constants as a function of $[H_2O_2]$ in Figure 3.22.

The number of enzyme turnovers occurring during the pre-steady-state reaction increases only slightly with increasing $[H_2O_2]$ and eventually, at sufficiently high $[H_2O_2]$, the number of enzyme turnovers that occur during the pre-steady-state reaction remain constant, Figure 3.21. The dependence of the rate of the pre-steady-state reaction on $[H_2O_2]$ indicates H_2O_2 is involved directly in the pre-steady-state reaction but does not affect the rate of the turnover limiting step that produces the hypo(pseudo)halite.

The rate of the steady-state reaction is largely independent of $[H_2O_2]$, Table 15. The slight variation in the observed rate constants for the steady-state reaction at low $[H_2O_2]$ is

due to the decrease in the linear portion of the reaction as can be observed by comparing traces B and C in Figure 3.20. This decreased accuracy in fitting the steady-state reaction is reflected in the increased error of the individual fits as [H_2O_2] is decreased, Table 15. The independence of the rate of the steady-state reaction on [H_2O_2] indicates, either, that H_2O_2 is not directly involved in the reaction represented by the steady-state kinetics or that the rate of enzyme turnover governs the rate of this reaction and steady-state active enzyme concentration is independent of [H_2O_2].

In addition to concentration-dependence studies, the effect that order of mixing of LPO, PsX^-, and H_2O_2 has on the reaction kinetics was also observed. For most experiments conducted to observe the LPO-catalyzed oxidation of PsX^- by H_2O_2, LPO and PsX^- were mixed by hand, then this solution was mixed with H_2O_2 in a single mixing stopped-flow experiment. The reactions observed when this mixing order was used were biphasic as seen in Figure 3.23. This mixing order was used to protect the enzyme from permanent inactivation by H_2O_2.[76] However, to test the hypothesis that the reaction of LPO with H_2O_2 reversibly produces an inactive form of the enzyme, H_2O_2 was reacted with LPO to produce this inactive species in the first mixing step of a double mixing stopped-flow experiment. After an age time of one second PsX^- was mixed with the oxidized LPO species to determine if the pre-steady-state reaction could still be observed. When LPO was reacted with H_2O_2 prior to mixing with PsX^- the pre-equilibrium could no longer be observed indicating that an inactive enzyme species was reversibly produced by the reaction of LPO with H_2O_2 in the first mixing cycle, Figure 3.24.

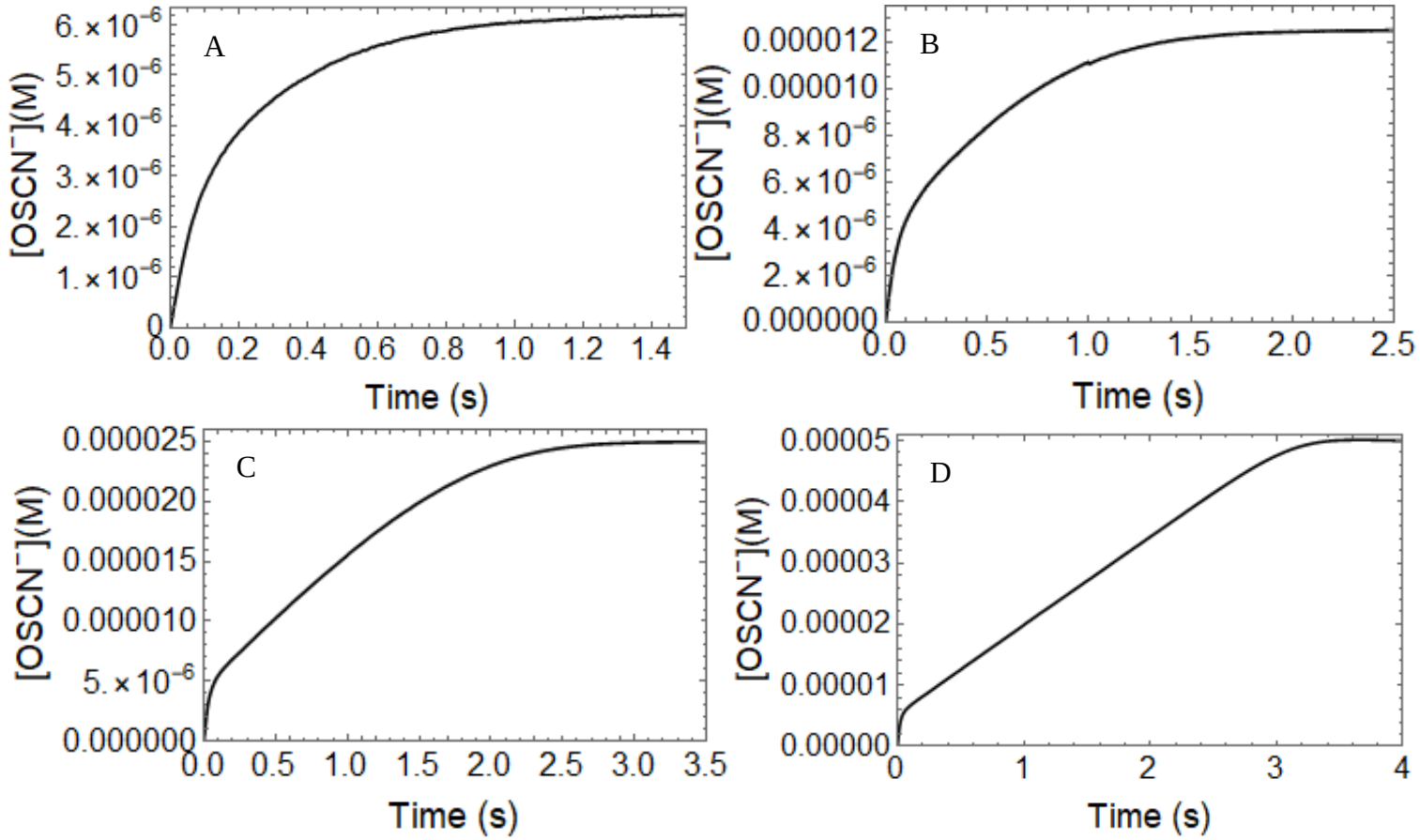

Figure 3.20 - Kinetic traces of the LPO-catalyzed oxidation of SCN^- by H_2O_2 as [H_2O_2] was varied. Post-mixing concentrations were [LPO] = 0.5 uM, [SCN^-] = 100 uM, [TNB] = 100 uM, and [H_2O_2] = 6.25, 12.5, 25, and 50 uM for A, B, C, and D, respectively. The change in scale of the y-axis due to varying [H_2O_2] should be noted.

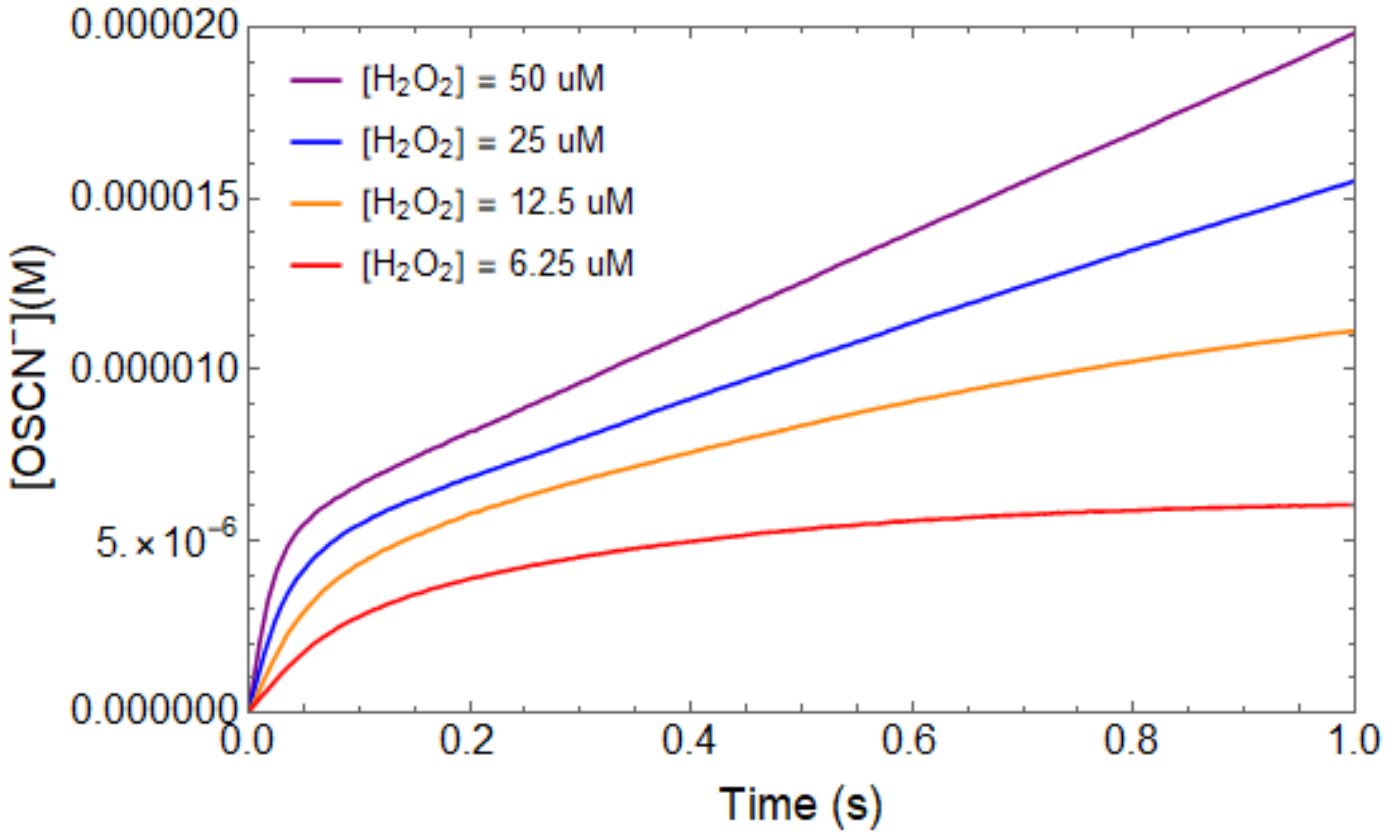

Figure 3.21 - Kinetic traces of the pre-steady-state reaction observed during the LPO-catalyzed oxidation of SCN^- by H_2O_2 as $[H_2O_2]$ was varied. Post-mixing concentrations were $[SCN^-]$ = 100 uM, [LPO] = 0.5 uM, [TNB] = 100 uM, and $[H_2O_2]$ = 6.25, 25, 12.5, and 6.25 uM.

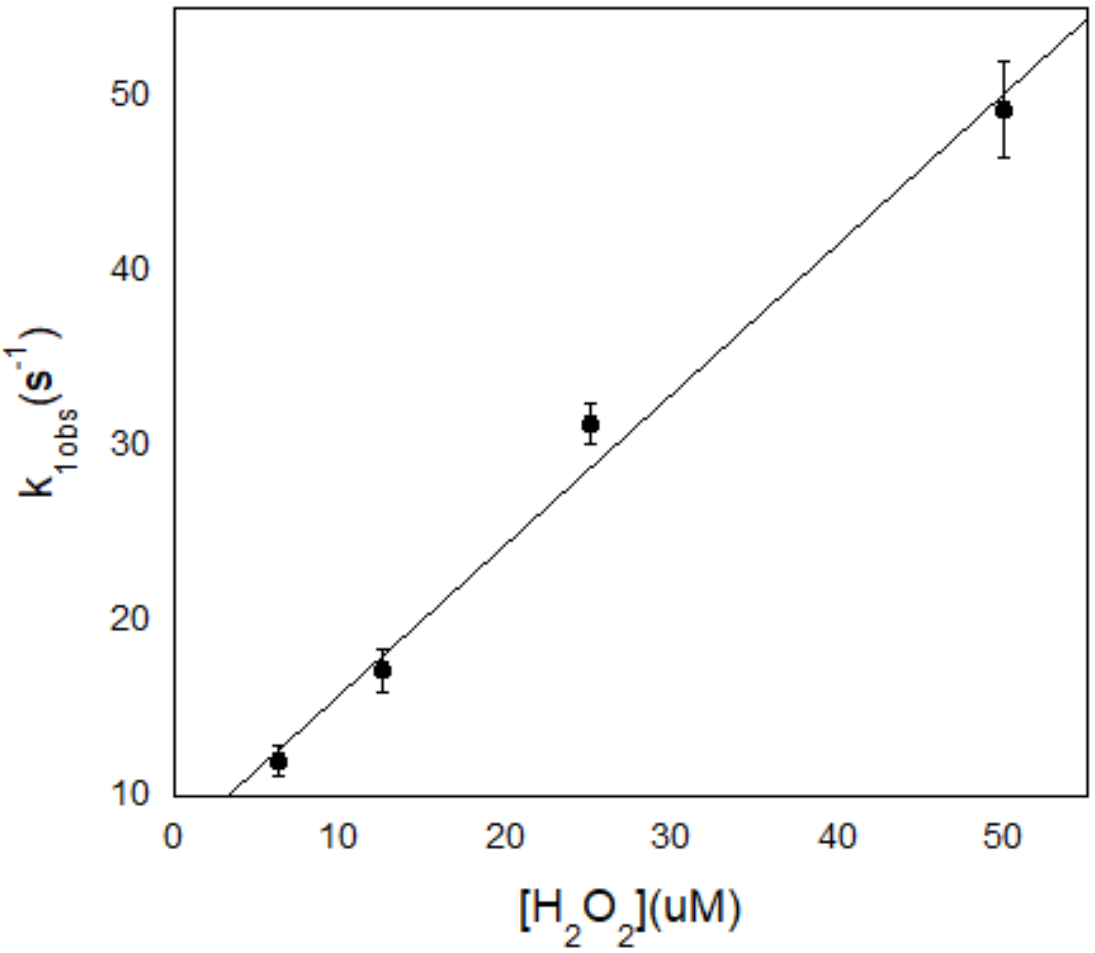

Figure 3.22 - Effect of $[H_2O_2]$ on k_{1obs} for the LPO-catalyzed oxidation of SCN^- by H_2O_2 under conditions of low concentration of $[SCN^-]$. Post-mixing concentrations were [LPO] = 0.5 uM, $[SCN^-]$ = 100 uM, [TNB] = 100 uM, and $[H_2O_2]$ = 6.25, 12.5, 25, and 50 uM. The estimated error shown by the error bars for the individual rate constants is for a least-squares fit of an average of five kinetic traces and has been multiplied by a factor of 10 so that the error bars would be visible on the plot.

Table 15 - Effect of varying [H_2O_2] on the rate of the steady-state reaction of the LPO-catalyzed oxidation of SCN^- by H_2O_2

[H_2O_2](uM)	**k_{2obs} ($M \cdot s^{-1}$)**
5	0.0212(1)
10	0.0284(1)
20	0.03210(6)
40	0.03290(6)
Average	0.028(5)

[a]The post-mixing concentrations were [LPO] = 0.1 uM, [SCN^-] = 100 uM, [TNB] = 100 uM, and [H_2O_2] = 5, 10, 20, and 40 uM.

[b]The estimated error, given by the parenthetical digits, for the individual rate constants is for a least-squares fit of an average of five kinetic traces.

[c]The average error of the model predicted rate constants was determined by the standard deviation of the individual fits.

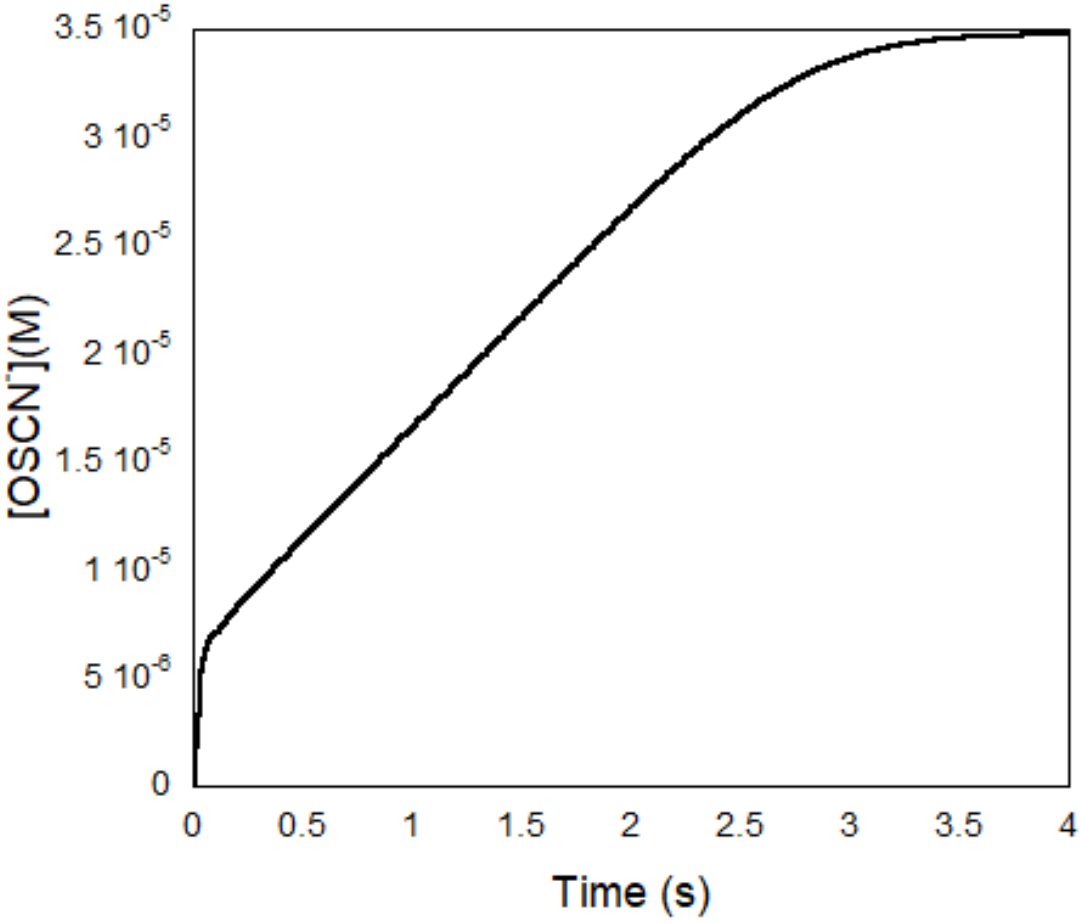

Figure 3.23 - Kinetic trace of the LPO-catalyzed oxidation of SCN^- by H_2O_2 under conditions of low concentration of [SCN^-] with LPO/SCN^- pre-equilibrium prior to mixing with H_2O_2. Post-mixing concentrations were [LPO] = 1 uM, [SCN^-] = 100 uM, [H_2O_2] = 40 uM, and [TNB] = 100 uM.

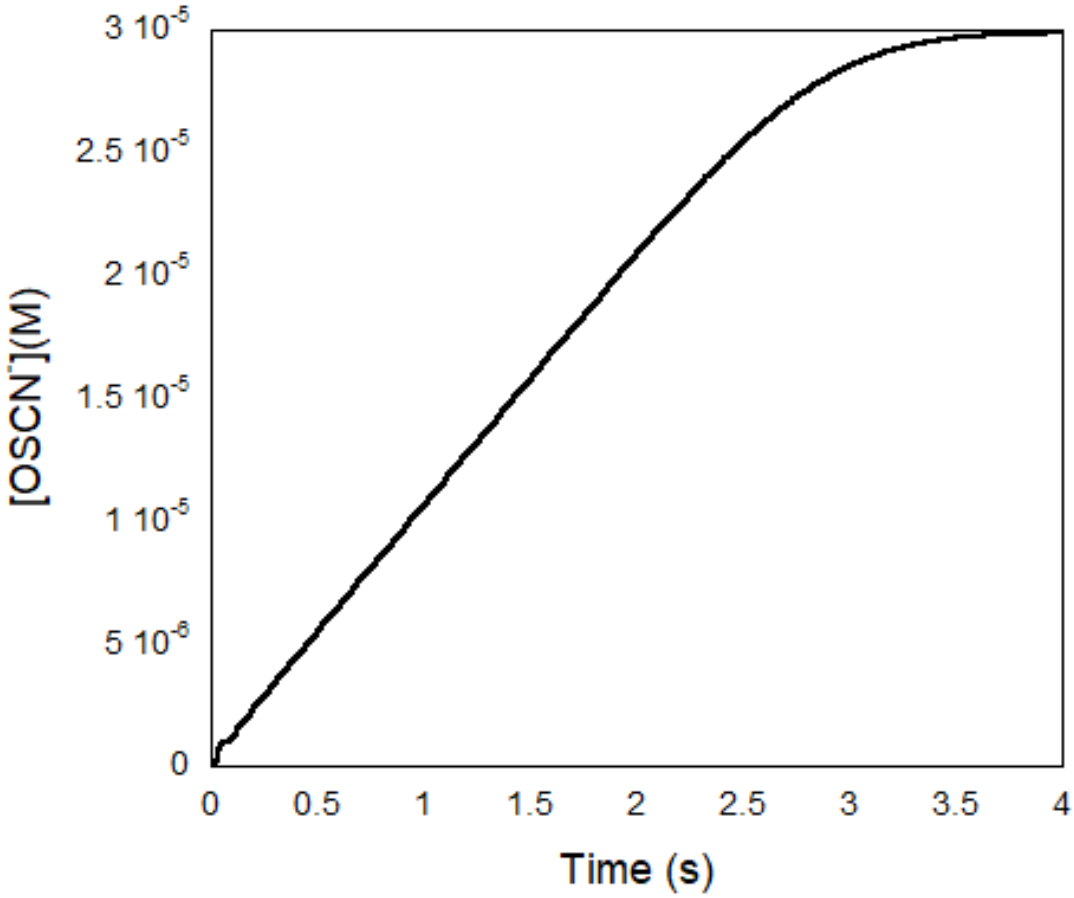

Figure 3.24 - Kinetic trace of the LPO-catalyzed oxidation of SCN^- by H_2O_2 under conditions of low concentration of [SCN^-] without LPO/SCN^- pre-equilibrium. H_2O_2 was reacted with LPO in the first step of a double mixing experiment. SCN^- was introduced in the second mixing cycle. Post-mixing concentrations were [LPO] = 1 uM, [SCN^-] = 100 uM, [H_2O_2] = 40 uM, and [TNB] = 100 uM. The age time was one second.

3.5.3 Effect of Varying Lactoperoxidase Concentration on the Lactoperoxidase-Catalyzed Oxidation of Pseudohalide by Hydrogen Peroxide Under Conditions of Low Pseudohalide Concentration

The lactoperoxidase-catalyzed oxidation of PsX^- by H_2O_2 under conditions of low [PsX^-] was observed as a function of [LPO] to determine the effects on the reaction rates. Figure 3.25 shows the kinetic traces of the reaction at varying concentrations of [LPO]. The kinetics of the steady-state reaction act predictably as [LPO] is varied for a catalysis reaction with a first-order dependence on [LPO] for the observed rate constant, Figure 3.27. However, when the data is fit to a simple biphasic kinetic model the observed rate constant of the pre-steady-state reaction is independent of [LPO], Table 16.

Additionally, the number of turnovers that occur during the pre-steady-state reaction increases with increasing [LPO], Figure 3.26. This indicates that increasing [LPO] increases the rate of turnover but has no effect on the observed rate constant of the inhibitory reaction which results in the pre-steady-state reaction, Figure 3.26. This would occur if the inhibitory reaction were not catalytic in nature, but rather pseudo-first-order in SCN^- or H_2O_2 with respect to LPO.

Given the first-order rate dependency of the observed rate constant for the pre-steady-state reaction on [H_2O_2] as discussed in section 3.5.2, it can be concluded that H_2O_2 reacts with LPO to inhibit the rate of LPO turnover. It may achieve this by producing an unproductive, or less productive, form of the enzyme in a reversible reaction.

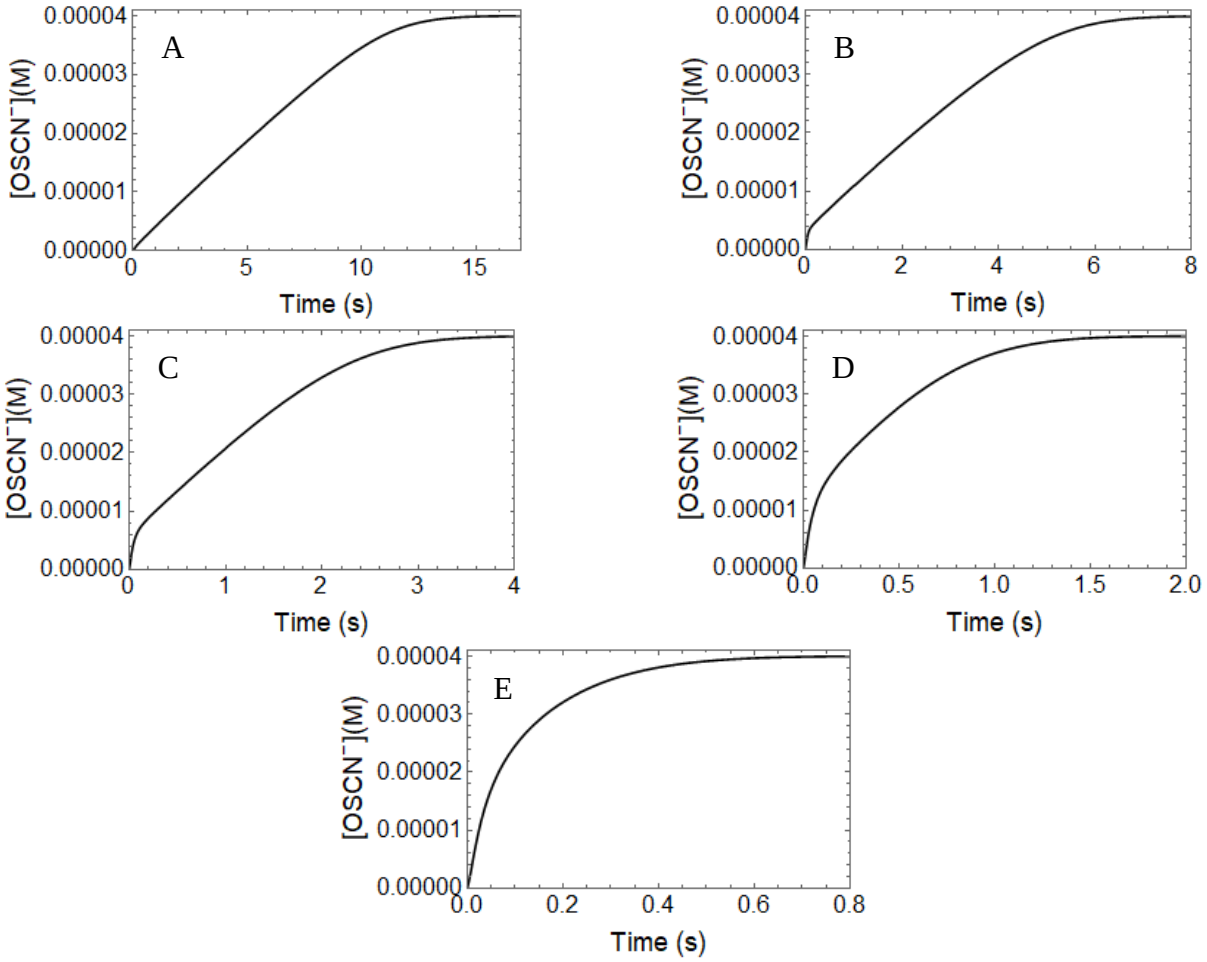

Figure 3.25 - Kinetic traces of the LPO-catalyzed oxidation of SCN^- by H_2O_2 as [LPO] is varied. Post-mixing concentrations were [SCN^-] = 200 uM, [H_2O_2] = 40 uM, [TNB] = 100 uM, and [LPO] = 0.125, 0.25, 0.5, 1, and 2 uM for A, B, C, D, and E, respectively.

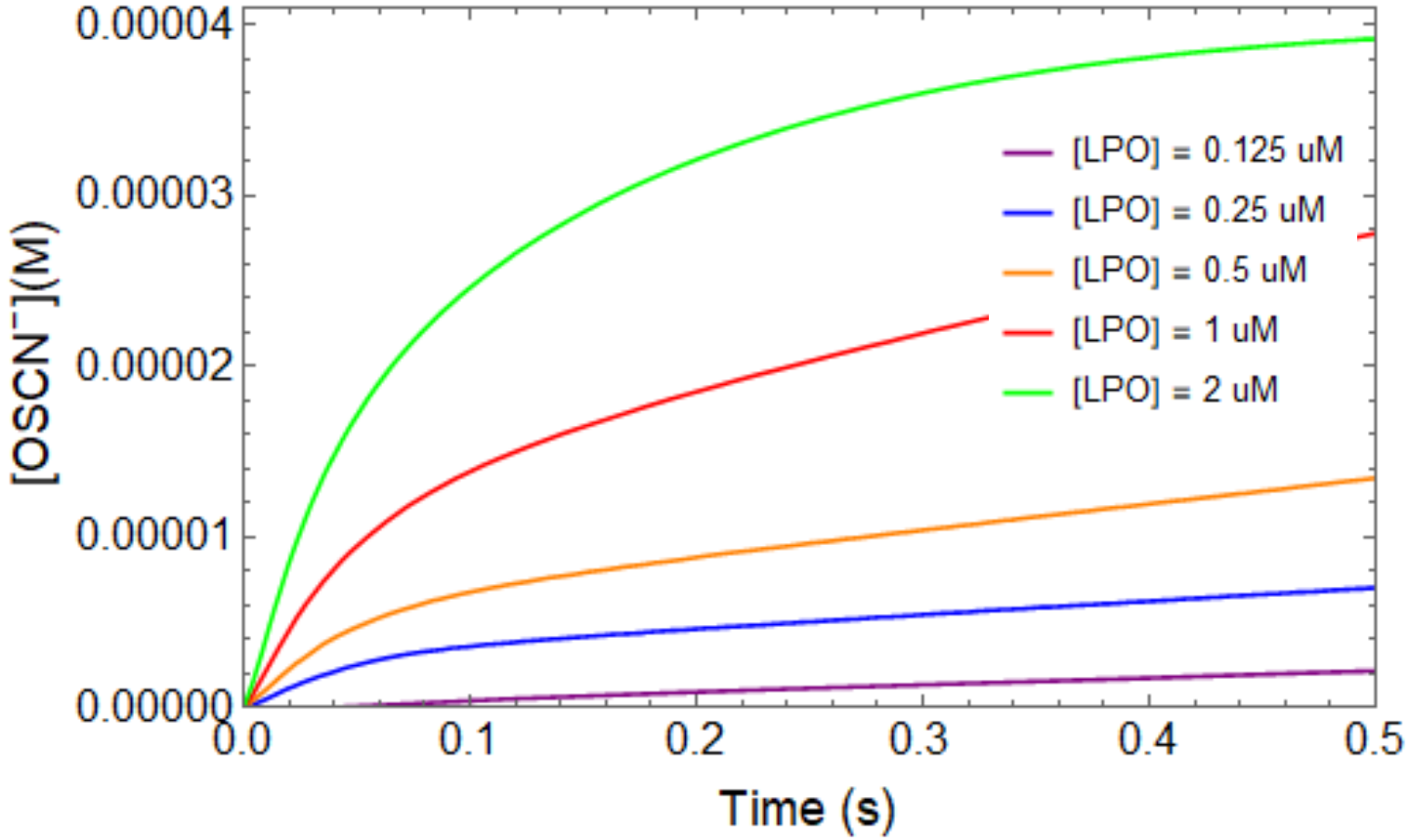

Figure 3.26 - Kinetic traces of pre-steady-state reaction of the LPO-catalyzed oxidation of SCN^- by H_2O_2 as [LPO] is varied. Post-mixing concentrations were [SCN^-] = 200 uM, [H_2O_2] = 40 uM, [TNB] = 100 uM, and [LPO] = 0.125-2 uM.

Table 16 - Effect of varying [LPO] on the rate of the pre-steady-state reaction for the LPO-catalyzed oxidation of SCN^- by H_2O_2.

[LPO](uM)	**$k_{1obs}(s^{-1})$**
0.25	23.5(1)
0.5	23.07(9)
1	20.7(1)
Average	22(2)

[a]Post-mixing concentrations were [SCN^-] = 200 uM, [H_2O_2] = 40 uM, [TNB] = 100 uM, and [LPO] = 0.25, 0.5, and 1 uM.

[b]The estimated error, given by the parenthetical digits, for the individual rate constants is for a least-squares fit of an average of five kinetic traces.

[c]The average error was calculated by the standard deviation of the individual fits.

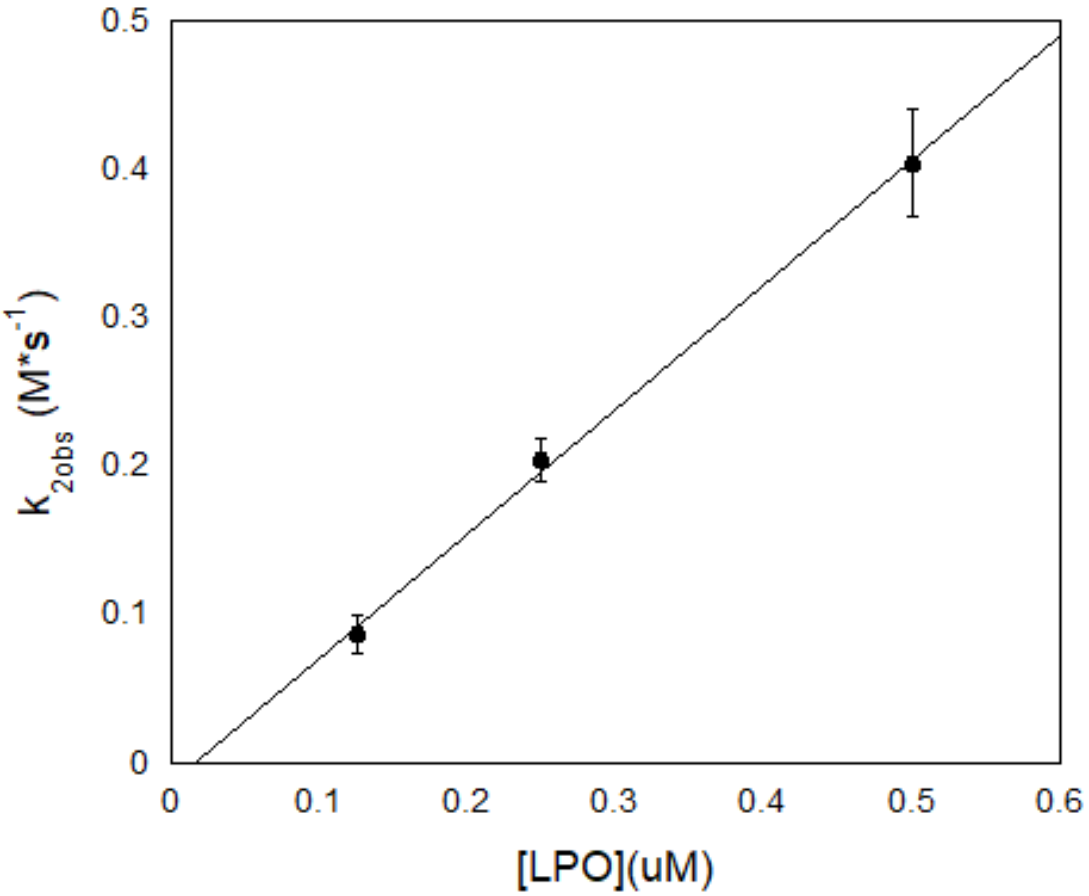

Figure 3.27 - Steady-state reaction rate dependence on [LPO] for the LPO-catalyzed oxidation of SCN^- by H_2O_2. Post-mixing concentrations were [SCN^-] = 200 uM, [H_2O_2] = 40 uM, [TNB] = 100 uM, and [LPO] = 0.125, 0.25, and 0.5 uM. The estimated error shown by the error bars for the individual rate constants is for a least-squares fit of an average of five kinetic traces and has been multiplied by a factor of 10 so that the error bars would be visible on the plot.

3.6 Proposed Mechanism and Fitted Data of the Lactoperoxidase-Catalyzed Oxidation of Halides and Pseduohalides - Ordered Sequential Mechanism and Hydrogen Peroxide Tight Binding Inhibition

A new mechanism is proposed here which explains the kinetics observed for the LPO-catalyzed oxidation of X^- by H_2O_2 at low concentration of X^-, Figure 3.28. This model depicts an ordered sequential mechanism with tight binding inhibition by hydrogen peroxide. The first productive step of the reaction is the reversible binding of LPO and X^- to produce LPOX. This bound species then reacts irreversibly in the turnover-limiting step with H_2O_2 to produce native LPO and the hypo(pseudo)halous acid or hypo(pseudo)halite, HOX/OX^-, referred to hereafter as OX^-. H_2O_2 acts as a tight binding inhibitor by reacting reversibly with native LPO to produce an oxidized species referred to in this model as LPO-H_2O_2. It is important to note that this LPO-H_2O_2 bound species is not equivalent to LPO compound I as the production of compound I is not considered to be reversible. This model differs from the literature model given in Equations 3.2.5 and 3.2.6 by the order in which the oxidizing and reducing substrates bind or react with LPO in the ordered sequential mechanism as well as the action of the H_2O_2 as a tight binding inhibitor.

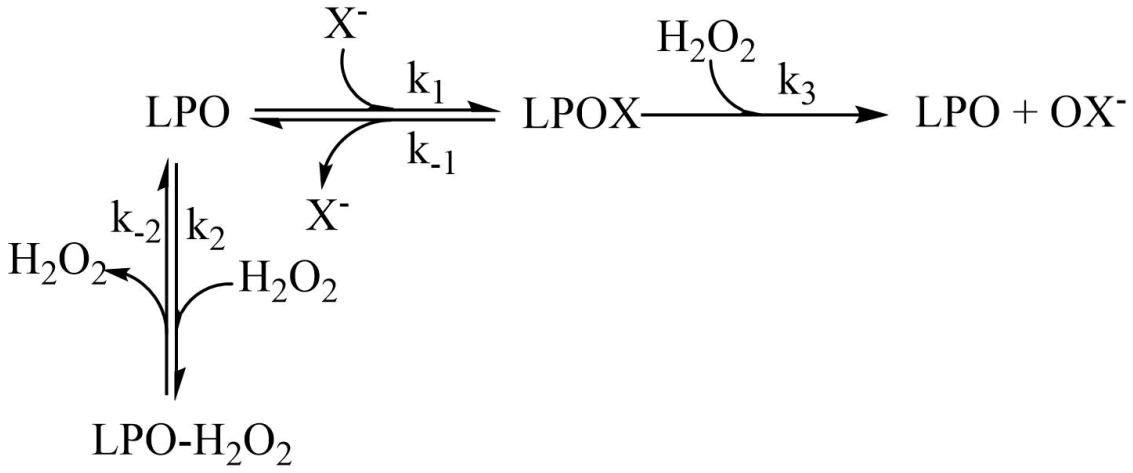

Figure 3.28 - Proposed mechanism for the LPO-catalyzed oxidation of X^- by H_2O_2.

3.6.1 Model of the Proposed Mechanism of the Lactoperoxidase-Catalyzed Oxidation of Halides - Ordered Sequential Mechanism and Hydrogen Peroxide Tight Binding Inhibition

A Mathematica model was made of the proposed mechanism given in Figure 3.28 for the lactoperoxidase-catalyzed oxidation of X^- by H_2O_2. For this model to reflect the biphasic kinetics observed experimentally the following conditions must be met: (1) the binding equilibrium for LPO and X^- must not be rate-limiting and lie toward the bound species, ($k_1 > k_3$) and ($k_1 >> k_{-1}$); (2) the reaction of LPO with H_2O_2 to form the unproductive LPO-H_2O_2 species must be competitive with the reaction of LPOX with H_2O_2 ($k_2 \approx k_3$); and (3) the equilibrium which produces the unproductive LPO-H_2O_2 species must lie toward the oxidized species ($k_2 >> k_{-2}$). Under these three conditions, the proposed mechanism explains what is observed experimentally and presented in section 3.5.

It is, again, important to note that the model was built to maintain a constant $[X^-]$ under conditions of both high and low $[X^-]$ due to the use of the TNB assay which produces X^- as discussed in section 2.3.1. The Mathematica code used to model the proposed reaction mechanism in given in section 5.3.5. In fact, so long as $[X^-]$ is kept under pseudo-first-order reaction conditions with respect to LPO, the $[X^-]$ can be considered constant.

The concentration of the various enzyme species during the pre-steady-state and steady-state phases of the reaction under low and high concentrations of X^- is critical in understanding the cause of the pre-steady-state reaction and effect of this reaction on the kinetic traces. Under conditions of high $[X^-]$, LPOX is produced rapidly and remains the primary enzyme species throughout the reaction, Figure 3.29. As a result, the reaction observed under conditions of high $[X^-]$ is first-order with the turnover-limiting step being the reaction of LPOX with H_2O_2, Figure 3.30.

When $[X^-]$ is low the rapid equilibrium of binding of native LPO and X^- causes the fast production of the active LPOX species. The competitive rate of k_2 and k_3 as well as the tight binding of H_2O_2 to native LPO causes a relatively slow conversion from LPOX as the primary enzyme species to the unproductive species LPO-H_2O_2, Figure 3.31. As LPOX is the productive enzyme species in the turnover limiting step, the enzyme becoming tied up as the unproductive species LPO-H_2O_2 causes a decrease in the rate of OX^- production, Figure 3.32. After steady-state concentrations have been reached, the reaction becomes zeroth-order, Figure 3.34. During the steady-state reaction the concentration of the unproductive enzyme species, LPO-H_2O_2, slowly decreases and is replaced by the X^- bound species, LPOX, until H_2O_2 has been depleted, the reaction is complete, and LPOX becomes the primary enzyme species, Figure 3.33.

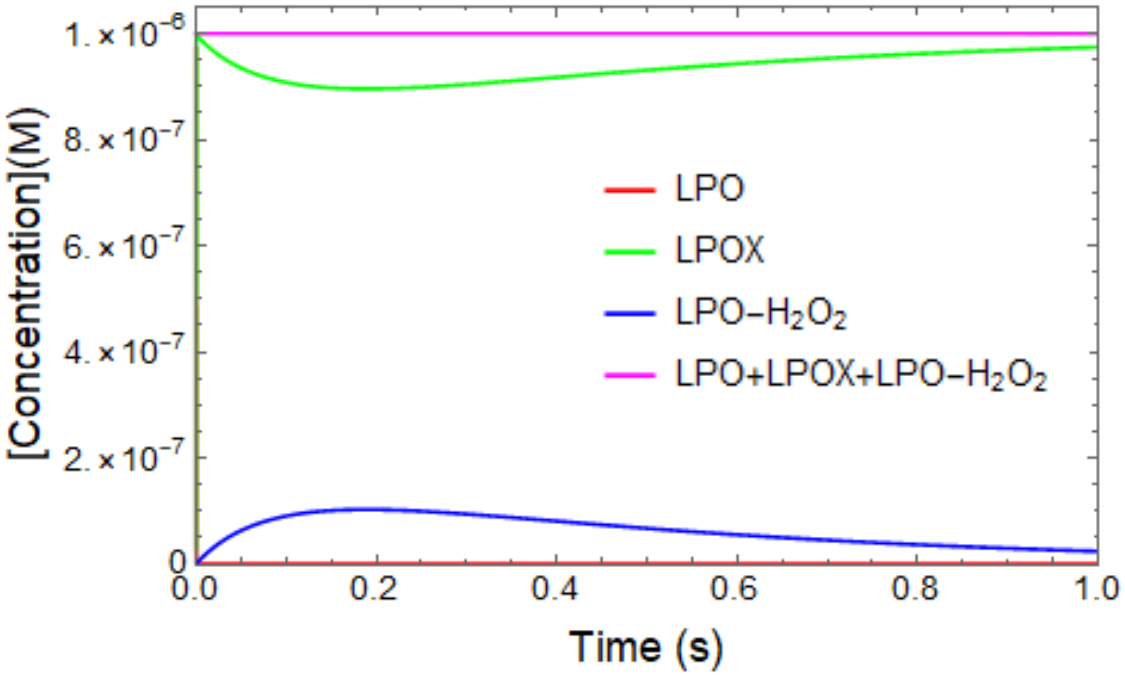

Figure 3.29 – Simulated enzyme species concentrations during the LPO-catalyzed oxidation of X^- by H_2O_2 for the proposed mechanism under high [X^-] conditions.

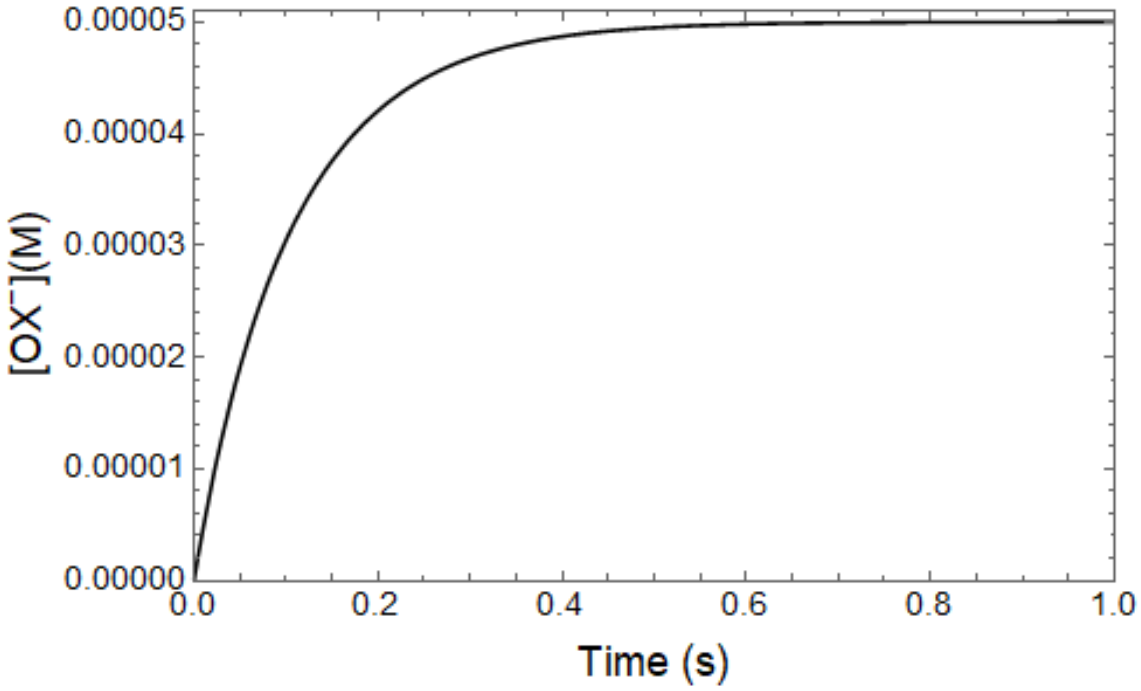

Figure 3.30 – Simulated trace of [OX^-] for the proposed mechanism for the LPO-catalyzed oxidation of X^- by H_2O_2 under conditions of high [X^-].

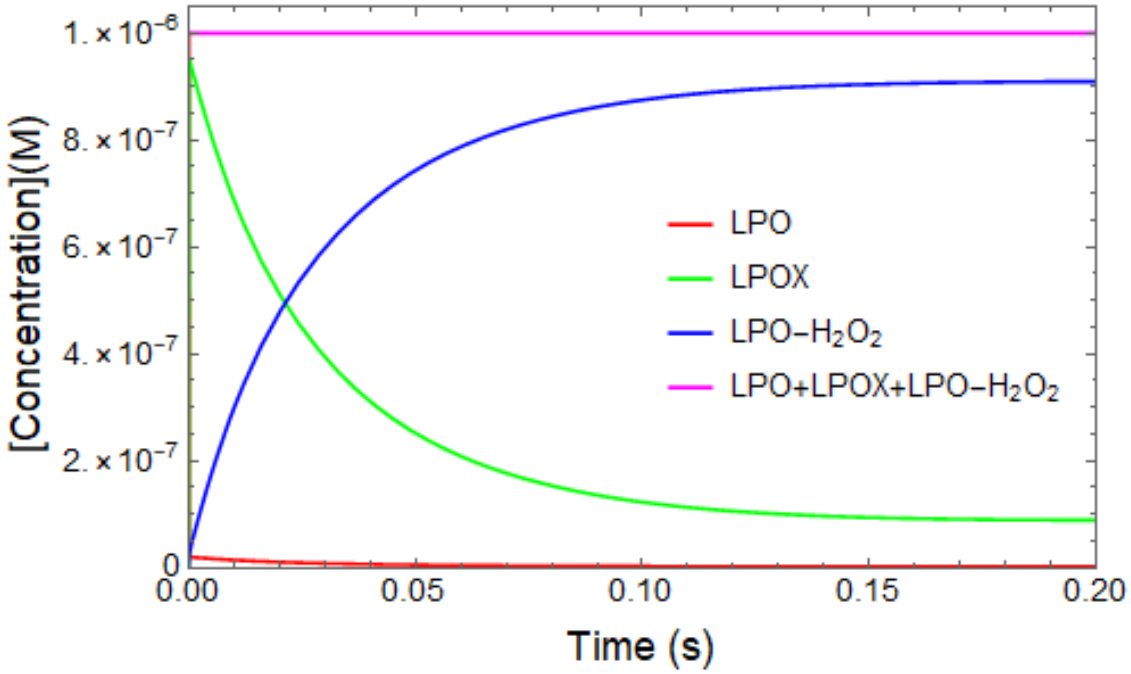

Figure 3.31 – Simulated enzyme species concentrations during the pre-steady-state reaction for the proposed mechanism for the LPO-catalyzed oxidation of X^- by H_2O_2 under conditions of low $[X^-]$.

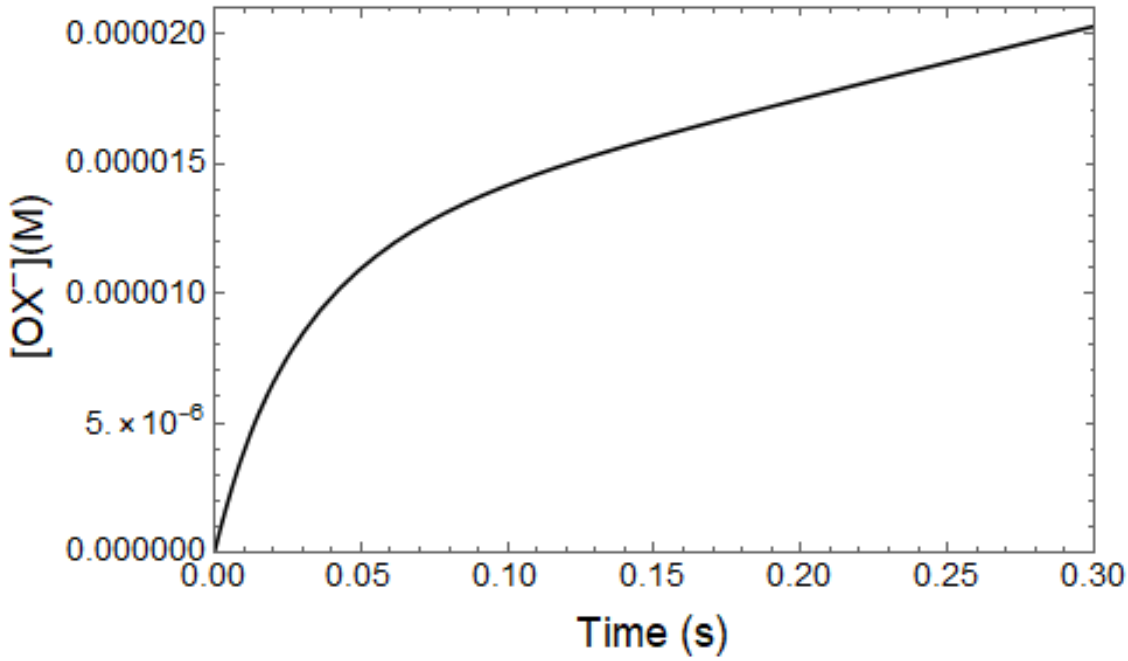

Figure 3.32 – Simulated trace of [OX^-] during the pre-steady-state reaction for the proposed mechanism for the LPO-catalyzed oxidation of X^- by H_2O_2 under conditions of low [X^-].

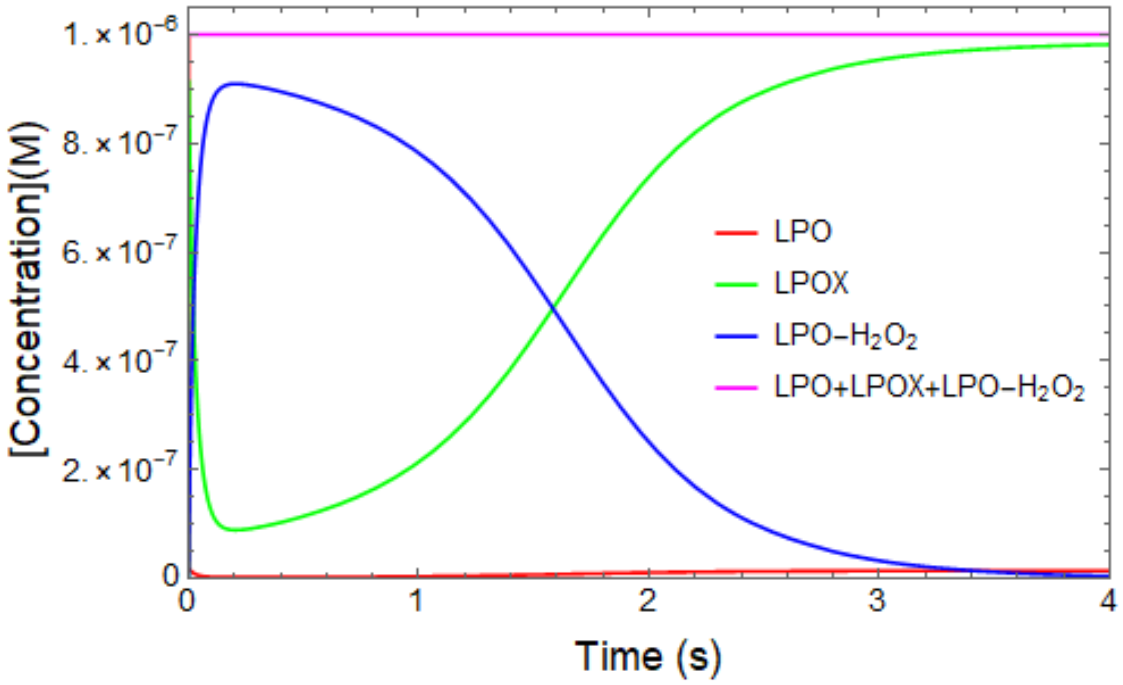

Figure 3.33 - Simulated enzyme concentrations during the reaction for the proposed mechanism for the LPO-catalyzed oxidation of X^- by H_2O_2 under conditions of low $[X^-]$.

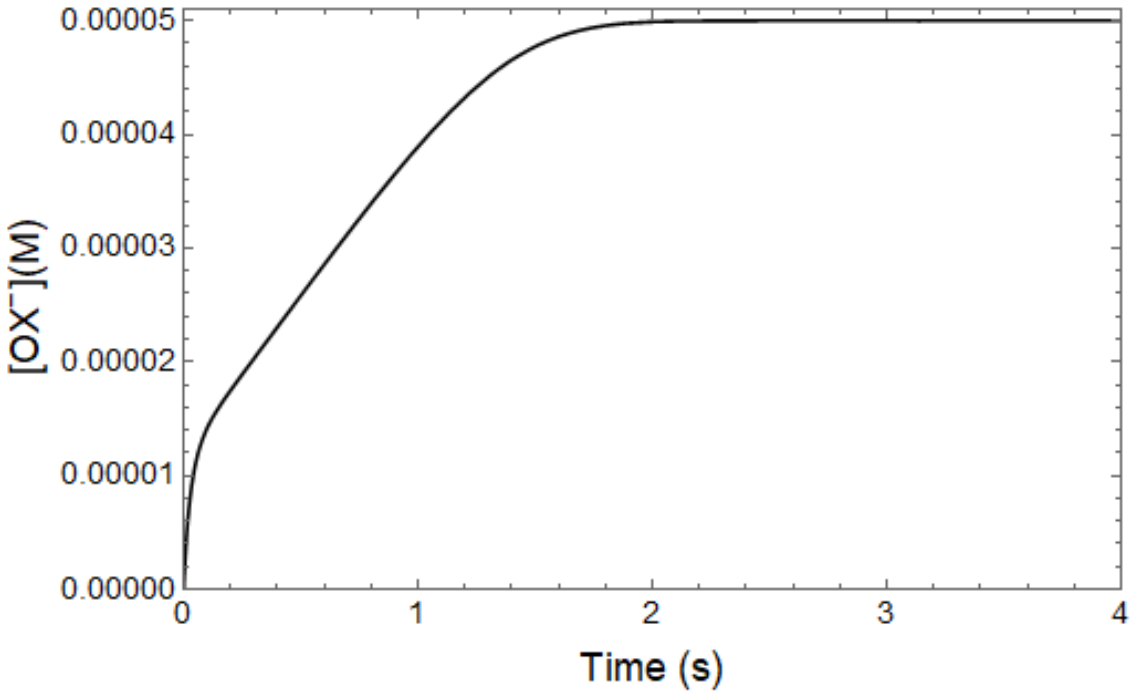

Figure 3.34 – Simulated trace of [OX^-] during the reaction for the proposed mechanism for the LPO-catalyzed oxidation of X^- by H_2O_2 under conditions of low [X^-].

A Mathematica model of the proposed mechanism of the lactoperoxidase-catalyzed oxidation of X^- by H_2O_2, Figure 3.28, was used to fit experimental data and to calculate the rate constants. The data for which the pre-steady-state reactions were well resolved from the steady-state reactions, as in traces A and B in Figure 3.35, were easily fit by the model and all the rate constants were fit simultaneously.

However, the rate constants for the data in which the pre-steady-state and steady-state reactions were not well resolved, as in trace C in Figure 3.35, could not be fit simultaneously. In these cases, rate constants which were not primary to the observed kinetics were fixed so that the rate constants related to the reactions which were able to be

clearly observed could be calculated, Tables 19-22. Kinetic fits can be seen in Figures 3.35-3.38.

Tables 17 and 18 show the average calculated rate constants for the model proposed in Figure 3.28 for SCN^- and $SeCN^-$, respectively. The predictions made concerning the relative magnitudes of the rate constants appear to be correct, i.e. ($k_1 > k_3$), ($k_1 >> k_{-1}$), ($k_2 \approx k_3$), and ($k_2 >> k_{-2}$). The rate constant k_1 is diffusion-controlled for both substrates. Furthermore, the rate constant k_{-1} was smaller for $SeCN^-$ than for SCN^-. This indicates that $SeCN^-$ binds more tightly to LPO than SCN^-. Rate constants k_2, k_{-2}, and k_3 are similar for SCN^- and $SeCN^-$, which is expected given that X^- is not involved in these steps.

Table 17 - Average rate constants for the proposed model of the LPO-catalyzed oxidation of [SCN^-] by H_2O_2

Rate Constant	Calculated Constants
$\mathbf{k_1}$	$1.4(2)\times10^9\ M^{-1}s^{-1}$
$\mathbf{k_{-1}}$	$3.94(5)\times10^3\ s^{-1}$
$\mathbf{k_2}$	$3(1)\times10^7\ M^{-1}s^{-1}$
$\mathbf{k_{-2}}$	$1.9(4)\ s^{-1}$
$\mathbf{k_3}$	$1.0(3)\times10^7\ M^{-1}s^{-1}$

[a]Calculated from Tables 19-21 for the proposed model of the LPO-catalyzed oxidation of [SCN^-] by H_2O_2.

[b]The average error given by the parenthetical digits were calculated by the standard deviation of the individual fits.

Table 18 - Average rate constants for the proposed model of the LPO-catalyzed oxidation of [$SeCN^-$] by H_2O_2

Rate Constant	Calculated Constants
$\mathbf{k_1}$	$1.250(7)x10^9\ M^{-1}s^{-1}$
$\mathbf{k_{-1}}$	$1.0(1)\ x10^3\ s^{-1}$
$\mathbf{k_2}$	$2.7(1)\ x10^7\ M^{-1}s^{-1}$
$\mathbf{k_{-2}}$	$1.5(1)\ s^{-1}$
$\mathbf{k_3}$	$1.2(2)\ x10^7\ M^{-1}s^{-1}$

[a]Average rate constants calculated from Table 22 for the proposed model of the LPO-catalyzed oxidation of [$SeCN^-$] by H_2O_2.

[b]The average error given by the parenthetical digits were calculated by the standard deviation of the individual fits from Table 22.

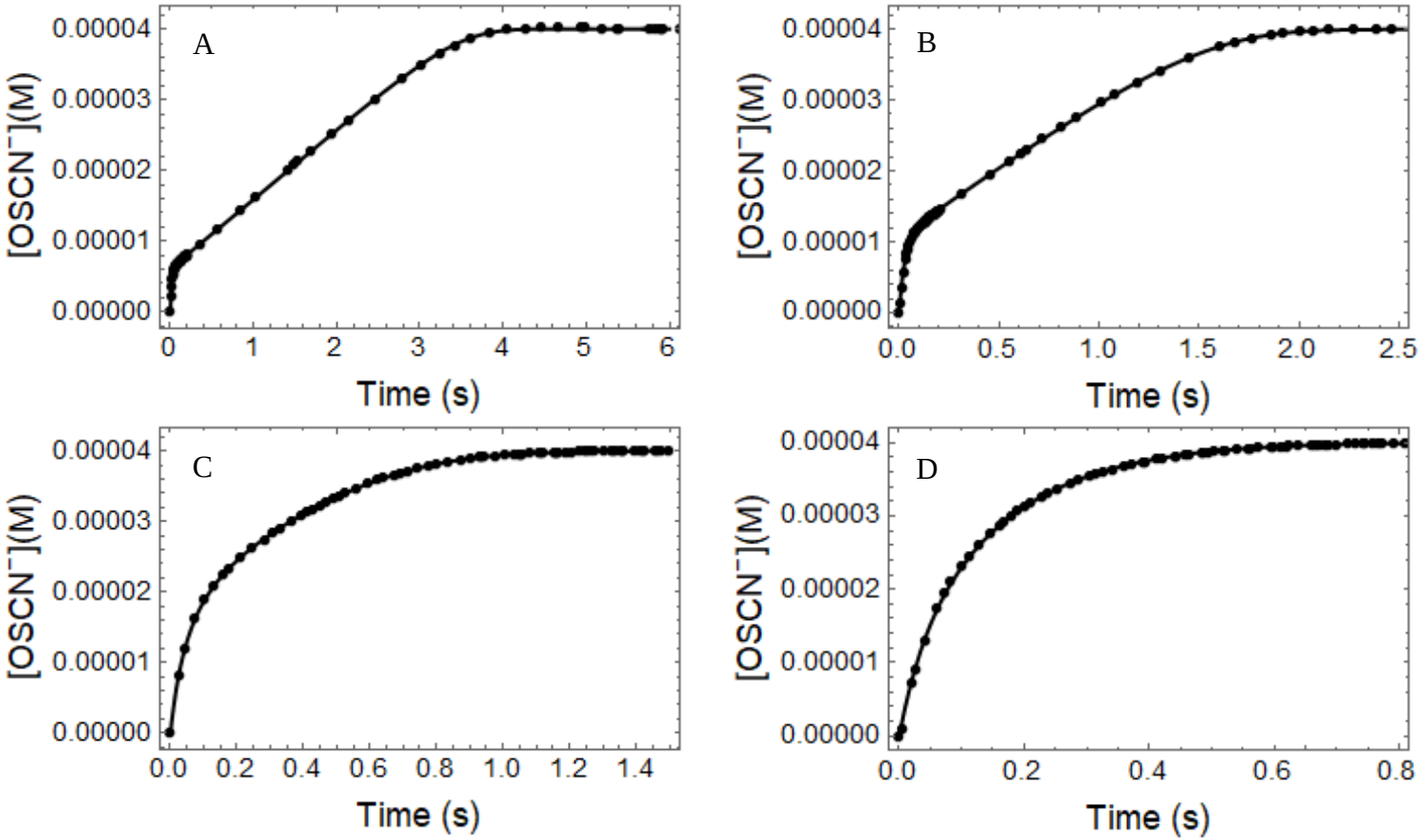

Figure 3.35 - Fitted kinetic traces for the lactoperoxidase-catalyzed oxidation of SCN^- by H_2O_2 as [SCN^-] is varied. The post-mixing concentrations were [LPO] = 1.2 uM, [H2O2] = 40 uM, [TNB] = 100 uM, and [SCN^-] = 53, 106, 213, and 6.25 uM for A, B, C, and, D, respectively. Rate constants produced by these fits are given in Table 19.

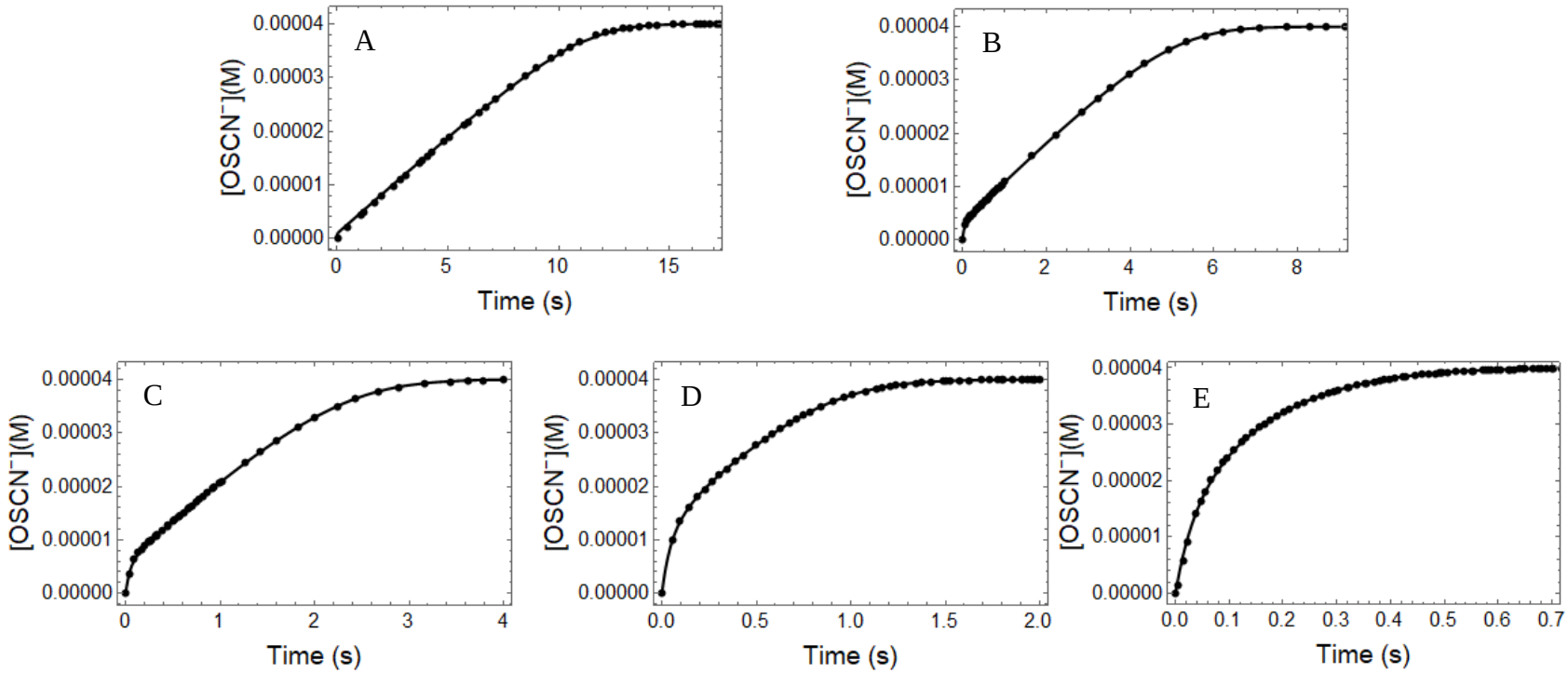

Figure 3.36 - Fitted kinetic traces for the lactoperoxidase-catalyzed oxidation of SCN^- by H_2O_2 as [LPO] was varied. Post-mixing concentrations were [SCN^-] = 200 uM, [H_2O_2] = 40 uM, [TNB] = 100 uM, and [LPO] = 0.125, 0.25, 0.5, 1, and 2 uM for A, B, C, D, and E, respectively. Rate constants produced by these fits are given in Table 20.

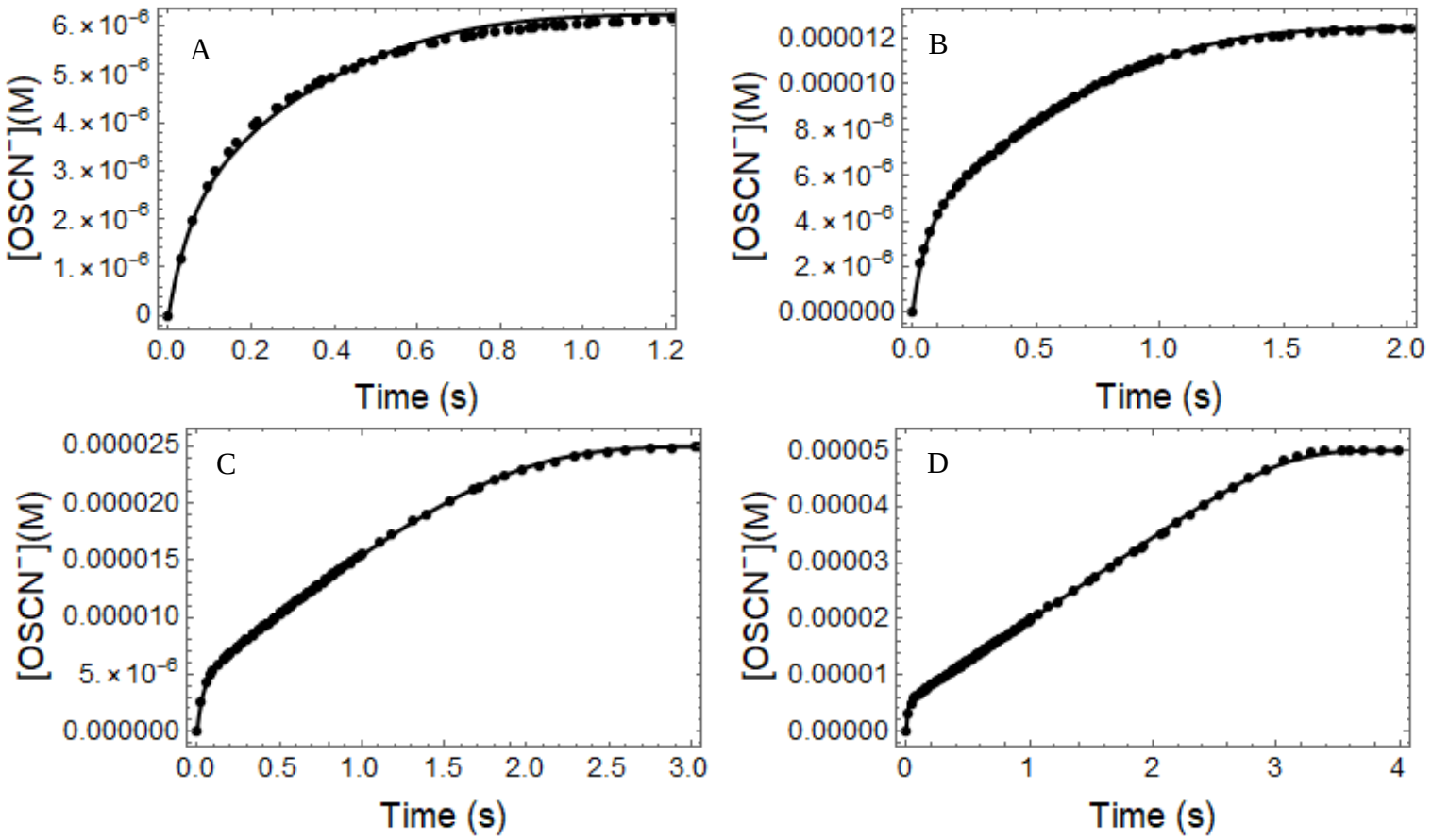

Figure 3.37 - Fitted kinetic traces for the lactoperoxidase-catalyzed oxidation of SCN^- by H_2O_2 as $[H_2O_2]$ was varied. Post-mixing concentrations were [LPO] = 0.5 uM, $[SCN^-]$ = 100 uM, [TNB] = 100 uM, and $[H_2O_2]$ = 6.25, 12.5, 25, and 50 uM for A, B, C, and D, respectively. Rate constants produced by these fits are given in Table 21.

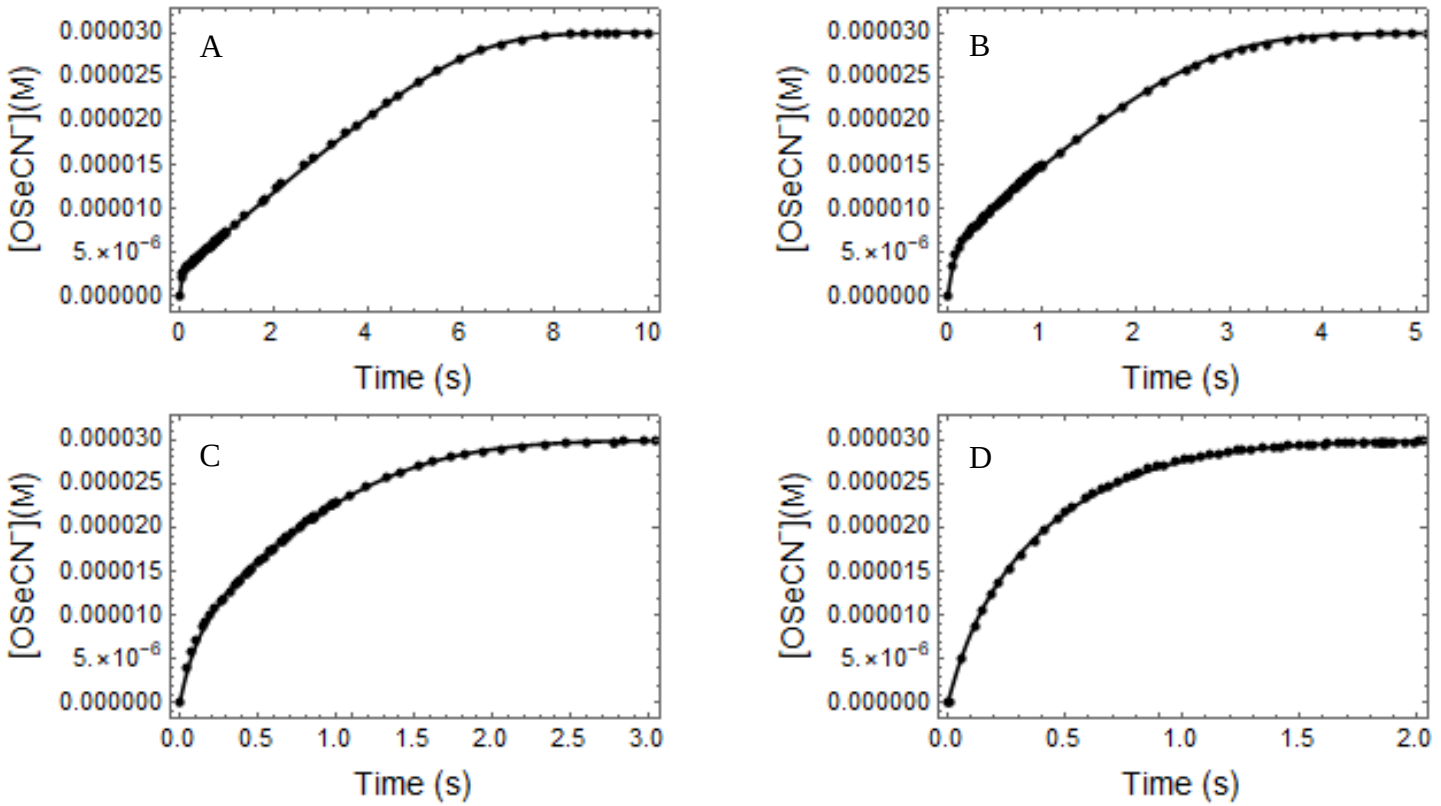

Figure 3.38 - Fitted kinetic traces for the lactoperoxidase-catalyzed oxidation of $SeCN^-$ by H_2O_2 as [$SeCN^-$] was varied. The post-mixing concentrations were [LPO] = 0.24 uM, [H_2O_2] = 30 uM, [TNB] = 100 uM, and [$SeCN^-$] = 42.5, 85, 170, and 340 uM for traces A, B, C, and D, respectively. Rate constants produced by these fits are given in Table 22.

Table 19 - Fitted rate constants for the proposed mechanism of the LPO-catalyzed oxidation of SCN^- by H_2O_2 as [SCN^-] was varied

[SCN^-](uM)	k_1 ($M^{-1}\cdot s^{-1}$)	k_{-1} (s^{-1})	k_2 ($M^{-1}\cdot s^{-1}$)	k_{-2} (s^{-1})	k_3 ($M^{-1}\cdot s^{-1}$)
53	$1.31(7)x10^9$	$4.6(3)x10^3$	$2.23(3)x10^7$	1.556(4)	$8.62(3)x10^6$
106	$1.33(3)x10^9$	$3.9(3)x10^3$	$3.04(1)\ x10^7$	1.760(3)	$9.24(3)x10^6$
213	$1.30\ x10^9$(fixed)	$3.93x10^3$(fixed)	$2.81(2)\ x10^7$	1.68(1)	$9.27(4)x10^6$
425	$1.30x10^9$(fixed)	$3.93x10^3$(fixed)	$2.65(3)\ x10^7$	1.72(fixed)	$9.44(4)\ x10^6$
Average	$1.32(1)x10^9$	$4.3(5)x10^3$	$2.7(3)x10^7$	1.7(1)	$9.1(4)x10^6$

[a]The post-mixing concentrations were [LPO] = 1.2 uM, [H_2O_2] = 40 uM, [TNB] = 100 uM, and [SCN^-] = 53, 106, 213, and 425 uM.*

Table 20 - Fitted rate constants for the proposed mechanism of the LPO-catalyzed oxidation of SCN^- by H_2O_2 as [LPO] was varied

[LPO](uM)	k_1 ($M^{-1}\cdot s^{-1}$)	k_{-1} (s^{-1})	k_2 ($M^{-1}\cdot s^{-1}$)	k_{-2} (s^{-1})	k_3 ($M^{-1}\cdot s^{-1}$)
0.125	$1.20x10^9$(fixed)	$4.20x10^3$	$2.42x10^7$(fixed)	1.98(1)	$7.39(2)x10^6$
0.25	$1.2(2)x10^9$	$4.2(4)x10^3$	$2.5(2)x10^7$	2.17(1)	$7.30(3)x10^6$
0.5	$1.17(2)x10^9$	$4.2(7)x10^3$	$2.5(4)x10^7$	2.35(1)	$7.32(5)x10^6$
1	$1.20x10^9$(fixed)	$4.20x10^3$(fixed)	$2.27(1)x10^7$	2.39(1)	$7.56(2)x10^6$
2	$1.20x10^9$(fixed)	$4.20x10^3$(fixed)	$1.79(1)x10^7$	2.30(fixed)	$7.19(2)x10^6$
Average	$1.20(4)x10^9$	$4.18(3)x10^3$	$2.3(3)x10^7$	2.2(2)	$7.4(1)x10^6$

[a]The post-mixing concentrations were [SCN^-] = 200 uM, [H_2O_2] = 40 uM, [TNB] = 100 uM, and [LPO] = 0.125, 0.25, 0.5, 1, and 2 uM.*

Table 21 - Fitted rate constants for the proposed mechanism of the LPO-catalyzed oxidation of SCN^- by H_2O_2 as $[H_2O_2]$ was varied

$[H_2O_2]$(uM)	k_1 ($M^{-1}\cdot s^{-1}$)	k_{-1} (s^{-1})	k_2 ($M^{-1}\cdot s^{-1}$)	k_{-2} (s^{-1})	k_3 ($M^{-1}\cdot s^{-1}$)
50	$1.58(2)\times10^9$	$3.5(3)\times10^3$	$5.91(3\times10^{-3})\times10^7$	2.58(2)	$1.84(4)\times10^7$
25	$1.8(4)\times10^9$	$3.2(7)\times10^3$	$4.8(4)\times10^7$	2.14(2)	$1.110(7)\times10^7$
12.5	1.65×10^9(fixed)	3.30×10^3(fixed)	$6.4(1)\times10^7$	2.30(fixed)	$1.44(2)\times10^7$
6.25	1.65×10^9(fixed)	3.30×10^3(fixed)	$4.9(2)\times10^7$	2.30(fixed)	$1.330(5)\times10^7$
Average	$1.7(1)\times10^9$	$3.3(2)\times10^3$	$5.5(8)\times10^7$	2.4(3)	$1.4(3)\times10^7$

[a]The post-mixing concentrations were $[SCN^-]$ = 100 uM, [LPO] = 0.5 uM, [TNB] = 100 uM, and $[H_2O_2]$ = 6.25, 12.5, 25, and 50 uM.*

Table 22 - Fitted rate constants for the proposed mechanism of the LPO-catalyzed oxidation of $[SeCN^-]$ by H_2O_2 with $[SeCN^-]$ varied

$[SeCN^-]$(uM)	k_1 ($M^{-1}\cdot s^{-1}$)	k_{-1} (s^{-1})	k_2 ($M^{-1}\cdot s^{-1}$)	k_{-2} (s^{-1})	k_3 ($M^{-1}\cdot s^{-1}$)
42.5	$1.25(5)\times10^9$	$9.16(3)\times10^2$	$2.71(8)\times10^7$	1.44(1)	$8.48(1)\times10^6$
85	$1.24(3)\times10^9$	$9.70(1)\times10^2$	$2.87(3)\times10^7$	1.33(4)	$1.23(2)\times10^7$
170	1.25×10^9(fixed)	$1.190(7)\times10^3$	2.79×10^7(fixed)	1.58(2)	$1.289(9)\times10^7$
340	1.25×10^9(fixed)	1.03×10^3(fixed)	2.79×10^7(fixed)	1.45(fixed)	$1.47(2)\times10^7$
Average	$1.250(7)\times10^9$	$1.0(1)\times10^3$	$2.8(1)\times10^7$	1.5(1)	$1.2(3)\times10^6$

[a]The post-mixing concentrations were [LPO] = 0.24 uM, $[H_2O_2]$ = 30 uM, [TNB] = 70 uM, $[SeCN^-]$ = 42.5, 85, 170, and 340 uM.*

*The estimated error, given by the parenthetical digits, for the individual rate constants is for a least-squares fit of an average of 5 kinetic traces. The average error was calculated by the standard deviation of the individual fits.

3.7 Conclusion

We present data that challenges the lactoperoxidase literature model for the mechanism of the lactoperoxidase-catalyzed oxidation of X^- by H_2O_2, presented in Equations 3.2.5 and 3.2.6. In particular, the biphasic nature of the reaction under conditions of low $[X^-]$ is inconsistent with the kinetics expected given the literature mechanism. To address the inconsistencies, a new mechanism is proposed consisting of an ordered sequential mechanism with tight binding inhibition by H_2O_2, shown in Figure 3.25. This mechanism is novel because it utilizes the bound LPOX species as the primary productive enzyme species rather than compound I, as discussed in section 1.2. Furthermore, the hydrogen peroxide bound enzyme species, LPO-H_2O_2, is considered unproductive. The primary evidence for the validity of this mechanism is the dependence of the observed rate constant of the pre-steady-state reaction on $[H_2O_2]$ and the increasing number of enzyme turnovers during the pre-steady-state reaction with increasing $[X^-]$ and [LPO].

The proposed mechanism, Figure 3.26, explains the observed kinetics at high and low $[PsX^-]$. Under conditions of high $[PsX^-]$, where the reaction has simple first-order kinetics, the reaction rate is primarily dependent on the turnover-limiting reaction of LPOX and H_2O_2, rate constant k_3. The rate of this reaction is independent of $[X^-]$ and first order in $[H_2O_2]$ as seen experimentally in section 3.4. This is because there is no appreciable production of the LPO-H_2O_2 species, so the pre-steady-state reaction indicative of H_2O_2 inhibition is not observed.

Under conditions of low $[PsX^-]$ there is competition for LPO binding of X^- by H_2O_2. The reaction of LPO with H_2O_2 produces the less reactive LPO-H_2O_2 species in a reaction which is pseudo-first-order with respect to $[H_2O_2]$. The production of LPO-H_2O_2 inhibits

the rate of [X^-] oxidation until an equilibrium has been reached and the reaction becomes zeroth-order. The rate of the zeroth-order reaction is independent of [H_2O_2] and has a first-order dependence on [X^-]. The first-order dependence on [X^-] of the steady-state reaction is due to increased competition with H_2O_2 for LPO binding which results in an increased steady-state concentration of LPOX and an increased rate of enzyme turnover. This increase in rate of enzyme turnover with increased [X^-] also causes the increased number of turnovers during the pre-steady-state reaction effectively stopping the reaction of LPO with H_2O_2 at sufficiently high [X^-].

Our proposed mechanism is the simplest explanation for the observed kinetic behavior of the reaction. As such, it should be noted that the actual catalysis mechanism may be more complicated than the mechanism proposed in Figure 3.26. For example, the reaction of LPO with H_2O_2 to produce the LPO-H_2O_2 bound species is considered in this mechanism to be reversible. This means that the LPO-H_2O_2 bound species cannot be compound I as this would require compound I to be able to oxidize water (within the environment of the enzyme active site) to produce H_2O_2. The redox potentials of LPO compound I and H_2O_2 at pH 7, shown in Table 1 in section 1.2.3, indicate that this oxidation should not be possible (unless the redox potential of water is markedly different in the enzyme binding pocket).

Overall our mechanism is novel compared to the other lactoperoxidase mechanisms reported in literature as well as the mechanisms of catalysis for other heme enzymes, reviewed in section 1.2, in that it depends on the initial binding of X^- for halogen cycle catalysis. This hypothesis rejects the commonly held belief that compound I is the active form of the enzyme and considers the LPO-H_2O_2 bound species to be an inactive species

which inhibits the oxidation of X^-. Furthermore, as the reaction of LPO with X^- is very fast, the LPO-H_2O_2 bound species is not produced in significant concentrations at high concentrations of X^-.

The biological relevance of the biphasic reaction kinetics depends upon the concentrations of LPO, SCN^-, and H_2O_2 *in vivo*. Due to the similarities in the k_2 and k_3 rate constants, the inhibition of LPO by H_2O_2 is observed under reaction conditions where near equimolar concentrations of H_2O_2 and SCN^- are present or when the concentration of H_2O_2 exceeds the concentration of SCN^-. We suggest that the kinetics of LPO catalysis observed experimentally under conditions of high SCN^- concentration and comparatively low H_2O_2 concentration reflect the kinetics observed for healthy biological systems. However, under certain disease conditions, H_2O_2 is produced at a higher rate and SCN^- concentration is low due to substrate depletion or restricted transport. Under such disease conditions, inhibition of LPO by H_2O_2 may become relevant *in vivo*.[153]

We suggest three representative physiological situations that may exhibit conditions that lead to LPO inhibition by H_2O_2. First, in the airway of a person afflicted with cystic fibrosis (CF). Due to damaged lung tissue, the transport of SCN^- to the airway mucous is inhibited and the concentration of SCN^- can be as low as 0.1 uM.[46] Furthermore, the prevalence of infection among CF patients causes the lungs to be in a state of oxidative stress and H_2O_2 concentration is high. Second, in the gingival crevasse there is a SCN^- concentration gradient which causes a low concentration of SCN^- in the gingival crevicular fluid (GCF). Again, under conditions of health, concentration of H_2O_2 is expected to be low in the GCF; however, under conditions of disease, neutrophilic polymorphonuclear leukocytes are introduced which promote higher concentrations of H_2O_2.[154] Lastly, the

LPO inhibition by H_2O_2 may occur in the oral biofilms responsible for dental caries (tooth decay). The commensal bacteria present in these biofilms produce H_2O_2 and the structure of the biofilm may decrease accessibility of SCN^- which could result in conditions for LPO inhibition by H_2O_2.[8]

The narrow range of conditions in which H_2O_2 inhibition by LPO is observed brings up further questions regarding the biological purpose of the inhibition. We propose that the inhibition of LPO by H_2O_2 results in two physiological consequences: decrease in the rate of production of $OSCN^-$ and the increase in local concentrations of H_2O_2. Since many pathogenic bacteria are obligate anaerobes (only grow in the absence of oxygen), inhibition of LPO by H_2O_2 to raise the concentration of H_2O_2 may help fight infection.[8] Further evidence for this hypothesis may be gathered by studying the other defensive peroxidases for inhibition by H_2O_2. Thus, future mechanistic studies on these peroxidases is warranted.

3.8 Future Work

The primary enzyme species present during the LPO catalysis at low concentration of reducing substrate should be determined. This may be done by observing the LPO-catalyzed oxidation of PsX^- under low concentration conditions using a thiol that does not absorb in the UV-Vis spectrum such as 2-mercaptoethanol as the OX^- scavenger in place of TNB. A higher concentration of LPO and H_2O_2 must be used so that LPO can be directly observed spectrophotometrically and H_2O_2 is competitive with X^-. The spectral signature of LPO during the catalysis may identify the dominant LPO species. The halogen cycle mechanisms of myeloperoxidase and eosinophil peroxidase should be also studied at low concentration of reducing substrate to determine if they share an analogous mechanism with lactoperoxidase.

Chapter 4 – LACTOPEROXIDASE BINDING AND COMPETITION STUDIES

4.1 Introduction

The binding constants of lactoperoxidase with its inorganic anion substrates (SCN^-, I^-, Br^-, Cl^-, etc.) have been determined spectrophotometrically[155] and by NMR spectroscopy.[37, 43, 156] These studies have given a wide range of values for the binding constant of SCN^-, the primary lactoperoxidase substrate, citing varied spectroscopic techniques and experimental conditions for the variation in reported constants.[155] However, the most likely reason for the varied binding constants is pH variation. It has been shown that SCN^-/lactoperoxidase binding constants are highly pH dependent ranging from approximately 0.5-100 mM from pH 3.8-6.8.[43,37,155, 157]

NMR and X-ray crystallography studies of lactoperoxidase have also been undertaken to determine the binding site of the various reducing substrates, discussed in section 1.1.2. It has been proposed using crystallography data that each substrate has a discreet binding site in the binding pocket and that the proximity of the binding sites to the heme center determines the enzymatic preference of substrate.[18] However, kinetic studies[41] disagree with the proposed crystallographic substrate preference and structural NMR studies[37, 43] disagree with the proposed binding site of thiocyanate when compared to the crystal structure data. Certainly, it is possible that the binding sites for the reducing substrate observed in the crystallography data are different than the actual catalytic binding sites for the enzyme in solution observed by NMR spectroscopy.

This chapter will present equilibrium binding studies, equilibrium competition studies, kinetic binding studies, and competition kinetic binding studies of various reducing

substrates with LPO. Equilibrium binding studies are used here to determine the binding constant of $SeCN^-$ as compared to SCN^- to LPO. Equilibrium competition studies are used to determine if SCN^-, $SeCN^-$, and F^- (fluoride) bind competitively to lactoperoxidase. Kinetic studies of the rates of binding of $SeCN^-$ as compared to SCN^- with LPO are also presented to determine if a difference in binding rate or mechanism can be determined. Competition kinetic binding studies are present to determine the effect of competing ions on the kinetics of binding.

4.2 Lactoperoxidase Halide and Pseudohalide Binding

Spectral titrations of lactoperoxidase were conducted with SCN^- and $SeCN^-$, PsX^-, to determine binding constants and stoichiometry of binding. Spectra were collected for LPO at varying concentrations of PsX^-. Some of the data collected exhibited a very small spectral change even at saturating substrate concentrations, i.e. SCN^- binding with LPO, Figure 4.1. Because of the difficulty in analyzing these very small changes, difference spectra were produced to determine the wavelengths at which the binding of PsX^- with LPO exhibited the largest spectral change. The differences in absorbance at the maxima and minima of these difference spectra at varying $[PsX^-]$ were used to create Hill plots and Scatchard plots.

Hill plots were produced by plotting the difference in absorbance at the maximum and minimum of the difference spectra at various $[PsX^-]$ against the $[PsX^-]$. Hill plots were used to determine binding constants according to the method by Ferrari et al. using the modified Hill equation given in Equation 4.1.1.[155] In the modified Hill equation $\Delta A_{max-min}$ is the difference in the absorbances of the difference spectra at the maximum and minimum. The ΔA_∞ is the maximum change in absorbance of the difference spectra at the maximum and

minimum achieved when LPO is completely bound to substrate. [PsX^-] is the concentration of unbound PsX^-. However, [PsX^-] is considered constant because [PsX^-]>>[LPO] so the ratio of PsX^- bound to LPO compared to free PsX^- is negligible. When $\Delta A_{max-min}$ is plotted against [PsX^-], the resulting plot is fit to the modified Hill equation, Equation 4.1.1, to determine the dissociation constant, K_D.

$$\Delta A_{max-min} = \frac{\Delta A_{\infty}[PsX^-]}{K_D + [PsX^-]} \qquad \text{Equation 4.1.1}$$

The Scatchard plots were used to determine the number of binding equivalents of substrate with respect to LPO using the modified Scatchard equation, Equation 4.1.2. When $\frac{\Delta A_{max-min}}{[PsX^-]}$ is plotted against $\Delta A_{max-min}$ the slope of the resulting line is $m = -\frac{1}{K_D}$. We can also determine from this plot the number of binding equivalents of PsX^- with respect to LPO. A linear plot indicates there is a single class of binding site of substrate to enzyme. However, a Scatchard plot which curves is indicative of multiple classes of binding sites. In the case of single substrate binding, a curve in the Scatchard plot could indicate multiple binding sites. The Scatchard plot has been previously used to determine K_D and, indeed, the modified Scatchard equation shows us that K_D can be calculated from the negative reciprocal of the slope. However, this is not best practice presently due to increased error associated with the Scatchard equation.[158] The modified Hill equation given in Equation 4.1.1 can be fit more accurately to a nonlinear model to calculate K_D.

$$\frac{\Delta A_{max-min}}{[PsX^-]} = -\frac{\Delta A_{max-min}}{K_D} + \frac{\Delta \varepsilon_{max-min} * [E_T]}{K_D} \qquad \text{Equation 4.1.2}$$

4.2.1 Lactoperoxidase –Thiocyanate Binding Constant

As discussed in section 4.1, the lactoperoxidase binding constant has been determined repeatedly at varying pH and using various spectroscopic methods. As such, the binding constant for thiocyanate with lactoperoxidase has been independently determined and reported here for direct comparison to the binding constant for selenocyanate with lactoperoxidase, section 4.2.2.

LPO has a strong Soret band absorption with a λ_{max} at 412 nm that shifts to 414 nm when SCN^- is bound, Figure 4.1. There is also an increase in intensities of the Q-band absorption at approximately 490 and 630 nm associated with the porphyrin spectra, when SCN^- is bound to LPO, Figure 4.2 inset. Because the spectral change was difficult to analyze, even when the concentration of [SCN^-] was high enough that LPO was saturated, the difference spectra was used to calculate the dissociation constant, Figure 4.2. The largest changes in absorbance were determined by the difference spectra and the difference in the absorption at the maxima and minima, at 426 and 406 nm, respectively, were used to produce a Hill plot and a Scatchard plot.

The Hill plot was used to determine the LPO-SCN dissociation constant, Figure 4.3. The dissociation constant was calculated to be 15.6(6) mM. The linearity of the Scatchard plot, Figure 4.4, indicates that there was a single class of binding site and only one binding equivalent of SCN^- to LPO.

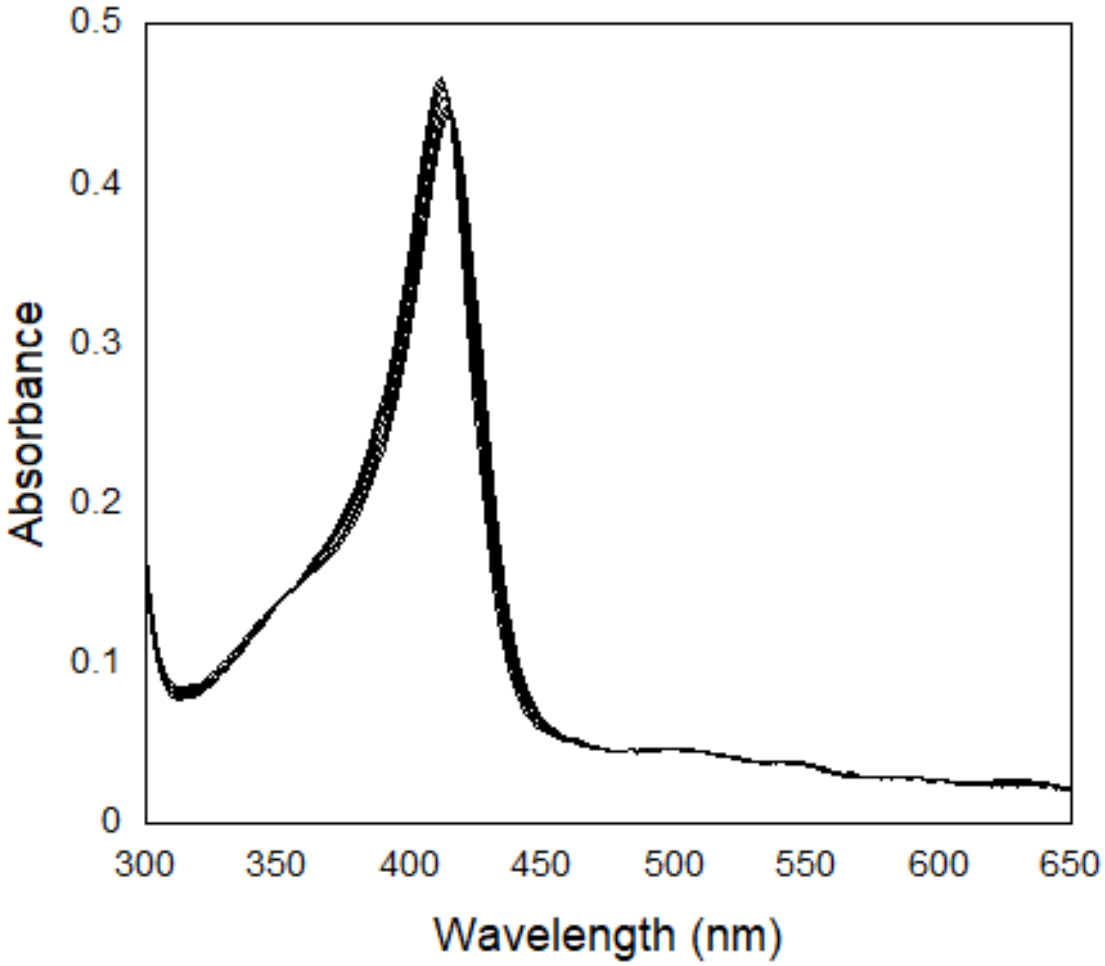

Figure 4.1 - Lactoperoxidase - Thiocyanate spectral titration.

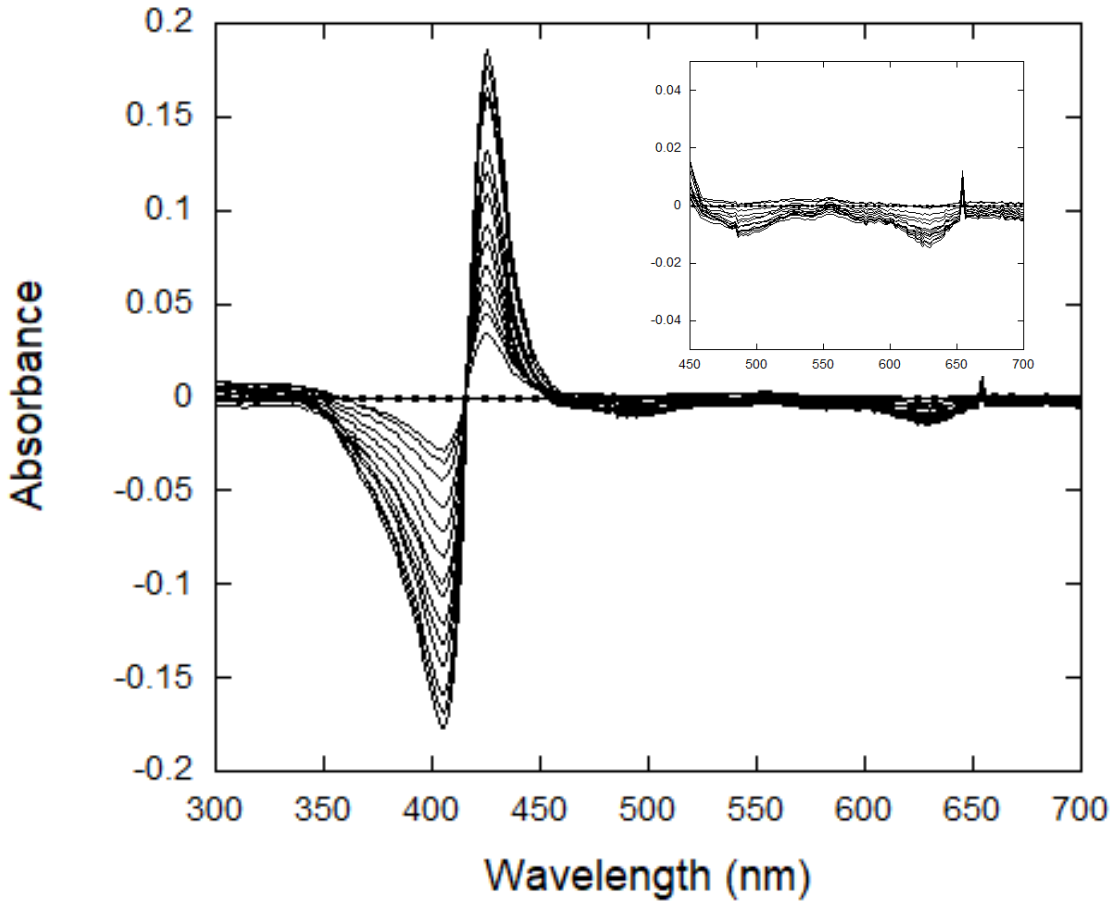

Figure 4.2 - Lactoperoxidase - Thiocyanate spectral titration difference spectra. The inset shows the Q-bands in more detail.

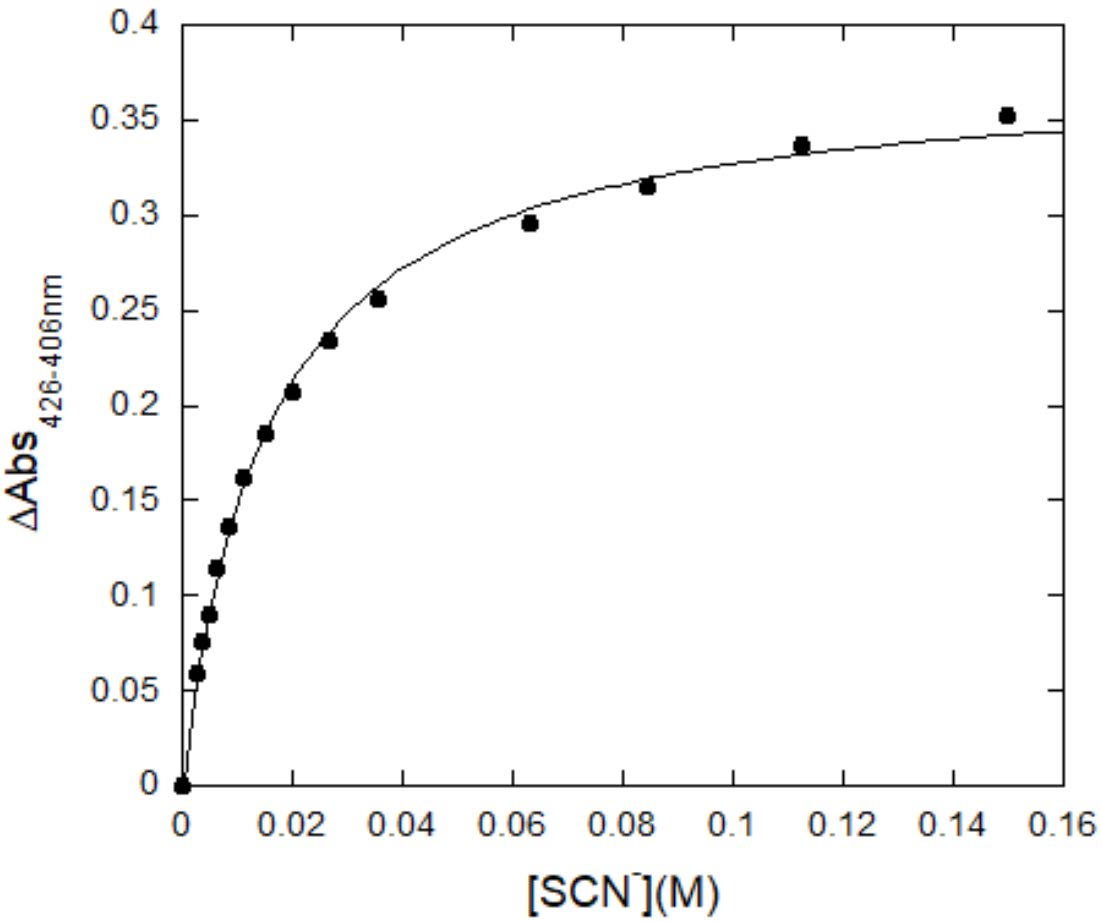

Figure 4.3 - Lactoperoxidase-Thiocyanate Hill plot. K_D = 15.6(6) mM. The estimated error, given by the parenthetical digit, is for a least-squares fit of the plot.

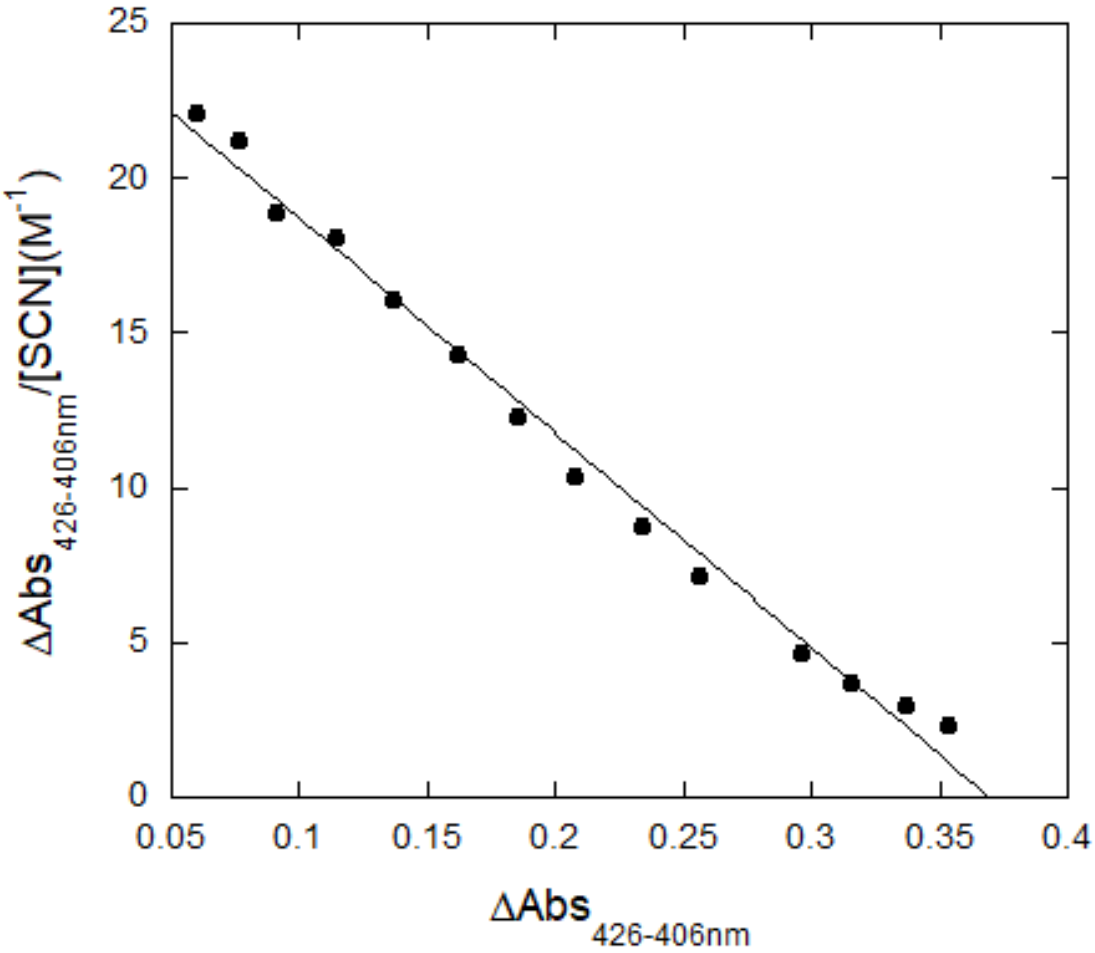

Figure 4.4 - Lactoperoxidase-Thiocyanate Scatchard Plot.

4.2.2 Lactoperoxidase – Selenocyanate Binding Constant

The binding constant of lactoperoxidase with selenocyanate was determined for comparison to thiocyanate using a spectral titration. The spectral changes for $SeCN^-$ binding to LPO were much more significant than those observed for SCN^- shown in Figure 4.1, section 4.2.1. There was a large shift in the Soret band from 412 nm for native LPO to 432 nm upon $SeCN^-$ binding, Figure 4.5. There was also an increase in absorbance of the Q-bands at 550 and 630 nm. When $SeCN^-$ binds to LPO, the Q-band peak at 630 nm is like the peak observed when SCN^- is bound to LPO, Figures 4.7 and 4.2, respectively, as both peaks decreased in intensity with increasing [PsX^-]. When $SeCN^-$ is bound to lactoperoxidase, the Q-band peak at 550 nm differs from the similar Q-band peak observed for SCN^- at 490 nm displayed in Figure 4.2. In addition to the wavelength shift, the Q-band peak at 490 nm for SCN^- binding is a negative peak in the difference spectra indicating a reduced peak intensity with increased [SCN^-]. However, the peak at 550 nm for $SeCN^-$ binding to LPO is a positive peak in the difference spectra indicating an increased peak intensity as [$SeCN^-$] increases.

The difference spectra in Figure 4.6 was used to determine the wavelengths of maximum change in the binding spectrum. The difference in the maximum and minimum peaks, at 432 and 407 nm at each [$SeCN^-$] were used to produce a Hill plot and a Scatchard plot. The Hill plot determined the dissociation constant for LPO and $SeCN^-$ to be 9.5(1) mM, Figure 4.7, which is less than the K_D of 15.6(6) mM calculated for SCN^- binding with LPO. The smaller K_D value indicates that $SeCN^-$ binds more tightly to LPO than SCN^-. The linearity of the Scatchard plot, Figure 4.8, indicates that, as with SCN^-, there is 1:1 binding stoichiometry with respect to LPO and $SeCN^-$.

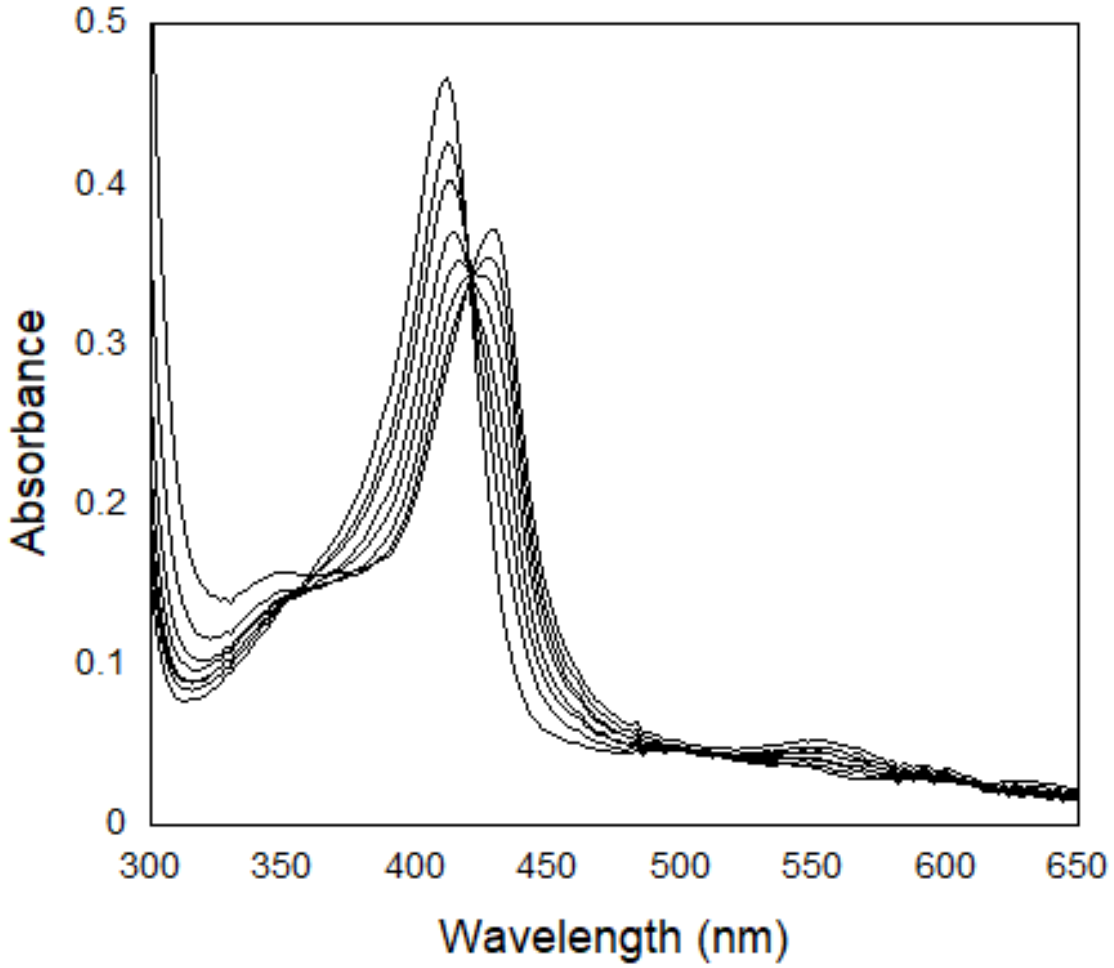

Figure 4.5 - Lactoperoxidase – selenocyanate spectral titration. A shift from the native LPO peak at 412 nm to the bound LPO-SeCN spectra at 432 nm is observed.

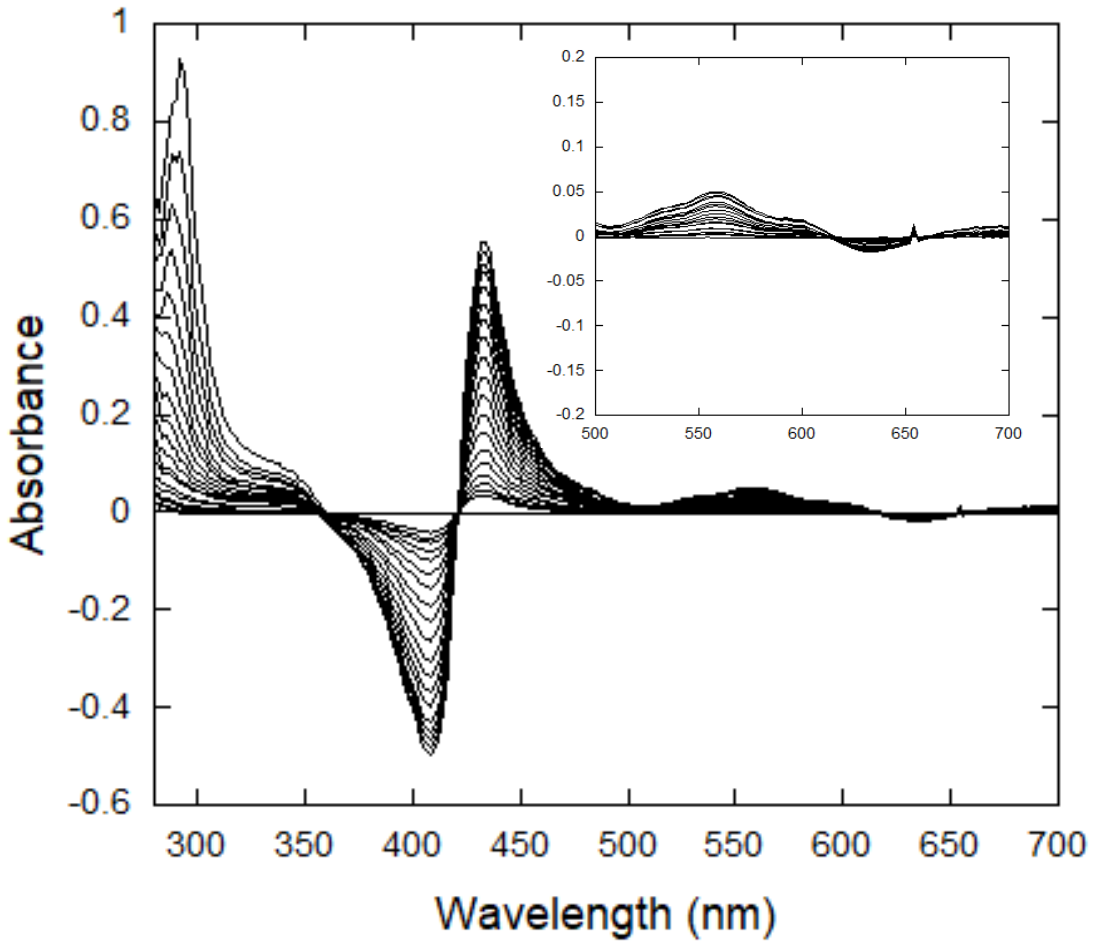

Figure 4.6 - Lactoperoxidase - selenocyanate spectral titration difference spectra. The inset shows the Q-bands in more detail.

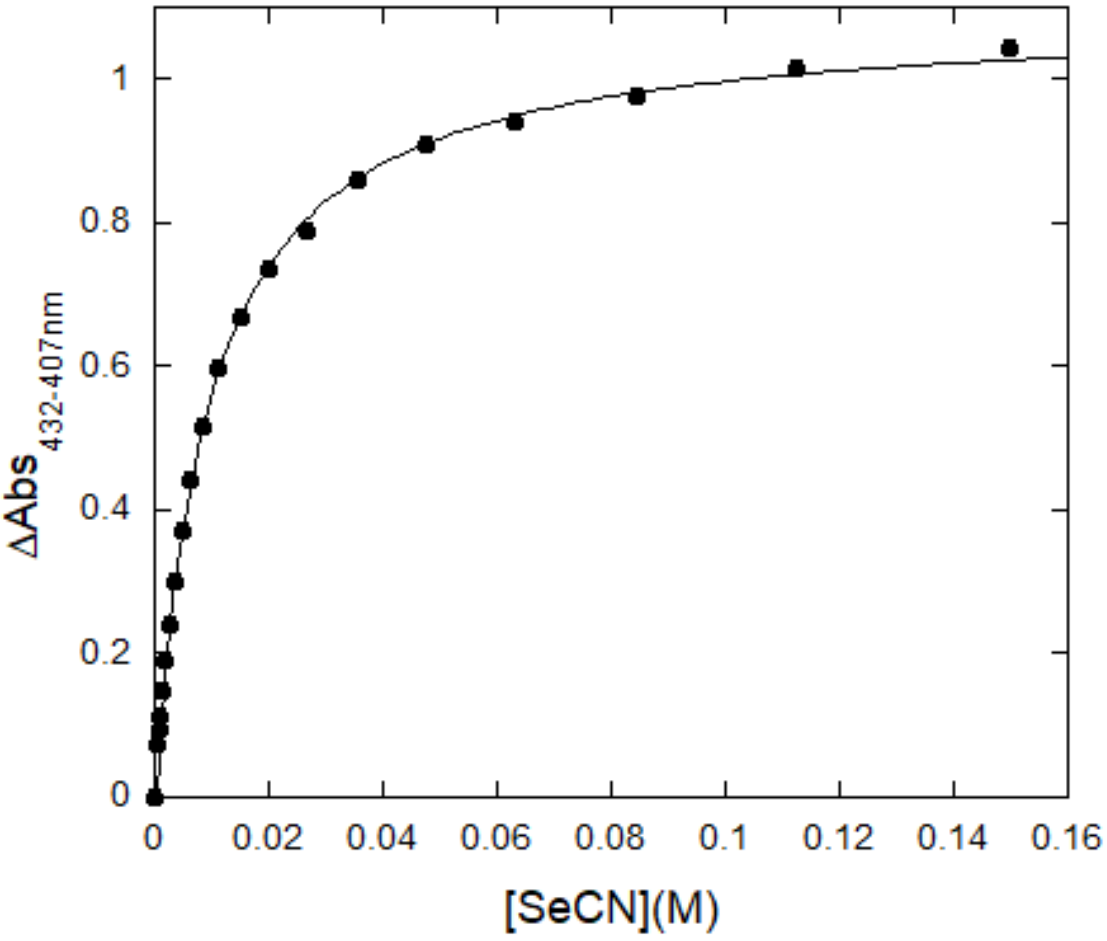

Figure 4.7 – Hill plot of selenocyanate binding to lactoperoxidase. K_D = 9.5(1) mM. The estimated error, given by the parenthetical digit, is for a least-squares fit of the data.

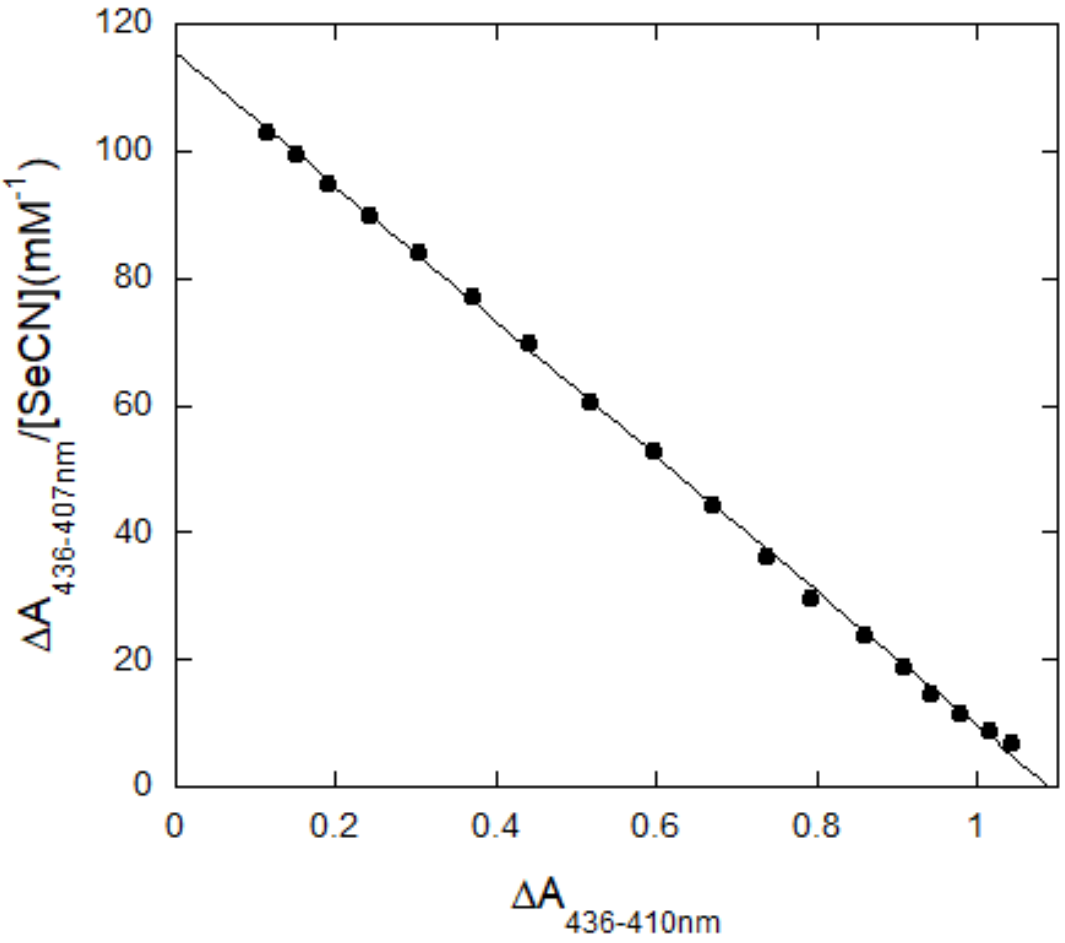

Figure 4.8 - Lactoperoxidase-Selenocyanate Scatchard Plot.

4.3 Lactoperoxidase Competition Binding Studies

Spectral titrations were also used in competition studies to determine if there was competitive binding between multiple LPO substrates. Thiocyanate competition with selenocyanate and fluoride competition with selenocyanate were tested. In these studies, the concentrations of a single substrate, SCN^- and F^- in these cases, were held constant and allowed to come to equilibrium binding with LPO. The concentration of the second substrate, $SeCN^-$, was varied to determine the effect on the pre-established equilibrium. These changes were used to determine the binding cooperativity between the two LPO substrates using Hill plots and logarithmic Hill plots.

Difference spectra were produced to determine the wavelengths that exhibited the largest spectral change for the equilibrium binding spectra. The differences in absorbance at the maxima and minima of these difference spectra at varying $[PsX^-]$ were used to create Hill plots and logarithmic Hill plots. The Hill plots were used to calculate the competition binding constant to compare to the binding constant in the absence of other substrates. The Hill plots were produced according to Equation 4.1.1 as discussed in section 4.2.

Logarithmic Hill plots were used to determine the Hill coefficients according to Equation 4.1.3. The Hill coefficient, n, indicates cooperativity such that when n > 1 there is positively cooperative binding, when n < 1 there is negatively cooperative binding, and when n = 1 there is non-cooperative binding. The fraction of bound LPO is referred to in Equation 4.1.3 as θ. When $\log\left(\frac{\theta}{1-\theta}\right)$ is plotted against $\log[PsX^-]$ the slope of the resulting line is the Hill coefficient n.

$$\log\left(\frac{\theta}{1-\theta}\right) = n * \log[PsX^-] - logK_D \qquad \text{Equation 4.1.3}$$

4.3.1 Thiocyanate and Selenocyanate Competition Studies

A competition study of the binding of thiocyanate and selenocyanate with lactoperoxidase was performed to determine if they bind competitively. In this study [SCN^-] was held constant at a concentration of more than double the binding constant for SCN^- with LPO. The initial spectra visible in the spectral titration, Figure 4.9, is that of LPO bound with SCN^- with a λ_{max} at 414 nm. As $SeCN^-$ is added, the lactoperoxidase Soret band peak shifts to 430 nm for the $SeCN^-$ bound to LPO.

The K_D calculated for the Hill plot of $SeCN^-$ binding with LPO in the presence of SCN^- was 14.3(5) mM, Figure 4.11. When compared to what was calculated for binding of $SeCN^-$ with LPO, 9.5(1) mM reported in section 4.2.3, the ratio is 1:1.5, indicating there is competitive binding between SCN^- and $SeCN^-$ for LPO binding. In addition to the ratio of observed binding constants which indicates competition between SCN^- and $SeCN^-$ for LPO binding sites, the logarithmic Hill plot, Figure 4.12, indicates that the Hill coefficient n is equal to 0.84(2). A Hill coefficient of $n < 1$ indicates negatively cooperative binding meaning that binding of SCN^- to LPO negatively effects the ability of $SeCN^-$ to bind to LPO. Negatively cooperative binding does not necessarily mean that SCN^- and $SeCN^-$ share a binding site, though that is one possible explanation; it means that the enzyme cannot efficiently bind both substrates.

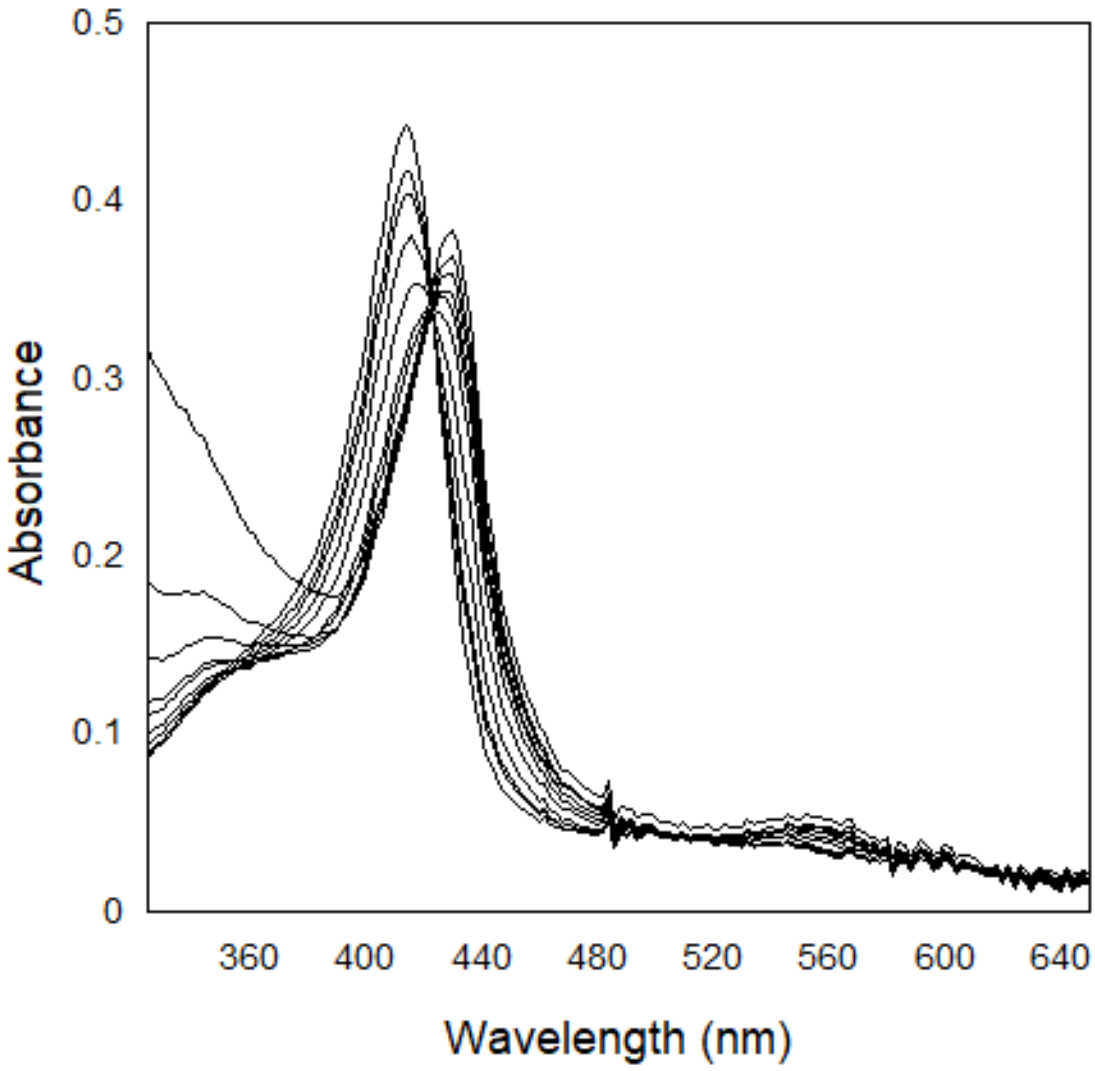

Figure 4.9 - Thiocyanate - Selenocyanate competition for lactoperoxidase binding spectral titration.

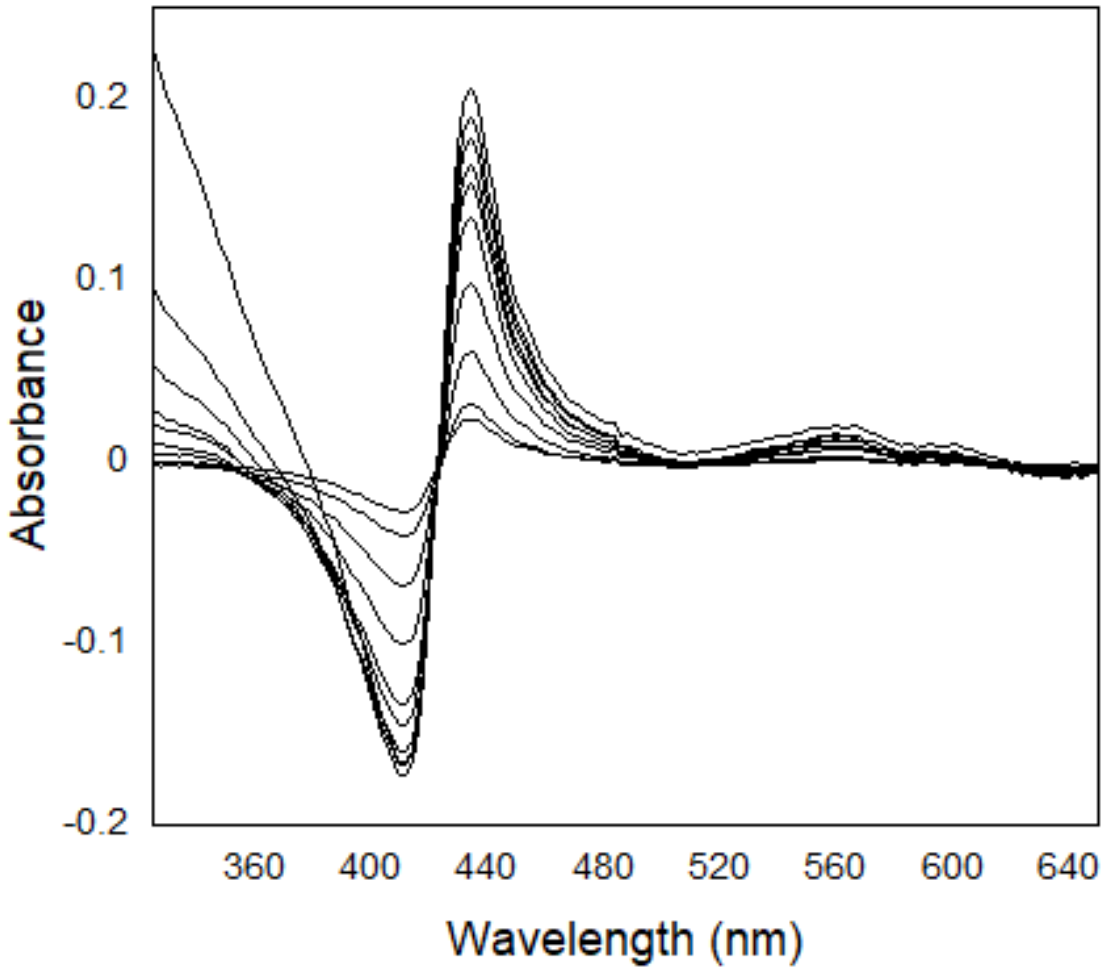

Figure 4.10 - Thiocyanate - Selenocyanate competition differences spectra.

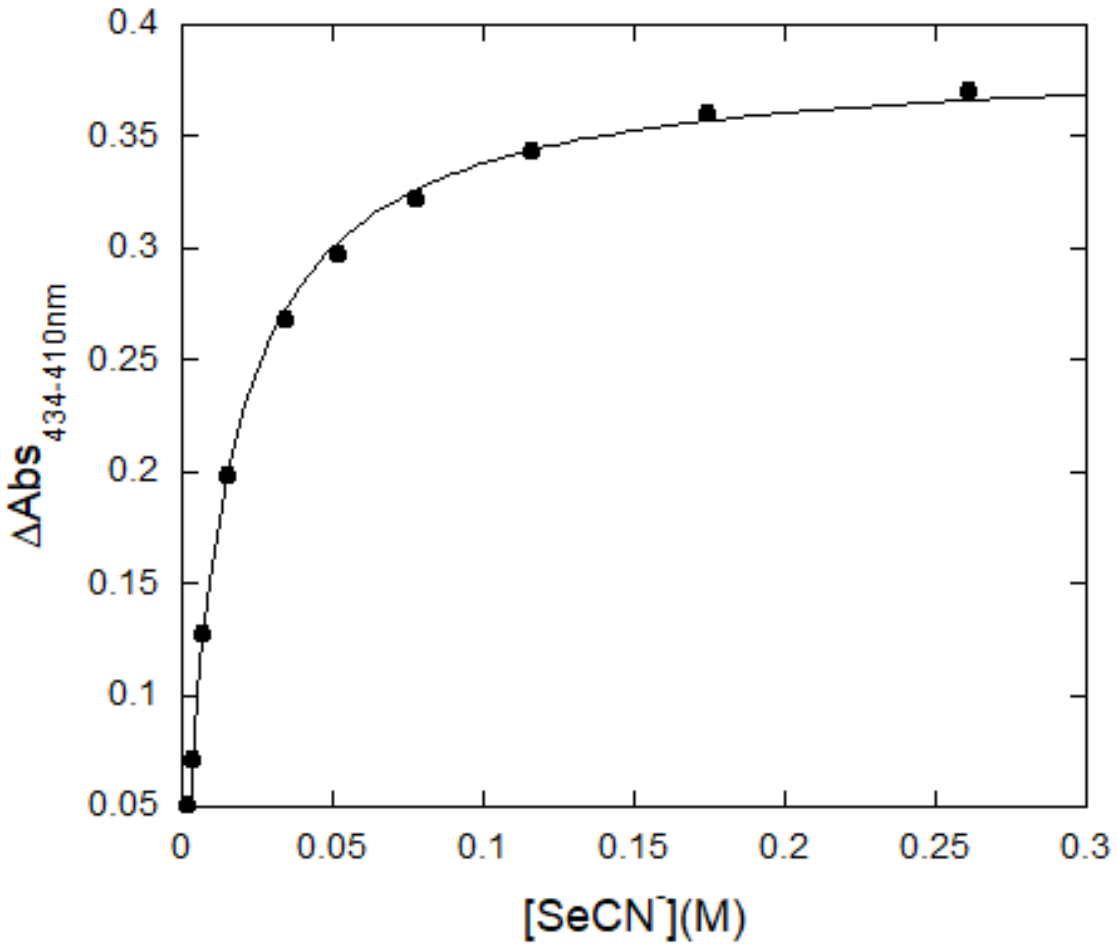

Figure 4.11 - Thiocyanate - Selenocyanate Hill plot for the competition of lactoperoxidase binding. K_D = 14.3(5) mM. The estimated error, given by the parenthetical digit, is for a least-squares fit.

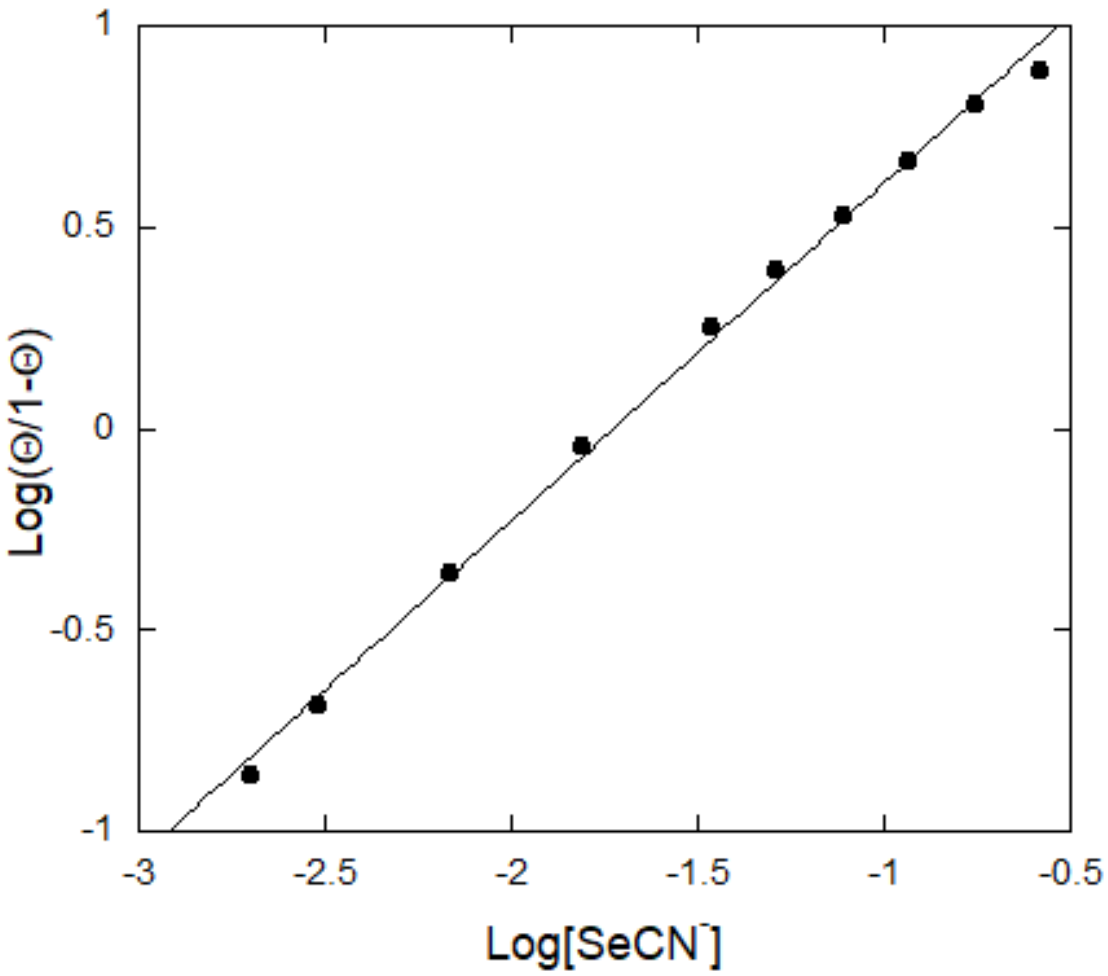

Figure 4.12 - Thiocyanate - Selenocyanate logarithmic Hill plot for the competition of binding with lactoperoxidase. The Hill coefficient calculated from the slope is n = 0.84(2). The estimated error, given by the parenthetical digit, is for a least-squares fit.

4.3.2 Selenocyanate and Fluoride Competition Studies

Fluoride binds reversibly to lactoperoxidase at the catalytic center of the heme.[159] This occurrence has been attributed to the hard nature of fluoride and its ability to interact directly with the iron heme center.[159] This interaction occurs relatively slowly, on a time scale which can be observed via time resolved UV-Vis spectroscopy. This reaction is pH-dependent due to the competition of fluoride with a hydroxyl ion at the catalytic site and has a pseudo-first-order rate constant of $9.7(4)x10^2$ $M^{-1}s^{-1}$.[79, 159] There is some disagreement in the literature reporting the spectral change upon F^- binding with LPO. Segal and Dunford report F^- binding to LPO to cause a shift in the Soret band from 412 nm for native LPO to 410 nm for the LPO-F complex.[79] However, Ferrari et al. report "a deep modification in the optical difference spectra pattern" although no specific shift or spectral data were given.[155] F^- has also exhibited a pH dependent inhibition of lactoperoxidase activity and production of hypothiocyanite in buffer and saliva.[78, 80]

The binding of $SeCN^-$ with LPO also occurs relatively slowly. Discussion of the kinetics of $SeCN^-$ binding to LPO is given in section 4.4. Slow binding of $SeCN^-$ to LPO, the large shift in the Soret band with $SeCN^-$ binding, and the apparent inhibition of lactoperoxidase by $SeCN^-$ in the kinetic studies led to the hypothesis that $SeCN^-$ may also bind to the LPO iron catalytic heme center. A spectral titration competition study was used to determine if $SeCN^-$ binds competitively with F^- at the iron center of the heme.

The spectral change observed upon LPO binding with F^- more closely resembled the change reported by Segal and Dunford with a very small shift in the Soret band from 412 nm for native LPO to 410 nm for the bound LPO-F species, Figure 4.13. The logarithmic Hill plot, Figure 4.15, indicates a Hill coefficient of 1.06(1). A Hill coefficient

of n = 1 indicates non-cooperative binding and suggests that $SeCN^-$ does not compete with F^- for binding to the LPO iron heme center.

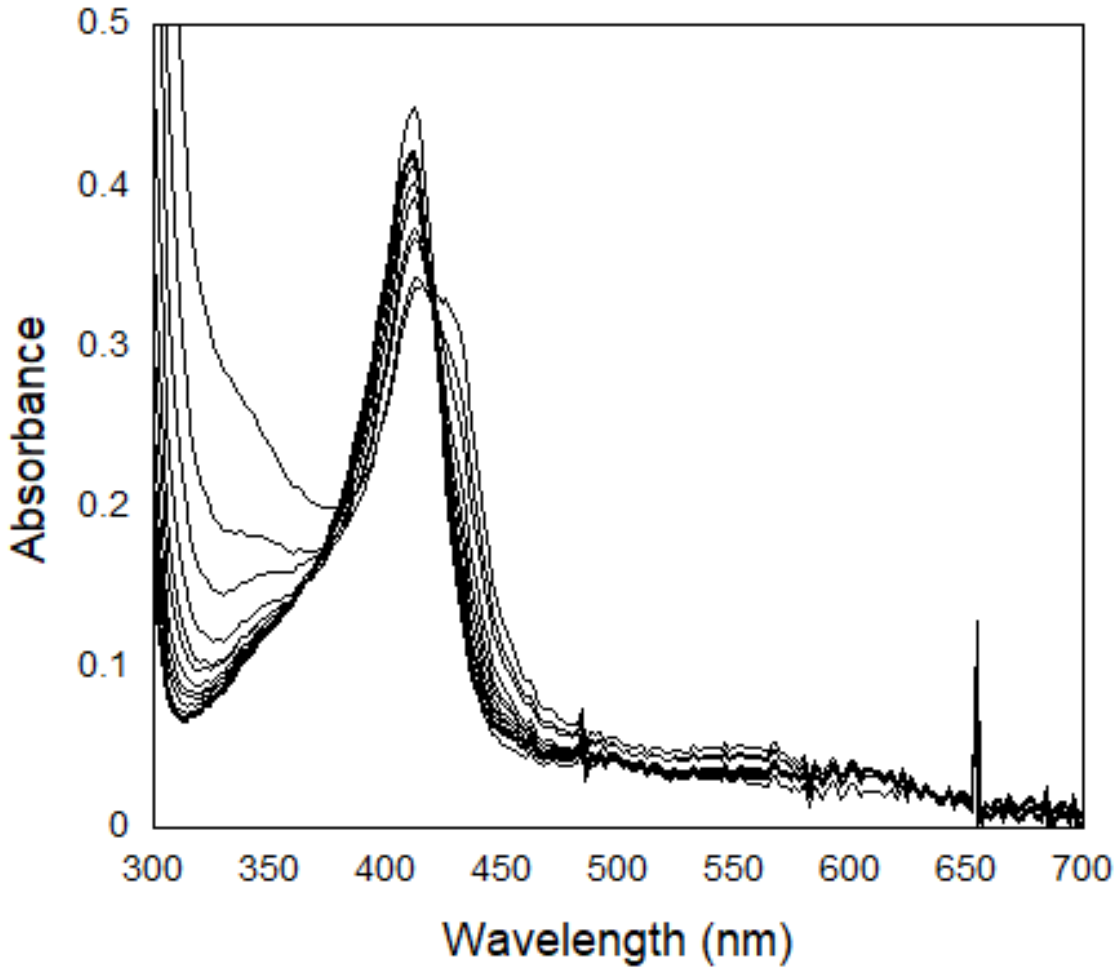

Figure 4.13 - Fluoride - Selenocyanate competition binding spectra.

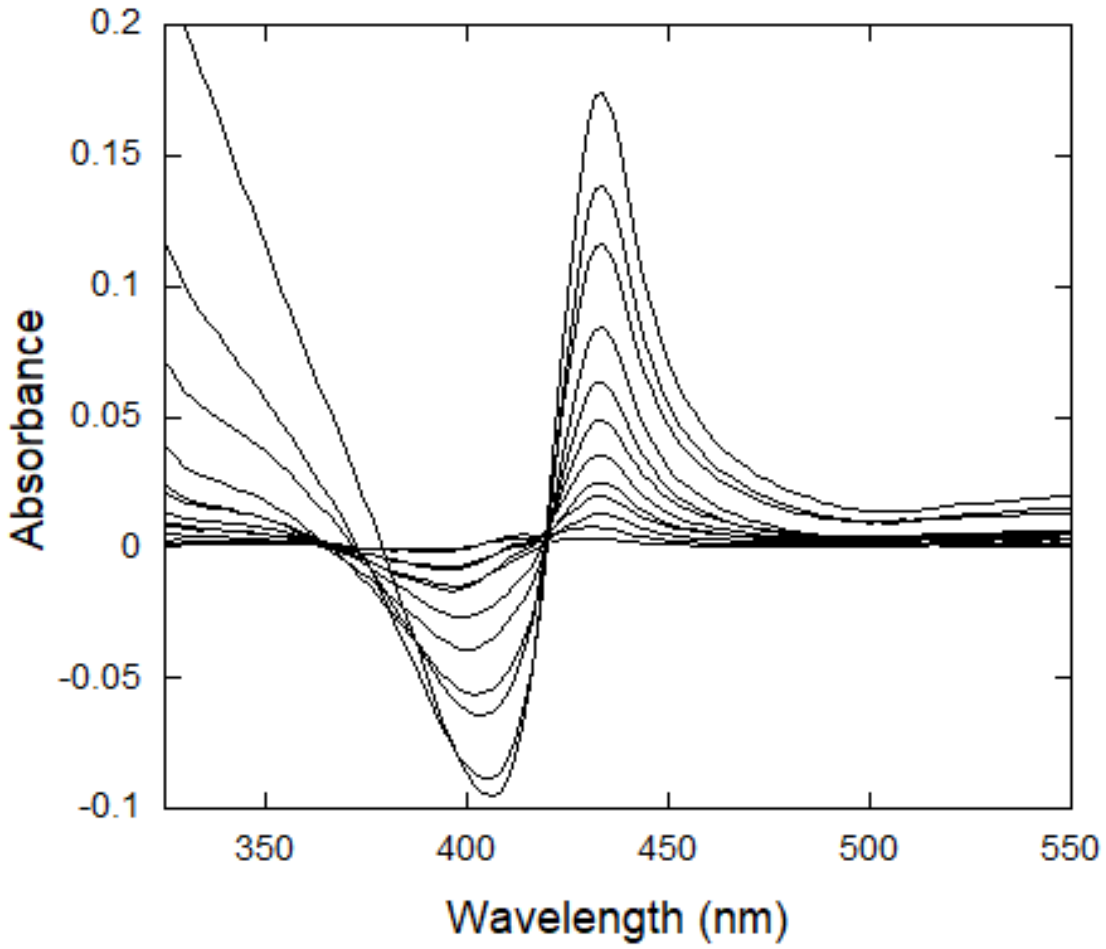

Figure 4.14 - Lactoperoxidase Binding Competition Study of Selenocyanate and Fluoride.

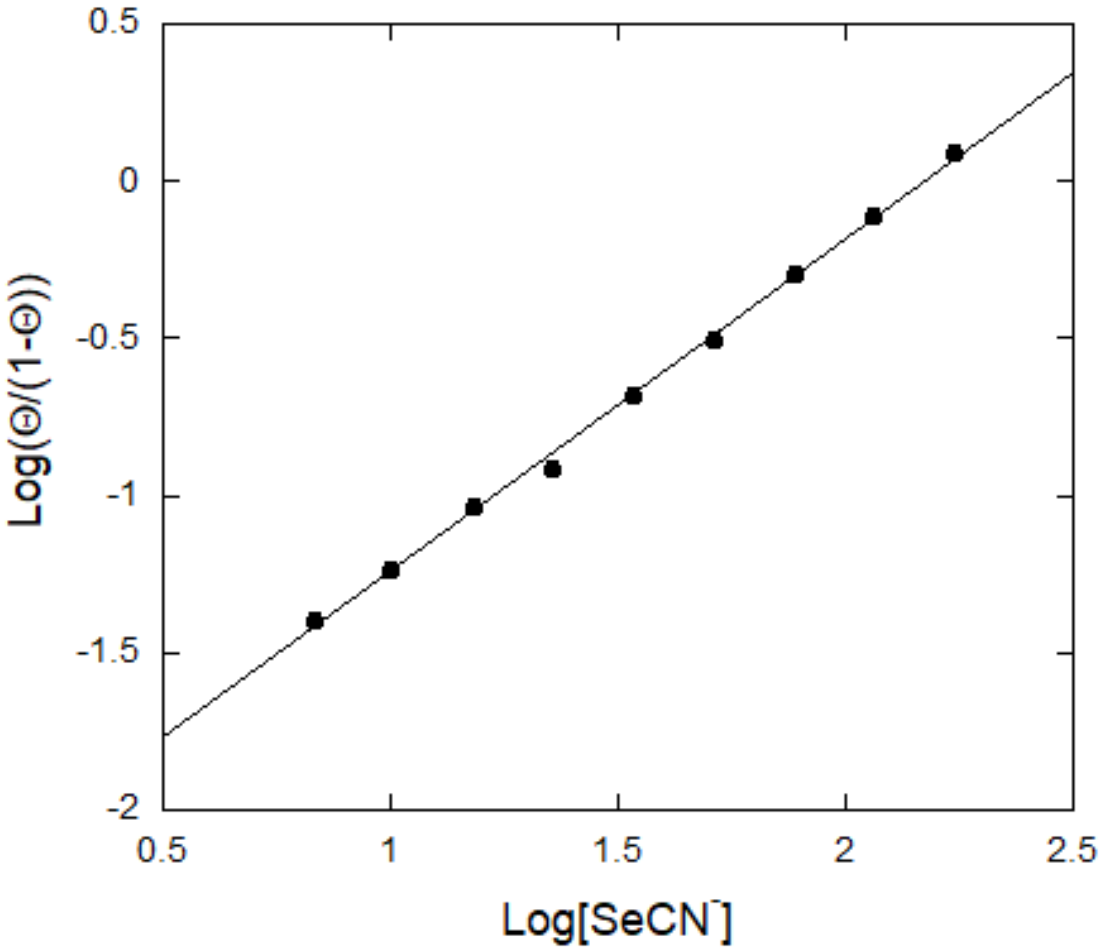

Figure 4.15 - Selenocyanate - Fluoride competition logarithmic Hill plot. n = 1.06(1). The estimated error, given by the parenthetical digit, is for a least-squares fit.

4.4 Kinetics of Pseudohalide Binding to Lactoperoxidase

The relatively slow binding of $SeCN^-$ to LPO enables the study of the mechanism of this binding via UV-Vis stopped-flow spectroscopy. The binding of SCN^-, however, was too fast to observe. This section discusses the mechanism of $SeCN^-$ binding to LPO. The effect of SCN^- as a competitive ligand on the rate of binding of LPO with $SeCN^-$ was also observed to further probe the binding mechanism.

4.4.1 Kinetics of Selenocyanate Binding to Lactoperoxidase

The kinetics of selenocyanate binding to lactoperoxidase were observed as a function of [$SeCN^-$], Figure 4.16. A reaction, which is slow enough to be observed using stopped-flow UV-Vis methods, occurs upon the mixing of $SeCN^-$ with LPO. When the kinetics of $SeCN^-$ binding to LPO were observed, the initial spectrum collected at t = 0 was not the spectrum of native LPO as expected. The change in spectra at t = 0 can be seen in the initial difference spectra in Figure 4.18. It appears that there is an equilibrium between LPO and $SeCN^-$ which is very fast, occurring in the mixing time, followed by a slower reaction which is observed.

A comparison was made between the initial spectra collected at t = 0 and the final spectra at the completion of the reaction, referred to here as $t = \infty$, for the reaction of $SeCN^-$ binding to LPO. The difference in the initial spectrum from the spectrum for native LPO and the slower reaction which follows indicate there are two phases of $SeCN^-$ binding to LPO. We propose that $SeCN^-$ binds to LPO at two separate binding sites or with two unique orientations, but is likely not bound at both sites simultaneously, given the linearity of the Scatchard plot, Figure 4.8, as discussed in section 4.2.2. Here we will consider these binding sites to be the kinetic and thermodynamic binding sites with the first, fast reaction

of LPO with $SeCN^-$ producing the LPO species with $SeCN^-$ bound to the kinetic binding site referred to as LPOSeCN. The second, slow reaction produces the LPO species with $SeCN^-$ bound to the thermodynamic binding site referred to as LPOSeCN*. The change in the difference spectra at t = 0, Figure 4.18, is very small compared to the total change in absorbance at $t = \infty$, Figure 4.20. There is also a shift in wavelengths of the maxima and minima of the difference spectra from 430 and 405 nm for the initial difference spectra to 432 and 407 nm for the final difference spectra.

In addition to the change in absorbance intensity and wavelength of maxima and minima in the difference spectra at t = 0 and $t = \infty$, there may also be a difference in binding constants between the initial and final binding of $SeCN^-$ to LPO. The dissociation constants of the initial and final binding of $SeCN^-$ to LPO, which were determined using the same methods presented in section 4.2 by fitting difference spectra absorbance data to the Hill equation, were calculated to be 29.2(3) mM and 9.6(5) mM, respectively, Figures 4.19 and 4.21. It should be noted that the initial dissociation constant is unreliable as true equilibrium has not been reached, but the initial dissociation constant is included here to illustrate the difference between the initial and final difference spectra.

The first phase of LPO binding to $SeCN^-$ is very fast and accounts for a very small change in the spectra. The change in spectra at t = 0 is similar to what is seen for complete binding of SCN^- to LPO which causes a very slight change in LPO spectra, Figures 4.1 and 4.2 in section 4.2.1. The binding of SCN^- with LPO occurs very quickly at the relatively high experimental concentrations of SCN^- used here. High concentrations of substrate must be used to produce a large enough change in the spectra to be accurately observed.

The binding kinetics of the second phase of LPO binding to $SeCN^-$ offer further evidence of the two-phase binding mechanism. The rate dependence of the second phase of the reaction on [$SeCN^-$] were not first-order as simple binding kinetics, under pseudo-first-order concentrations of $SeCN^-$ with respect to LPO, would predict. Instead, the binding of $SeCN^-$ with LPO exhibits a rate dependence on $SeCN^-$ that is nonlinear with the observed rate constants becoming constant at higher concentrations of $SeCN^-$, Figure 4.17. The dependence of the observed rate constant on [$SeCN^-$] can be explained by two consecutive equilibria as seen in the mechanism given in Figure 4.16. The first equilibrium, which is very fast, produces the LPO species with $SeCN^-$ bound to the kinetic binding site, LPOSeCN. The second equilibrium is the first-order conversion of the LPOSeCN species to the LPO species with the $SeCN^-$ bound to the thermodynamic binding site, LPOSeCN*.

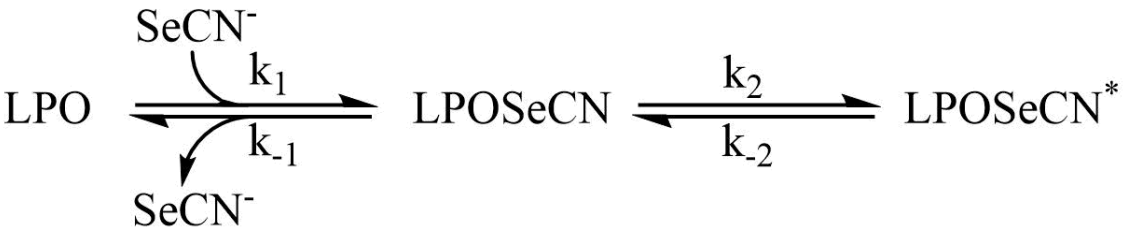

Figure 4.16 - Mechanism of binding of $SeCN^-$ to Lactoperoxidase.

The conversion of LPOSeCN to LPOSeCN* exhibits a dependence on [$SeCN^-$] because increased [$SeCN^-$] pushes the equilibria toward the bound species. The derived rate equation given in Equation 4.4.6 shows the rate dependence on [$SeCN^-$] and the first equilibrium, K_1. At high [$SeCN^-$] the first equilibrium is effectively pushed completely to the bound species and the rate of the second equilibrium becomes independent of [$SeCN^-$]. The rate law to produce LPOSeCN* is derived using the steady-state approximation in equations 4.4.1-4.4.6:

$$\frac{+d[LPOSeCN]}{dt} = k_1[LPO][SeCN^-] - k_{-1}[LPOSeCN] - k_2[LPOSeCN] + k_{-2}[LPOSeCN^*] = 0 \quad \text{Equation 4.4.1}$$

$$k_1[LPO][SeCN^-] + k_{-2}[LPOSeCN^*] = (k_{-1}k_2)[LPOSeCN] \quad \text{Equation 4.4.2}$$

$$[LPOSeCN]_{SS} = \frac{k_1[LPO][SeCN^-] + k_{-2}[LPOSeCN^*]}{(k_{-1}k_2)} \quad \text{Equation 4.4.3}$$

$$\frac{+d[LPOSeCN^*]}{dt} = k_2[LPOSeCN] - k_{-2}[LPOSeCN^*] \quad \text{Equation 4.4.4}$$
$$= \frac{k_1[LPO][SeCN^-] + k_{-2}[LPOSeCN^*]}{k_{-1}} - k_{-2}[LPOSeCN^*]$$

$$\frac{+[LPOSeCN^*]}{dt} = k_2[LPOSeCN] - k_{-2}[LPOSeCN^*] \quad \text{Equation 4.4.5}$$
$$= k_2\left(\frac{k_1[LPO][SeCN] + k_{-2}[LPOSeCN^*]}{k_{-1}}\right) - k_{-2}[LPOSeCN^*]$$

Assuming $k_1[LPO][SeCN^-] >> k_{-1}[LPOSeCN]$ and pseudo-first-order conditions with respect to $SeCN^-$:

$$\frac{+d[LPOSeCN^*]}{dt} = k_2 * K_1[LPO][SeCN] \quad \text{Equation 4.4.6}$$

The rate constants k_1 and k_{-1} could not be determined as that reaction was too fast to be observed. However, the data was fit to the proposed model given in Figure 4.16 using SpecFit[160] and the equilibrium constant was varied manually to obtain an unvaried rate constant, k_2, Table 23. Using this method, an approximate association equilibrium constant K_1 of 200 M^{-1} was used to calculate the rate constant k_2 to be 51.4(9) s^{-1}. The exact rate constants k_1, k_{-1}, or k_{-2}, or the exact equilibrium constants K_1 and K_2, could not be calculated from this data.

Given the proposed mechanism it should also be noted that the effective dissociation constant for the binding of $SeCN^-$ with LPO, K_{Deff} = 9.6(5) mM for the final equilibrium, is best represented by Equation 4.4.7. Using the equation for K_{Deff} and the approximate K_1 equilibrium constant, the approximate equilibrium constant K_2 can be estimated to be 0.5.

$$K_{Deff} = \frac{1}{K_1 * K_2} = \frac{k_{-1}k_{-2}}{k_1 k_2} \qquad \text{Equation 4.4.7}$$

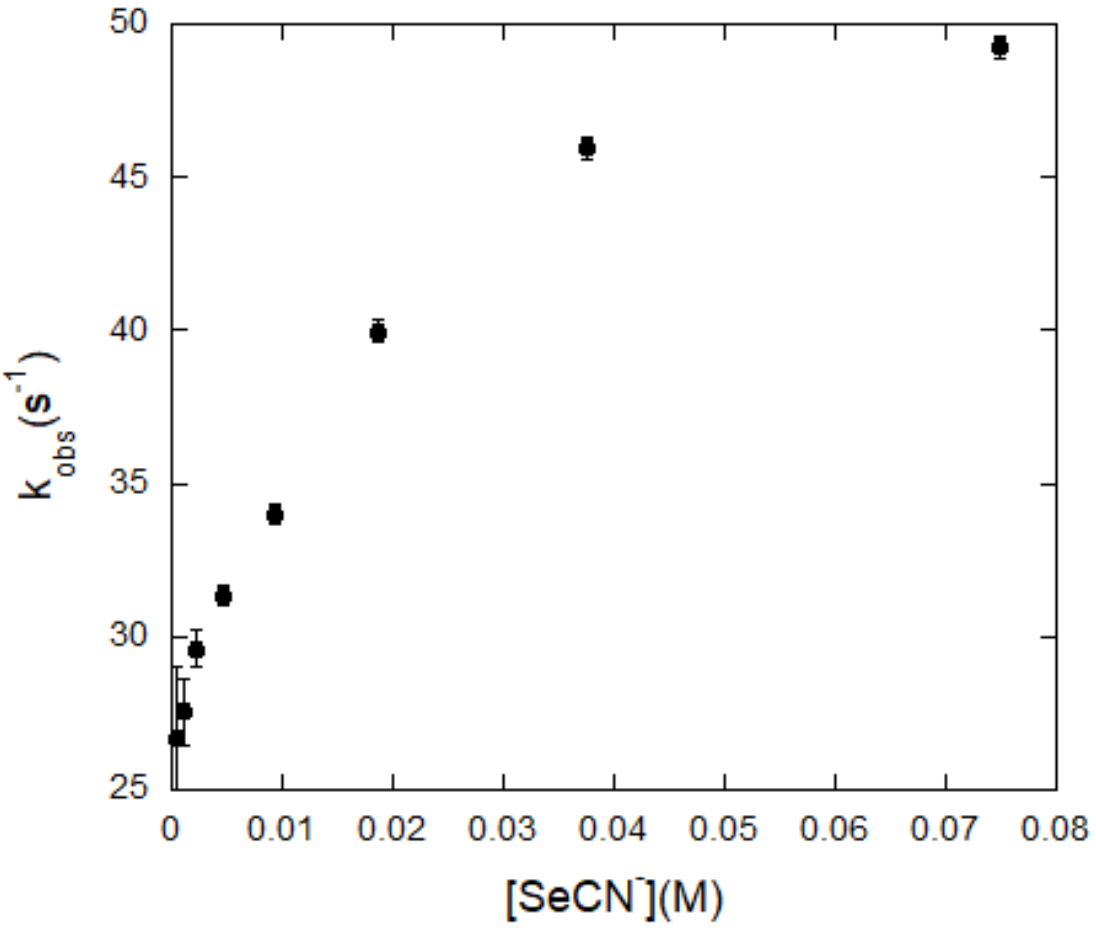

Figure 4.17 - Observed rate constants for the binding of $SeCN^-$ with LPO. Post-mixing concentrations were [LPO] = 8 uM and [$SeCN^-$] = 0.56-75 mM. The estimated error shown by the error bars for the individual rate constants is for a least-squares fit of an average of five kinetic traces and has been multiplied by a factor of 10 so that the error bars would be visible on the plot.

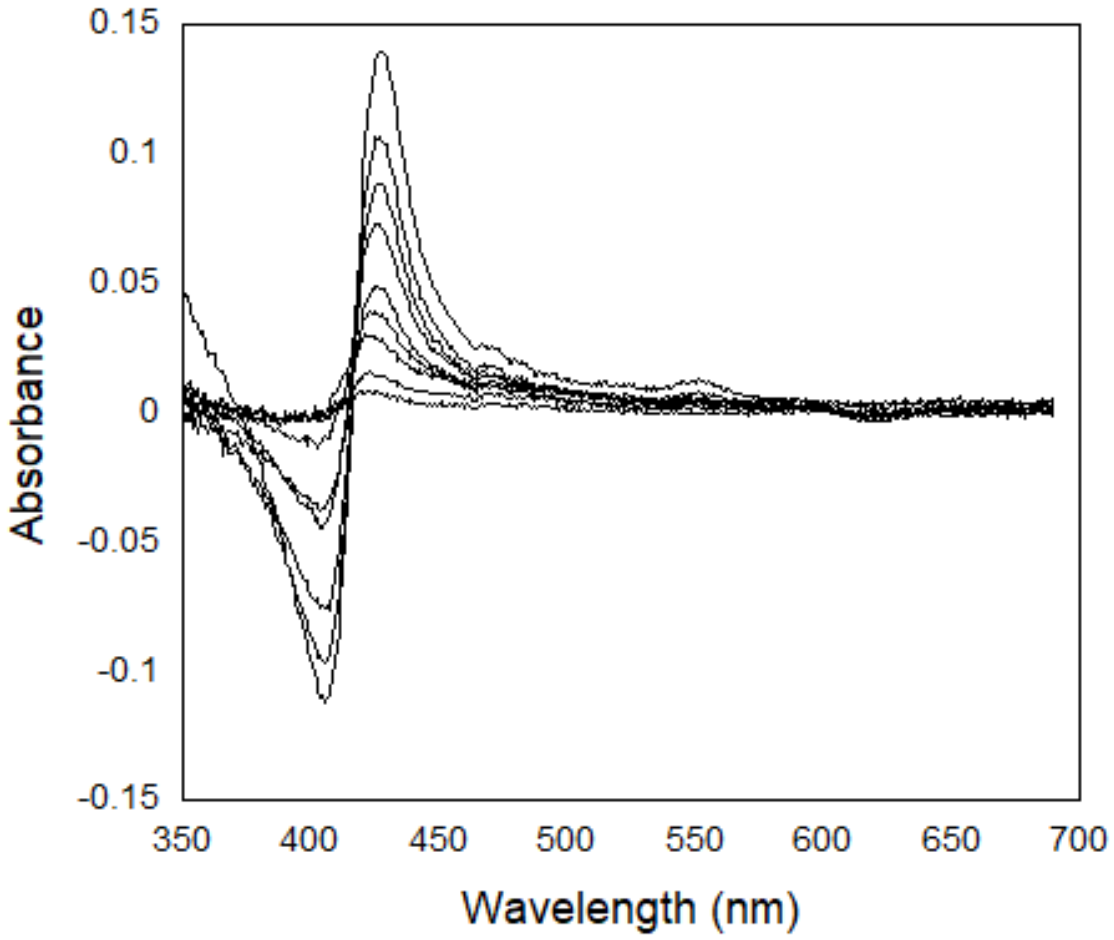

Figure 4.18 - Initial difference spectra at t = 0 for $SeCN^-$ binding to LPO.

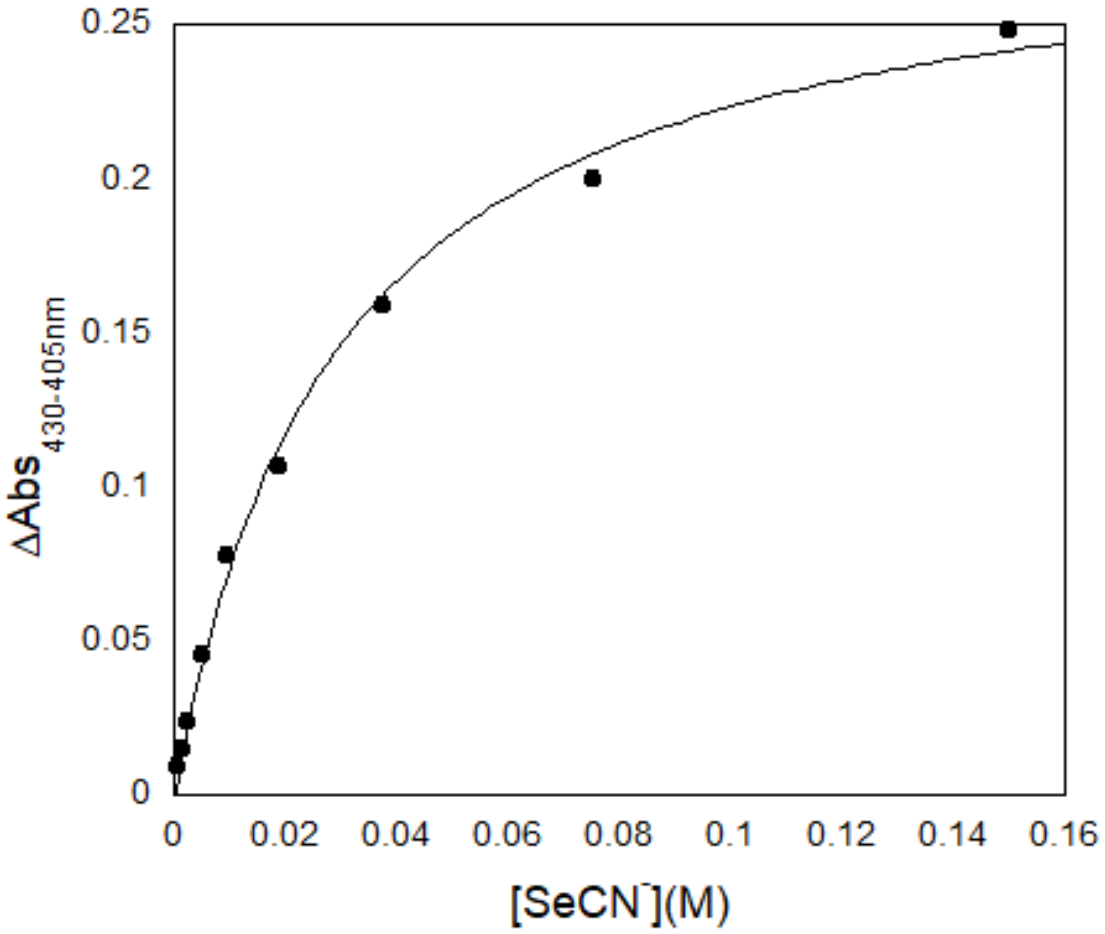

Figure 4.19 – Hill Plot for the initial binding of $SeCN^-$ with LPO. The dissociation constant was calculated to be K_D = 29.2(3) mM. The estimated error, given by the parenthetical digit, is for a least-squares fit.

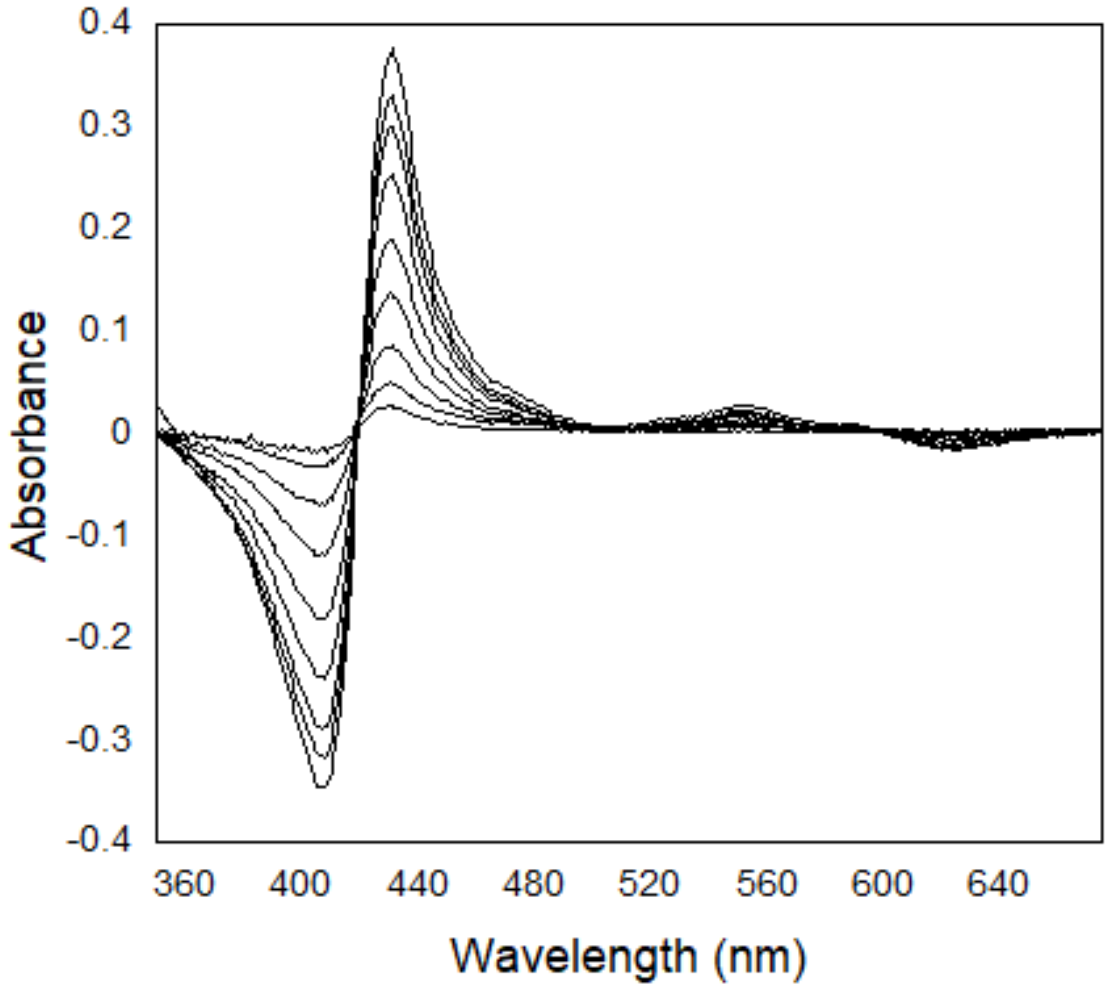

Figure 4.20 - Final difference spectra for $SeCN^-$ binding to LPO.

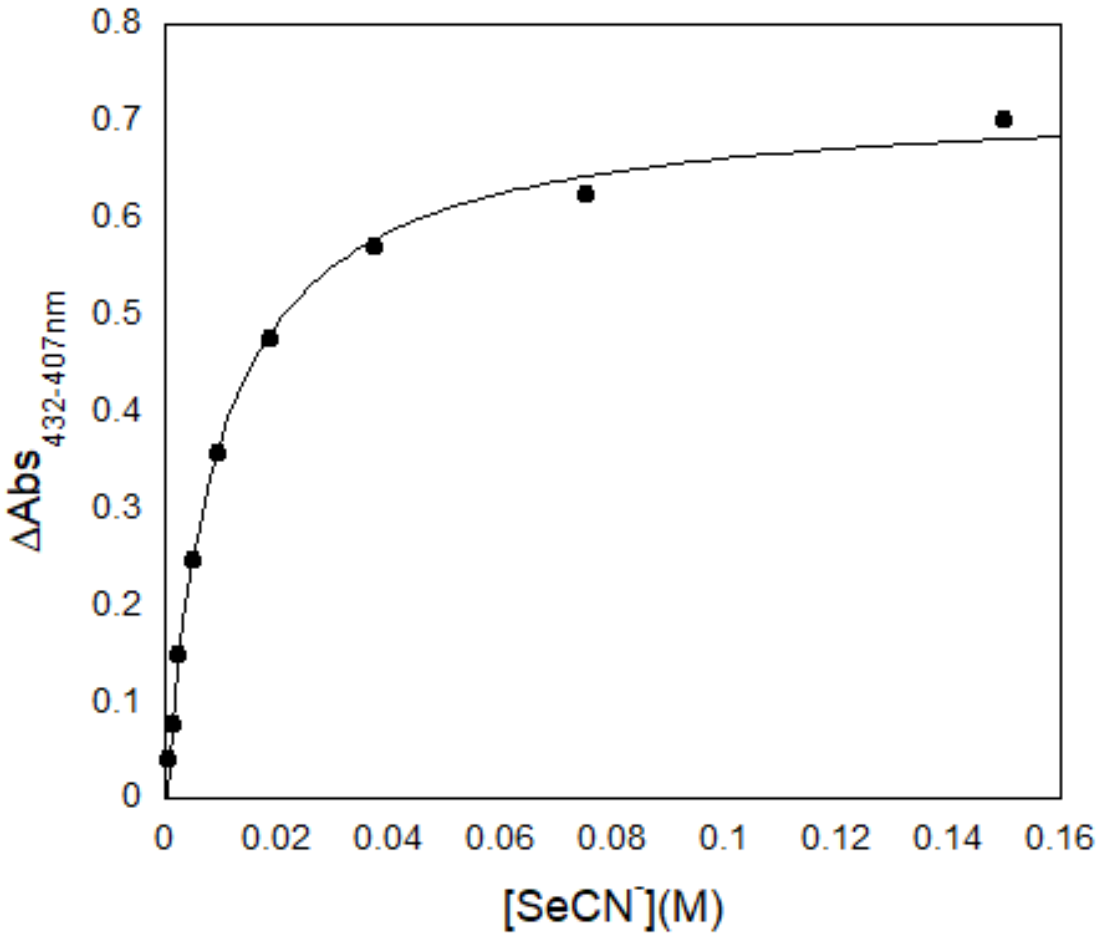

Figure 4.21 – Hill Plot for the final binding of $SeCN^-$ with LPO. The dissociation constant was calculated to be K_D = 9.6(5) mM. The estimated error, given by the parenthetical digit, is for a least-squares fit.

Table 23 - Calculated rate constant for the conversion of LPOSeCN to LPOSeCN* during the binding of LPO with $SeCN^-$

[$SeCN^-$](mM)	k(s^{-1})
9.4	52.0(4)
18.75	50.1(3)
37.5	51.4(3)
75	51.9(3)
Average	51.4(9)

[a]The estimated error given by the parenthetical digit is for a least-squares fit of the global spectral analysis.

[b]The average error represents the standard deviation of the individual fits.

4.4.2 Kinetics of Pseudohalide Competition Binding

The effect of competing substrates on the observed rate of $SeCN^-$ binding to LPO was observed to further explore the proposed binding mechanism given in Figure 4.16. These competition binding experiments were done by allowing LPO to come to pre-equilibrium with either SCN^- or $SeCN^-$ prior to the addition of the other substrate. The concentrations of SCN^- and $SeCN^-$ were independently varied to determine the effect on the rate of the observed reaction. Since LPOSeCN* is the predominantly observed species and the equilibrium represented by K_2 is the rate-limiting reaction, the kinetics of the production of LPOSeCN* were observed when $SeCN^-$ was added to an equilibrium solution of LPOSCN. The kinetics of the loss of LPOSeCN* was observed when SCN^- was added to an equilibrium solution containing LPOSeCN*. We know from our equilibrium

competitive binding experiments, results presented in section 4.3.1, that SCN^- and $SeCN^-$ bind to LPO competitively so the effect of varying the concentrations of SCN^- and $SeCN^-$ on the observed rate constants identifies which binding sites are occupied by SCN^- and $SeCN^-$.

Figure 4.22 shows the proposed mechanism of the observed reaction during the SCN^- and $SeCN^-$ competition studies. This mechanism incorporates the proposed mechanism of $SeCN^-$ binding to LPO, Figure 4.16 in section 4.4.1, and adds the competing equilibrium of SCN^- with LPO.

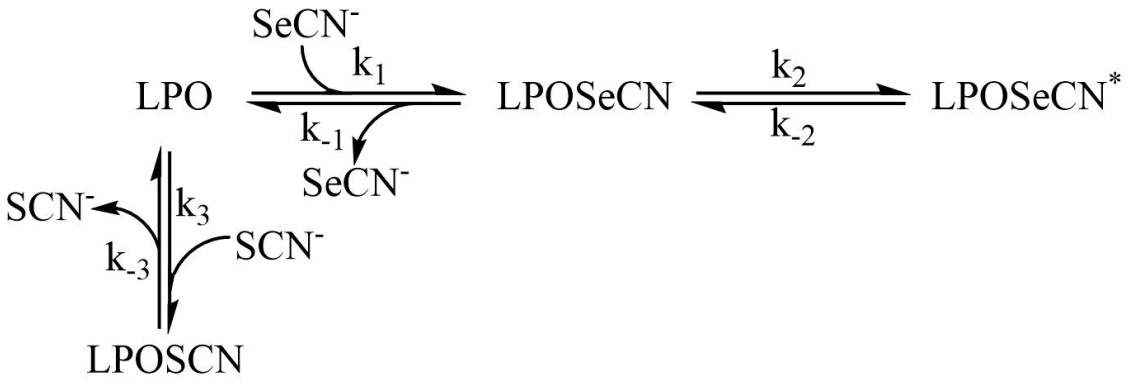

Figure 4.22 - Mechanism of lactoperoxidase binding kinetics for the competition of SCN^- and $SeCN^-$ binding to LPO.

LPO was allowed to come to equilibrium with $SeCN^-$ to produce LPOSeCN* prior to the addition of SCN^- making $SeCN^-$ the competing ligand. When $SeCN^-$ acts as the competing ligand increasing [$SeCN^-$] increased the observed rate constant, Figure 4.24. Increasing [SCN^-] decreased the observed rate constant, Figure 4.25. The rate of this reaction is dependent on k_{-2}, Figure 4.22, as the conversion of LPOSeCN* to LPOSeCN is rate-limiting which is independent of SCN^- and $SeCN^-$. When LPO was allowed to come to equilibrium with SCN^- to produce LPOSCN prior to the addition of $SeCN^-$ increasing [$SeCN^-$] increased observed rate constant and increasing [SCN^-] decreased the observed rate constant, Figures 4.26 and 4.27, respectively. When SCN^- acts as the competing substrate the reaction of LPOSeCN going to LPOSeCN* becomes rate-limiting.

The mechanism in Figure 4.22 can be simplified to a competition equilibrium mechanism to better understand the rate dependencies. Since the rate constants k_2 and k_{-2} are considered rate-limiting in the model for LPO binding with $SeCN^-$, as seen in Figure 4.16, and LPO binding to SCN^- is known to be fast, the intermediate LPOSeCN was excluded to simplify the resulting model in Figure 4.23. While the entire mechanism given in Figure 4.22 should be used in further studies to fit all rate constants as the first $SeCN^-$ binding equilibrium with LPO does affect the binding kinetics, the rate equation for the simplified mechanism, Figure 4.23, can be derived to understand the dependencies. The derived rate equation, Equation 4.4.11, shows the reason for the dependence on [$SeCN^-$] and inverse dependence on [SCN^-] regardless of mixing order as [$SeCN^-$] is found in the numerator and [SCN^-] in the denominator of the equation.

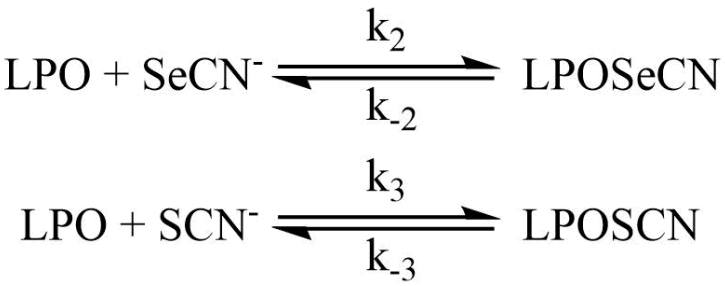

Figure 4.23 - Simplified competition mechanism for the competition of SCN^- and $SeCN^-$ binding to lactoperoxidase.

The rate equation for the model in figure 4.23 can be derived using the steady-state approximation:

$$\frac{+d[LPO]}{dt} = -k_2[LPO][SeCN^-] + -k_{-2}[LPOSeCN^*] - k_3[LPO][SCN^-] \qquad \text{Equation 4.4.8}$$

$$+ -k_{-3}[LPOSCN] = 0$$

$$[LPO]_{SS} = \frac{k_{-3}[LPOSCN] + k_{-2}[LPOSeCN^*]}{k_3[SCN^-] + k_2[SeCN^-]} \qquad \text{Equation 4.4.9}$$

$$\frac{+d[LPOSeCN^*]}{dt} = k_2[LPO][SeCN^-] - k_{-2}[LPOSeCN^*] \qquad \text{Equation 4.4.10}$$

$$= k_2\left(\frac{k_{-3}[LPOSCN] + k_{-2}[LPOSeCN^*]}{k_3[SCN^-] + k_2[SeCN^-]}\right)[SeCN^-] - k_{-2}[LPOSCN^*]$$

Assuming $k_2[SeCN^-] << k_3[SCN^-]$,

$$\frac{+d[LPOSeCN^*]}{dt} = k_2[SeCN^-]\left(\frac{k_{-3}[LPOSCN] + k_{-2}[LPOSeCN^*]}{k_3[SCN^-]}\right) \qquad \text{Equation 4.4.11}$$

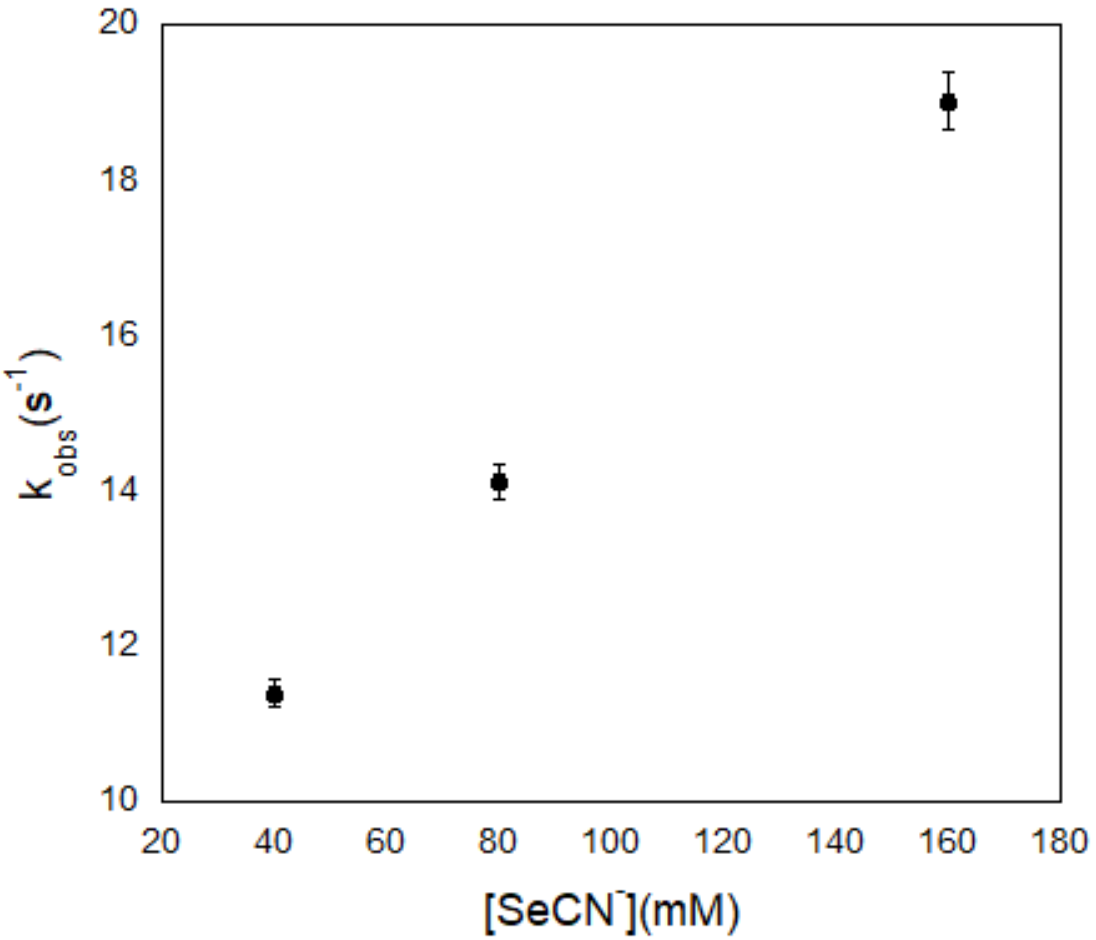

Figure 4.24 - Kinetics of the approach to equilibrium of LPO bound to $SeCN^-$ upon the addition of SCN^- as a function of [$SeCN^-$]. Final concentrations were [LPO] = 4.9, [SCN^-] = 320 mM, and [$SeCN^-$] = 40-160 mM. The estimated error shown by the error bars is for a least-squares fit of the global spectral analysis.

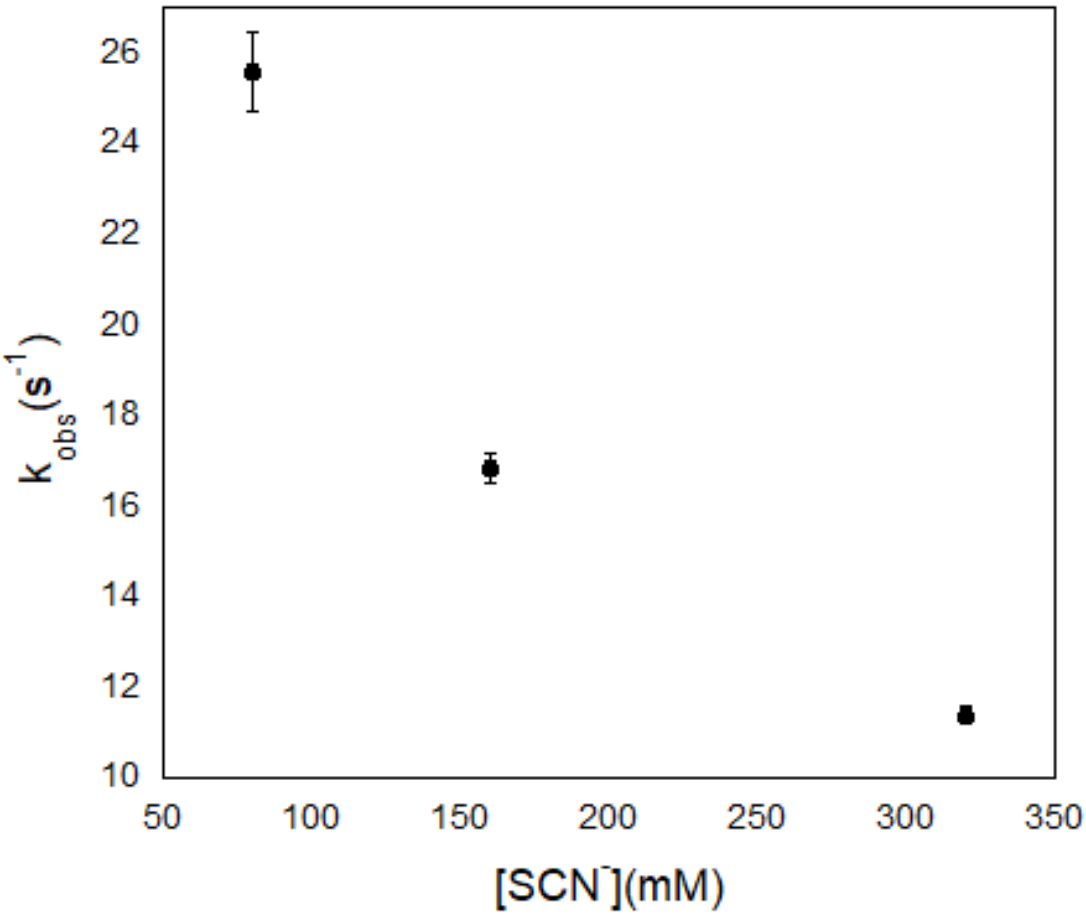

Figure 4.25 - Kinetics of the approach to equilibrium of LPO bound to $SeCN^-$ upon the addition of SCN^- as a function of [SCN^-]. Final concentrations were [LPO] = 4.9, [$SeCN^-$] = 40 mM, and [SCN^-] = 80-320 mM. The estimated error shown by the error bars is for a least-squares fit of the global spectral analysis.

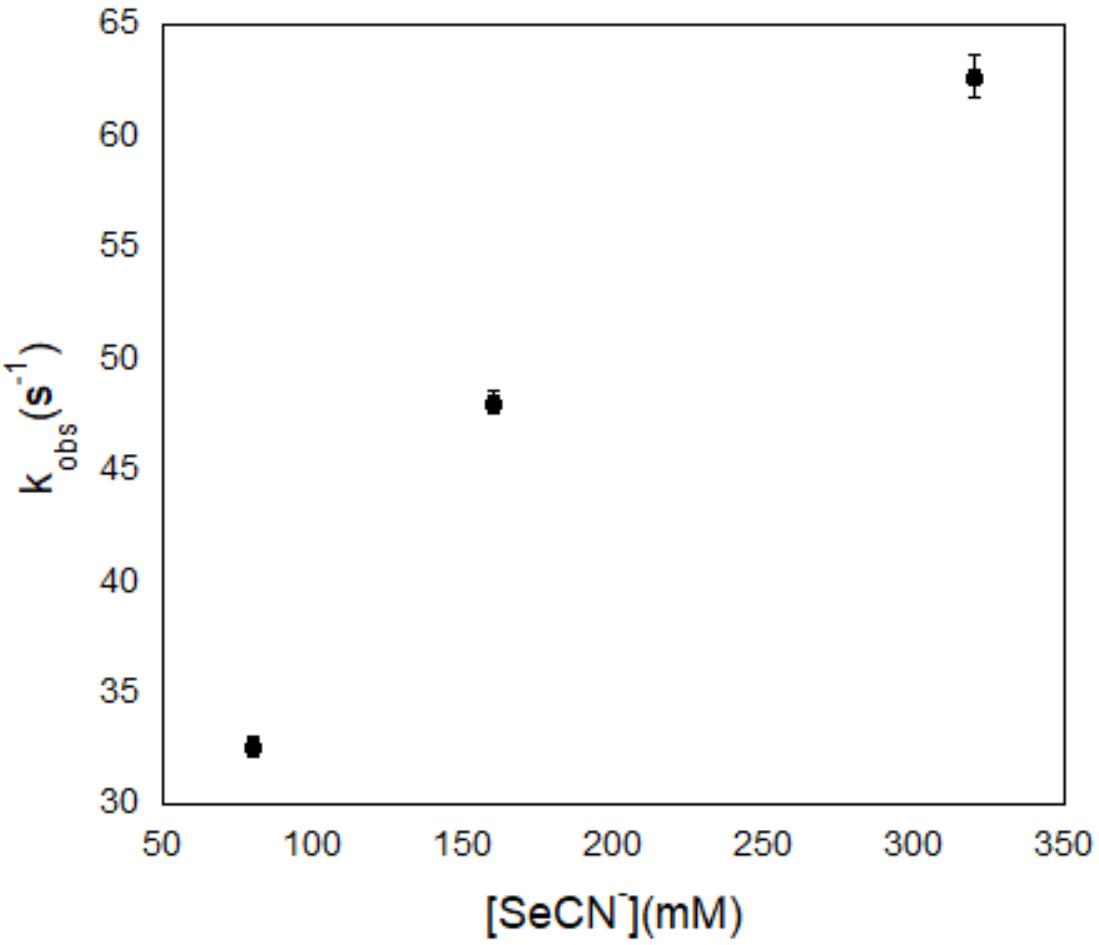

Figure 4.26 - Kinetics of the approach to equilibrium of LPO bound to SCN^- upon the addition of $SeCN^-$ as a function of [$SeCN^-$]. Final concentrations were [LPO] = 5.1 uM, [SCN^-] = 40 mM, and [$SeCN^-$] = 80-320 mM. The estimated error shown by the error bars is for a least-squares fit of the global spectral analysis.

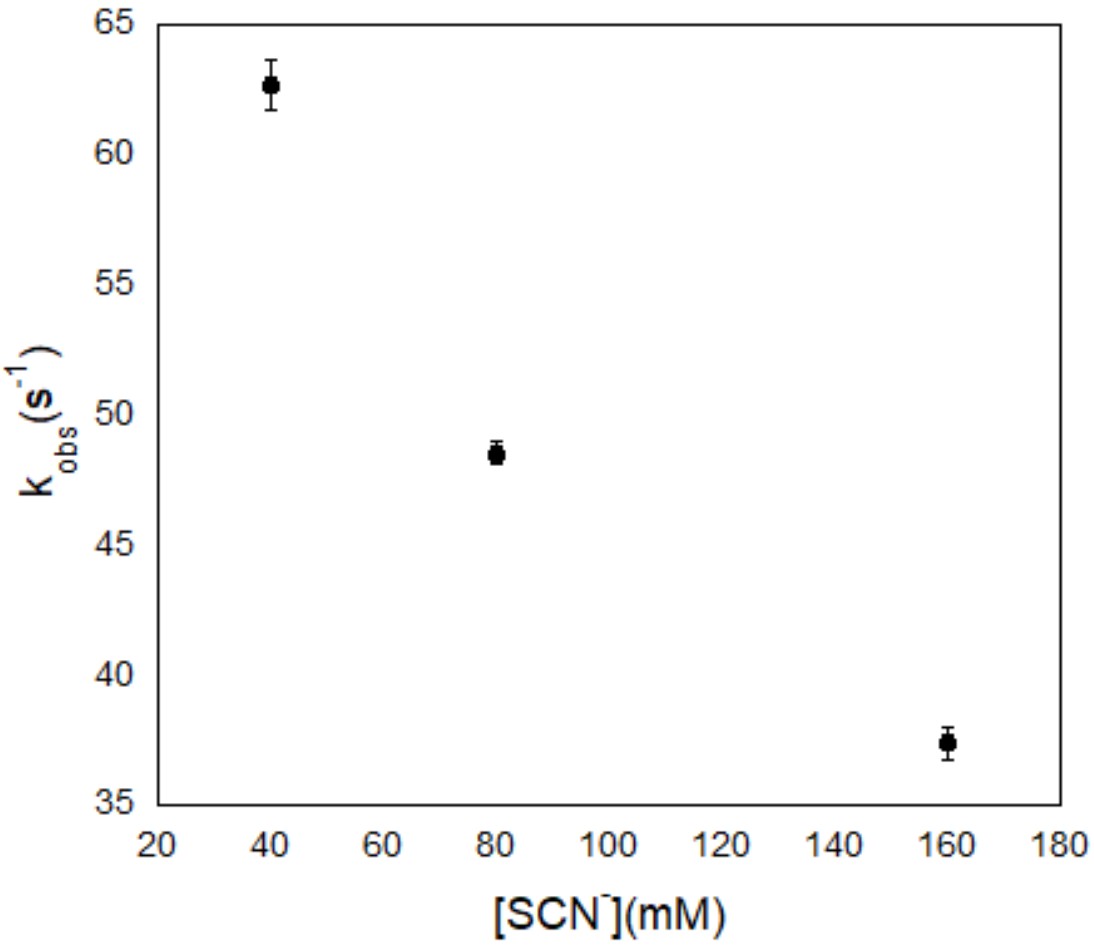

Figure 4.27 - Kinetics of the approach to equilibrium of LPO bound to SCN^- upon the addition of $SeCN^-$ as a function of [$SeCN^-$]. Final concentrations were [LPO] = 5.1 uM, [$SeCN^-$] = 320 mM, and [SCN^-] = 40-160 mM. The estimated error shown by the error bars is for a least-squares fit of the global spectral analysis.

4.5 Conclusion

The binding constant of $SeCN^-$ with LPO was determined using a spectral titration of K_D = 9.5(1) mM which is smaller than the dissociation constant calculated for the SCN^- binding constant of K_D = 15.6(6) mM. The difference in binding constants indicates a tighter binding for $SeCN^-$ relative to SCN^- to LPO.

The tighter binding of $SeCN^-$ than SCN^- to LPO may be due to the differences in the mechanism and available binding sites. We have presented evidence that $SeCN^-$ binds to LPO in a two-phase reaction and can occupy two separate binding sites within LPO. The first reaction is the binding of $SeCN^-$ to the kinetic binding site of LPO and is very fast as is the binding of SCN^- to LPO. In the second equilibrium, the bound $SeCN^-$ shifts to the thermodynamic binding site. However, SCN^- binding kinetics show no spectral evidence that SCN^- moves to a second binding site. The thermodynamic binding site for $SeCN^-$ is likely closer to the heme than the kinetic binding site or has a different orientation with respect to the heme which would cause the increased Soret band shift as well as increased absorption change of the Q-bands. However, given the lack of competition between $SeCN^-$ and F^-, it is unlikely that $SeCN^-$ binds directly to the iron of the heme, section 4.3.2.

Also notable is the lack of evidence of the difference in binding of $SeCN^-$ to LPO as compared to SCN^- in the catalytic mechanism for the LPO-catalyzed oxidation of PsX^- discussed in section 3.4. The shift in binding site/orientation of $SeCN^-$ has a first-order rate constant of 51.4 s^{-1}. The calculated first-order rate constant for the reaction of LPOSeCN with H_2O_2, k_3 in the proposed LPO catalysis mechanism given in Figure 3.28, was 60 s^{-1} at the lowest concentration of H_2O_2 of 5 uM. The larger first-order rate constant for the reaction of the LPOSeCN species with H_2O_2 than that of the shift from the

kinetically bound LPOSeCN species to the thermodynamically bound LPOSeCN* species indicated that the production of the LPOSeCN* was not kinetically competent and should not be expected to affect the LPO catalysis kinetics. The competitive rates of binding of LPO with $SeCN^-$ and SCN^- given in section 3.6.1 in addition to the likelihood that SCN^- would be much more prevalent in physiological fluids as compared to $SeCN^-$ indicate that it is unlikely that $SeCN^-$ would be competitive with SCN^- for LPO binding *in vivo*. Lack of competition of $SeCN^-$ for LPO binding also makes it unlikely that $OSeCN^-$ is a naturally occurring species.

4.6 Future Work

Additional $SeCN^-$ binding studies should be done to determine the exact values of the individual rate constants and for the proposed mechanism of $SeCN^-$ binding to LPO, Figure 4.16, to determine how these relate to the binding observed in the catalytic mechanism. Also, more detailed $SCN^-/SeCN^-$ competition binding studies may be the key to determining the backward rate constant for the conversion of LPOSeCN* to LPOSeCN.

Chapter 5 – EXPERIMENTAL METHODS

5.1 Synthesis and Study of Hyposelenocyanite at Alkaline pH

5.1.1 Materials

Potassium selenocyanate, KSeCN, was obtained from Milipore Sigma. Chlorine gas, Cl_2, was obtained from Sigma Aldrich. Sodium hydroxide, NaOH, was obtained from Fisher Scientific. Water was doubly distilled in glass. Sodium hypochlorite, NaOCl, was prepared by sparging Cl_2 gas into 0.3 M sodium hydroxide until the solutions reached concentration of approximately 0.1 M. NaOCl solution was standardized spectrophotometrically, $\varepsilon(OCl^-)_{292\ nm} = 350\ M^{-1}cm^{-1}$.[142]

Kinetic data was collected using a Hi-Tech SF-61 DX2 stopped-flow instrument with a xenon arc lamp at 25 °C. Polychromatic data was collected using a photodiode array detector and single wavelength data was collected using a photomultiplier tube detector. Absorbance spectra were collected using a HP8452 A Diode array spectrophotometer. The pH of the final solutions were determined using an Orion Research Expandable ionAnalyzer EA 920 with a VWR symphony combination pH probe.

Polychromatic kinetic data was analyzed using SPECFIT Version 3.0.40. Least-squares analysis of the single wavelength kinetic data were fit using Kinetic Studio Version 1.0.12.19577.[161] Least-squares analysis to determine the relationship of observed rate constants was done using KaleidaGraph Version 3.5.[162]

5.1.2 Synthesis of Hyposelenocyanite by the Oxidation of Selenocyanate by Hypochlorous Acid at Alkaline pH

Solutions of KSeCN and NaOCl were prepared in 0.1 M sodium hydroxide. The concentration of KSeCN was varied to determine rate dependencies for the production of

$OSeCN^-$. The concentrations of KSeCN were maintained at 100 times the concentration of NaOCl to minimize overoxidation of $OSeCN^-$.

NaOCl and KSeCN were reacted in a single mixing stopped-flow experiment, Figure 5.1. The rate of the reaction of NaOCl was observed at 292 nm. An average of five kinetic traces were fit to a first-order integrated rate equation for each concentration condition.

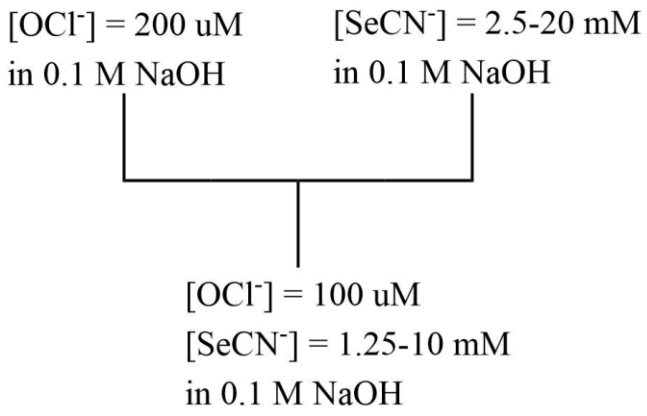

Figure 5.1 - Reaction mixing scheme for the single mixing stopped-flow experiment for the synthesis of $OSeCN^-$ at alkaline pH as $[SeCN^-]$ was varied. This mixing scheme was used to produce the data in Figure 2.3 in section 2.2.1.

5.1.3 Determination of the Rate of Decomposition of Hyposelenocyanite at Alkaline pH

NaOCl and KSeCN solutions were made in 0.1 M NaOH. The concentrations of NaOCl were at least 3 mM so $OSeCN^-$ could be observed spectrophotometrically. Pseudo-first-order conditions with respect to $SeCN^-$ were used to minimize overoxidation.

NaOCl and KSeCN were reacted in a single mixing stopped-flow experiment with monochromatic data collection at 378 nm to directly observe the decomposition of $OSeCN^-$. The concentrations of NaOCl and KSeCN were independently varied to determine the effect on the reaction rate, Figure 5.2.

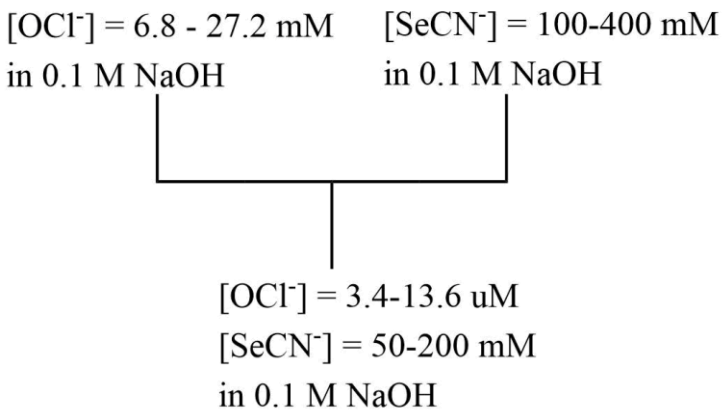

Figure 5.2 - Reaction mixing scheme for the single mixing stopped-flow experiment for the decomposition of $OSeCN^-$ at alkaline pH as $[SeCN^-]$ and $[OCl^-]$ was varied. This mixing scheme was used to produce the data in Tables 3 and 4 in section 2.2.1.

5.2 Observation of Hyposelenocyanite at Neutral pH Produced by the Lactoperoxidase-Catalyzed Oxidation of Selenocyanate by Hydrogen Peroxide

5.2.1 Materials

KSeCN was obtained from Milipore Sigma. Sodium hydroxide, NaOH, was obtained from Fisher Scientific. Water was doubly distilled in glass. Phosphate buffer was made using anhydrous monosodium phosphate, NaH_2PO4, obtained from Fisher Scientific and disodium phosphate, Na_2HPO4, obtained from Mallinckrodt Chemicals. The pH of the phosphate buffer was adjusted using NaOH and measured using an Orion Research Expandable ionAnalyzer EA 920 with a VWR symphony combination pH probe. Hydrogen peroxide 30%, H_2O_2, was obtained from Fisher Scientific.

Lactoperoxidase was dissolved in 100 mM pH 7 phosphate buffer and standardized spectrophotometrically, $\varepsilon(LPO)_{412\ nm}$ = 112,000 $M^{-1}cm^{-1}$.[12] H_2O_2 was diluted from 30% with water and standardized spectrophotometrically, $\varepsilon(H_2O_2)_{240\ nm}$ = 36.4 $M^{-1}cm^{-1}$.[163] TNB was dissolved in 100 mM pH 7 phosphate buffer and standardized spectrophotometrically, $\varepsilon(TNB)_{412\ nm}$ = 14,150 $M^{-1}cm^{-1}$.[146]

Absorption spectra were collected using a HP 8452 A Diode array spectrophotometer. Time-resolved stopped-flow measurements were collected using a Hi-Tech SF-61 DX2 stopped-flow instrument with a xenon arc lamp at 25 °C. Polychromatic data was collected using a photodiode array detector and single wavelength data was collected using a photomultiplier tube detector. This instrument is equipped with a xenon arc lamp and a 1.00 cm path length quartz sample cell.

5.2.2 Rate of Production and Stoichiometry of Hyposelenocyanite Produced by the Lactoperoxidase-Catalyzed Oxidation of Selenocyanate by Hydrogen Peroxide

A single mixing experiment was performed with data collection at 324 nm to observe the production of DTNB and determine the rate at which $OSeCN^-$ is produced by the LPO-catalyzed oxidation of $SeCN^-$ by H_2O_2 as a function of [LPO]. A mixture of KSeCN, LPO, and TNB was reacted with H_2O_2 according to the scheme in Figure 5.3. An average of five kinetic traces for each concentration condition was fit to a first-order integrated rate equation to determine the observed rate constants.

The LPO-catalyzed oxidation of $SeCN^-$ by H_2O_2 was also studied as a function of [H_2O_2] to determine the stoichiometry of $OSeCN^-$ production and H_2O_2. A single mixing stopped flow experiment according to the mixing scheme in Figure 5.3 was used with final reactant concentrations of [LPO] = 1 uM, [$SeCN^-$] = 1 mM, [TNB] = 70 uM, and [H_2O_2] = 7.5-30 uM.

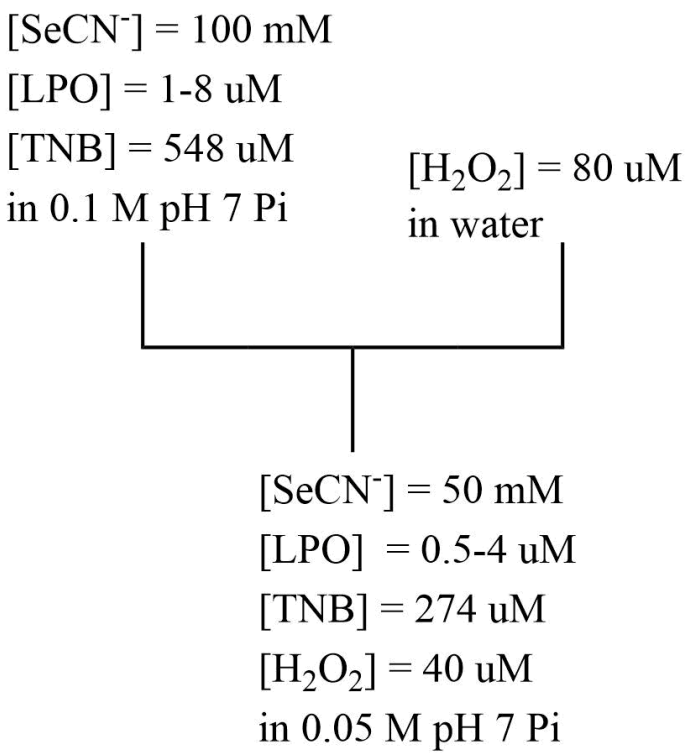

Figure 5.3 - Reaction mixing scheme for the single mixing stopped-flow experiment to observe rate of production of $OSeCN^-$ at neutral pH by the LPO-catalyzed oxidation of $SeCN^-$ by H_2O_2. This mixing scheme was used to produce the data in Figure 2.6 in section 2.3.1. The experiment in Table 5 used this scheme as well with varied concentrations.

5.2.3 Determination of the Rate of Decomposition of Hyposelenocyanite at Alkaline pH

Double mixing experiments were performed with data collection at 412 nm to observe the lifetime of $OSeCN^-$ at pH 7. $OSeCN^-$ was produced in the first mixing cycle by the LPO-catalyzed oxidation of KSeCN by H_2O_2. This was achieved by reacting a mixture of LPO and KSeCN, buffered at pH 7 in 100 mM phosphate buffer, with H_2O_2. This reaction was performed under pseudo-first-order conditions with respect to KSeCN

to minimize overoxidation. LPO was kept at catalytic concentrations of less than 10% [H_2O_2]. This reaction was observed in a single mixing experiment to determine the minimum age time necessary to complete the $OSeCN^-$ in the first mixing cycle. The minimum age time for the double mixing experiment was set to four half-lives of this reaction.

The age time after the first mixing cycle was varied from 0.2-1.6 seconds before the addition of TNB in the second mixing cycle. The change in TNB concentration from a blank with no [H_2O_2] added was used to determine the concentration of the remaining product. Data was collected monochromatically at 412 nm to observe the change in [TNB] as [$OSeCN^-$] was produced.

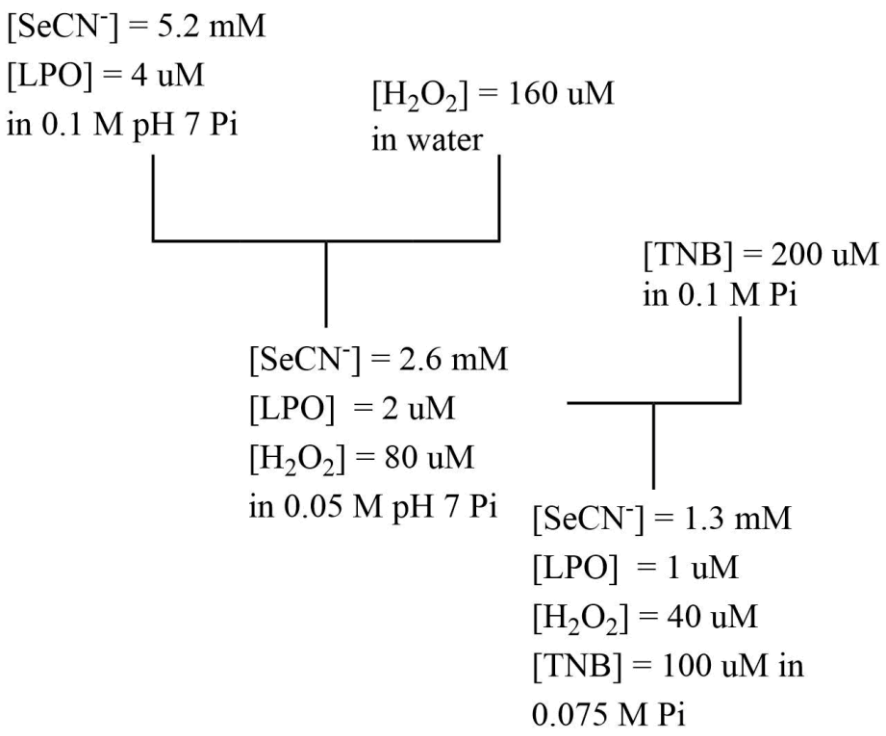

Figure 5.4 - Reaction mixing scheme for the double mixing stopped-flow experiment to observe the rate of decomposition of $OSeCN^-$ at neutral pH. This mixing scheme was used to produce the data in Figure 2.7 in section 2.3.2.

5.3 Lactoperoxidase Mechanistic Studies

5.3.1 Materials

Water was doubly distilled in glass. NaSCN was obtained from Sigma-Aldrich. KSeCN was obtained from Millipore Sigma. H_2O_2 was obtained from Fisher Scientific and the concentration was determined spectrophotometrically, $\varepsilon(H_2O_2)_{240\ nm}$ = 36.4 $M^{-1}cm^{-1}$.[163] LPO concentration was determined spectrophotometrically, $\varepsilon(LPO)_{412\ nm}$ = 112,000 $M^{-1}cm^{-1}$.[12] TNB was standardized spectrophotometrically, $\varepsilon(TNB)_{412\ nm}$ = 14,150 $M^{-1}cm^{-1}$.[146]

Solutions of NaSCN, KSeCN, and LPO were buffered in 100 mM pH 7 phosphate buffer. Phosphate buffer was made using anhydrous monosodium phosphate, NaH_2PO4, obtained from Fisher Scientific and disodium phosphate, Na_2HPO4, obtained from Mallinckrodt Chemicals. NaOH was obtained from Fisher Scientific and was used to adjust the buffer pH. The pH was measured using an Orion Research Expandable ionAnalyzer EA 920 with a VWR symphony combination pH probe. Buffers were treated with Chelex-100 to remove divalent metals.

Absorbance measurements were measured using a HP 8452A diode array spectrophotometer. Stopped-flow measurements were collected using a Hi-Tech SF-661 DX2 instrument equipped with a photomultiplier tube for single wavelength detection and a diode array for collection of polychromatic data. This instrument is equipped with a xenon arc lamp and a 1.00 cm path length quartz sample cell.

Polychromatic kinetic data was analyzed using SPECFIT Version 3.0.40.[160] Single wavelength kinetic data was analyzed using Kinetic Studio Version 1.0.12.19577.[161] Least-squares analysis to determine the relationship of observed rate constants was done using KaleidaGraph Version 3.5.[162] Mathematica was used to model the data and a nonlinear fit was used to determine the rate constants.[164]

Polychromatic kinetic data was deconvoluted and fit using SPECFIT Version 3.0.40.[160] Single wavelength kinetic data was analyzed using Kinetic Studio Version 1.0.12.19577.[161] Least-squares analysis to determine order dependency was done using KaleidaGraph Version 3.5.[162]

5.3.2 Collection of Stopped-Flow Kinetic Data for the Lactoperoxidase-Catalyzed Oxidation of Pseudohalides by Hydrogen Peroxide

Single mixing stopped-flow experiments according to the scheme in Figure 5.3 were used to probe the mechanism of the LPO-catalyzed oxidation of $SeCN^-$ and H_2O_2. Experiments were done under what will be considered "high concentration" and "low concentration" of reducing substrates. High concentration of reducing substrates refers, in general, to experiments we conducted where $[PsX^-] \geq 1$ mM, [LPO] ≥ 1 uM, and pseudo-first-order conditions of $[PsX^-]$ with respect to $[H_2O_2]$ were used. Low concentration of reducing substrates refers, in general, to experiments conducted under conditions of $[PsX^-] \leq 1$ mM, stoichiometric or near stoichiometric conditions of $[PsX^-]$ with respect to $[H_2O_2]$, and [LPO] ≤ 1 uM. High and low concentration conditions were optimized to observe the effects of varying reactant and enzyme concentrations where first-order and biphasic reaction trace kinetics were observed, respectively.

Experimental traces were collected at 412 nm to observe the change in TNB during the LPO catalysis. Five runs were averaged and fit to a Mathematica model given in section 5.3.5. Data from the experiments where the biphasic reaction kinetics were observed was collected for the pre-steady-state reaction independently to obtain more resolved traces. Data was then collected over the entire reaction time and the data sets were merged.

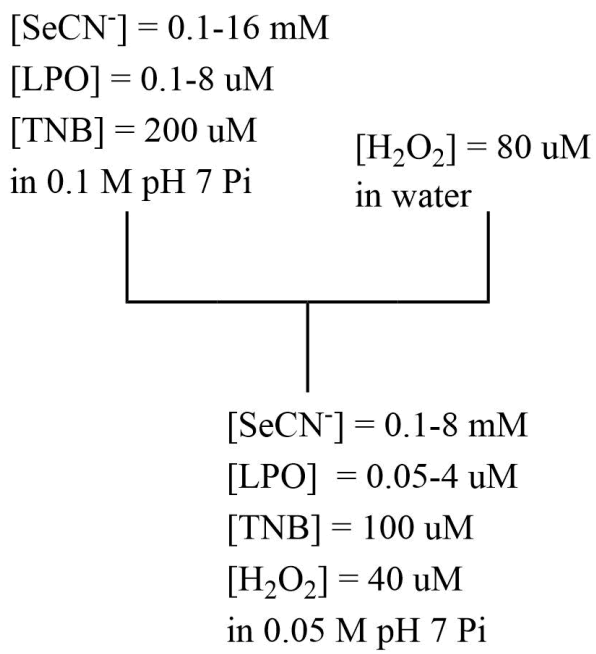

Figure 5.5 - Reaction mixing scheme for the single mixing stopped-flow experiment to observe the rate of the LPO-catalyzed oxidation of $SeCN^-$ by H_2O_2 at neutral pH. This mixing scheme was used to produce the data in Chapter 3.

5.3.3 Determining the Effect of Mixing order on the Lactoperoxidase-Catalyzed Oxidation of Pseudohalides by Hydrogen Peroxide

The effect of the order of mixing of LPO with PsX^- and H_2O_2 on the reaction kinetics of the LPO-catalyzed oxidation of PsX^- under low PsX^- concentration conditions. Two double mixing stopped-flow experiments were performed which first allowed LPO and SCN^- to come to equilibrium in the first mixing cycle, then added H_2O_2 in the second mixing cycle to initiate catalysis. A second double mixing experiment reacted LPO with

H_2O_2 in the first mixing cycle, then added SCN^- in the second mixing cycle. The age time in both experiments was 0.5 seconds.

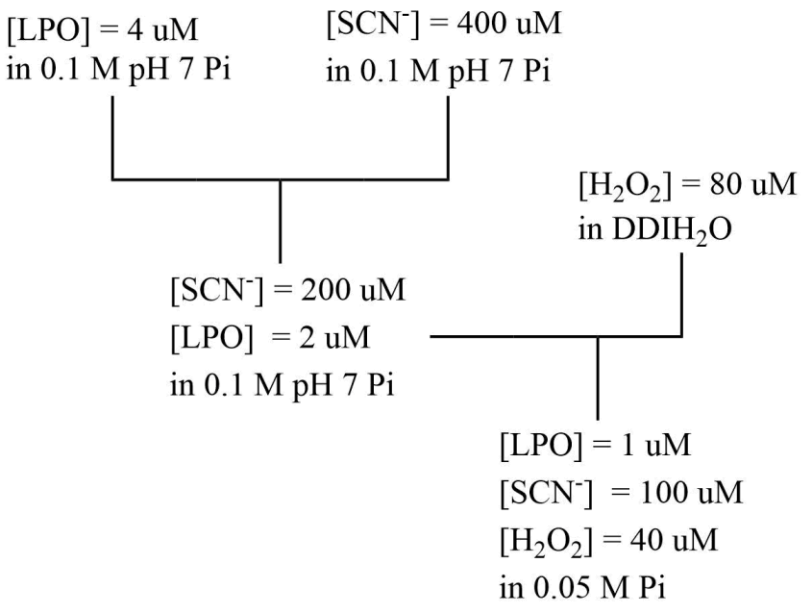

Figure 5.6 - Reaction mixing scheme for the double mixing stopped-flow experiment to observe the effect of mixing LPO and PsX^- in the first mixing cycle prior to the addition of H_2O_2 on the LPO-catalyzed oxidation of PsX^- by H_2O_2 at neutral pH. This mixing scheme was used to produce the data in Figure 3.22.

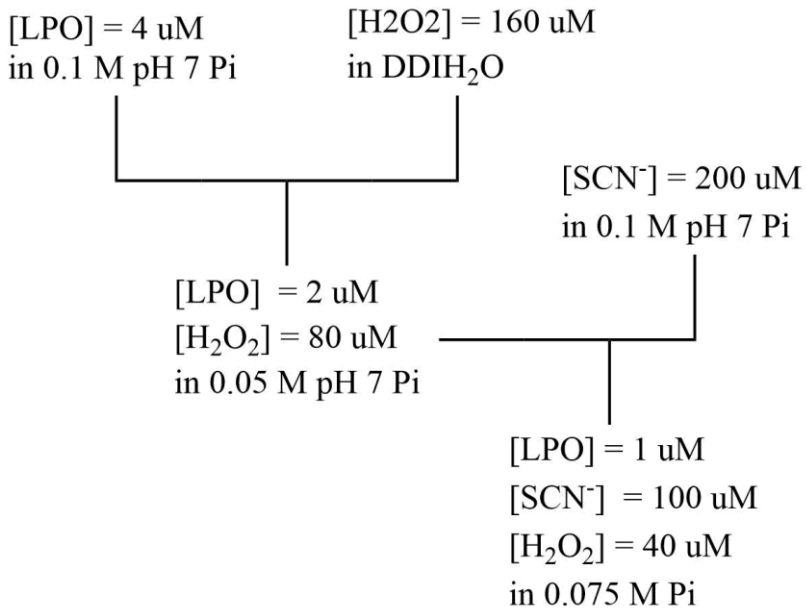

Figure 5.7 - Reaction mixing scheme for the double mixing stopped-flow experiment to observe the effect of mixing LPO and H_2O_2 in the first mixing cycle prior to the addition of PsX^- on the LPO-catalyzed oxidation of PsX^- by H_2O_2 at neutral pH. This mixing scheme was used to produce the data in Figure 3.23.

5.4 Lactoperoxidase Binding Studies

5.4.1 Materials

Potassium selenocyanate, KSeCN, was obtained from Millipore Sigma. Sodium thiocyanate was obtained from Sigma-Aldrich. Phosphate buffer was made using anhydrous monosodium phosphate, NaH_2PO4, obtained from Fisher Scientific and disodium phosphate, Na_2HPO4, obtained from Mallinckrodt Chemicals. The pH was adjusted using concentrated NaOH obtained from Fisher Scientific and measured using an Orion Research Expandable ionAnalyzer EA 920 with a VWR symphony combination pH

probe. Water was doubly distilled in glass. Lactoperoxidase was dissolved in 100 mM pH 5.5 phosphate buffer and standardized spectrophotometrically, $\varepsilon(LPO)_{412\ nm}$ = 112,000 $M^{-1}cm^{-1}$.[12] NaSCN and KSeCN were weighed out and dissolved in 100 mM pH 5.5 phosphate buffer.

Absorption spectra were measured using a HP 8452A diode array spectrophotometer. Stopped-flow measurements were collected using a Hi-Tech SF-661 DX2 instrument equipped with a photomultiplier tube for single wavelength detection and a diode array for collection of polychromatic data. This instrument is equipped with a xenon arc lamp and a 1.00 cm path length quartz sample cell.

Polychromatic kinetic data was analyzed using SPECFIT Version 3.0.40.[160] Single wavelength kinetic data was analyzed using Kinetic Studio Version 1.0.12.19577.[161] Scatchard Plots, Hill Plots, and least-squares analysis on the datasets were done using Kaleidagraph Version 3.5. [162]

5.4.2 Spectral Titrations

Spectral titrations of NaSCN and KSeCN with LPO were conducted to determine the dissociation constants of the substrates with LPO.[155] Spectral titrations with LPO were conducted by adding 200 µL of NaSCN or KSeCN of varying concentrations to 2 mL of LPO in a 1 cm quartz cuvette using micropipettes. Stock lactoperoxidase concentrations were approximately 4.4 uM so that the after mixing concentration was 4 uM. Stock NaSCN and KSeCN solutions were varied such that final [NaSCN] and [KSeCN] varied from approximately 1-300 mM. Solutions were mixed well in a 1 cm quartz cuvette and allowed to come to equilibrium for approximately one minute before polychromatic absorption spectra were collected.

5.4.3 Lactoperoxidase Competition Studies

Spectral titrations of competition of thiocyanate and selenocyanate as well as fluoride and selenocyanate for lactoperoxidase binding were conducted.[155] Thiocyanate, selenocyanate, fluoride, and lactoperoxidase solutions were prepared in 100 mM phosphate buffer at pH 5.5.

Lactoperoxidase (1 mL of 9.2 uM) and sodium fluoride (1 mL of 29.6 mM) were added to a 1x1 cm cuvette using a micropipette and mixed well. 300 uL of potassium selenocyanate of varying concentration form 2-0.077 M was added to the cuvette. The solution was mixed well and allowed to come to equilibrium for one minute. A blank, made by adding 1 mL of 9.2 uM, and 1.3 mL of 100 mM pH 5.5 phosphate buffer to a 1x1 cm cuvette, was used to blank the instrument so difference spectra could be collected.

5.4.4 Scatchard Analysis

Scatchard analyses were performed to determine the binding constants and number of binding equivalents. The concentration of lactoperoxidase and bound lactoperoxidase could not be calculated directly due to the small shift in absorbance for the bound and unbound protein so the difference spectra were used to analyze the data and the following mathematical analysis was used to fit the data. In the analysis below, E = LPO, X = SCN/SeCN, EX = Bound LPO.

$$EX \rightleftharpoons E + X \qquad \text{Equation 6.4.1}$$

$$K_d = \frac{[E] * [X]}{[EX]} \qquad \text{Equation 6.4.2}$$

$$[E_T] = [E] + [EX] \qquad \text{Equation 6.4.3}$$

Enzyme spectra were recorded before and after addition of X and the difference spectra of the two spectra was taken. The wavelengths with maximum positive and negative absorbance were determined which are referred to as peak and valley, p and v, respectively. So,

$$A_{X,p} = \varepsilon_{p,E}[E] + \varepsilon_{p,EX}[EX] \qquad \text{Equation 6.4.4}$$

When no X has been added,

$$A_{0,p} = \varepsilon_{p,E}[E_T] \qquad \text{Equation 6.4.5}$$

The change in absorbance can be written as,

$$\Delta A_p = A_{X,p} - A_{0,p} \qquad \text{Equation 6.4.6}$$

$$= \varepsilon_{p,E}[E] + \varepsilon_{p,EX}[EX] - \varepsilon_{p,E}[E_T]$$

Substituting Equation 6.4.3, solved for [E]

$$\Delta A_p = \varepsilon_{p,E}[E_T] - \varepsilon_{p,E}[EX] + \varepsilon_{p,EX}[EX] \qquad \text{Equation 6.4.7}$$

$$- \varepsilon_{p,E}[E_T]$$

Simplify

$$\Delta A_p = -\varepsilon_{p,E}[EX] + \varepsilon_{p,EX}[EX] \qquad \text{Equation 6.4.8}$$

Separate variables

$$\Delta A_p = \left(\varepsilon_{p,EX} - \varepsilon_{p,E}\right)[EX] \qquad \text{Equation 6.4.9}$$

Given that Equations 6.4.4-6.4.9 also have analogous equation for the valley,

$$\Delta A_{p-v} = \Delta A_p - \Delta A_v \qquad \text{Equation 6.4.10}$$

$$= \left(\varepsilon_{p,EX} - \varepsilon_{p,E}\right)[EX] - \left(\varepsilon_{v,EX} - \varepsilon_{v,E}\right)[EX]$$

Rearrange

$$\Delta A_{p-v} = \left(\varepsilon_{p,EX} - \varepsilon_{p,E} - \varepsilon_{v,EX} + \varepsilon_{v,E}\right)[EX] \qquad \text{Equation 6.4.11}$$

The constant $\varepsilon_{p,EX} - \varepsilon_{p,E} - \varepsilon_{v,EX} + \varepsilon_{v,E}$ can be renamed $\Delta\varepsilon_{p-v}$ to give,

$$\Delta A_{p-v} = \left(\Delta\varepsilon_{p-v}\right)[EX] \qquad \text{Equation 6.4.12}$$

Solving Equation 6.4.2 for EX and then substituting into equation 6.4.12 gives

$$\Delta A_{p-v} = \left(\Delta\varepsilon_{p-v}\right)\left[\frac{[X] * [E]}{K_d}\right] \qquad \text{Equation 6.4.13}$$

Substitute Equation 6.4.3, solved for E

$$\Delta A_{p-v} = \left(\Delta\varepsilon_{p-v}\right)\left[\frac{[X] * [E_T - EX]}{K_d}\right] \qquad \text{Equation 6.4.14}$$

Rearranging and substituting Equation 6.4.12 in the form of $EX = \frac{\Delta A_{p-v}}{\Delta \varepsilon_{p-v}}$ gives,

$$\frac{\Delta A_{p-v}}{[X]} = \Delta \varepsilon_{p-v}\left[-\frac{\Delta A_{p-v}}{\Delta \varepsilon_{p-v} * K_d} + \frac{E_T}{K_d}\right] \qquad \text{Equation 6.4.15}$$

Combining terms gives,

$$\frac{\Delta A_{p-v}}{[X]} = -\frac{\Delta A_{p-v}}{K_d} + \frac{\Delta \varepsilon_{p-v} * [E_T]}{K_d} \qquad \text{Equation 6.4.16}$$

Using equation 16 and plotting $\frac{\Delta A_{p-v}}{[X]}$ vs. ΔA_{p-v}, a linear plots result given there is only one binding site. In these plots $m = -\frac{1}{K_d}$ and $y_{int} = \frac{\Delta \varepsilon_{p-v} * [E_T]}{K_d}$.

5.4.5 Logarithmic Hill Plot

The logarithmic Hill plot was used to calculate the Hill coefficients and determine the cooperativity of binding between LPO reducing substrates. Using equation 6.4.16 given in section 6.4.3 the term $\Delta \varepsilon_{p-v}$ can be calculated using the y-intercept of the Scatchard plots. Given that the logarithmic form of the Hill equation is,

$$\log\left(\frac{\theta}{1-\theta}\right) = n * \log(X^-) - logK_D \qquad \text{Equation 6.5.1}$$

And θ is equal to the fraction of the protein bound to substrate,

$$\theta = \frac{[EX]}{[E] + [EX]}$$ Equation 6.5.2

And,

$$[E]_T = [E] + [EX]$$ Equation 6.5.3

$[E]_T$ can be substituted into equation 6.5.2 to give,

$$\theta = \frac{[EX]}{[E]_T}$$ Equation 6.5.4

Equation 6.4.12 from section 6.4 can be solved for [EX] and substituted into Equation 6.5.4 to give,

$$\theta = \frac{\Delta A_{p-v}}{\Delta \varepsilon_{p-v} * E_T}$$ Equation 6.5.5

$\Delta \varepsilon_{p-v}$ can be calculated from the y-intercept of the Scatchard plots, Equation 6.4.16 for each substrate to calculate θ.

5.4.6 LPO Binding Kinetics

A single mixing stopped-flow experiment was used to observe the kinetics of $SeCN^-$ to LPO. Final LPO concentrations were approximately 8 uM so that the absorbance would be suitable for analysis, approximately 0.9 absorbance units. Post-mixing KSeCN concentrations were varied from approximately 1-80 mM. The instrument was blanked by mixing stock LPO with the buffer solution so that difference spectra were observed.

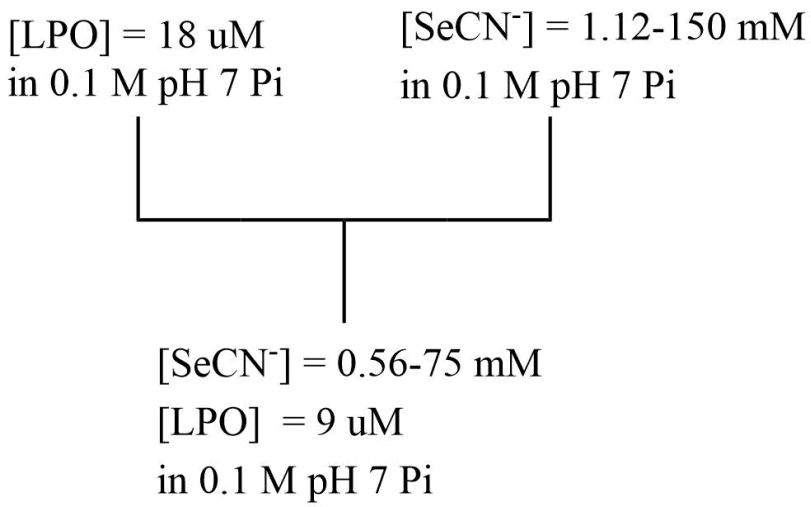

Figure 5.8 - Reaction mixing scheme for the single mixing stopped-flow experiment to observe the rate $SeCN^-$ binding to LPO at pH 5.5 in 100 mM phosphate buffer. This mixing scheme was used to produce the data in section 4.4.1.

5.4.7 Lactoperoxidase Competition Binding Kinetics

A double mixing experiment was used to determine the effect of SCN^- and $SeCN^-$ as competing ions on the rate of binding of each substrate with LPO. LPO and the first binding substrate were mixed in the first mixing cycle via the hand mixer and allowed to come to equilibrium. The second substrate was introduced in the second mixing cycle and was completed using the stopped-flow instrument. In addition to the second substrate, an equimolar concentration of the first substrate after the first mixing cycle was also added in the second mixing cycle so the concentration of the competing substrate would remain constant and the entire spectral change could be attributed to the competing substrate, Figure 5.6. Experiments were done with both SCN^- and $SeCN^-$ functioning as the competitive ligand as a function of both [SCN^-] and [$SeCN^-$].

Final concentration of LPO was maintained at approximately 4-5 uM, 0.4-0.5 absorbance units. The concentration of the initial binding substrate was kept at approximately three times or greater than the dissociation constant calculated in section 4.2. The ligand added in the second mixing cycle was at least double the concentration of the initial ligand.

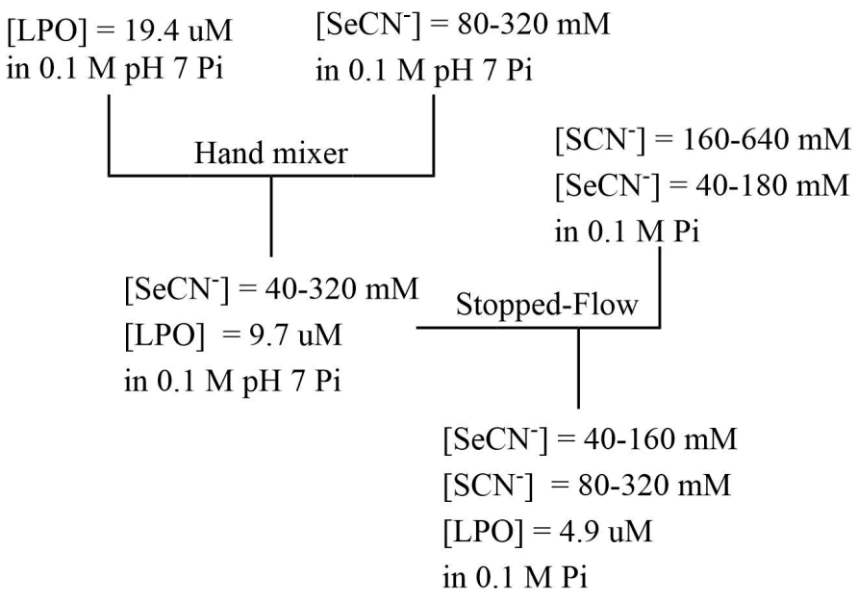

Figure 5.9 - Reaction mixing scheme for the double mixing experiment to observe the rate effect of a competitive binding ligand on the kinetics of binding of SCN^- and $SeCN^-$ to LPO at pH 5.5 in 100 mM phosphate buffer. This mixing scheme was used to produce the data in section 4.4.2.

REFERENCES

1. Cheng, G.; Salerno, J. C.; Cao, Z.; Pagano, P. J.; Lambeth, J. D., Identification and characterization of VPO1, a new animal heme-containing peroxidase. *Free Radic Biol Med* **2008,** *45* (12), 1682-94.

2. Ruf, J.; Carayon, P., Structural and functional aspects of thyroid peroxidase. *Archives of Biochemistry and Biophysics* **2006,** *445* (2), 269-277.

3. Evans, J. S.; Cope, T. A., The Bactericidal Property of Milk. *Univ. Penn. Med. Bull.* **1909,** *21*, 264-74.

4. Hanssen, F. S., The bactericidal property of milk. *Br. J. Exp. Pathol.* **1924,** *5*, 271-80.

5. Jones, F. S.; Little, R. B., Bactericidal property of cow milk. *J. Exp. Med.* **1927,** *45*, 319-35.

6. Mickelson, M. N., Effect of lactoperoxidase and thiocyanate on the growth of Streptococcus pyogenes and Streptococcus agalactiae in a chemically defined culture medium. *Journal of General Microbiology* **1966,** *43* (1), 31-43.

7. Mosimann, W., Salivary peroxidase. *Archives of Biochemistry and Biophysics* **1951,** *33*, 487.

8. Ashby, M. T.; Kreth, J.; Soundarajan, M.; Sivuilu, L. S., Influence of a model human defensive peroxidase system on oral streptococcal antagonism. *Microbiology (Reading, United Kingdom)* **2009,** *155* (11), 3691-3700.

9. Martin, A. P.; Neufeld, H. A.; Lucas, F. V.; Stotz, E., Characterization of uterine peroxidase. *Journal of Biological Chemistry* **1958,** *233*, 206-8.

10. Gerson, C.; Sabater, J.; Scuri, M.; Torbati, A.; Coffey, R.; Abraham, J. W.; Lauredo, I.; Forteza, R.; Wanner, A.; Salathe, M.; Abraham, W. M.; Conner, G. E., The lactoperoxidase system functions in bacterial clearance of airways. *American Journal of Respiratory Cell and Molecular Biology* **2000,** *22* (6), 665-671.

11. Bafort, F.; Parisi, O.; Perraudin, J. P.; Jijakli, M. H., Mode of action of lactoperoxidase as related to its antimicrobial activity: a review. *Enzyme Res.* **2014**, 517164/1-517164/14.

12. Pruitt, K. M.; Tenovuo, J. O.; Editors, *Immunology Series, Vol. 27: The Lactoperoxidase System: Chemistry and Biological Significance*. 1985; p 257 pp.

13. Pruitt, K. In *Lactoperoxidase*, Kluwer Academic/Plenum Publishers: 2003; pp 563-570.

14. Pruitt, K. M.; Kamau, D. N. In *The lactoperoxidase systems of bovine and human milk*, Elsevier: 1991; pp 133-74.

15. Everse, J.; Everse, K. E.; Grisham, M. B.; Editors, *Peroxidases in Chemistry and Biology, Vol. 1*. CRC Press: 1990; p 400 pp.

16. Ghibaudi, E.; Laurenti, E., Unraveling the catalytic mechanism of lactoperoxidase and myeloperoxidase: A reflection on some controversial features. *European Journal of Biochemistry* **2003,** *270* (22), 4403-4412.

17. Sarr, D.; Toth, E.; Gingerich, A.; Rada, B., Antimicrobial actions of dual oxidases and lactoperoxidase. *J Microbiol* **2018,** *56* (6), 373-386.

18. Sharma, S.; Singh, A. K.; Kaushik, S.; Sinha, M.; Singh, R. P.; Sharma, P.; Sirohi, H.; Kaur, P.; Singh, T. P., Lactoperoxidase: structural insights into the function, ligand binding and inhibition. *Int. J. Biochem. Mol. Biol.* **2013,** *4* (3), 108-128.

19. Earnshaw, R. G.; Banks, J. G.; Francotte, C.; Defrise, D., Inhibition of Salmonella typhimurium and Escherichia coli in an infant milk formula by an activated lactoperoxidase system. *J. Food Prot.* **1990,** *53* (2), 170-2.

20. Elliot, R. M.; McLay, J. C.; Kennedy, M. J.; Simmonds, R. S., Inhibition of foodborne bacteria by the lactoperoxidase system in a beef cube system. *Int. J. Food Microbiol.* **2004,** *91* (1), 73-81.

21. Davidson, P. M.; Cekmer, H. B.; Monu, E. A.; Techathuvanan, C., The use of natural antimicrobials in food: an overview. *Woodhead Publ. Ser. Food Sci., Technol. Nutr.* **2015,** *269* (Handbook of Natural Antimicrobials for Food Safety and Quality), 1-27.

22. Epstein, J. B.; Emerton, S.; Le, N. D.; Stevenson-Moore, P., A double-blind crossover trial of Oral Balance gel and Biotene toothpaste versus placebo in patients with xerostomia following radiation therapy. *Oral Oncol* **1999,** *35* (2), 132-7.

23. Shin, K.; Wakabayashi, H.; Yamauchi, K.; Teraguchi, S.; Tamura, Y.; Kurokawa, M.; Shiraki, K., Effects of orally administered bovine lactoferrin and lactoperoxidase on influenza virus infection in mice. *J. Med. Microbiol.* **2005,** *54* (8), 717-723.

24. Shin, K.; Hayasawa, H.; Lonnerdal, B., Inhibition of Escherichia coli respiratory enzymes by the lactoperoxidase-hydrogen peroxide-thiocyanate antimicrobial system. *J. Appl. Microbiol.* **2001,** *90* (4), 489-493.

25. Allen, P. Z.; Morrison, M., Lactoperoxidase. IV. Immunological analysis of bovine lactoperoxidase preparations obtained by a simplified fractionation procedure. *Archives of Biochemistry and Biophysics* **1963,** *102*, 106-13.

26. Dumontet, C.; Rousset, B., Identification, purification, and characterization of a non-heme lactoperoxidase in bovine milk. *Journal of Biological Chemistry* **1983,** *258* (23), 14166-72.

27. Cals, M. M.; Mailliart, P.; Brignon, G.; Anglade, P.; Dumas, B. R., Primary structure of bovine lactoperoxidase, a fourth member of a mammalian heme peroxidase family. *European Journal of Biochemistry* **1991,** *198* (3), 733-9.

28. Kumar, R.; Bhatia, K. L.; Dauter, Z.; Betzel, C., Purification, crystallization and preliminary x-ray crystallographic analysis of lactoperoxidase from buffalo milk. *Acta Crystallogr., Sect. D: Biol. Crystallogr.* **1995,** *D51* (6), 1094-6.

29. Singh, A. K.; Singh, N.; Sharma, S.; Singh, S. B.; Kaur, P.; Bhushan, A.; Srinivasan, A.; Singh, T. P., Crystal Structure of Lactoperoxidase at 2.4 Å Resolution. *J. Mol. Biol.* **2007,** *376* (4), 1060-1075.

30. Rae, T. D.; Goff, H. M., The heme prosthetic group of lactoperoxidase. Structural characteristics of heme l and heme l-peptides. *Journal of Biological Chemistry* **1998,** *273* (43), 27968-27977.

31. Suriano, G.; Watanabe, S.; Ghibaudi, E. M.; Bollen, A.; Pia Ferrari, R.; Moguilevsky, N., Glu375Gln and Asp225Val mutants: About the nature of the covalent linkages between heme group and apo-protein in bovine lactoperoxidase. *Bioorganic & Medicinal Chemistry Letters* **2001,** *11* (21), 2827-2831.

32. Davey, C. A.; Fiedler, T.; Fenna, R. E. In *X-ray crystallographic studies of human myeloperoxidase*, Springer-Verlag: 2000; pp 31-37.

33. Sheikh, I. A.; Singh, A. K.; Singh, N.; Sinha, M.; Singh, S. B.; Bhushan, A.; Kaur, P.; Srinivasan, A.; Sharma, S.; Singh, T. P., Structural Evidence of Substrate Specificity in Mammalian Peroxidases: Structure of the thiocyanate complex with lactoperoxidase and its interactions at 2.4 Å resolution. *Journal of Biological Chemistry* **2009,** *284* (22), 14849-14856.

34. Al-Mustafa, J. I.; Alshbool, T., Fourier Transform Infrared Spectroscopic Investigation of the Binary and Ternary Cyanide Adducts of the Oxidized Horseradish Peroxidase: Identification of a Second Stretching Mode for the Carbon-Nitrogen Bond of the Bound Cyanide Ion. *Spectrosc. Lett.* **2014,** *47* (4), 281-291.

35. Kooter, I. M.; Pierik, A. J.; Merkx, M.; Averill, B. A.; Moguilevsky, N.; Bollen, A.; Wever, R., Difference Fourier Transform Infrared Evidence for Ester Bonds Linking the Heme Group in Myeloperoxidase, Lactoperoxidase, and Eosinophil Peroxidase. *Journal of the American Chemical Society* **1997,** *119* (47), 11542-11543.

36. Marechal, A.; Ingledew, W. J.; Rich, P. R., Time-resolved FTIR study of CO recombination with horseradish peroxidase. *Biochemical Society Transactions* **2008,** *36* (6), 1165-1168.

37. Modi, S.; Behere, D. V.; Mitra, S., Binding of thiocyanate to lactoperoxidase: proton and nitrogen-15 nuclear magnetic resonance studies. *Biochemistry* **1989,** *28* (11), 4689-94.

38. Sakurada, J.; Takahashi, S.; Shimizu, T.; Hatano, M.; Nakamura, S.; Hosoya, T., Proton and iodine-127 nuclear magnetic resonance studies on the binding of iodide by lactoperoxidase. *Biochemistry* **1987,** *26* (20), 6478-83.

39. Singh, A. K.; Pandey, N.; Sinha, M.; Kaur, P.; Sharma, S.; Singh, T. P., Structural evidence for the order of preference of inorganic substrates in mammalian heme peroxidases: crystal structure of the complex of lactoperoxidase with four inorganic substrates, SCN-, I-, Br- and Cl. *Int. J. Biochem. Mol. Biol.* **2011,** *2* (4), 328-339.

40. Mohammed, O. F.; Pines, D.; Dreyer, J.; Pines, E.; Nibbering, E. T. J., Sequential Proton Transfer Through Water Bridges in Acid-Base Reactions. *Science (Washington, DC, United States)* **2005,** *310* (5745), 83-86.

41. Furtmuller, P. G.; Jantschko, W.; Regelsberger, G.; Jakopitsch, C.; Arnhold, J.; Obinger, C., Reaction of lactoperoxidase compound I with halides and thiocyanate. *Biochemistry* **2002,** *41* (39), 11895-11900.

42. Furtmuller, P. G.; Burner, U.; Obinger, C., Reaction of myeloperoxidase compound I with chloride, bromide, iodide, and thiocyanate. *Biochemistry* **1998,** *37* (51), 17923-30.

43. Crull, G. B.; Goff, H. M., NMR relaxation studies of the interaction of thiocyanate with lactoperoxidase. *Journal of Inorganic Biochemistry* **1993,** *50* (3), 181-92.

44. Blair-Johnson, M.; Fiedler, T.; Fenna, R., Human myeloperoxidase: structure of a cyanide complex and its interaction with bromide and thiocyanate substrates at 1.9 A resolution. *Biochemistry* **2001,** *40* (46), 13990-7.

45. Schultz, C. P.; Ahmed, M. K.; Dawes, C.; Mantsch, H. H., Thiocyanate levels in human saliva: quantitation by Fourier-transform infrared spectroscopy. *Analytical Biochemistry* **1996,** *240* (1), 7-12.

46. Lorentzen, D.; Durairaj, L.; Pezzulo, A. A.; Nakano, Y.; Launspach, J.; Stoltz, D. A.; Zamba, G.; McCray, P. B., Jr.; Zabner, J.; Welsh, M. J.; Nauseef, W. M.; Banfi, B., Concentration of the antibacterial precursor thiocyanate in cystic fibrosis airway secretions. *Free Radical Biology & Medicine* **2011,** *50* (9), 1144-1150.

47. Ligeti, E.; Mocsai, A., Exocytosis of neutrophil granulocytes. *Biochemical Pharmacology* **1999,** *57* (11), 1209-1214.

48. Oka, S.; Sibazaki, Y.; Tahara, S., Direct Potentiometric Determination of Chloride Ion in Whole

Blood. *Anal. Chem.* **1981,** *53* (4), 588-593.

49. Ashby, M. T.; Carlson, A. C.; Scott, M. J., Redox Buffering of Hypochlorous Acid by Thiocyanate in Physiologic Fluids. *Journal of the American Chemical Society* **2004,** *126* (49), 15976-15977.

50. Kohler, H.; Taurog, A.; Dunford, H. B., Spectral studies with lactoperoxidase and thyroid peroxidase: Interconversions between native enzyme, Compound II, and Compound III. *Archives of Biochemistry and Biophysics* **1988,** *264* (2), 438-449.

51. Lardinois, O. M.; Medzihradszky, K. F.; De Montellano, P. R. O., Spin trapping and protein cross-linking of the lactoperoxidase protein radical. *Journal of Biological Chemistry* **1999,** *274* (50), 35441-35448.

52. Courtin, F.; Deme, D.; Virion, A.; Michot, J. L.; Pommier, J.; Nunez, J., The role of lactoperoxidase-H2O2 compounds in the catalysis of thyroglobulin iodination and thyroid hormone synthesis. *European Journal of Biochemistry* **1982,** *124* (3), 603-9.

53. Chance, B., The properties of the enzyme-substrate compounds of horse-radish and lacto-peroxidase. *Science (Washington, DC, United States)* **1949,** *109*, 204-8.

54. Theorell, H.; Akesson, A., Purified milk peroxidase. *Ark. Kemi, Mineral. Geol.* **1943,** *17B* (No. 7), 6 pp.

55. Chance, B., Enzyme-substrate compounds of horseradish peroxidase and peroxides. II. Kinetics of formation and decomposition of the primary and secondary complexes. *Arch. Biochem.* **1949,** *22*, 224-52.

56. Furtmuller, P. G.; Jantschko, W.; Zederbauer, M.; Jakopitsch, C.; Arnhold, J.; Obinger, C., Kinetics of interconversion of redox intermediates of lactoperoxidase, eosinophil peroxidase and myeloperoxidase. *Japanese journal of infectious diseases* **2004,** *57* (5), S30-1.

57. Furtmuller, P. G.; Arnhold, J.; Jantschko, W.; Zederbauer, M.; Jakopitsch, C.; Obinger, C., Standard reduction potentials of all couples of the peroxidase cycle of lactoperoxidase. *Journal of Inorganic Biochemistry* **2005,** *99* (5), 1220-1229.

58. Koppenol, W. H., Thermodynamic considerations on the formation of reactive species from hypochlorite, superoxide and nitrogen monoxide. Could nitrosyl chloride be produced by neutrophils and macrophages? *FEBS Letters* **1994,** *347* (1), 5-8.

59. Arnhold, J.; Monzani, E.; Furtmueller, P. G.; Zederbauer, M.; Casella, L.; Obinger, C., Kinetics and thermodynamics of halide and nitrite oxidation by mammalian heme peroxidases. *European Journal of Inorganic Chemistry* **2006,** (19), 3801-3811.

60. Arnhold, J.; Furtmueller, P. G.; Obinger, C., Redox properties of myeloperoxidase. *Redox Rep.* **2003,** *8* (4), 179-186.

61. Ball, R.; Brindley, J., The life story of hydrogen peroxide II: a periodic pH and thermochemical drive for the RNA world. *J. R. Soc. Interface* **2015,** *12* (109), 1-11.

62. Loew, O., Catalase, a new enzyme of general occurrence, with special reference to the tobacco plant. *U.S. Dept. Agr., Rep.* **1901,** (No. 68), 47 pp.

63. Bonnischen, R. K.; Chance, B.; Theorell, H., Catalase activity. *Acta Chemica Scandinavica (1947-1973)* **1947,** *1* (No. 8), 685-708.

64. Watanabe, Y.; Nakajima, H.; Ueno, T., Reactivities of Oxo and Peroxo Intermediates Studied by Hemoprotein Mutants. *Accounts of Chemical Research* **2007,** *40* (7), 554-562.

65. Alfonso-Prieto, M.; Biarnes, X.; Vidossich, P.; Rovira, C., The Molecular Mechanism of the Catalase Reaction. *Journal of the American Chemical Society* **2009,** *131* (33), 11751-11761.

66. Chance, B.; Herbert, D., Catalases and peroxides. XIV. Enzyme-substrate compounds of bacterial catalase and peroxides. *Biochemical Journal* **1950,** *46*, 402-14.

67. Kato, S.; Ueno, T.; Fukuzumi, S.; Watanabe, Y., Catalase Reaction by Myoglobin Mutants and Native Catalase: Mechanistic Investigation by Kinetic Isotope Effect. *Journal of Biological Chemistry* **2004,** *279* (50), 52376-52381.

68. Ogura, Y., Catalase activity at high concentration of hydrogen peroxide. *Archives of Biochemistry and Biophysics* **1955,** *57*, 288-300.

69. Kettle, A. J.; Winterbourn, C. C., A Kinetic Analysis of the Catalase Activity of Myeloperoxidase. *Biochemistry* **2001,** *40* (34), 10204-10212.

70. Thomas, J. A.; Morris, D. R.; Hager, L. P., Chloroperoxidase. VII. Classical peroxidatic, catalatic, and halogenating forms of the enzyme. *Journal of Biological Chemistry* **1970,** *245* (12), 3129-34.

71. Nakajima, R.; Yamazaki, I., The mechanism of oxyperoxidase formation from ferryl peroxidase and hydrogen peroxide. *Journal of Biological Chemistry* **1987,** *262* (6), 2576-81.

72. Bolshakov, I. A.; Vygodina, T. V.; Gennis, R.; Karyakin, A. A.; Konstantinov, A. A., Catalase Activity of Cytochrome c Oxidase Assayed with Hydrogen Peroxide-Sensitive Electrode Microsensor. *Biochemistry (Moscow)* **2010,** *75* (11), 1352-1360.

73. Vlasits, J.; Jakopitsch, C.; Bernroitner, M.; Zamocky, M.; Furtmueller, P. G.; Obinger, C., Mechanisms of catalase activity of heme peroxidases. *Archives of Biochemistry and Biophysics* **2010,** *500* (1), 74-81.

74. Jenzer, H.; Jones, W.; Kohler, H., On the molecular mechanism of lactoperoxidase-catalyzed hydrogen peroxide metabolism and irreversible enzyme inactivation. *Journal of Biological Chemistry* **1986,** *261* (33), 15550-6.

75. Jantschko, W.; Furtmuller, P. G.; Zederbauer, M.; Neugschwandtner, K.; Jakopitsch, C.; Obinger, C., Reaction of ferrous lactoperoxidase with hydrogen peroxide and dioxygen: an anaerobic stopped-flow study. *Archives of Biochemistry and Biophysics* **2005,** *434* (1), 51-59.

76. Huwiler, M.; Jenzer, H.; Kohler, H., The role of compound III in reversible and irreversible inactivation of lactoperoxidase. *European Journal of Biochemistry* **1986,** *158* (3), 609-14.

77. Kohler, H.; Jenzer, H., Interaction of lactoperoxidase with hydrogen peroxide. Formation of enzyme intermediates and generation of free radicals. *Free Radic Biol Med* **1989,** *6* (3), 323-39.

78. Thibodeau, E. A.; Bowen, W. H.; Marquis, R. E., pH-Dependent fluoride inhibition of peroxidase activity. *Journal of Dental Research* **1985,** *64* (10), 1211-13.

79. Segal, R.; Dunford, H. B.; Morrison, M., Kinetics of fluoride binding by lactoperoxidase. *Can. J. Biochem.* **1968,** *46* (12), 1471-4.

80. Hannuksela, S.; Tenovuo, J.; Roger, V.; Lenander-Lumikari, M.; Ekstrand, J., Fluoride inhibits the antimicrobial peroxidase systems in human whole saliva. *Caries Research* **1994,** *28* (6), 429-34.

81. Tenovuo, J., Inhibition by thiocyanate of lactoperoxidase-catalyzed oxidation and iodination reactions. *Arch. Oral Biol.* **1978,** *23* (10), 899-903.

82. Kalmar, J.; Woldegiorgis, K. L.; Biri, B.; Ashby, M. T., Mechanism of Decomposition of the Human Defense Factor Hypothiocyanite Near Physiological pH. *Journal of the American Chemical Society* **2011,** *133* (49), 19911-19921.

83. Doerge, D. R.; Niemczura, W. P., Suicide inactivation of lactoperoxidase by 3-amino-1,2,4-triazole. *Chem Res Toxicol* **1989,** *2* (2), 100-3.

84. Doerge, D. R., Mechanism-based inhibition of lactoperoxidase by thiocarbamide goitrogens. Identification of turnover and inactivation pathways. *Biochemistry* **1988,** *27* (10), 3697-700.

85. Koeksal, Z.; Kalin, R.; Gerni, S.; Guelcin, I.; Oezdemir, H., The inhibition effects of some natural products on lactoperoxidase purified from bovine milk. *J. Biochem. Mol. Toxicol.* **2017,** *31* (9), n/a.

86. Roy, G.; Jayaram, P. N.; Mugesh, G., Inhibition of Lactoperoxidase-Catalyzed Oxidation by Imidazole-Based Thiones and Selones: A Mechanistic Study. *Chem. - Asian J.* **2013,** *8* (8), 1910-1921.

87. Lemma, K.; Ashby, M. T., Reactive sulfur species: kinetics and mechanism of the reaction of hypothiocyanous acid with cyanide to give dicyanosulfide in aqueous solution. *Chemical Research in Toxicology* **2009,** *22* (9), 1622-1628.

88. Nagy, P.; Jameson, G. N. L.; Winterbourn, C. C., Kinetics and Mechanisms of the Reaction of Hypothiocyanous Acid with 5-Thio-2-nitrobenzoic Acid and Reduced Glutathione. *Chemical Research in Toxicology* **2009,** *22* (11), 1833-1840.

89. McNaught, A. D.; Wilkinson, A., *Compendium of Chemical Terminology, 2nd Edition*. Blackwell: 1997; p 496 pp.

90. Below, J. F., Jr.; Connick, R. E.; Coppel, C. P., Kinetics of the formation of the ferric thiocyanate complex. *Journal of the American Chemical Society* **1958,** *80*, 2961-7.

91. Leung, A. M.; LaMar, A.; He, X.; Braverman, L. E.; Pearce, E. N., Iodine status and thyroid function of Boston-area vegetarians and vegans. *J. Clin. Endocrinol. Metab.* **2011,** *96* (8), E1303-E1307.

92. Han, H.; Kwon, H., Estimated dietary intake of thiocyanate from Brassicaceae family in Korean diet. *J. Toxicol. Environ. Health, Part A* **2009,** *72* (21 & 22), 1380-1387.

93. Wrobel, M.; Jurkowska, H.; Sliwa, L.; Srebro, Z., Sulfurtransferases and cyanide detoxification in mouse liver, kidney, and brain. *Toxicology Mechanisms and Methods* **2004,** *14* (6), 331-337.

94. Ashby, M. T., Hypothiocyanite. *Advances in Inorganic Chemistry* **2012,** *64*, 263-303.

95. Thomas, E. L., Lactoperoxidase-catalyzed oxidation of thiocyanate: equilibria between oxidized forms of thiocyanate. *Biochemistry* **1981,** *20* (11), 3273-80.

96. Aune, T. M.; Thomas, E. L., Accumulation of Hypothiocyanite Ion During Peroxidase-Catalyzed Oxidation of Thiocyanate Ion. *European Journal of Biochemistry* **1977,** *80* (#1), 209-214.

97. Cegolon, L.; Salata, C.; Piccoli, E.; Juarez, V.; Palu, G.; Mastrangelo, G.; Calistri, A., In vitro antiviral activity of hypothiocyanite against A/H1N1/2009 pandemic influenza virus. *Int. J. Hyg. Environ. Health* **2014,** *217* (1), 17-22.

98. Nagy, P.; Beal, J. L.; Ashby, M. T., Thiocyanate Is an Efficient Endogenous Scavenger of the Phagocytic Killing Agent Hypobromous Acid. *Chemical Research in Toxicology* **2006,** *19* (4), 587-593.

99. Thomas, E. L.; Aune, T. M., Lactoperoxidase, peroxide, thiocyanate antimicrobial system: correlation of sulfhydryl oxidation with antimicrobial action. *Infection and Immunity* **1978,** *20* (2), 456-63.

100. Thomas, E. L.; Aune, T. M., Susceptibility of Escherichia coli to bactericidal action of lactoperoxidase, peroxide, and iodide or thiocyanate. *Antimicrob. Agents Chemother.* **1978,** *13* (2), 261-5.

101. White, W. E., Jr.; Pruitt, K. M.; Mansson-Rahemtulla, B., Peroxidase-thiocyanate-peroxide antibacterial system does not damage DNA. *Antimicrob. Agents Chemother.* **1983,** *23* (2), 267-72.

102. Cupp-Sutton, K. A.; Ashby, M. T., Biological chemistry of hydrogen selenide. *Antioxidants* **2016,** *5* (4), 42/1-42/18.

103. Steinmann, D.; Nauser, T.; Koppenol, W. H., Selenium and Sulfur in Exchange Reactions: A Comparative Study. *Journal of Organic Chemistry* **2010,** *75* (19), 6696-6699.

104. Seby, F.; Potin-Gautier, M.; Giffaut, E.; Borge, G.; Donard, O. F. X., A critical review of thermodynamic data for selenium species at 25°C. *Chemical Geology* **2001,** *171* (3-4), 173-194.

105. Frost, A. A., Oxidation potential-free energy diagrams. *Journal of the American Chemical Society* **1951,** *73*, 2680-2.

106. Slater, J. C., Atomic radii in crystals. *Journal of Chemical Physics* **1964,** *41* (10), 3199-3204.

107. Allen, F. H., The Cambridge Structural Database: a quarter of a million crystal structures and rising. *Acta Crystallographica, Section B: Structural Science* **2002,** *B58* (3, No. 1), 380-388.

108. Nicovich, J. M.; Kreutter, K. D.; Van Dijk, C. A.; Wine, P. H., Temperature-dependent kinetics studies of the reactions bromine atom(2P3/2) + hydrogen sulfide ↔ mercapto + hydrogen bromide and bromine atom(2P3/2) + methanethiol ↔ methylthiol + hydrogen bromide. Heats of formation of mercapto and methylthio radicals. *Journal of Physical Chemistry* **1992,** *96* (6), 2518-28.

109. Berkowitz, J.; Ellison, G. B.; Gutman, D., Three methods to measure RH bond energies. *Journal of Physical Chemistry* **1994,** *98* (11), 2744-65.

110. Guziec, F. S., Jr., Seleno- and telluro-carbonyl compounds. *Chemistry of Organic Selenium and Tellurium Compounds* **1987,** *2*, 215-73.

111. Gonzales, J. M.; Musaev, D. G.; Morokuma, K., Theoretical Studies of Oxidative Addition of E-E Bonds (E = S, Se, Te) to Palladium(0) and Platinum(0) Complexes. *Organometallics* **2005,** *24* (21), 4908-4914.

112. Moore, C. E., *Ionization Potentials and Ionization Limits Derived from the Analyses of Optical Spectra*. National Bureau of Standards, Washington, D.C.: 1970; p 22 pp.

113. Hotop, H.; Lineberger, W. C., Binding energies in atomic negative ions. *Journal of Physical and Chemical Reference Data* **1975,** *4* (3), 539-76.

114. Allred, A. L., Electronegativity values from thermochemical data. *Journal of Inorganic and Nuclear Chemistry* **1961,** *17*, 215-21.

115. Widmer, M.; Schwarzenbach, G., Acidity of the hydrosulfide ion HS. *Helvetica Chimica Acta* **1964,** *47* (1), 266-71.

116. Hagisawa, H., The glass electrode and its applications. XII. Dissociation constants of hydrogen selenide. *Rikagaku Kenkyusho Iho* **1941,** *20*, 384-9.

117. Levy, D. E.; Myers, R. J., Spectroscopic determination of the second dissociation constant of hydrogen selenide and the activity coefficients and spectral shifts of its ions. *Journal of Physical Chemistry* **1990,** *94* (20), 7842-7.

118. Schwarz, K.; Foltz, C. M., Selenium as an integral part of factor 3 against dietary necrotic liver degeneration. *Journal of the American Chemical Society* **1957,** *79*, 3292-3.

119. Garousi, F., The essentiality of selenium for humans, animals, and plants, and the role of selenium in plant metabolism and physiology. *Acta Univ. Sapientiae, Aliment.* **2017,** *10* (1), 75-90.

120. Ullah, H.; Liu, G.; Yousaf, B.; Ali, M. U.; Irshad, S.; Abbas, Q.; Ahmad, R., A comprehensive review on environmental transformation of selenium: recent advances and research perspectives. *Environmental Geochemistry and Health* **2018**, Ahead of Print.

121. Muntau, A. C.; Streiter, M.; Kappler, M.; Roschinger, W.; Schmid, I.; Rehnert, A.; Schramel, P.; Roscher, A. A., Age-related reference values for serum selenium concentrations in infants and children. *Clinical Chemistry (Washington, DC, United States)* **2002,** *48* (3), 555-560.

122. *Toxicological Profile for selenium*; 1989; p 194 pp.

123. MacFarquhar Jennifer, K.; Broussard Danielle, L.; Melstrom, P.; Hutchinson, R.; Wolkin, A.; Martin, C.; Burk Raymond, F.; Dunn John, R.; Green Alice, L.; Hammond, R.; Schaffner, W.; Jones Timothy, F., Acute selenium toxicity associated with a dietary supplement. *Archives of internal medicine* **2010,** *170* (3), 256-61.

124. Tinggi, U., Selenium toxicity and its adverse health effects. *Reviews in Food and Nutrition Toxicity* **2005,** *4*, 29-55.

125. Boeck, A.; Thanbichler, M., Selenocysteine. *EcoSal Plus* **2014**, 1-12.

126. Block, E.; Birringer, M.; Jiang, W.; Nakahodo, T.; Thompson, H. J.; Toscano, P. J.; Uzar, H.; Zhang, X.; Zhu, Z., Allium chemistry: synthesis, natural occurrence, biological activity, and chemistry of Se-alk(en)ylselenocysteines and their γ-glutamyl derivatives and oxidation products. *Journal of Agricultural and Food Chemistry* **2001,** *49* (1), 458-470.

127. Lu, J.; Holmgren, A., Selenoproteins. *Journal of Biological Chemistry* **2009,** *284* (2), 723-727.

128. Shi, Z.; Pan, P.; Feng, Y.; Kan, Z.; Li, Z.; Wei, F., Environmental water chemistry and possible correlation with Kaschin-Beck Disease (KBD) in northwestern Sichuan, China. *Environ. Int.* **2017,** *99*, 282-292.

129. Muth, O. H.; Oldfield, J. E.; Remmert, L. F.; Schubert, J. R., Effects of selenium and vitamin E on white muscle disease. *Science (New York, N.Y.)* **1958,** *128* (3331), 1090.

130. Spallholz, J. E., On the nature of selenium toxicity and carcinostatic activity. *Free Radic Biol Med* **1994,** *17* (1), 45-64.

131. Raisbeck, M. F., Selenosis. *The Veterinary clinics of North America. Food animal practice* **2000,** *16* (3), 465-80.

132. Spallholz, J. E., Free radical generation by selenium compounds and their prooxidant toxicity. *Biomedical and environmental sciences : BES* **1997,** *10* (2-3), 260-70.

133. Anan, Y.; Kimura, M.; Hayashi, M.; Koike, R.; Ogra, Y., Detoxification of Selenite to Form Selenocyanate in Mammalian Cells. *Chemical Research in Toxicology* **2015,** *28* (9), 1803-1814.

134. Wolff, J.; Maurey, J. R., Thyroidal iodide transport. IX. The accumulation and metabolism of selenocyanate. *Endocrinology* **1966,** *79* (4), 795-800.

135. Ashby, M. T.; Carlson, A. C.; Scott, M. J., Redox buffering of hypochlorous acid by thiocyanate in physiologic fluids. *J Am Chem Soc* **2004,** *126* (49), 15976-7.

136. Nagy, P.; Beal, J. L.; Ashby, M. T., Thiocyanate is an efficient endogenous scavenger of the phagocytic killing agent hypobromous acid. *Chem Res Toxicol* **2006,** *19* (4), 587-93.

137. Nagy, P.; Alguindigue, S. S.; Ashby, M. T., Lactoperoxidase-Catalyzed Oxidation of Thiocyanate by Hydrogen Peroxide: A Reinvestigation of Hypothiocyanite by Nuclear Magnetic Resonance and Optical Spectroscopy. *Biochemistry* **2006,** *45* (41), 12610-12616.

138. Pruitt, K. M.; Tenovou, J., Kinetics of hypothiocyanite production during peroxidase-catalyzed oxidation of thiocyanate. *Biochimica et Biophysica Acta (BBA)/Protein Structure and Molecular* **1982,** *704* (2), 204-214.

139. Dua, S.; Maclean, M. J.; Fitzgerald, M.; McAnoy, A. M.; Bowie, J. H., Is the Hypothiocyanite Anion (OSCN)- the Major Product in the Peroxidase Catalyzed Oxidation of the Thiocyanate Anion (SCN)-? A Joint Experimental and Theoretical Study. *Journal of Physical Chemistry A* **2006,** *110* (14), 4930-4936.

140. Wilson, I. R.; Harris, G. M., The oxidation of thiocyanate ion by hydrogen peroxide. I. The pH-independent reaction. *Journal of the American Chemical Society* **1960,** *82*, 4515-17.

141. CRC Handbook of Chemistry and Physics: A Ready-Reference of Chemical and Physical Data, 85th ed, Edited by David R. Lide. *Journal of the American Chemical Society* **2005,** *127* (12), 4542.

142. Morris, J. C., The acid ionization constant of HOCl from 5 to 35°. *Journal of Physical Chemistry* **1966,** *70* (12), 3798-805.

143. Nagy, P.; Wang, X.; Lemma, K.; Ashby, M. T., Reactive Sulfur Species: Hydrolysis of Hypothiocyanite To Give Thiocarbamate-S-oxide. *Journal of the American Chemical Society* **2007,** *129* (51), 15756-15757.

144. Gau, J.; Arnhold, J.; Flemmig, J.; Furtmuller, P.-G.; Obinger, C.; Arnhold, J.; Flemmig, J., Enhancing hypothiocyanite production by lactoperoxidase - mechanism and chemical properties of promotors. *Biochem Biophys Rep* **2015,** *4*, 257-267.

145. Flemmig, J.; Rusch, D.; Czerwinska, M. E.; Rauwald, H.-W.; Arnhold, J., Components of a standardised olive leaf dry extract (Ph. Eur.) promote hypothiocyanite production by lactoperoxidase. *Archives of Biochemistry and Biophysics* **2014,** *549*, 17-25.

146. Eyer, P.; Worek, F.; Kiderlen, D.; Sinko, G.; Stuglin, A.; Simeon-Rudolf, V.; Reiner, E., Molar absorption coefficients for the reduced Ellman reagent: reassessment. *Analytical Biochemistry* **2003,** *312* (2), 224-227.

147. Plano, D.; Lizarraga, E.; Font, M.; Palop, J. A.; Sanmartin, C., Thermal stability and decomposition of sulphur and selenium compounds. *J. Therm. Anal. Calorim.* **2009,** *98* (2), 559-566.

148. Greenwood, N. N.; Earnshaw, A., *Chemistry of the Elements, 2nd Edition*. 1997; p No pp given.

149. Carroll, L.; Pattison, D. I.; Fu, S.; Schiesser, C. H.; Davies, M. J.; Hawkins, C. L., Reactivity of selenium-containing compounds with myeloperoxidase-derived chlorinating oxidants: Second-order rate constants and implications for biological damage. *Free Radical Biology & Medicine* **2015,** *84*, 279-288.

150. Hamada, S., Decomposition equilibrium of selenocyanate ion. *Nippon Kagaku Zasshi* **1961,** *82*, 1327-30.

151. Jakopitsch, C.; Pirker, K. F.; Hofbauer, S.; Furtmuller, P. G.; Flemmig, J.; Arnhold, J.; Schlorke, D.; Obinger, C., Mechanism of reaction of chlorite with mammalian heme peroxidases. *Journal of Inorganic Biochemistry* **2014,** *135*, 10-19.

152. Cook, P. F.; Cleland, W. W.; Editors, *Enzyme Kinetics and Mechanism*. Garland Science: 2007; p 404 pp.

153. Sies, H., Hydrogen peroxide as a central redox signaling molecule in physiological oxidative stress: Oxidative eustress. *Redox Biol* **2017,** *11*, 613-619.

154. Ashby, M. T., Inorganic chemistry of defensive peroxidases in the human oral cavity. *Journal of Dental Research* **2008,** *87* (10), 900-914.

155. Ferrari, R. P.; Ghibaudi, E. M.; Traversa, S.; Laurenti, E.; De, G. L.; Salmona, M., Spectroscopic and binding studies on the interaction of inorganic anions with lactoperoxidase. *J Inorg Biochem* **1997,** *68* (1), 17-26.

156. Modi, S.; Behere, D. V.; Mitra, S., Binding of aromatic donor molecules to lactoperoxidase: proton NMR and optical difference spectroscopic studies. *Biochimica et Biophysica Acta, Protein Structure and Molecular Enzymology* **1989,** *996* (3), 214-25.

157. Sievers, G., The thiocyanate binding to lactoperoxidase. *Protides of the Biological Fluids* **1985,** *32*, 129-32.

158. Feldman, H. A., Statistical limits in Scatchard analysis. *Journal of Biological Chemistry* **1983,** *258* (21), 12865-7.

159. Theorell, H.; Paul, K. G., Dissociation constants and their relations to the activity in peroxidases. *Ark. Kemi, Mineral. Geol.* **1944,** *18A* (No. 12), 23 pp.

160. *SPECFIT*, Spectrum Software Associates: 1993-2007.

161. *Kinetic Studio*, TKG Scientific: 2009.

162. *KaleidaGraph* 2.5; Synergy Software: 2000.

163. Beers, R. F., Jr.; Sizer, I. W., A spectrophotometric method for measuring the breakdown of hydrogen peroxide by catalase. *Journal of Biological Chemistry* **1952,** *195*, 133-40.

164. Wofram Research, I. *Mathematica*, 11.2; Wolfram Research, Inc.: 2017.

APPENDICES

Appendix A - Modeling of the Literature Mechanism of the Halogen Cycle of Lactoperoxidase

Mathematica was used to make and probe a mathematical model of the lactoperoxidase halogen cycle as reported by Furmüller and shown in Equations 3.2.5 and 3.2.6.[41] An NDSolve of the differential equations was used to model the reaction. In the model EE = LPO, Ox = H_2O_2, EOx = compound I, S = PsX^-.

```
Clear[EE, ES, EOx, S, Ox, P, Ox0, t, k1, k2];

equations = {
  EE'[t] == -k1*EE[t]*Ox[t] + k2*EOx[t]*S,
  EOx'[t] == +k1*EE[t]*Ox[t] - k2*EOx[t]*S,
  Ox'[t] == -k1*EE[t]*Ox[t],
  P'[t] == k2*EOx[t]*S,
  EE[0] == EE0,
  EOx[0] == 0,
  Ox[0] == Ox0,
  P[0] == 0
  };

k1 = 1.1*10^7;
k2 = 2*10^8;
```

```
EE0 = 1*10^-6;

S = 1*10^-4;

Ox0 = 5*10^-5;


timeframe = 5;


answer = NDSolve[equations, P[t] , {t, 0, timeframe};


EE[t_] = EE[t] /. answer;

EOx[t_] = EOx[t] /. answer;

Ox[t_] = Ox[t] /. answer;

P[t_] = P[t] /. answer;
```

A parametricNDSolve was used to observe the effect of varying concentrations of reactants on the model.

```
Clear[EE, EOx, S, Ox, P, S0, Ox0, EEO, t, k1, k2, a];


k1 = 1.1*10^7;

k2 = 4*10^4;

EE0 = 1*10^-6;

Ox0 = 5*10^-5;

S = 5*10^-5*a;
```

```
timeframe = 10000;


pfun = ParametricNDSolveValue[
  {
   EE'[t] == -k1*EE[t]*Ox[t] + k2*EOx[t]*S,
   EOx'[t] == +k1*EE[t]*Ox[t] - k2*EOx[t]*S,
   Ox'[t] == -k1*EE[t]*Ox[t],
   P'[t] == k2*EOx[t]*S,
   EE[0] == EE0,
   EOx[0] == 0,
   Ox[0] == Ox0,
   P[0] == 0
   }
  , P, {t, 0, 10000}, {a}];
```

Appendix B - Modeling of the Proposed Mechanism of the Lactoperoxidase-Catalyzed Oxidation of Pseudohalide

Mathematica was used to make and probe a mathematical model of the proposed lactoperoxidase halogen cycle mechanism as discussed in section 3.6.1 of this work. An NDSolve of the differential equations was used to model the reaction with the rate constants caculated from experimental data. In the model EE = LPO, ES =

LPOSCN/LPOSeCN, Ox = H_2O_2, EOx = $LPOH_2O_2$, S = PsX^-, and P = $OPsX^-$. The rate constants were approximated from the fitted rate constants in section 3.6.1.

```
Clear[EE,ES,EOx,S, Ox, P,Ox0, t,k1, km1,k2, km2, k3];

equations = {
  EE'[t] == -k1*EE[t]*S+km1*ES[t]-k2*EE[t]*Ox[t]+km2*EOx[t]+k3*ES[t]*Ox[t],
  ES'[t] == k1*EE[t]*S-km1*ES[t]-k3*ES[t]*Ox[t],
  EOx'[t] == k2*EE[t]*Ox[t]-km2*EOx[t],
  Ox'[t] == -k3*ES[t]*Ox[t],
  P'[t] == k3*ES[t]*Ox[t],
  EE[0] == EE0,
  ES[0]== 0,
  EOx[0]== 0,
  Ox[0]== Ox0,
  P[0]== 0};

k1=1.4*10^9;
km1=3940;
k2=3.48*10^7;
km2=2.07;
k3=1*10^7;
EE0=1*10^-6;
```

```
S=1*10^-4;
Ox0=5*10^-5;

timeframe = 6;

answer=NDSolve[equations, {EE[t], ES[t], EOx[t],S[t], Ox[t], P[t]}, {t,0,timeframe}];

EE[t_]=EE[t]/.answer;
ES[t_]=ES[t]/.answer;
EOx[t_]=EOx[t]/.answer;
S[t_]=S[t]/.answer;
Ox[t_]=Ox[t]/.answer;
P[t_]=P[t]/.answer;
```

Appendix C - Fitting Experimental Data Using the Proposed Mechanism of the Lactoperoxidase-Catalyzed Oxidation of Pseudohalide

Experimental kinetic traces collected using methods discussed in section 6.3 of this work were fit to the proposed model for the lactoperoxidase-catalyzed oxidation of PsX^- at low [PsX^-] discussed in section 3.6.2 of this work to determine rate constants k_1, k_{-1}, k_2, k_{-2}, and k_3.

As the data was collected through the TNB assay, the fitted kinetic trace data was manipulated to match the predictions of the model. The reactions involving the TNB assay were omitted so as not to over complicate the model. The molar extinction coefficeint,

$\varepsilon_{412(TNB)}$ = 14,150 $M^{-1}cm^{-1}$, was used to calculate the trace as [$OPsX^-$].[146] Multiplication of the entire dataset by an appropriate factor to account for the entire consumption of H_2O_2 was done to allow for the model to fit the data.

A ParametricNDSolve was used to model the mechanism and a NonlinearRegression was used to calculate fitted rate constants. Initial parameters were determined by allowing all rate constants to vary for a set of data where the pre-equilibrium and steady-state reaction could both be clearly observed, such as trace B in Figure 3.28. The rate constants calculated here were used as initial parameter values to fit the traces which were less well-defined. In some cases, where the pre-equilibrium reaction and steady-state reactions were especially undefined, such as traces C and D in Figure 3.28, appropriate rate constants were fixed to allow the calculation of the rate constants for the dominant reaction which could be clearly observed in the trace. In the model EE = LPO, ES = LPOSCN/LPOSeCN, Ox = H_2O_2, EOx = LPO-H_2O_2, S = PsX^-, and P = $OPsX^-$.

```
SetDirectory["C:/Users/Kellye Sutton/Documents/Graduate Research/ExpB188"];
data1=ReadList["ExpB18804-06.Product.v4.txt",{Number,Number}];

Clear[EE,ES,EOx,S,Ox,P,k1,k2,k3,k4,k5];

totaltime=6;

S=5.3*10^-5;
```

```
model=ParametricNDSolveValue[
  {
   EE'[t] == -k1*EE[t]*S+k2*ES[t]-k3*EE[t]*Ox[t]+k4*EOx[t]+k5*ES[t]*Ox[t],
   ES'[t] == k1*EE[t]*S-k2*ES[t]-k5*ES[t]*Ox[t],
   EOx'[t] == k3*EE[t]*Ox[t]-k4*EOx[t],
   Ox'[t] == -k5*ES[t]*Ox[t],
   P'[t] == k5*ES[t]*Ox[t],
   EE[0] == 1.20*10^-6,
   ES[0]== 0,
   EOx[0]== 0,
   Ox[0]==4.0*10^-5,
   P[0]== 0},P,{t,0,totaltime},{k1,k2,k3,k4,k5}];

Clear[EE,ES,EOx,S,Ox,P,k1,k2,k3,k4,k5];
Needs["NonlinearRegression`"]
NonlinearRegress[data1,model[k1,k2,k3,k4,k5][t],{{k1,1*10^9},{k2,4000},{k3,3*10^7}
,{k4,2},{k5,9*10^6}},t]
```

Appendix D - Model of LPO Competition Binding Kinetics

A model was built of the proposed binding mechanism for SeCN- to LPO given in Figure 4.16. In the model LPO = EE, EX = LPOSeCN, EXp = LPOSeCN*, EY = LPOSCN, X = SCN^-, and Y = $SeCN^-$. The ParametricNDSolve is used to give a solve the differential equations and vary [SCN^-] and [$SeCN^-$] individually to determine the effect on the model.

The rate constants used were estimated based on the calculated constants from section 4.4.2.

```
(*LPO*SCN Pre-Equilibrium
SCN Varied*)

Clear[EE, EX, EXp, EY, t, k1, km1, k2, km2, k3, km3, X, Y]

k1 = 1*10^9;
km1 = 5000000;
k2 = 50;
km2 = 1;
k3 = 1*10^9;
km3 = 10000000;
X = 0.32;
Y = 0.04*a;
EE0 = 4.6*10^-6;
pfun = ParametricNDSolveValue[
  {
   EE'[t] == -k1*EE[t]*X + km1*EX[t] - k3*EE[t]*Y + km3*EY[t],
   EX'[t] == k1*EE[t]*X - km1*EX[t] - k2*EX[t] + km2*EXp[t],
   EXp'[t] == k2*EX[t] - km2*EXp[t],
   EY'[t] == k3*EE[t]*Y - km3*EY[t],
```

```
    EE[0] == EE0 - (k1*EE0*Y/km1)/(1 + Y*k1/km1),
    EX[0] == 0,
    EXp[0] == 0,
    EY[0] == (k1*EE0*Y/km1)/(1 + Y*k1/km1)
    }
   , EXp, {t, 0, 10000}, {a}];
timeframe = 0.4;
Plot[Evaluate[Table[pfun[a][t], {a, {1, 2, 4, 8, 32}}]], {t, 0,
  timeframe}, PlotRange -> {0, 4.6*10^-6}]
```